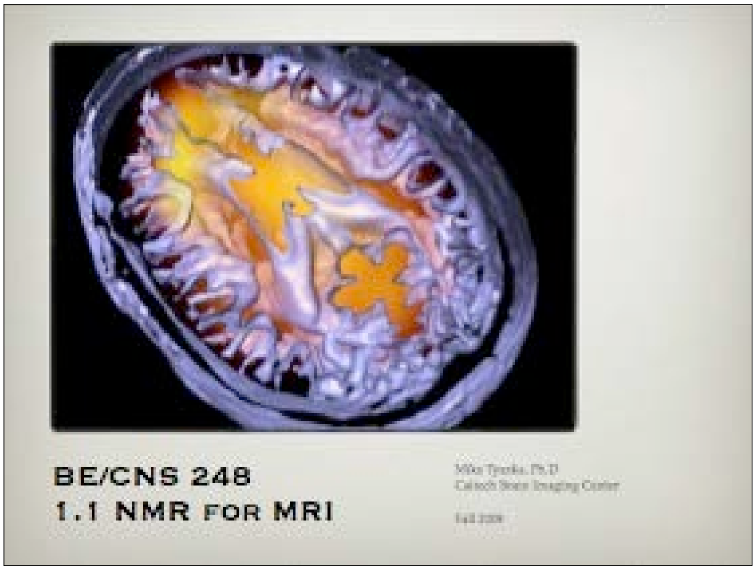
BE/CNS 248
1.1 NMR for MRI

1

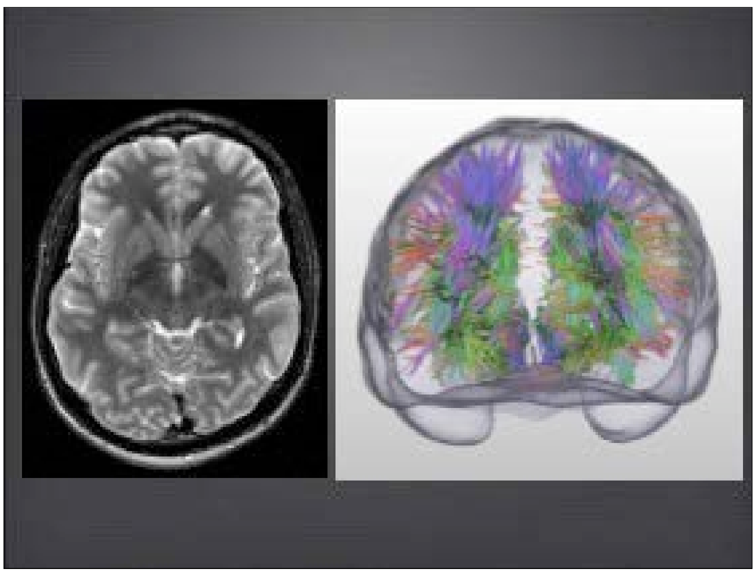

2

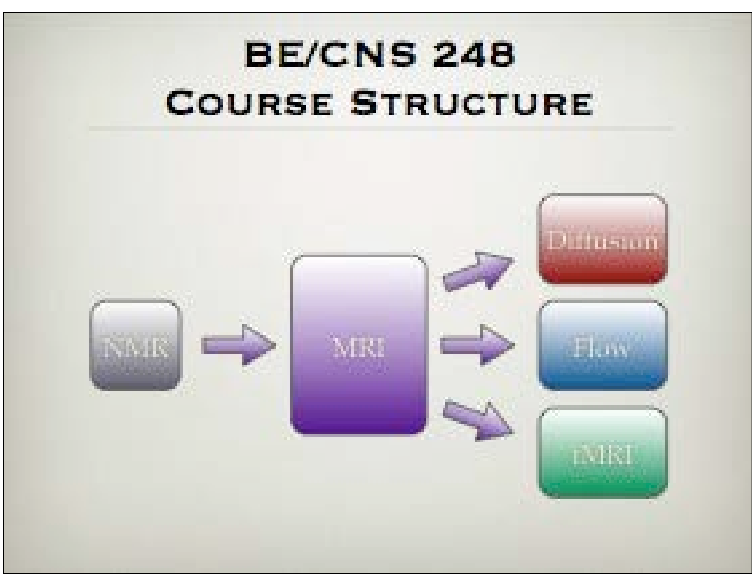
BE/CNS 248
Course Structure
NMR
MRI
Diffusion
Flow
fMRI

3

Web Resources

http://www.its.caltech.edu/~jmt/BE248

4

Lecture Summary

- 1.1 Basic NMR
  - a. A Brief History of NMR and MRI
  - b. Magnetism and Magnetic Materials
  - c. The Zeeman effect
  - d. Nuclear spin polarization
  - e. The Larmor relation
  - f. Nuclear shielding and chemical shift
  - g. Nuclear spin quantum mechanics
  - h. The Semi-classical Vector Model
  - i. The Bloch Equation
  - i. The Rotating Frame

5

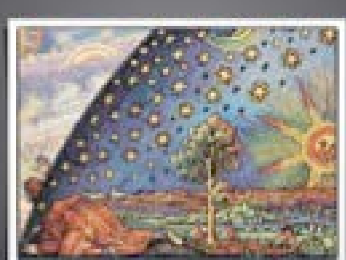

History of MRI

6

1891: Optical Hyperfine Splitting

A.A. Michelson observes optical hyperfine splitting as early as 1891. A full explanation of the effect had to wait more than 40 years for Pauli to suggest that the nucleus had a magnetic dipole. The orbital angular momentum of the electron interacts with the nuclear dipole, resulting in hyperfine splitting of absorption and emission lines.

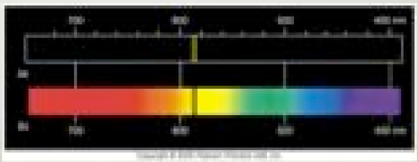

7

1896: Larmor Precession

1896 Sir Joseph Larmor publishes magnetic field effect on radiation frequency. Relates the precession frequency of the magnetic dipole associated with an orbiting electron to an externally applied magnetic field.

8

1896: Zeeman Effect

1896 Pieter Zeeman observes sodium D line splitting in an applied magnetic field. The effect arises from the interaction of the total (ie orbital + intrinsic) angular momentum of an electron.

Zeeman P. Nature 1897;55:347

9

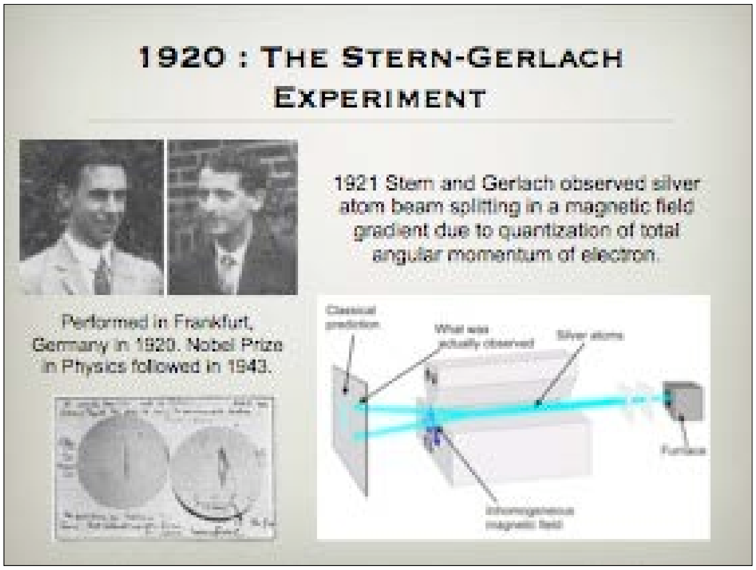
1920 : THE STERN-GERLACH EXPERIMENT
1921 Stern and Gerlach observed silver atom beam splitting in a magnetic field gradient due to quantization of total angular momentum of electron.
Performed in Frankfurt, Germany in 1920. Nobel Prize in Physics followed in 1943.
Classical prediction
What was actually observed
Silver atoms
Furnace
Inhomogeneous magnetic field

10

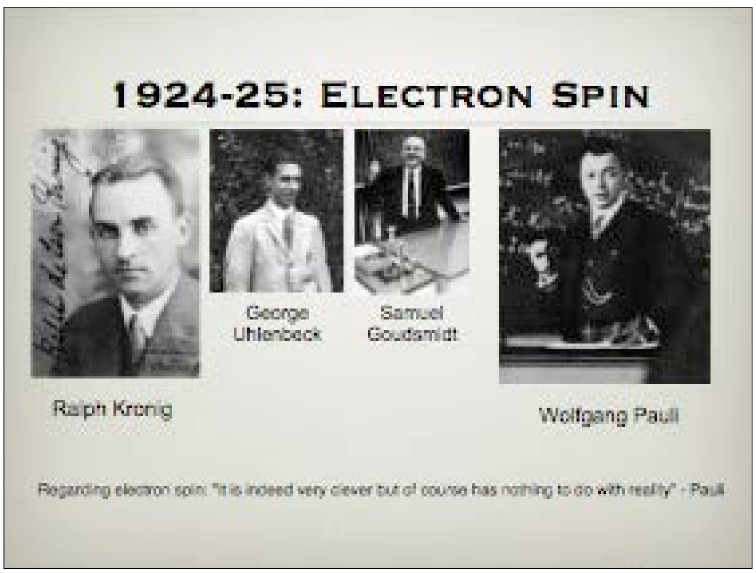
1924-25: ELECTRON SPIN
George Uhlenbeck
Samuel Goudsmidt
Ralph Kronig
Wolfgang Pauli
Regarding electron spin: "It is indeed very clever but of course has nothing to do with reality" - Pauli

11

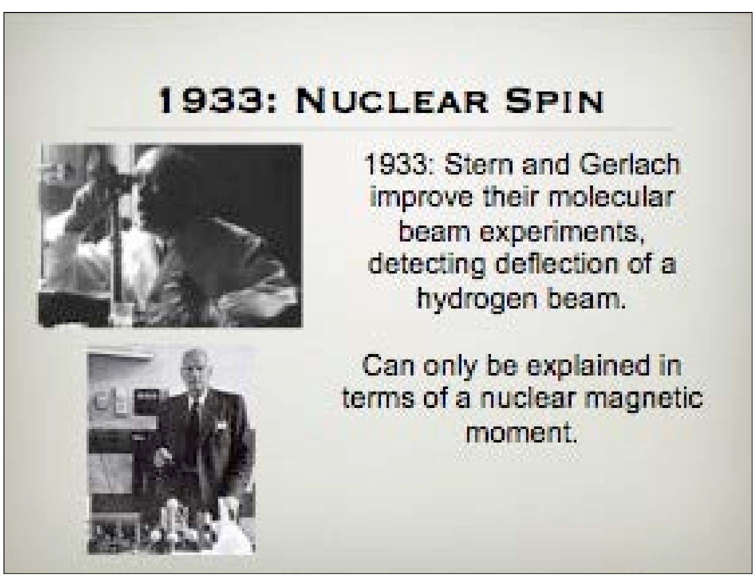
1933: NUCLEAR SPIN
1933: Stern and Gerlach improve their molecular beam experiments, detecting deflection of a hydrogen beam.
Can only be explained in terms of a nuclear magnetic moment.

12

1936-37: Nuclear Spin Resonance

1936 C.J. Gorter attempts to use nuclear resonance to study nuclear paramagnetism.

1937 I.I. Rabi succeeds with first NMR experiment. LiCl beam passed through a combined static and oscillating magnetic field. RF absorption increased at Larmor frequency.

13

1945: Bloch and Purcell

Felix Bloch
Stanford

Edward Purcell
Harvard

1945 within 3 weeks of each other, Bloch at Stanford and Purcell at Harvard observe ^{1}H NMR in water at 8MHz and Paraffin at 30MHz respectively.

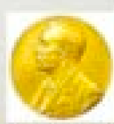

1952 Nobel Prize in Physics

14

1950: The Hahn Echo

1950 Erwin Hahn observes the first nuclear spin echo.

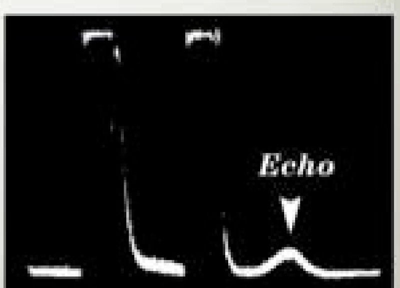

15

1973: Paul Lauterbur

Paul Lauterbur

1973 Paul Lauterbur at SUNY publishes Nature article describing a method for generating MR images using gradient frequency encoding and back projection reconstruction.

16

1977: Echo Planar Imaging

1977 Peter Mansfield publishes echo planar imaging method. EPI later becomes workhorse imaging sequence for fMRI with the advent of high performance gradient hardware.

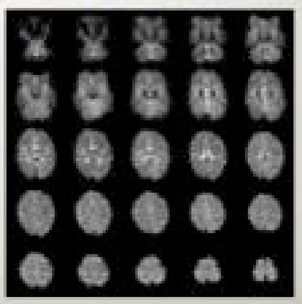

17

1970s Raymond Damadian

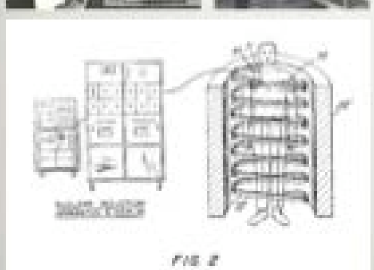

Patent awarded 1974

1970 Damadian at SUNY publishes Science article on relaxation time differences between normal and cancerous tissue. His 1974 patent did not describe a methods to generate images. By 1977 constructs human imager ("Indomitable") and acquires first MRI in a human.

See www.fonar.com for Damadian's argument supporting his claim to the 2003 Nobel Prize.

18

1990s BOLD fMRI

Seiji Ogawa

1990-1992 Seiji Ogawa and Ken Kwong introduce blood oxygenation level dependent (BOLD) contrast MRI. SFN is never the same again.

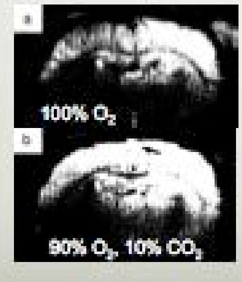

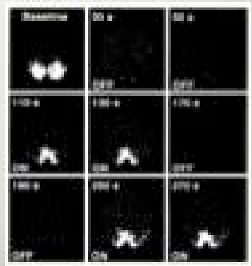

19

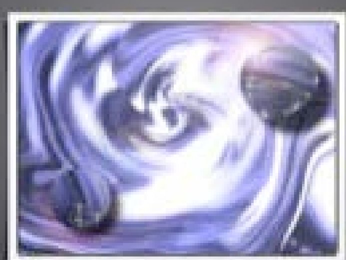

Magnetism

20

Forms of Magnetism

- Paramagnetism
  - Electronic Paramagnetism
  - NUCLEAR PARAMAGNETISM
  - Superparamagnetism
- Diamagnetism
  - Most organic compounds
- Ferromagnetism
  - Metallic Fe, Ni, Co

21

Magnetic Susceptibility

Susceptibility is dimensionless and relates the magnetization of a material to an applied magnetic field.

$$\begin{aligned} \mathbf{M} &= \chi \mathbf{H} \\ \mathbf{B} &= \mu_0 (\mathbf{H} + \mathbf{M}) \\ &= \mu_0 \mathbf{H} (1 + \chi) \end{aligned}$$

22

"Magnetic Field"

- H and B are strictly not the same thing.
- H aka the "auxilliary field"
- B aka the "magnetic induction"
- B is the total flux density due to external H field and resulting magnetization.
- B has units of Tesla (kg s^{-2} A^{-1})

23

Susceptibility Spectrum

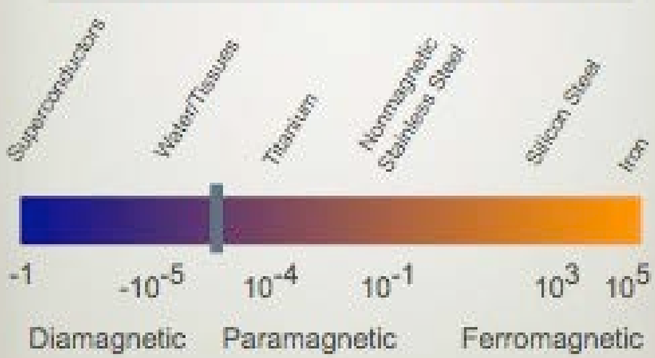

24

Meisner Effect

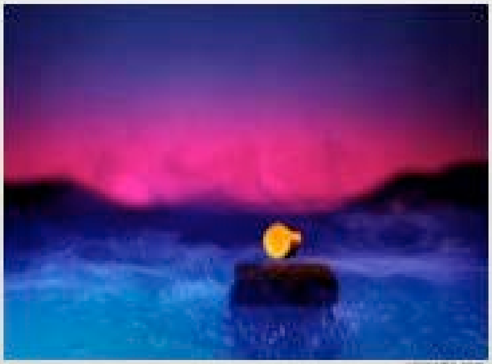

wikipedia.com

Magnet floating over HTC superconductor in liquid nitrogen

25

Spin Angular Momentum

For a nucleus with a spin quantum number, I

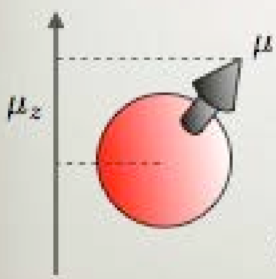

Magnetic field parallel to z axis

Dipole moment

$$\mu = \gamma\hbar\sqrt{I(I+1)}$$

z-component of dipole moment

$$\mu_z = \gamma m_I \hbar$$

Magnetic quantum number

$$m_I = -I, -I+1, \ldots, I$$

26

Spin 1/2 Nucleus

Dipole moment

$$\mu = \gamma\hbar\frac{\sqrt{3}}{2}$$

z-component of dipole moment

$$\mu_z = \pm\gamma\frac{\hbar}{2}$$

Magnetic quantum number

$$m_I = \pm\frac{1}{2}$$

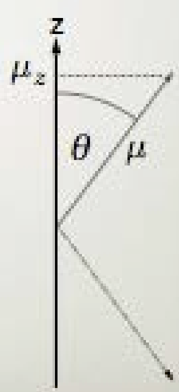

27

Important NMR Nuclei

Nucleus	Spin	γ (MHz/T)	Nat Abundance	Rel Sensitivity
^{1}H	½	42.58	99.99	100%
^{2}H	1	6.54	0.015	1.0%
^{12}C	0	-	-	-
^{13}C	½	10.71	1.1	1.6%
^{15}N	½	4.32	0.37	0.1%
^{19}F	½	40.01	100.0	83%
^{31}P	½	17.24	100.0	6.6%
^{23}Na	3/2	11.26	100.0	9.3%

28

Nuclear Magnetic Resonance

Continuous Wave Absorption

Pulsed RF Excitation

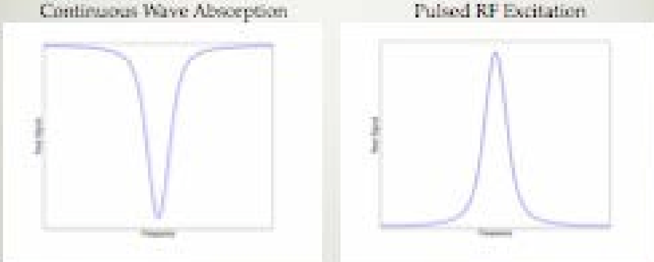

Increasing RF Frequency
Constant Field Strength

Increasing RF Frequency
Constant Field Strength

Increasing Field Strength
Constant RF Frequency

29

Nuclear Zeeman Effect

A magnetic field forces nuclei with a net magnetic moment to align in two or more energy states.

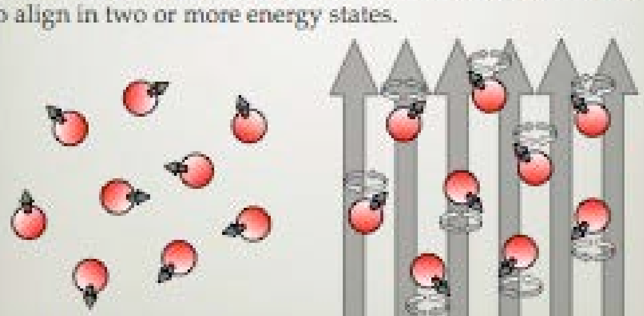

Spins align randomly in absence of a magnetic field

Magnetic Field

30

Larmor Equation

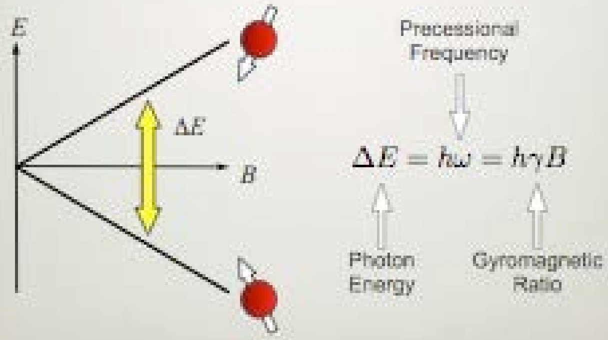

31

Population of Energy Levels

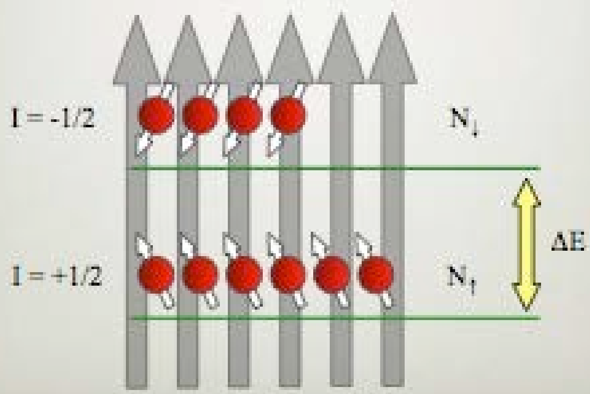

32

Population of Energy Levels

Boltzmann distribution of ¹H energy level populations

$$N_R = \frac{N_\downarrow}{N_\uparrow} = e^{-\Delta E/kT} = e^{-\hbar\gamma B/kT} < 1$$

Excess fraction in low energy state (paramagnetic)

$$\Delta N_R = \frac{N_\uparrow - N_\downarrow}{N_\uparrow + N_\downarrow} = \frac{1 - N_R}{1 + N_R}$$

33

Population of Energy Levels

Excess spins in low energy state in ppm

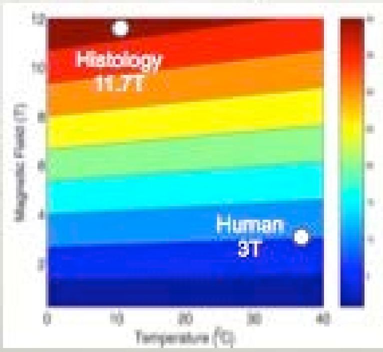

34

Bulk Magnetization

35

Bulk Magnetization

Spin Ensemble

Bulk Magnetization

- Equilibrium Bulk Magnetization does NOT precess
- A typical MRI voxel (1μl) contains roughly 10^{19} spins

36

Forces on a Dipole in a Magnetic Field

A magnetic dipole or current loop experiences a torque in a magnetic field

$$\mathbf{N} = \mu \times \mathbf{B}$$

37

The Bloch Equation

Provides a classical description for the evolution of the magnetization with time.

$$\frac{\partial \mathbf{M}}{\partial t} = \gamma \mathbf{M} \times \mathbf{B}$$

Rate of change of magnetization vector due to the application of an external field

38

Faraday Induction

$$emf = \frac{d\Phi}{dt}$$

$$\Phi = \int_A \mathbf{B} \cdot \mathbf{dS}$$

See Haacke 7.1, 7.2, 7.3 for details

39

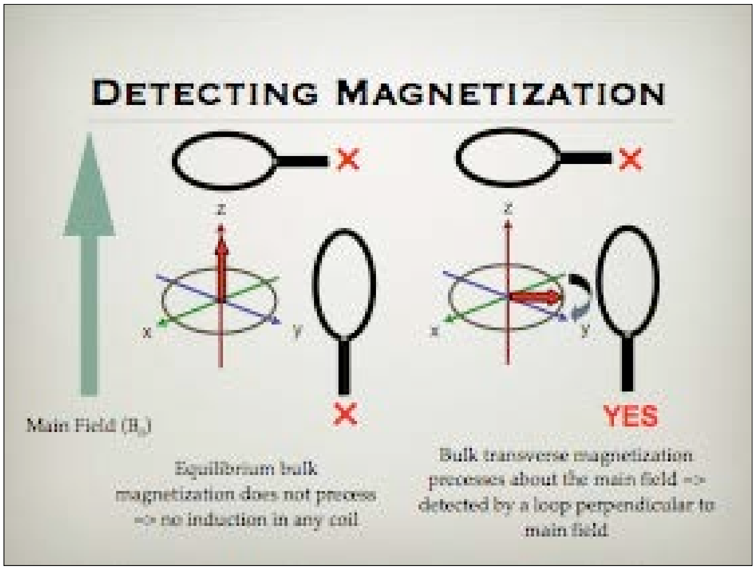

DETECTING MAGNETIZATION
z
x
y
YES
Main Field (B_0)
Equilibrium bulk magnetization does not process => no induction in any coil
Bulk transverse magnetization processes about the main field => detected by a loop perpendicular to main field

40

CREATING TRANSVERSE MAGNETIZATION

41

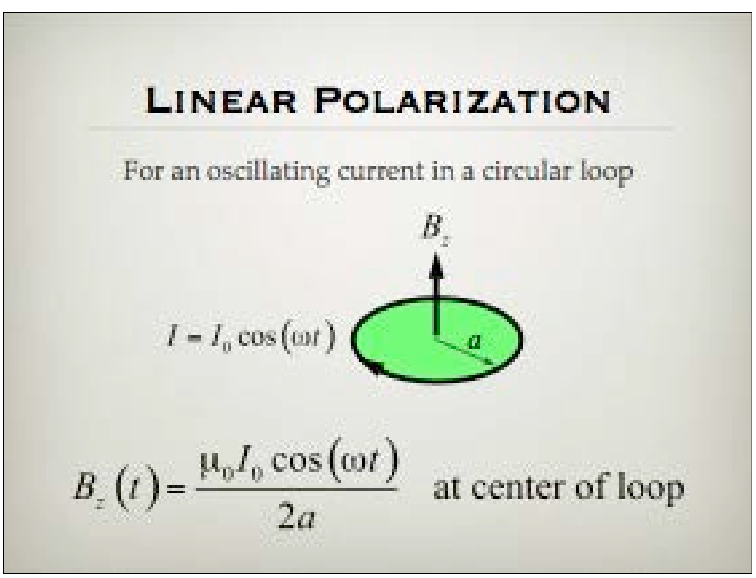

LINEAR POLARIZATION
For an oscillating current in a circular loop
B_z
$I = I_0 \cos(\omega t)$
a
$B_z(t) = \frac{\mu_0 I_0 \cos(\omega t)}{2a}$ at center of loop

42

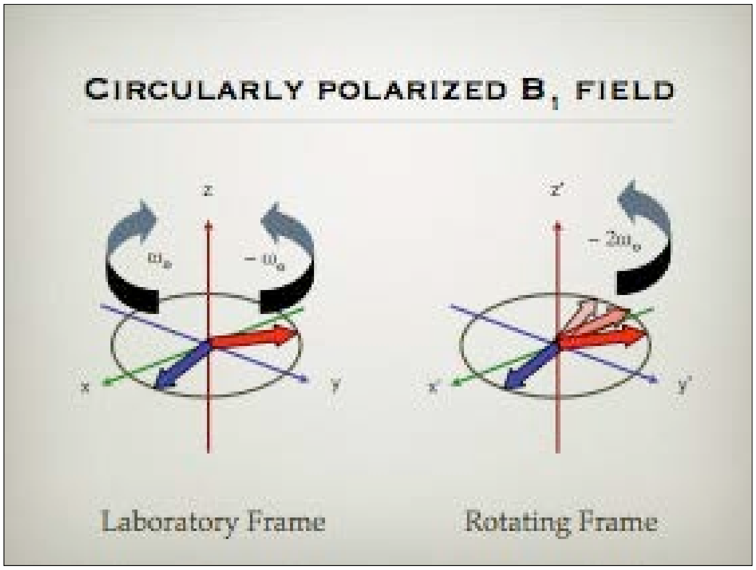
CIRCULARLY POLARIZED B_1 FIELD
z
ω_o
$-\omega_o$
x
y
z'
$-2\omega_o$
x'
y'
Laboratory Frame
Rotating Frame

43

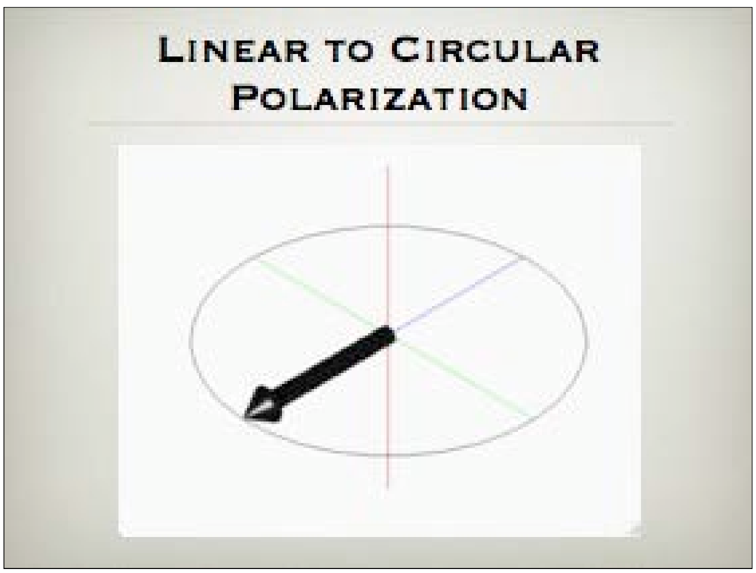
LINEAR TO CIRCULAR POLARIZATION

44

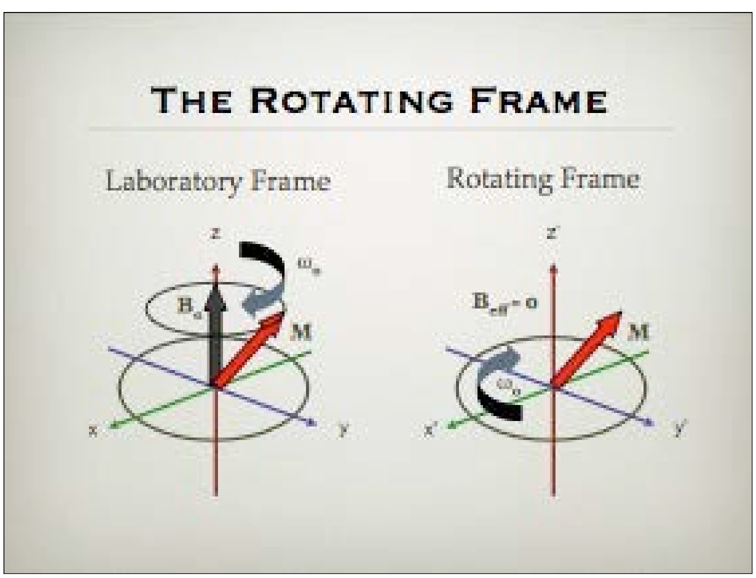
THE ROTATING FRAME
Laboratory Frame
Rotating Frame
z
ω_o
B_o
M
x
y
z'
$B_{eff} = 0$
M
ω_o
x'
y'

45

Bloch Equation in the Rotating Frame

Introduce effective magnetic field seen by magnetization

$$\mathbf{B}_{\text{eff}} = \left(B_0 - \frac{\omega_{rf}}{\gamma}\right)\hat{\mathbf{z}}$$
$$\frac{\partial \mathbf{M}}{\partial t} = \gamma \mathbf{M} \times \mathbf{B}_{\text{eff}}$$

46

Off-Resonance in the Rotating Frame

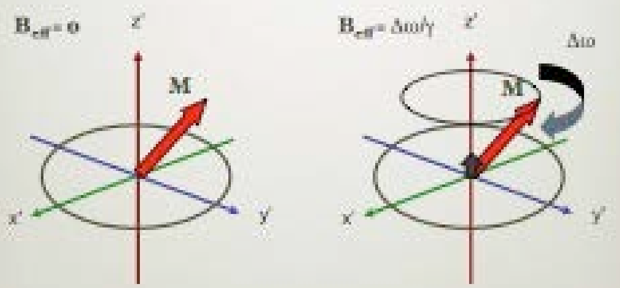

47

Adding RF B₁ Field to the Bloch Equation

In the rotating frame:

$$\mathbf{B}_{\text{eff}} = \left(\mathbf{B}_0 - \frac{\omega_{\mathbf{rf}}}{\gamma}\right)\hat{\mathbf{z}} + \mathbf{B}_1\hat{\mathbf{x}}$$

48

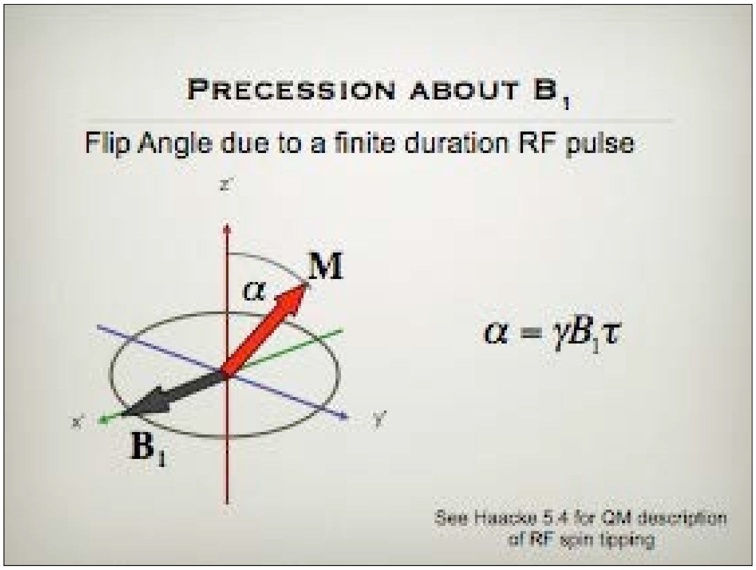
PRECESSION ABOUT B_1
Flip Angle due to a finite duration RF pulse
z'
M
α
x'
y'
B_1
$\alpha = \gamma B_1 \tau$
See Haacke 5.4 for QM description of RF spin tipping

49

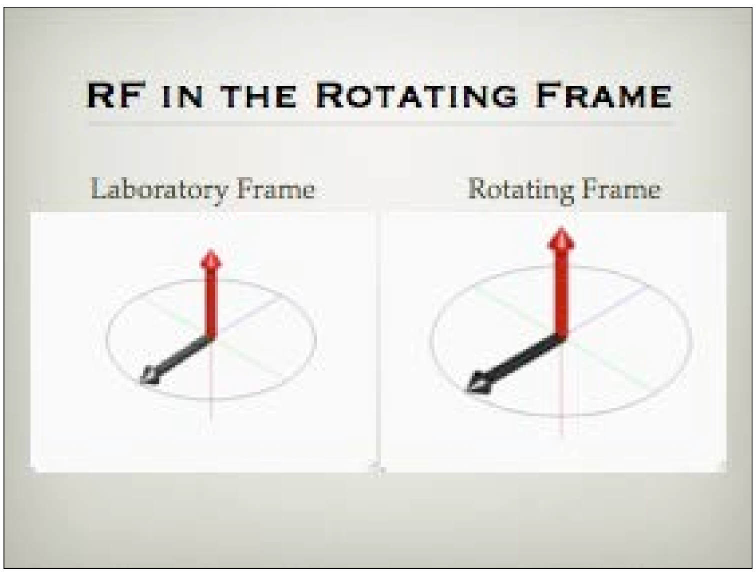
RF IN THE ROTATING FRAME
Laboratory Frame
Rotating Frame

50

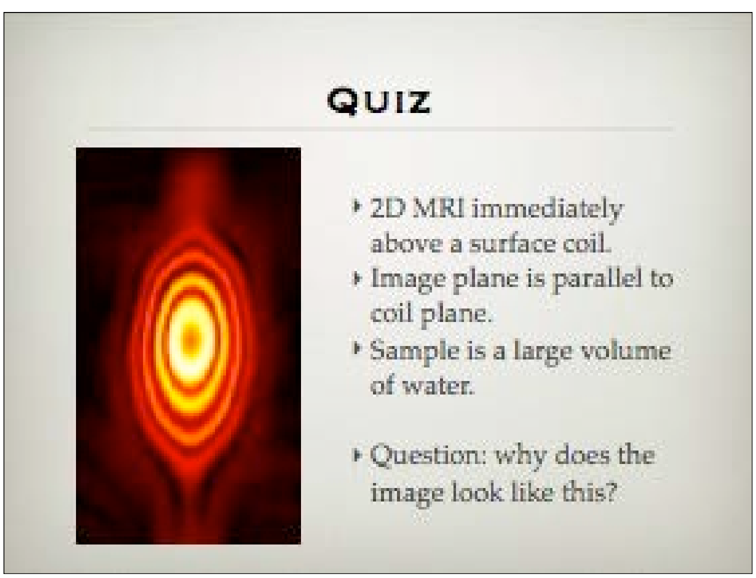
QUIZ
2D MRI immediately above a surface coil.
Image plane is parallel to coil plane.
Sample is a large volume of water.
Question: why does the image look like this?

51

Next Lecture

- 1.2 NMR for MRI

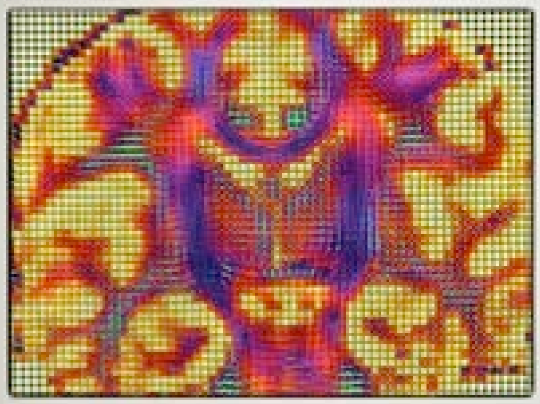

BE/CNS 248
1.2 NMR for MRI

Mike Tyszka, Ph.D
Caltech Brain Imaging Center

Fall Semester 2006-2007

1

Lecture Summary

- 1.2 Basic NMR
  - The Free Induction Decay
  - Relaxation
    - Spectral density function
    - Spin-lattice interactions and T1
    - Spin-spin interactions and T2
    - Field homogeneity and T2*
    - Spin-locked relaxation and $T_{1\rho}$
  - Basic Pulse Sequences
    - Pulse-acquire
    - Hahn Spin Echo
    - CPMG Sequence
    - Inversion Recovery
    - Saturation Recovery
    - Stimulated Echo
- Steady-State NMR

2

Free Induction Decay

3

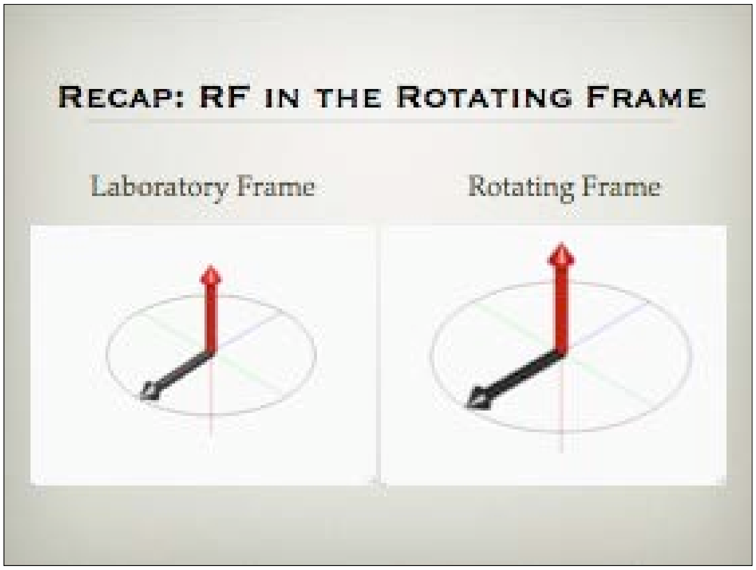
Recap: RF in the Rotating Frame
Laboratory Frame
Rotating Frame

4

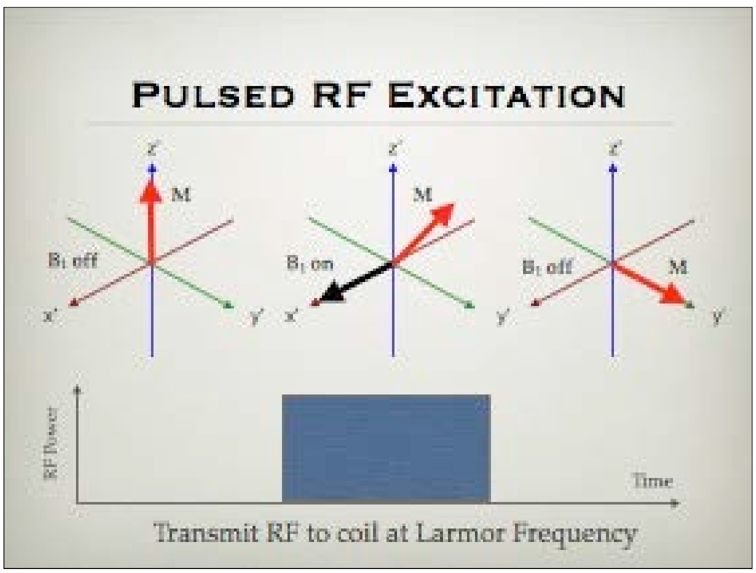
Pulsed RF Excitation
z'
M
B1 off
x'
y'
B1 on
RF Power
Time
Transmit RF to coil at Larmor Frequency

5

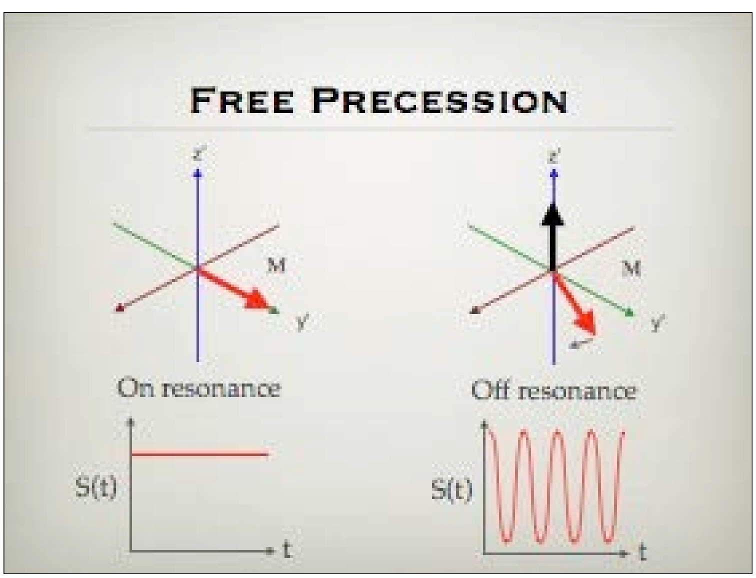
Free Precession
z'
M
y'
On resonance
Off resonance
S(t)
t

6

MR Signal as a Complex Quantity

- Signal detection is phase sensitive, so both Mx and My components of precessing magnetization can be measured.
- Two signal channels are commonly referred to as "real" and "imaginary".

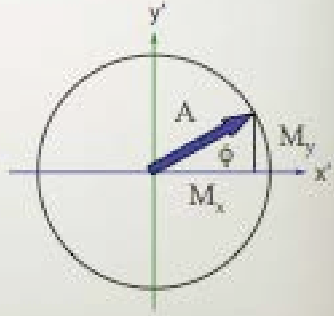

7

Complex Signal

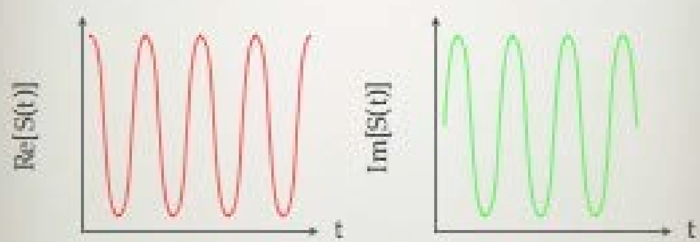

$$
\begin{aligned}
M &= Ae^{i\phi} \\
&= A\cos(\phi) + iA\sin(\phi) \\
&= M_x + iM_y
\end{aligned}
$$

8

RF Pulse Phasing

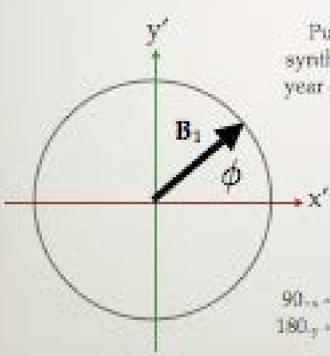

Pulse phase defined in relation to synthesizer (Typical accuracy: 1 ppm/year drift, < 0.5 degree phase precision at 100MHz)

Example Notation:

90_{-x} = 90 degree pulse phased along -x
180_{-y} = 180 degree pulse phased along -y

9

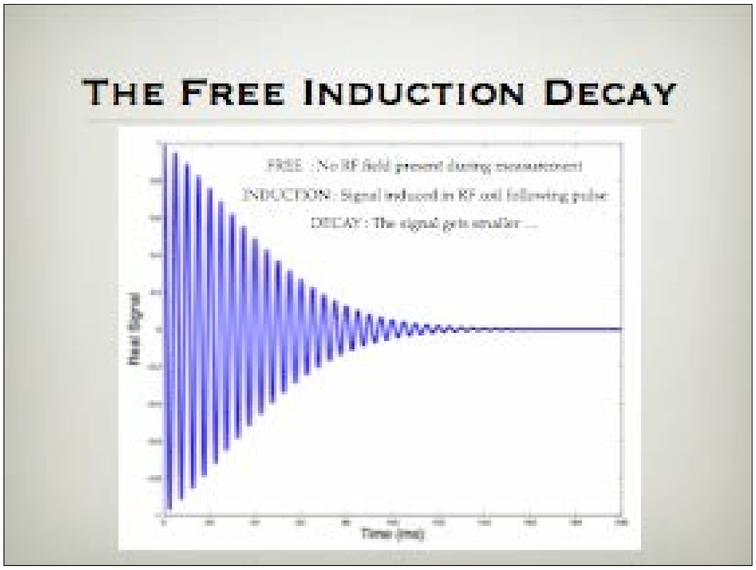
THE FREE INDUCTION DECAY
FREE : No RF field present during measurement
INDUCTION : Signal induced in RF coil following pulse
DECAY : The signal gets smaller ...
Real Signal
Time (ms)

10


RELAXATION

11

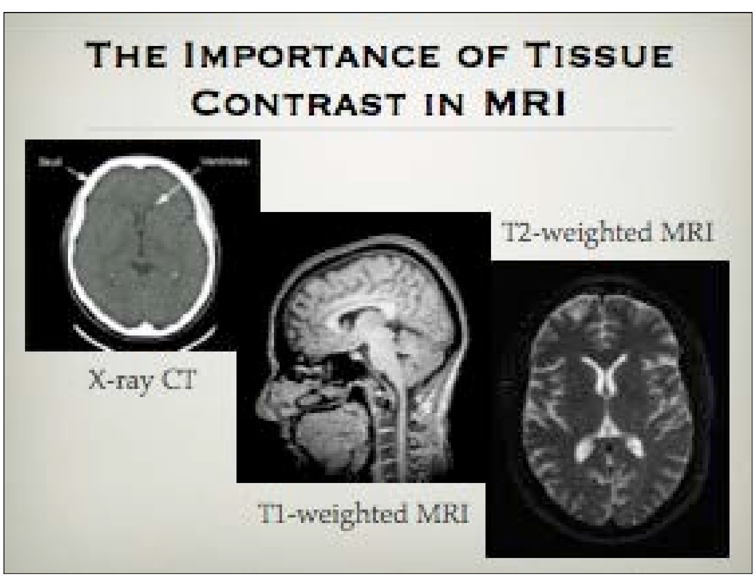
THE IMPORTANCE OF TISSUE CONTRAST IN MRI
X-ray CT
T1-weighted MRI
T2-weighted MRI

12

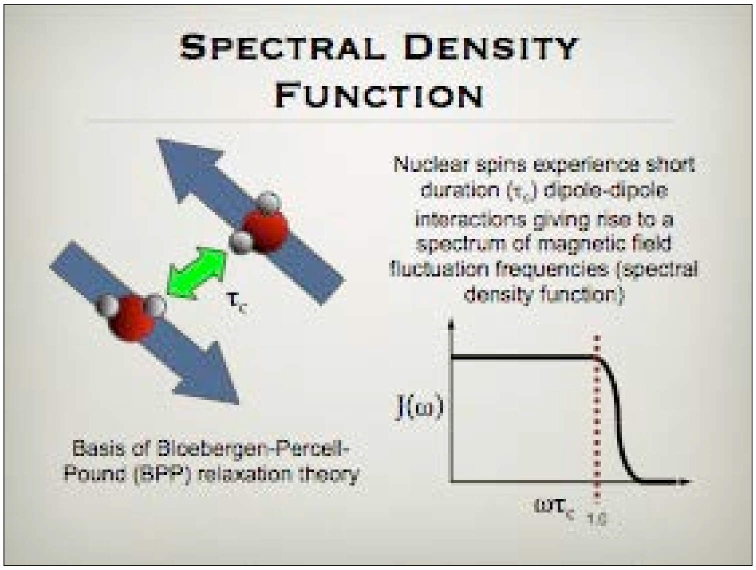
SPECTRAL DENSITY FUNCTION
Nuclear spins experience short duration (τ_c) dipole-dipole interactions giving rise to a spectrum of magnetic field fluctuation frequencies (spectral density function)
τ_c
$J(\omega)$
$\omega\tau_c$
1.0
Basis of Bloebergen-Percell-Pound (BPP) relaxation theory

13

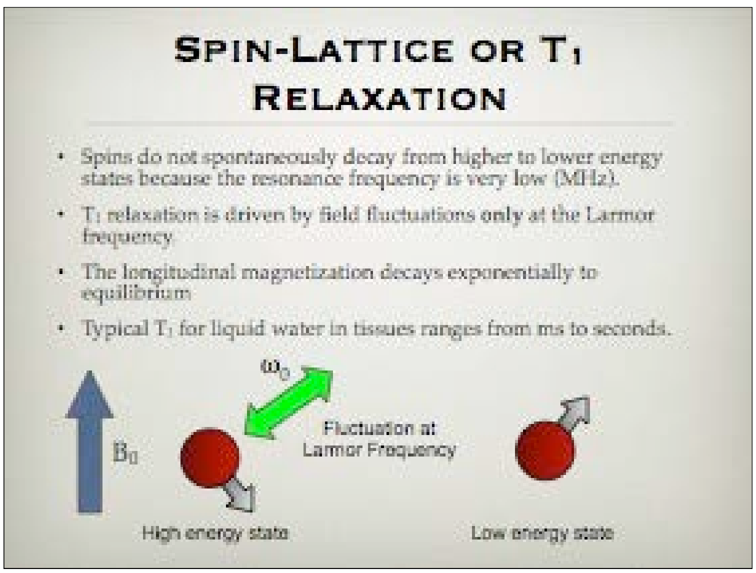
SPIN-LATTICE OR T_1 RELAXATION
• Spins do not spontaneously decay from higher to lower energy states because the resonance frequency is very low (MHz).
• T_1 relaxation is driven by field fluctuations only at the Larmor frequency
• The longitudinal magnetization decays exponentially to equilibrium
• Typical T_1 for liquid water in tissues ranges from ms to seconds.
ω_0
B_0
Fluctuation at Larmor Frequency
High energy state
Low energy state

14

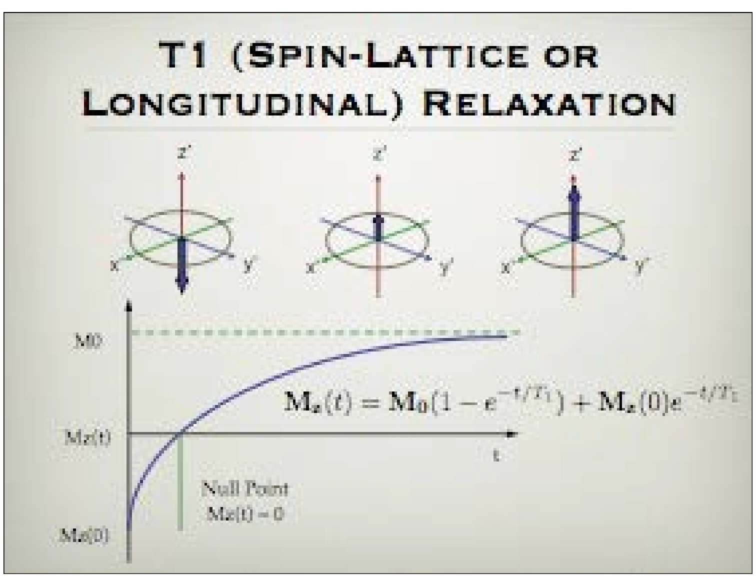
T1 (SPIN-LATTICE OR LONGITUDINAL) RELAXATION
z'
x'
y'
M0
Mz(t)
Mz(0)
t
$\mathbf{M}_z(t) = \mathbf{M}_0(1 - e^{-t/T_1}) + \mathbf{M}_z(0)e^{-t/T_1}$
Null Point
Mz(t) = 0

15

T2 (Spin-Spin or Transverse) Relaxation

- T2 relaxation is driven by field fluctuations at both zero frequency **and** the Larmor frequency.
- Spins are in phase following an RF pulse.
- The transverse magnetization decays exponentially to zero due to cumulative dephasing.
- Typical T2 for liquid water in tissues ranges from ms to seconds.

16

T2 (Spin-Spin or Transverse) Relaxation

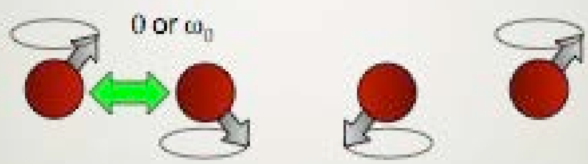

Fluctuation at either zero frequency or the Larmor Frequency causes spin-spin energy exchange.

Total energy preserved. Phase randomized.

17

T2 (Spin-Spin) Relaxation

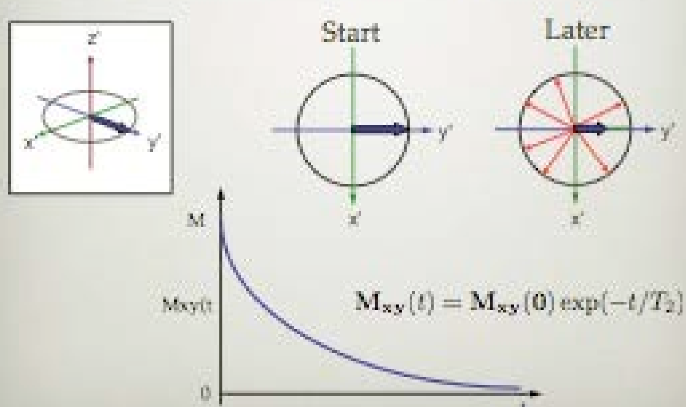

18

Relaxation Times at 3T

Table 1
T_1 and T_2 Relaxation Times at 3T and 1.5T Measured at 37°C. Literature data is also shown.

Tissue	T_2—3 T [ms]		T_1—3 T [ms]		T_2—1.5 T [ms]		T_1—1.5 T [ms]	
	This study	Literature	This study	Literature	This study	Literature	This study	Literature
Liver	42 ± 3		812 ± 64		46 ± 6	54 ± 8	576 ± 30	~600
Skeletal muscle	50 ± 4	35 ± 2	1412 ± 13	1420 ± 38	44 ± 6	35 ± 4	1008 ± 20	1060 ± 155
Heart	47 ± 11		1471 ± 31		40 ± 6	44 ± 6	1030 ± 34	
Kidney	56 ± 4		1194 ± 27		55 ± 3	61 ± 11	690 ± 30	704 ± 60
Cartilage 0°	27 ± 3	37 ± 4	1168 ± 18	~1240	30 ± 4	42 ± 7	1024 ± 70	~1060
Cartilage 90°	43 ± 2	45 ± 67	1156 ± 10		44 ± 3		1036 ± 67	
White matter	69 ± 3	56 ± 4	1084 ± 45	1110 ± 45	72 ± 4	79 ± 8	884 ± 50	778 ± 84
Gray matter	99 ± 7	71 ± 10	1820 ± 114	1470 ± 50	95 ± 8	~95	1124 ± 50	1086 ± 228
Optic nerve	78 ± 5		1083 ± 39		77 ± 9		815 ± 30	
Spinal cord	78 ± 2		993 ± 47		74 ± 6		745 ± 37	
Blood	275 ± 50		1932 ± 85	~1550	290 ± 30	327 ± 40	1441 ± 120	~1200

Stanisz GJ, et al. "T1, T2 Relaxation and Magnetization Transfer in Tissue at 3T" Magn Reson Med 2005;54:507-512.

19

Relaxation and the Bloch Equation

Separate equations of motion for each magnetization component. Add relaxation terms.

$$\frac{\partial M_x}{\partial t} = \gamma(M_y B_z - M_z B_y) - \frac{1}{T_2} M_x$$
$$\frac{\partial M_y}{\partial t} = \gamma(M_z B_x - M_x B_z) - \frac{1}{T_2} My$$
$$\frac{\partial M_z}{\partial t} = \gamma(M_x B_y - M_y B_x) - \frac{1}{T_1}(1 - M_z)$$

20

Analytical Solutions

Torque on magnetization causes precession:

Rotation about B_{eff}

Relaxation processes cause:

Exponential Decays

21

Other Contrast Mechanisms

22

T2* Relaxation

- B_0 inhomogeneities within a volume (right) cause additional dephasing of total Mxy.
- Decreases apparent T_2 by providing an additional dephasing mechanism.
- T_2^* is NOT an exponential process - B_0 distribution (below right) would have to be Lorentzian).
- Basis of BOLD and susceptibility sensitive imaging.
- Addressed in part by magnetic field shimming (homogeneity optimization)

23

B_0 Homogeneity in the Human Head

Following whole brain ideal linear shimming

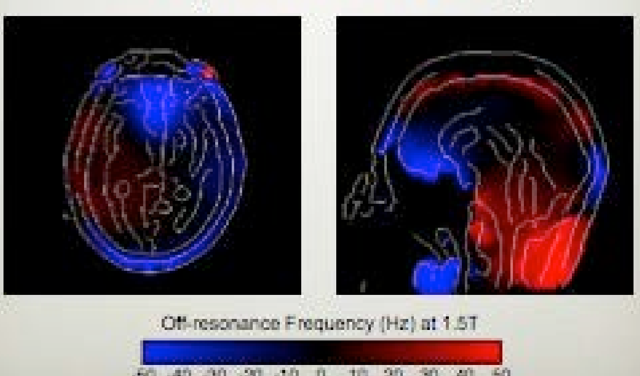

24

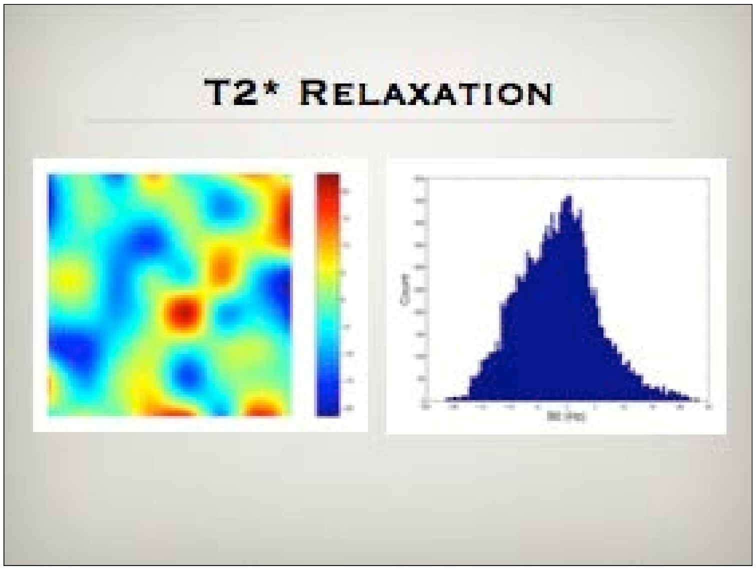
T2* RELAXATION

25

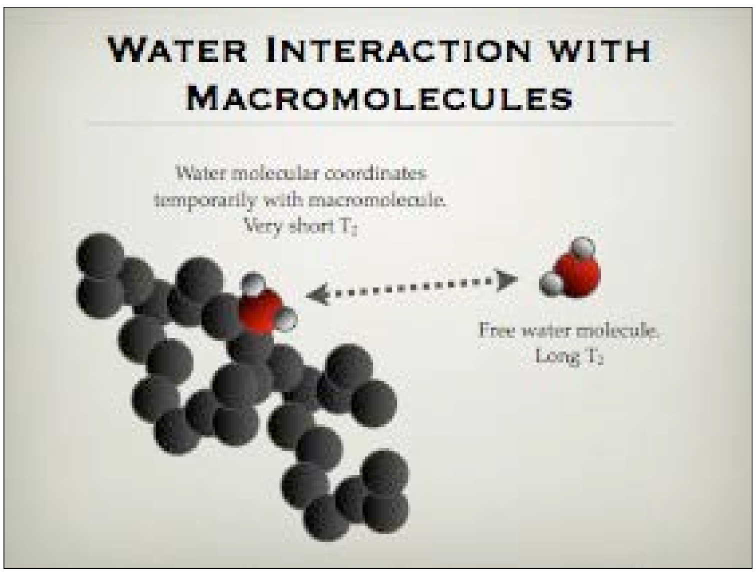
WATER INTERACTION WITH MACROMOLECULES
Water molecular coordinates temporarily with macromolecule. Very short T_2
Free water molecule. Long T_2

26

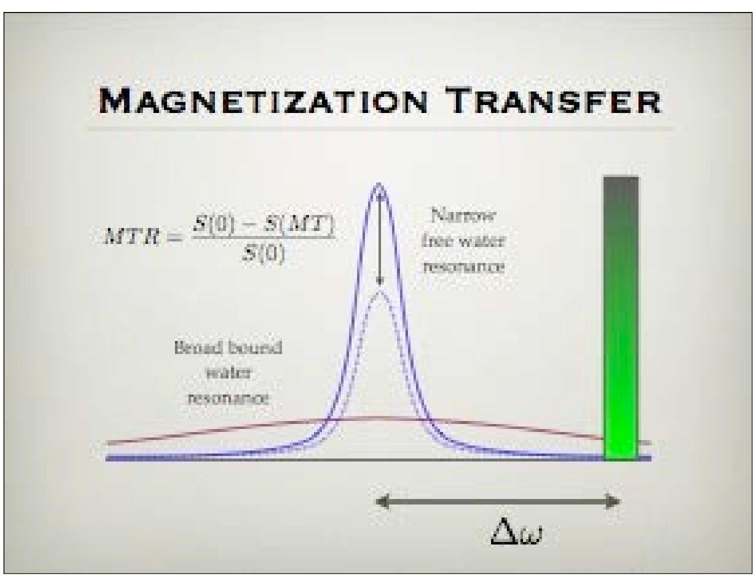
MAGNETIZATION TRANSFER
$MTR = \frac{S(0) - S(MT)}{S(0)}$
Narrow free water resonance
Broad bound water resonance
$\Delta\omega$

27

Magnetization Transfer Ratios at 3T

Table 2
Magnetization Transfer Parameters at 3 T Compared to Literature Data at 1.5 T

Tissue	This paper measured at 3 T				Literature at 1.5 T		
	M_{0B} (%)	R (s^{-1})	T_{2B} (µs)	MTR (%)	M_{0B} (%)	R (s^{-1})	T_{2B} (µs)
Liver	6.9 ± 0.7	61 ± 10	7.7 ± 0.2	77 ± 5		53 ± 8	7.8 ± 0.8
Skeletal muscle	7.4 ± 1.0	66 ± 6	6.7 ± 0.1	66 ± 2	9.9 ± 1.8	70 ± 4	8.2 ± 0.8
Heart	6.7 ± 0.2	50 ± 7	6.1 ± 0.1	66 ± 1	7.2 ± 0.7	37 ± 3	8.4 ± 0.4
Kidney	7.1 ± 1.0	46 ± 7	6.1 ± 0.3	62 ± 1			
Cartilage 0°	17.1 ± 2.4	57 ± 5	6.3 ± 0.1	65 ± 1			
Cartilage 55°	18.2 ± 0.6	60 ± 5	6.3 ± 0.1	66 ± 1			
White matter	13.9 ± 2.8	23 ± 4	10.3 ± 1.3	60 ± 1	15.2 ± 2.0	30 ± 6	11.3 ± 1.6
Gray matter	5.0 ± 0.5	40 ± 1	9.1 ± 0.2	54 ± 1	7.2 ± 1.0	28 ± 9	11.1 ± 1.1
Optic nerve	15.8 ± 1.1	23 ± 2	10.5 ± 0.9	66 ± 2		20 ± 3	10.5 ± 0.5
Spinal cord	12.8 ± 1.8	28 ± 5	10.5 ± 0.8	60 ± 1			
Blood	2.8 ± 0.7	35 ± 7	290 ± 16	11 ± 4	3.5 ± 0.8	40 ± 5	340 ± 40

MTR is measured at the RF saturation pulse amplitude, [illegible], and the offset frequency of the saturation, [illegible] (optimum MT experimental parameters to achieve maximum MT effect for most of the tissues).

Stanisz GJ, et al. "T1, T2 Relaxation and Magnetization Transfer in Tissue at 3T" Magn Reson Med 2005;54:507-512.

28

Magnetization Transfer Background suppression

de Boer, (c) Philips Medical Systems

29

T1ρ Relaxation

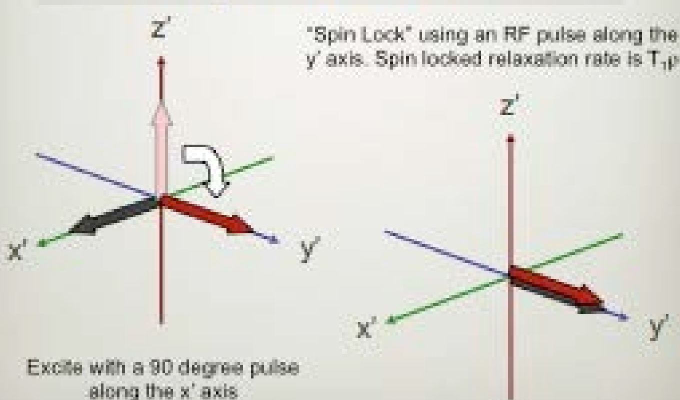

30

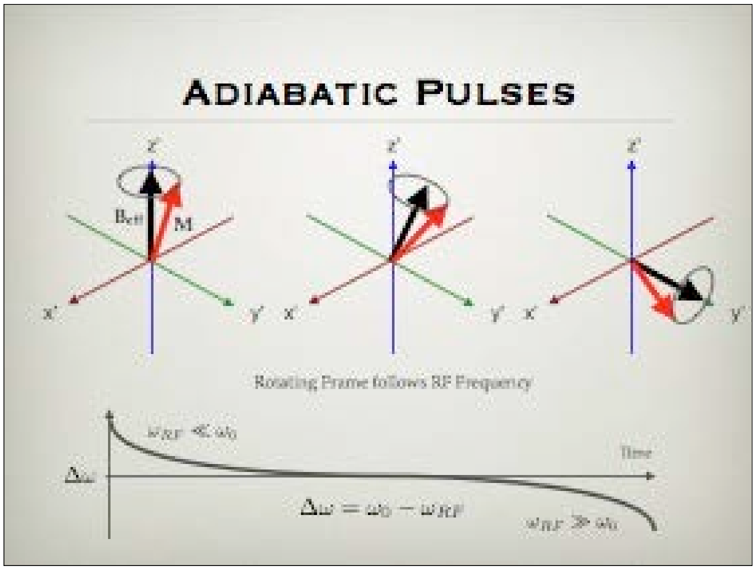
ADIABATIC PULSES
z'
B_{eff}
M
x'
y'
Rotating Frame follows RF Frequency
$\omega_{RF} \ll \omega_0$
Time
$\Delta\omega$
$\Delta\omega = \omega_0 - \omega_{RF}$
$\omega_{RF} \gg \omega_0$

31

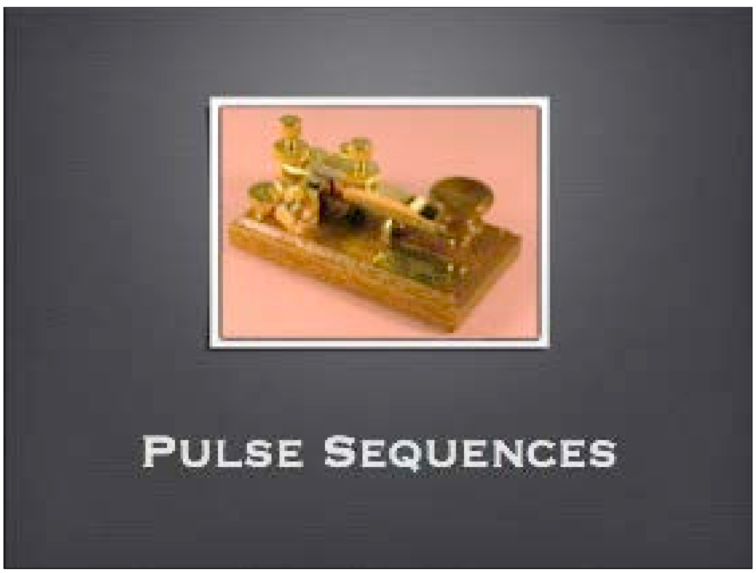
PULSE SEQUENCES

32

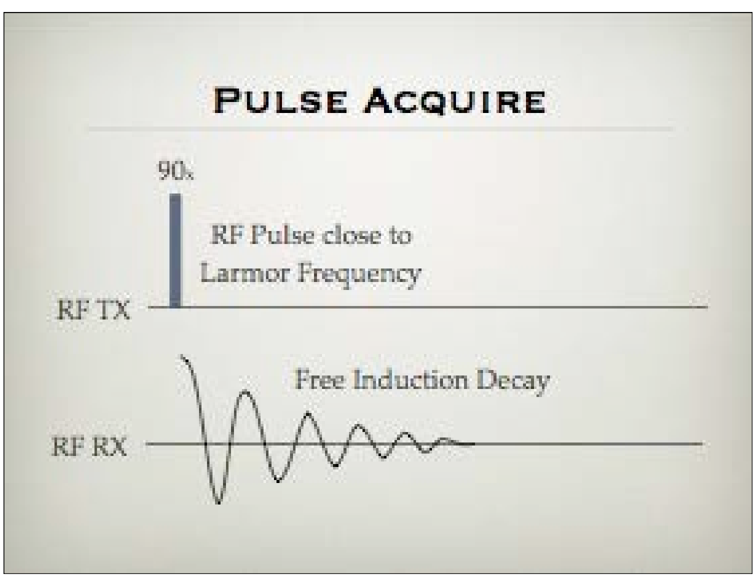
PULSE ACQUIRE
90_x
RF Pulse close to
Larmor Frequency
RF TX
Free Induction Decay
RF RX

33

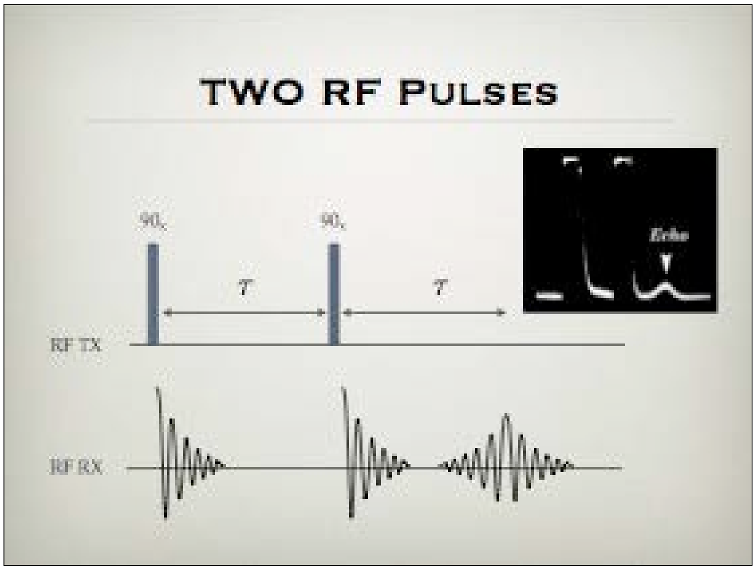
TWO RF PULSES
RF TX
RF RX
Echo

34

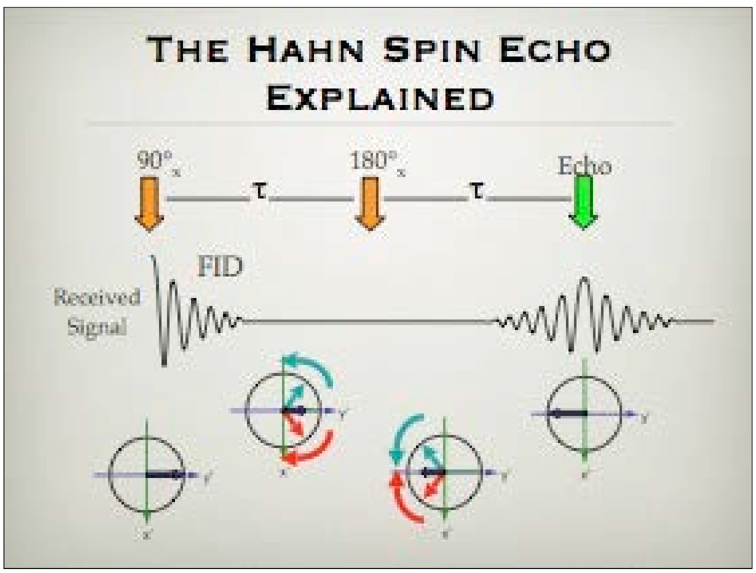
THE HAHN SPIN ECHO EXPLAINED
90°_x
180°_x
τ
τ
Echo
FID
Received Signal

35

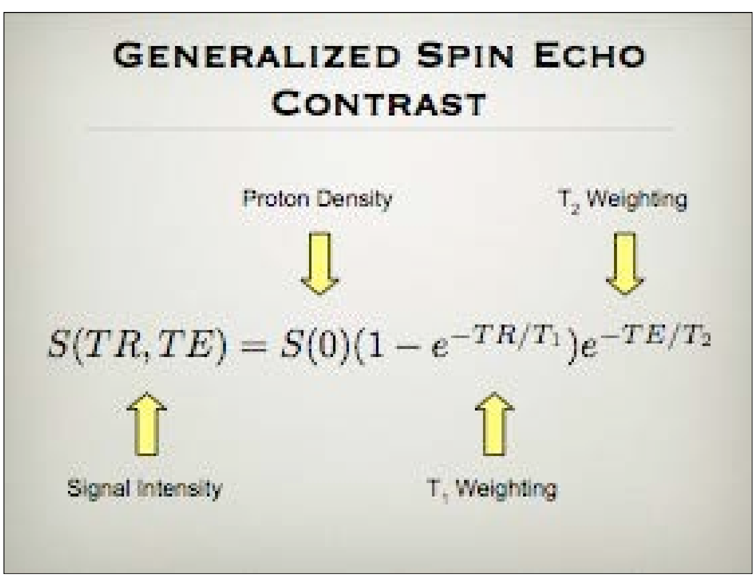
GENERALIZED SPIN ECHO CONTRAST
Proton Density
T_2 Weighting
$S(TR,TE) = S(0)(1 - e^{-TR/T_1})e^{-TE/T_2}$
Signal Intensity
T_1 Weighting

36

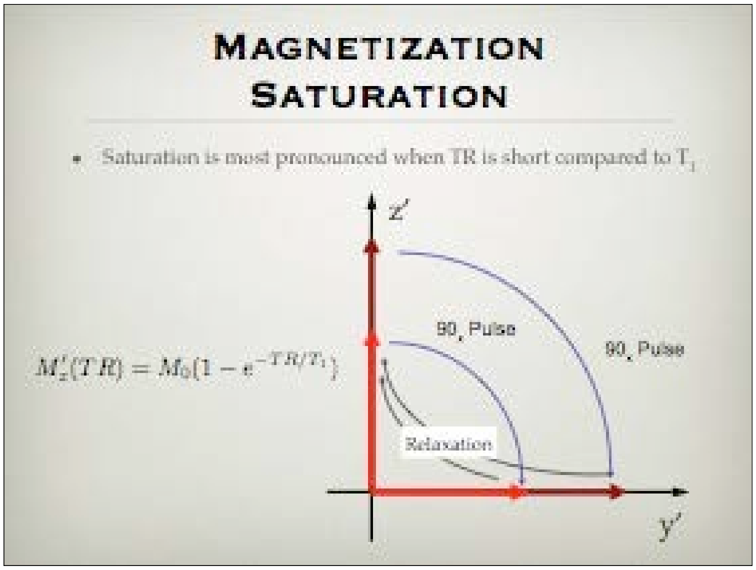

MAGNETIZATION SATURATION
• Saturation is most pronounced when TR is short compared to T_1
$M_z'(TR) = M_0(1 - e^{-TR/T_1})$
z'
90x Pulse
90x Pulse
Relaxation
y'

37

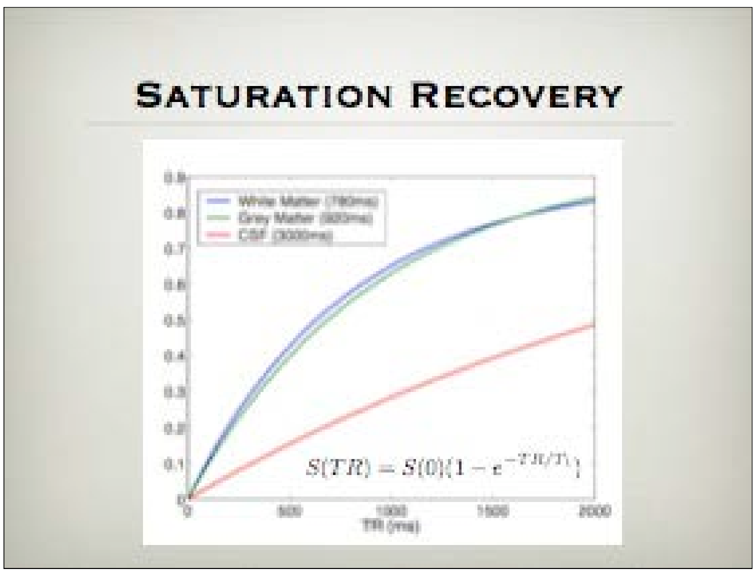

SATURATION RECOVERY
$S(TR) = S(0)(1 - e^{-TR/T_1})$
TR (ms)

38

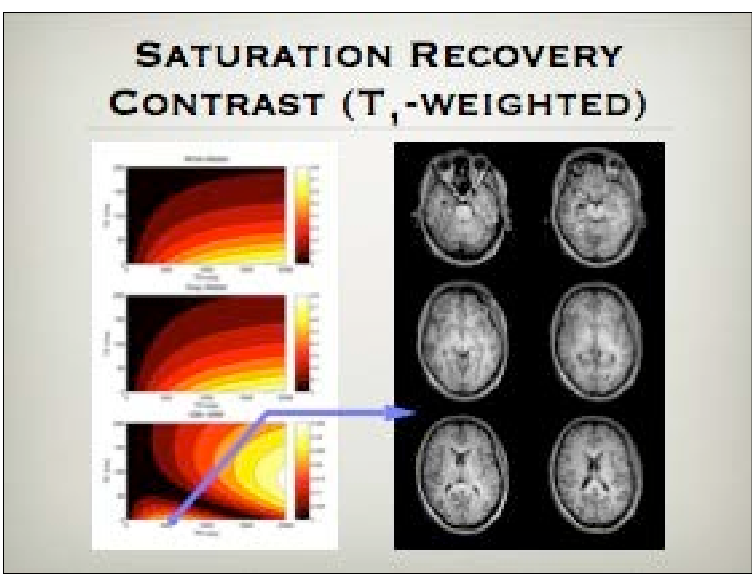

SATURATION RECOVERY CONTRAST (T_1-WEIGHTED)

39

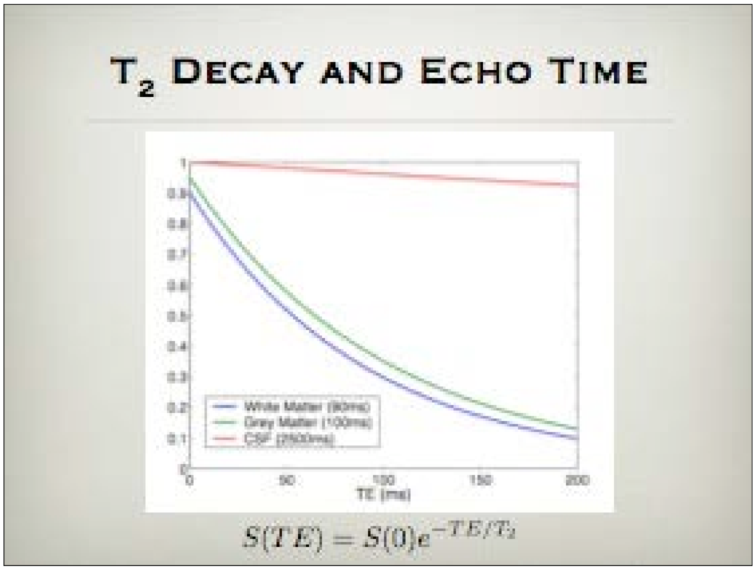
T2 Decay and Echo Time
White Matter (80ms)
Grey Matter (100ms)
CSF (2500ms)
TE (ms)
$S(TE) = S(0)e^{-TE/T_2}$

40

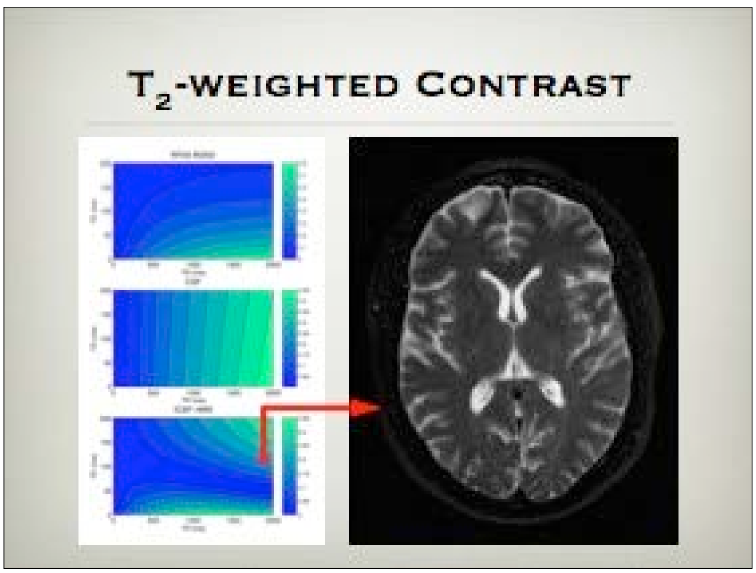
T2-Weighted Contrast

41

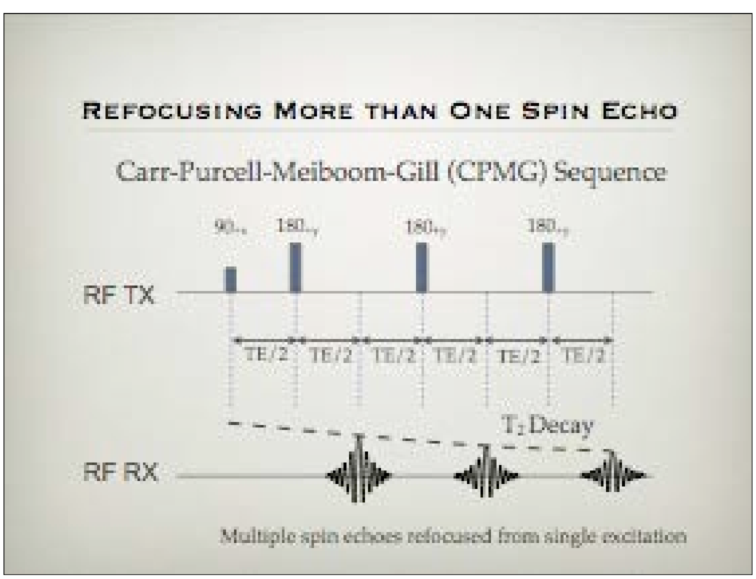
Refocusing More than One Spin Echo
Carr-Purcell-Meiboom-Gill (CPMG) Sequence
RF TX
TE/2
T2 Decay
RF RX
Multiple spin echoes refocused from single excitation

42

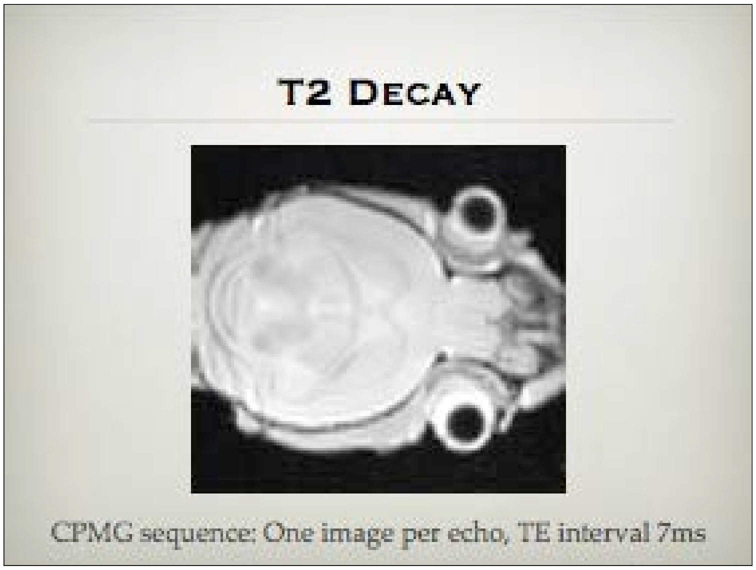
T2 Decay
CPMG sequence: One image per echo, TE interval 7ms

43

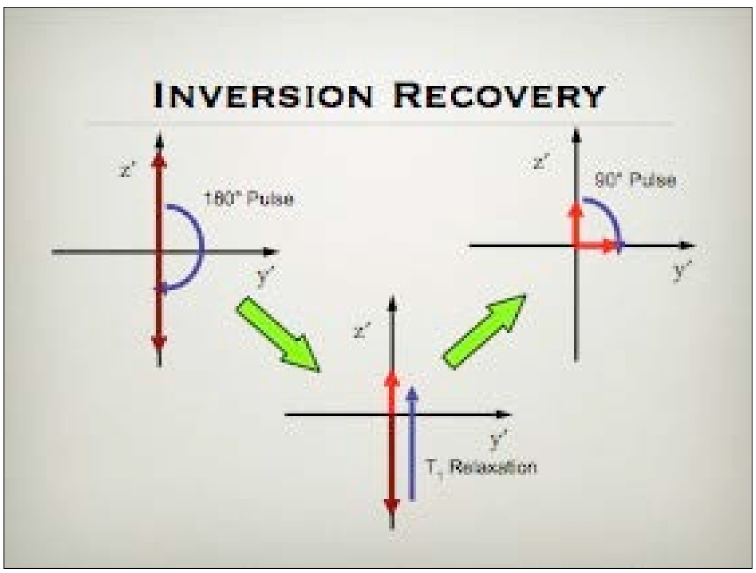
Inversion Recovery
z'
180° Pulse
y'
z'
90° Pulse
y'
z'
y'
T1 Relaxation

44

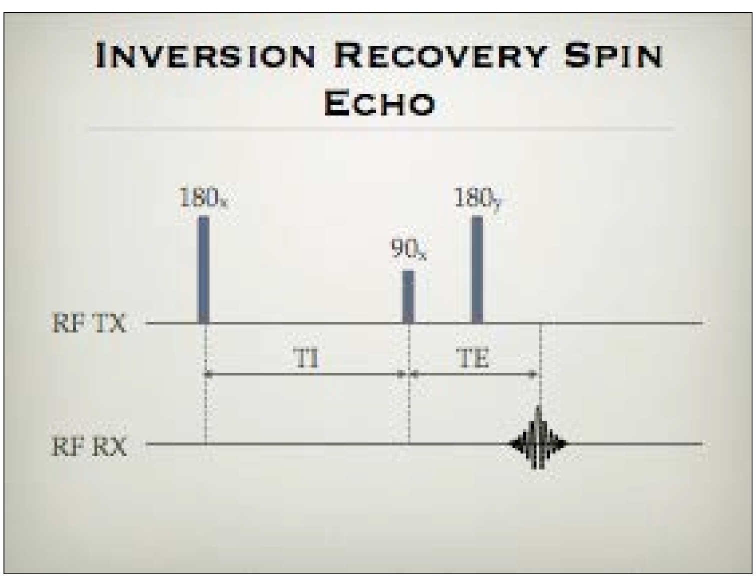
Inversion Recovery Spin Echo
180x
90x
180y
RF TX
TI
TE
RF RX

45

Inversion Recovery Weighting

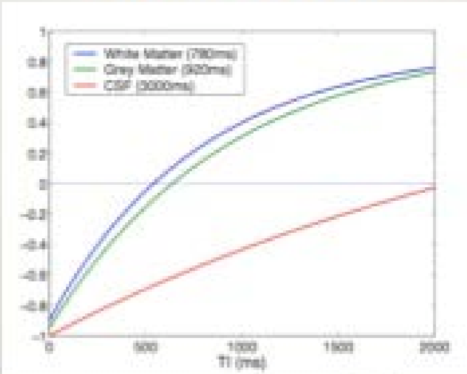

$$S(TI,TE) = S(0)(1 - 2e^{-TR/T_1})e^{-TE/T_2}$$

46

Magnitude Inversion Recovery Weighting

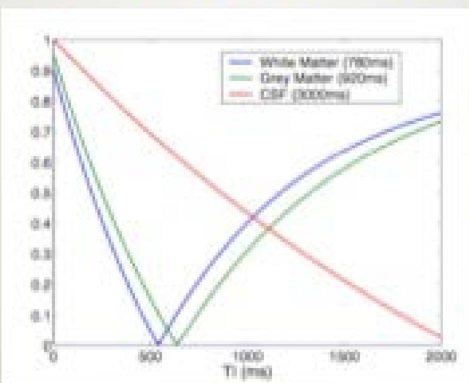

$$S(TI,TE) = |S(0)(1 - 2e^{-TR/T_1})e^{-TE/T_2}|$$

47

Inversion Recovery Contrast

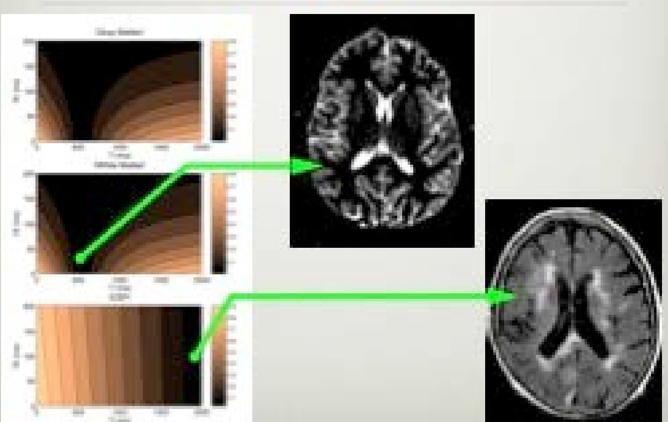

48

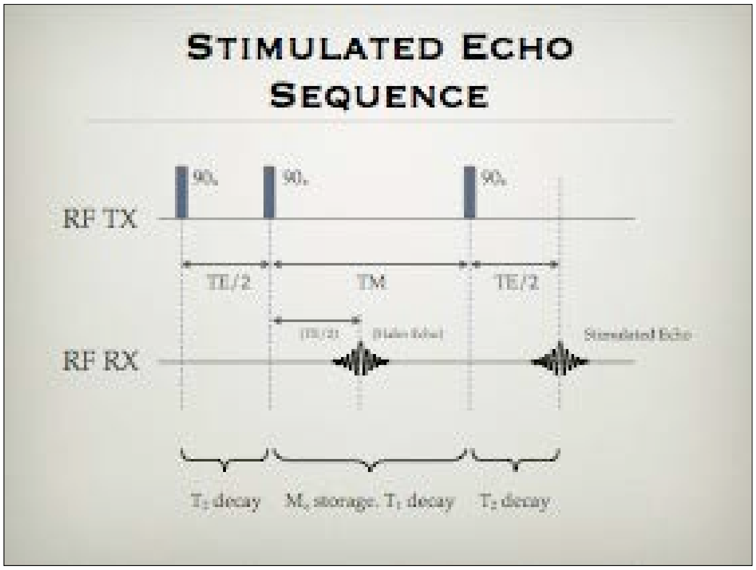
STIMULATED ECHO SEQUENCE
RF TX
TE/2
TM
TE/2
RF RX
Stimulated Echo
T_2 decay
M_z storage. T_1 decay
T_2 decay

49


THE STEADY STATE

50

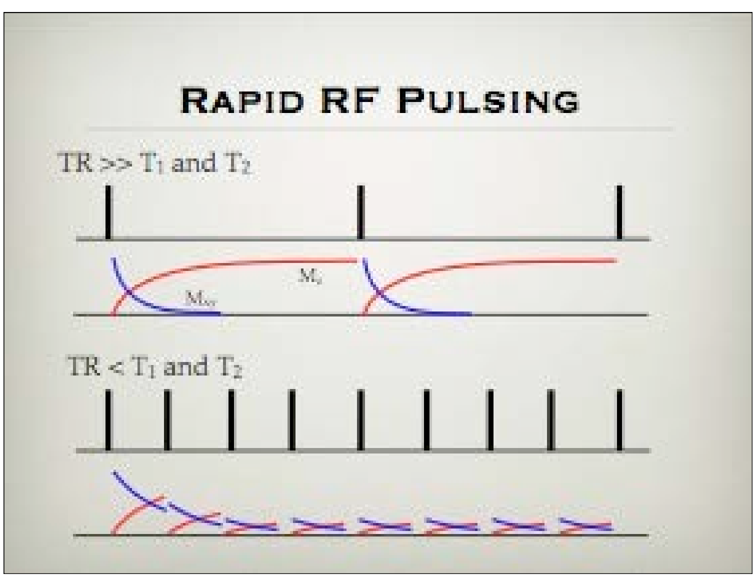
RAPID RF PULSING
TR >> T_1 and T_2
M_z
M_{xy}
TR < T_1 and T_2

51

Magnetization and the Steady-State

Define Normalized Time within interpulse period

$$t_n = t - nTR$$

Transverse magnetization T_2 decay

$$M_{xy}(t_n) = M_{xy}(0^+)e^{-t_n/T_2}$$

Longitudinal magnetization T_1 recovery

$$M_z(t_n) = M_0(1 - e^{-t_n/T_1}) + M_z(0^-)e^{-t_n/T_1}$$

52

Steady-State Incoherent (SSI)

Assume T2 << TR so no memory of Mxy across TR intervals

$$E_1 = e^{TR/T_1} \qquad E_2 = e^{TR/T_2} = 0$$

If a steady-state exists then the following must be true:

$$M_{nTR^-} = M_{ze} = M_{ze}E_1\cos\theta + M_0(1 - E1)$$

and therefore

$$M_{ze} = \frac{M_0(1 - E1)}{(1 - E_1\cos\theta)}$$

53

SSI Signal

Applying a flip and T_2 decay gives us the signal

$$M_{xy}(\theta, t_n) = \frac{M_0(1 - E_1)}{(1 - E_1\cos\theta)}e^{-t_n/T_2}\sin\theta$$

54

SSI Tissue Contrast

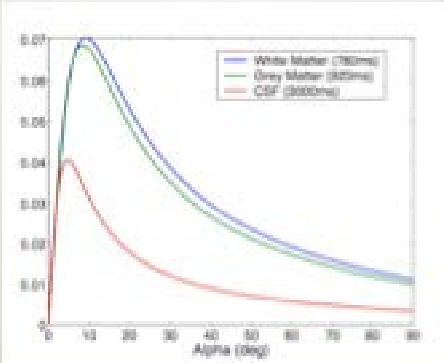

$$S(TR, TE, \alpha) = S(0)\sin(\alpha)\frac{1 - e^{-TR/T_1}}{1 - \cos(\alpha)e^{-TR/T_1}}e^{-TE/T_2}$$

55

The Ernst Angle

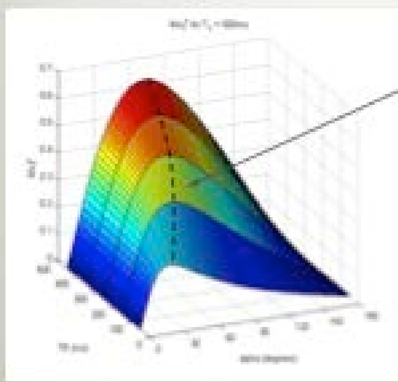

$$\theta_E = cos^{-1}(e^{-TR/T_1})$$

Maximum signal obtained at Ernst angle, **not 90°** when $TR < T_1$

56

Approach to SSI

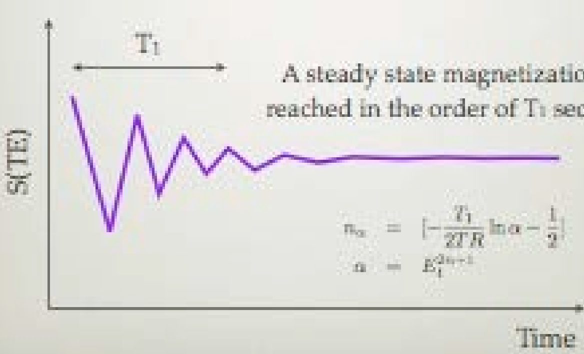

A steady state magnetization is reached in the order of T_1 seconds

$$\begin{aligned} n_\alpha &= [-\frac{T_1}{2TR}\ln\alpha - \frac{1}{2}] \\ \alpha &= E_1^{2n-1} \end{aligned}$$

57

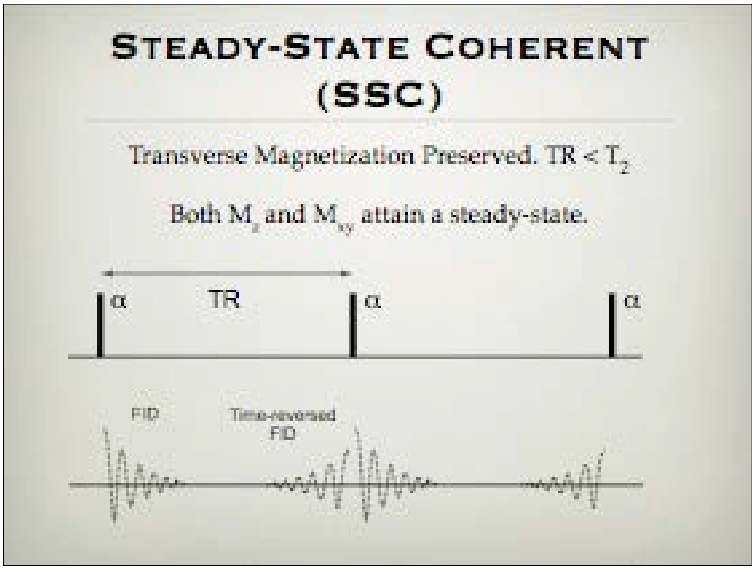
STEADY-STATE COHERENT (SSC)
Transverse Magnetization Preserved. TR < T_2
Both M_z and M_{xy} attain a steady-state.
α
TR
α
α
FID
Time-reversed FID

58

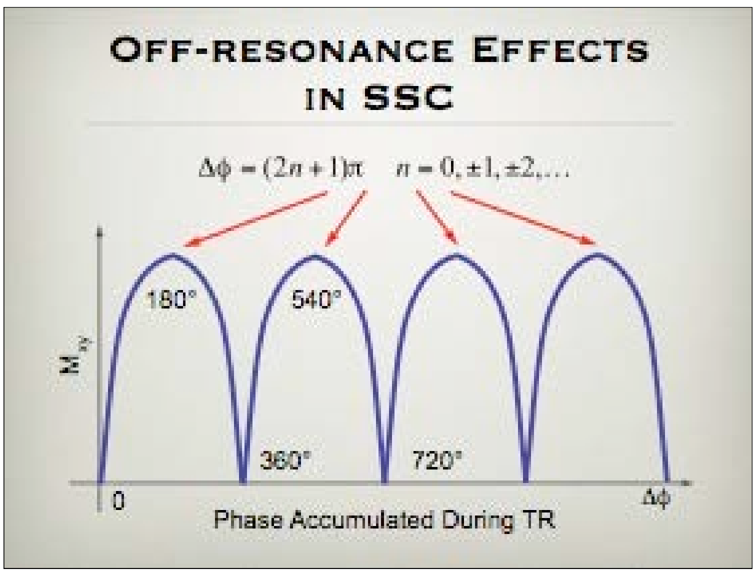
OFF-RESONANCE EFFECTS IN SSC
$\Delta\phi = (2n+1)\pi \quad n = 0, \pm1, \pm2, \ldots$
180°
540°
M_{xy}
360°
720°
0
$\Delta\phi$
Phase Accumulated During TR

59

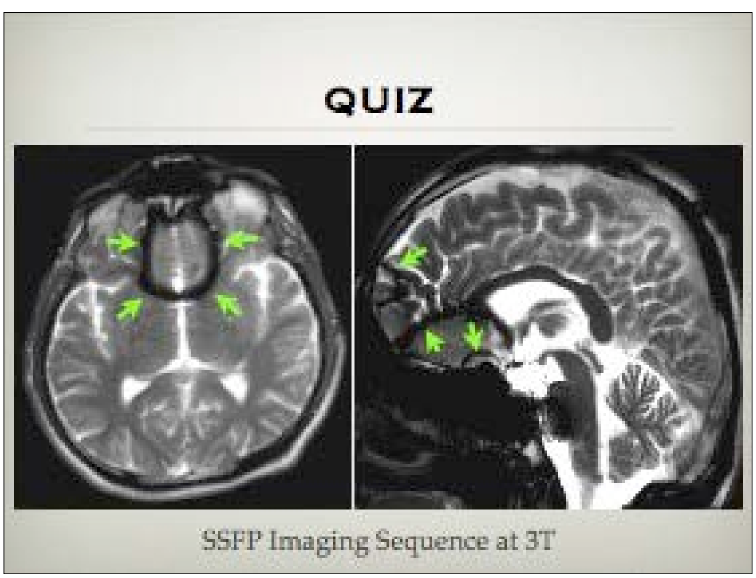
QUIZ
SSFP Imaging Sequence at 3T

60

Off-resonance artifacts SSFP at 12 Tesla

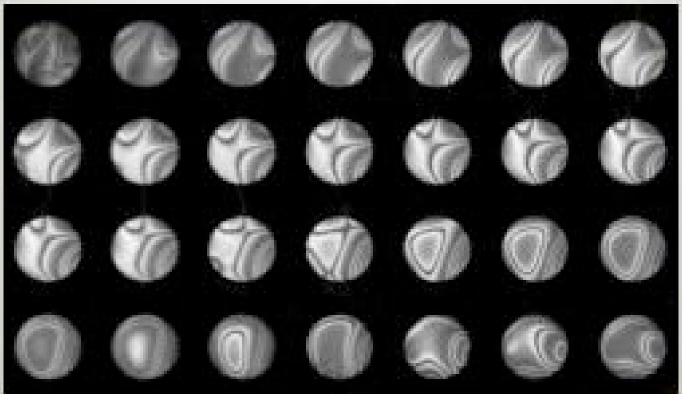

61

Next Lecture

- MR Image Formation I

62

BE/CNS 248
3.2 Imaging Motion

1

Lecture Summary

- 4.1 MRI of Flow and Motion
  - Motion in a gradient
  - Higher order gradient moments
  - Phase contrast MRI
  - Phase difference vs Complex difference
  - Fourier flow MRI
  - Pressure MRI

2

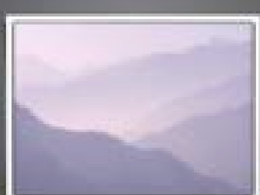

Motion in a Field Gradient

3

Coherent Motion

- Non-random bulk motion of a liquid, elastic, plastic or solid material
- Time- and length-scale dependent
- Coherent Motion
  - Laminar blood flow
  - CSF flow
  - Myocardial motion
- Incoherent Motion
  - Molecular self-diffusion
  - Capillary flow on a large length scale (Pseudo-diffusion)

4

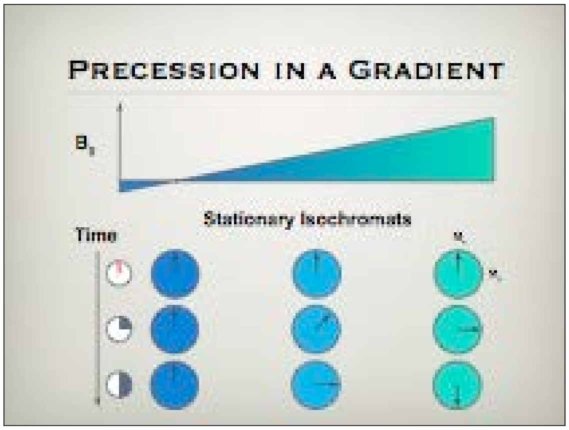

5

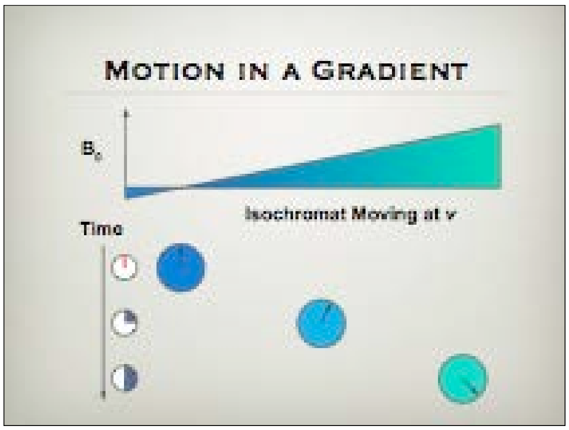

6

Higher order motion

Maclauren expansion of position as a function of time

$$x(t) = x(0) + x'(0)t + \frac{1}{2!}x''(0)t^2 + \ldots + \frac{1}{n!}x^{(n)}(0)t^n + \ldots$$

$$\begin{aligned} x'(0) &= v(0) && \text{Initial Velocity} \\ x''(0) &= a(0) && \text{Initial Acceleration} \\ &\vdots && \text{Initial Jerk ...} \end{aligned}$$

7

Gradient Moment Expansion

Substitute into 1D phase accumulation equation

$$\begin{aligned} \phi(T) &= \gamma \int_0^T dt G(t) x(t) \\ &= \gamma \left[x(0) \int_0^T dt G(t) + x'(0) \int_0^T dt G(t) t + \ldots \right] \\ &= \gamma \left[x(0) m_0(T) + v(0) m_1(T) + a(0) m_2(T) + \ldots \right] \end{aligned}$$

8

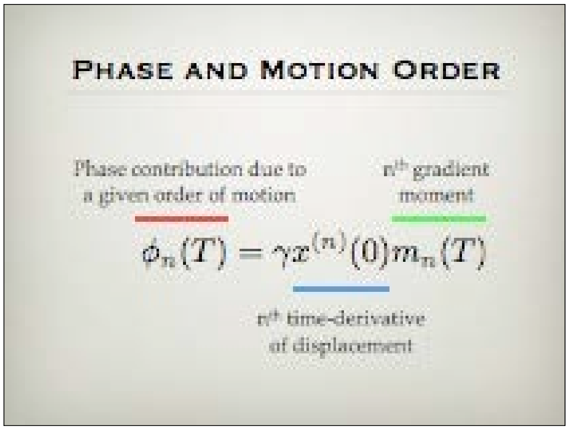
Phase and Motion Order
Phase contribution due to a given order of motion
n^{th} gradient moment
$$\phi_n(T) = \gamma x^{(n)}(0) m_n(T)$$
n^{th} time-derivative of displacement

9

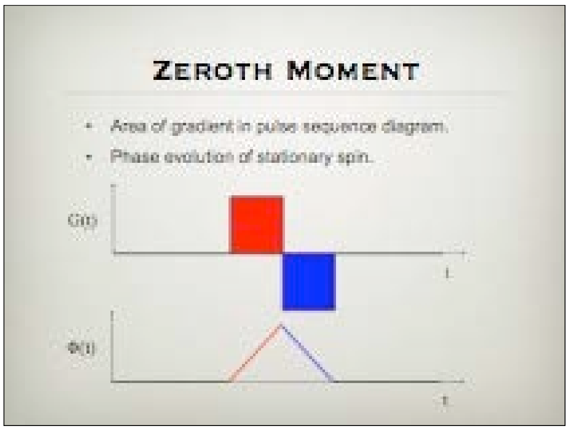
Zeroth Moment
- Area of gradient in pulse sequence diagram.
- Phase evolution of stationary spin.
G(t)
t
Φ(t)
t

10

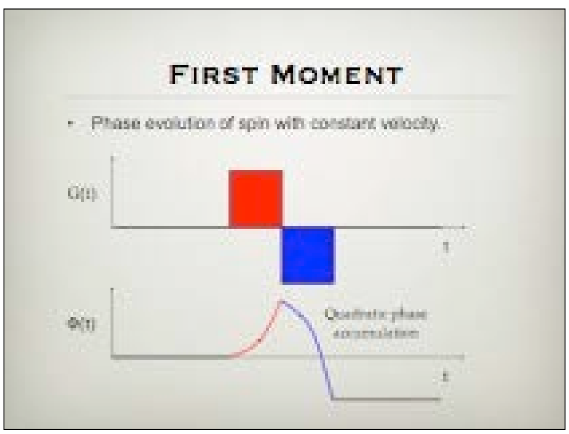
First Moment
- Phase evolution of spin with constant velocity.
G(t)
t
Φ(t)
Quadratic phase accumulation
t

11

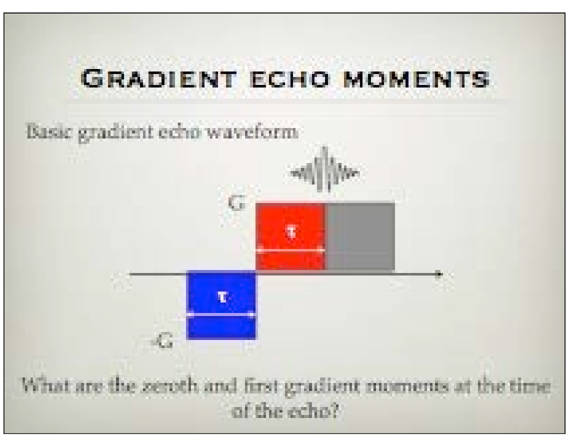
Gradient echo moments
Basic gradient echo waveform
G
τ
τ
-G
What are the zeroth and first gradient moments at the time of the echo?

12

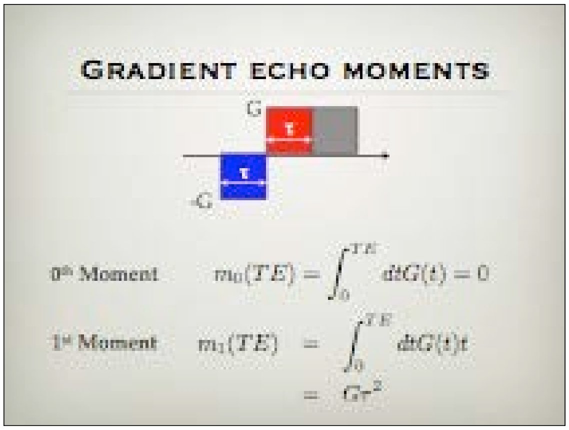
Gradient echo moments
G
τ
τ
-G
0th Moment $m_0(TE) = \int_0^{TE} dt G(t) = 0$
1st Moment $m_1(TE) = \int_0^{TE} dt G(t) t = G\tau^2$

13


Flow Compensation

14

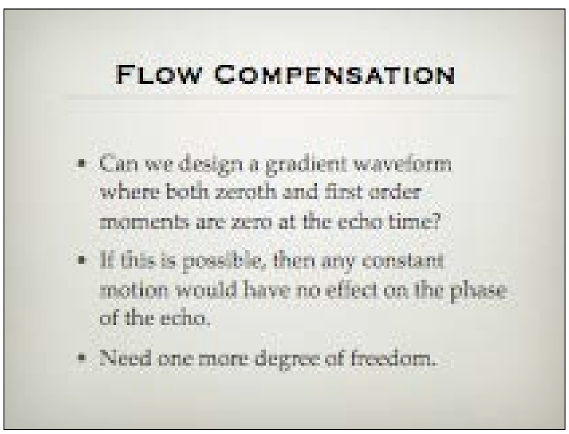
Flow Compensation
• Can we design a gradient waveform where both zeroth and first order moments are zero at the echo time?
• If this is possible, then any constant motion would have no effect on the phase of the echo.
• Need one more degree of freedom.

15

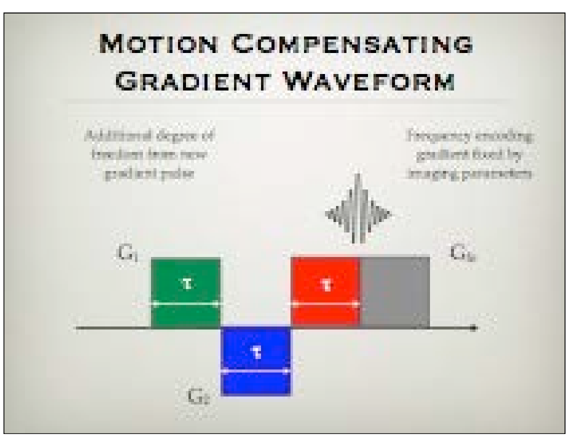
Motion Compensating Gradient Waveform
Additional degree of freedom from new gradient pulse
Frequency encoding gradient fixed by imaging parameters
G_1
G_{fe}
τ
τ
τ
G_2

16

Moment Equations

Gradient echo with equal duration gradient pulses

$$m_0(TE) = \tau(G_1 + G_2 + G_{fe})$$
$$m_1(TE) = \frac{1}{2}\tau^2(G_1 + 3G_2 + 5G_{fe})$$

17

Motion Compensation Solution

$m_0(TE) = m_1(TE) = 0$

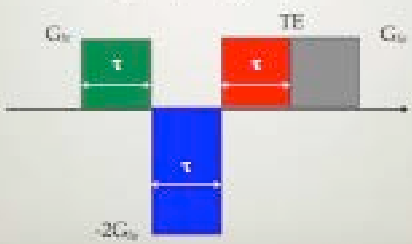

18

Even Echo Flow Compensation

First moment nulled intrinsically for even echos in both gradient and spin echo trains

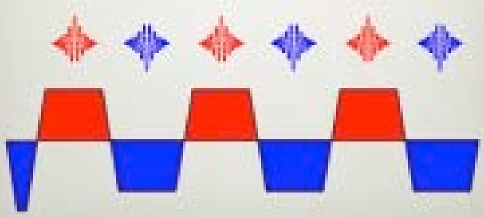

19

Flow Compensated Slice Selection and Phase Encoding

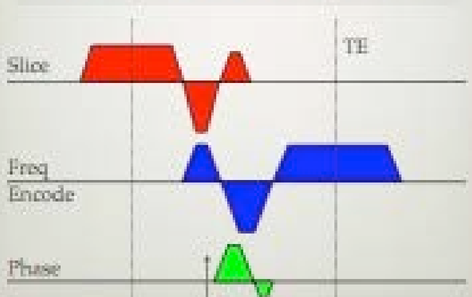

20

Flow Encoding

21

Phase Encoding of Flow

- Can a gradient waveform be designed that gives the echo a phase proportional to velocity in a given direction?
- Requires that zeroth moment is zero and first moment is finite at the echo time.
- More convenient still to have independent control over first moment.

22

Biopolar Flow Encoding Pulses

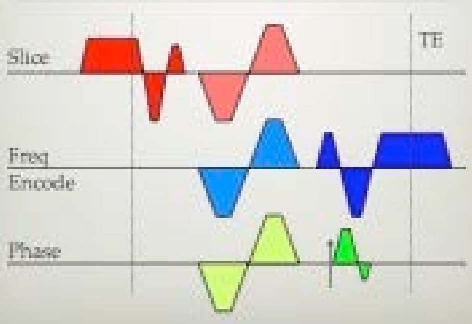

23

Background Phase

- The voxel phase without velocity encoding cannot be assumed to be zero.
- Many contributions to background phase:
  - B_0 inhomogeneity
  - Gradient eddy currents
  - Other orders of motion
  - Deliberate offsetting of echo position
  - ...

24

Removing Background Phase

General velocity encoded magnetization

$$\tilde{\rho} = \rho_0 e^{i(\phi_b + \phi_v)}$$

Acquire two images with opposite sign bipolar gradient pulses

$$\tilde{\rho}_{\pm} = \rho_0 e^{i(\phi_b \pm \phi_v)}$$

$$\phi_v = \frac{1}{2}(\angle\tilde{\rho}_+ - \angle\tilde{\rho}_-)$$

25

Phase Difference

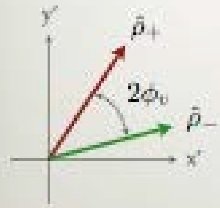

Difference in phase of transverse magnetization between positive and negative velocity encoded acquisitions.

26

Principle of Phase Contrast

Background phase arises from B_0 inhomogeneities, echo timing offsets, eddy currents, Maxwell terms, ...

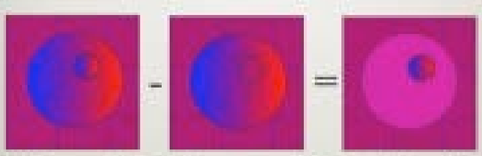

Velocity encoded through plane — Velocity compensated reference — Corrected phase velocity image

27

Encoding Schemes

6 Point Scheme — 4 Point Scheme

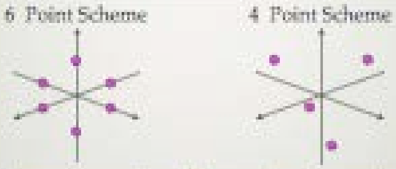

[illegible]	[illegible]	[illegible]	[illegible]
1	+	0	0
2	-	0	0
3	0	+	0
4	0	-	0
5	0	0	+
6	0	0	-

[illegible]	[illegible]	[illegible]	[illegible]
1	[illegible]	[illegible]	[illegible]
2	[illegible]	[illegible]	[illegible]
3	[illegible]	[illegible]	[illegible]
4	[illegible]	[illegible]	[illegible]

Scale gradients by 1/sqrt(3)

28

Recovering Velocity from 4-point Encoding

Use linear combinations of the voxel phase from each acquisition. For example, for the phase encoded z-component of velocity:

$$\phi_z = \frac{1}{2}\left[(\phi_3 + \phi_4) - (\phi_1 + \phi_2)\right]$$

29

Aliasing Velocity : VENC

Phase is modulo 2π so we expect to see phase aliasing if the velocity exceeds a certain value.
This critical velocity is called the encoding velocity or V_{enc}

$$V_{enc} = \frac{\pi}{\gamma m_1 (TE)}$$

30

Phase Unwrapping

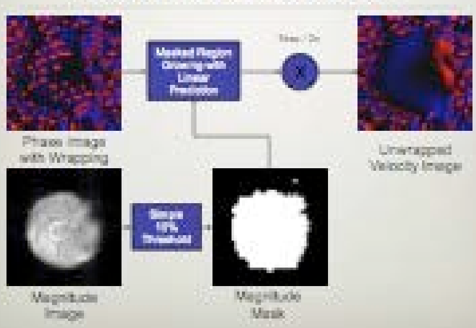

31

Velocity Imaging

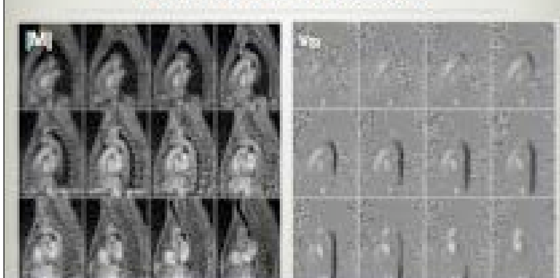

32

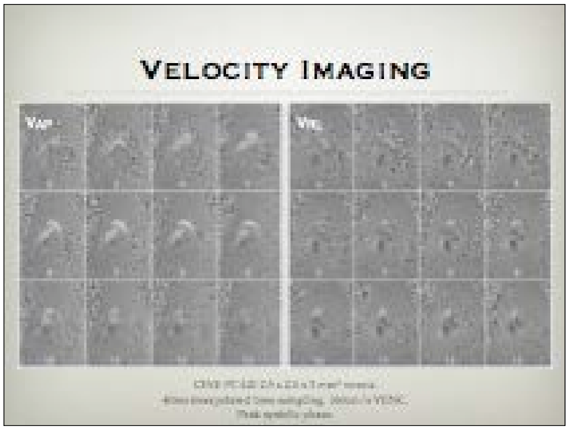
Velocity Imaging

33

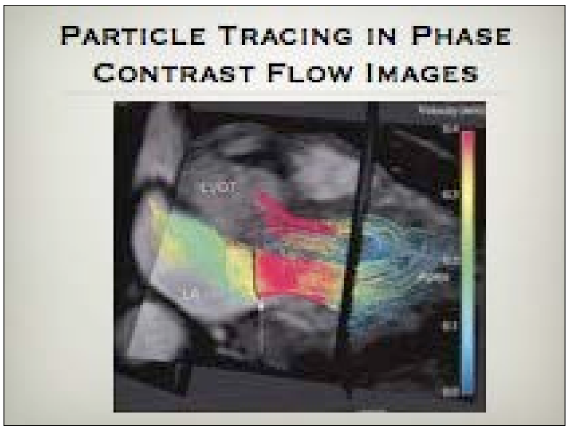
Particle Tracing in Phase
Contrast Flow Images

34

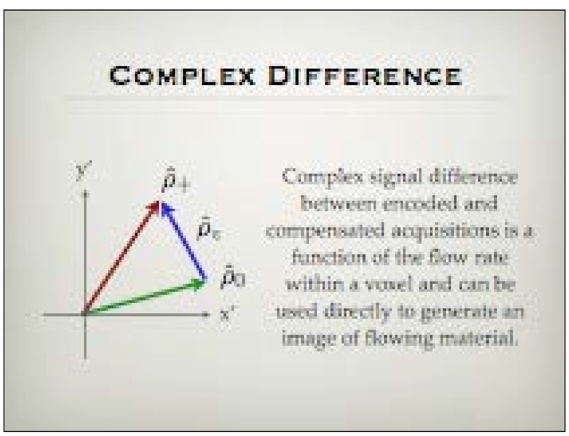
Complex Difference
y'
x'
Complex signal difference between encoded and compensated acquisitions is a function of the flow rate within a voxel and can be used directly to generate an image of flowing material.

35

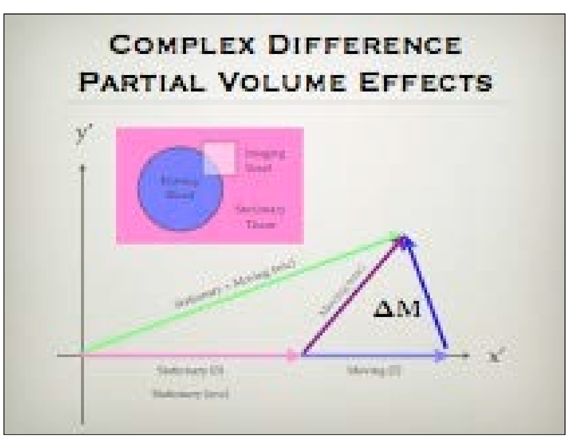
Complex Difference
Partial Volume Effects
y'
x'
ΔM

36

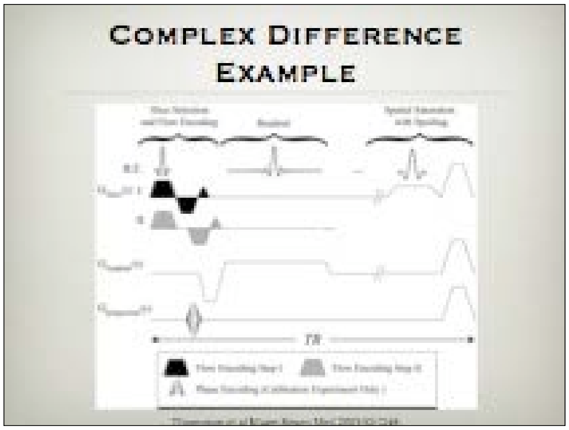
COMPLEX DIFFERENCE
EXAMPLE

37

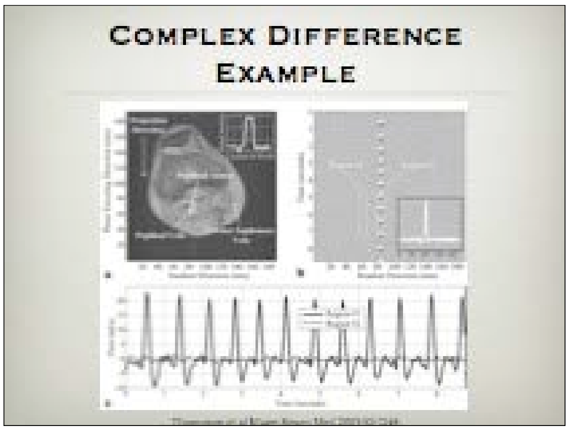
COMPLEX DIFFERENCE
EXAMPLE

38


TIME-RESOLVED FLOW
MEASUREMENT

39

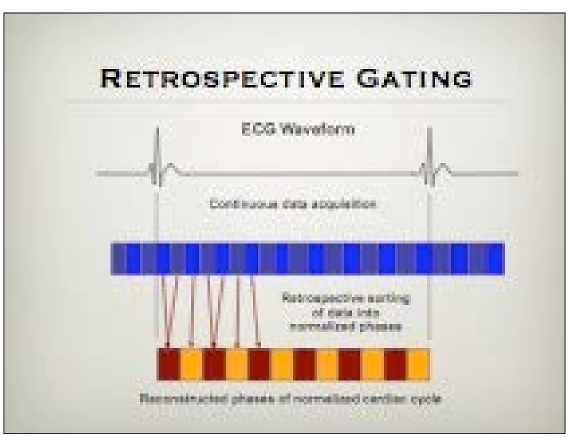
RETROSPECTIVE GATING
ECG Waveform
Continuous data acquisition
Retrospective sorting
of data into
normalized phases
Reconstructed phases of normalized cardiac cycle

40

Retrospectively Gated Phase Contrast MRI

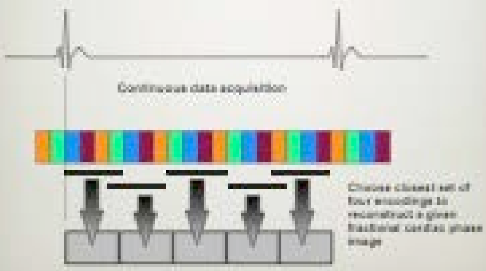

41

3D Phase Contrast CINE

SI Flow AP Flow

42

Real-time Velocity MRI

Spiral MRI with compensated and encoded acquisitions at 18 fps

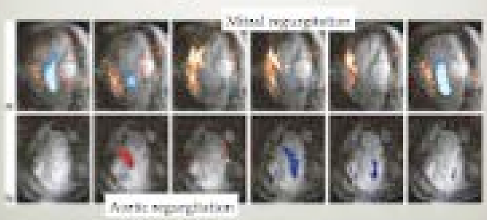

43

New velocity Dimension

Compare phase encoding of displacement

$$S(x) = \int_{-\infty}^{\infty} dt S(0) e^{-ik_x x}$$

with phase encoding of velocity

$$S(v) = \int_{-\infty}^{\infty} dt S(0) e^{-iq_v v_x}$$

44

Fourier Flow Encoding

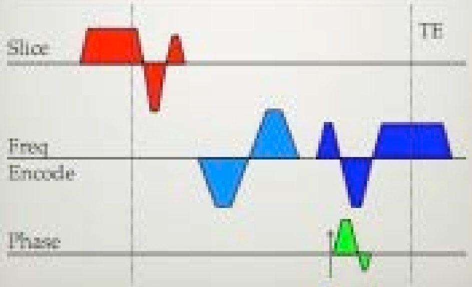

45

Realtime Fourier Velocity MRI

Velocity encoded EPI

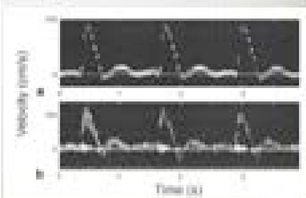

Aortic Flow Spectrum

46

Pressure Calculation

- The Navier-Stokes Equation relates velocity and relative pressure.
- Flow is viscous, time-varying and rotational.

$$-\nabla p = \rho \frac{\partial \mathbf{u}}{\partial t} + \rho \mathbf{u} \cdot \nabla \mathbf{u} + \eta \nabla \times \nabla \times \mathbf{u}$$

47

MRI Pressure Imaging

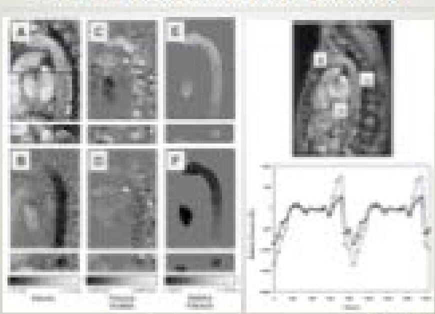

48

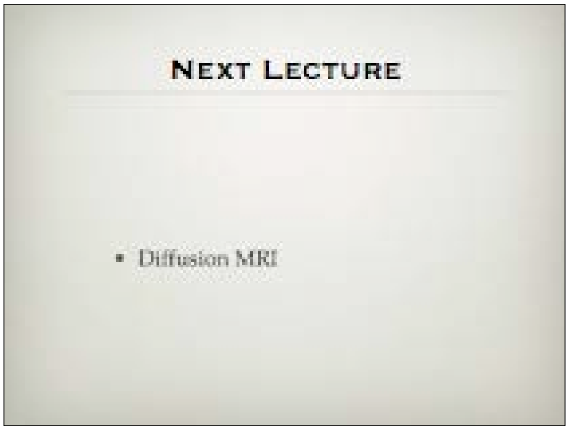

49

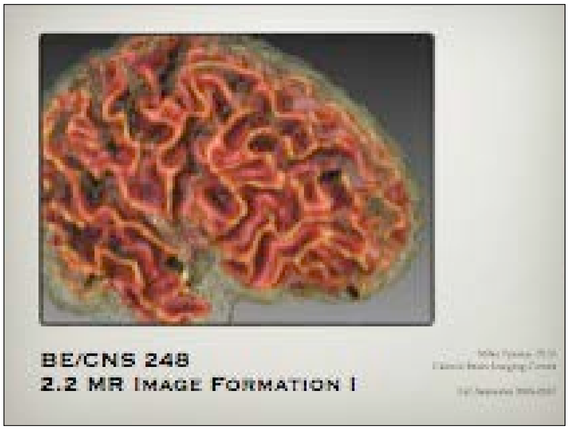
BE/CNS 248
2.2 MR Image Formation I

1

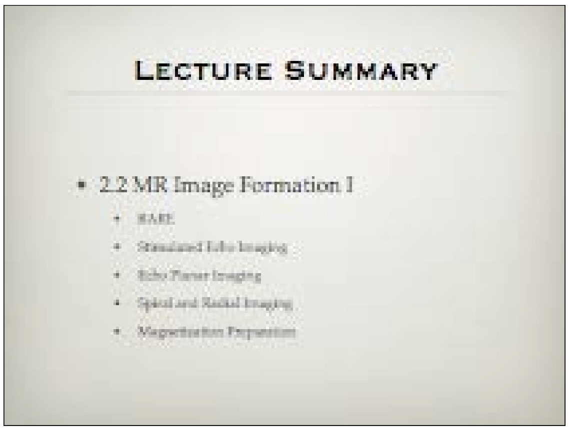
Lecture Summary
2.2 MR Image Formation I
RARE
Stimulated Echo Imaging
Echo Planar Imaging
Spiral and Radial Imaging
Magnetization Preparation

2


RARE and Turbo Spin Echo

3

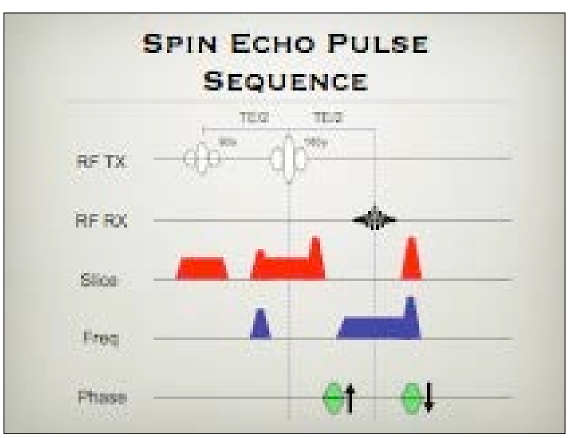
Spin Echo Pulse Sequence
TE/2
TE/2
RF TX
RF RX
Slice
Freq
Phase

4

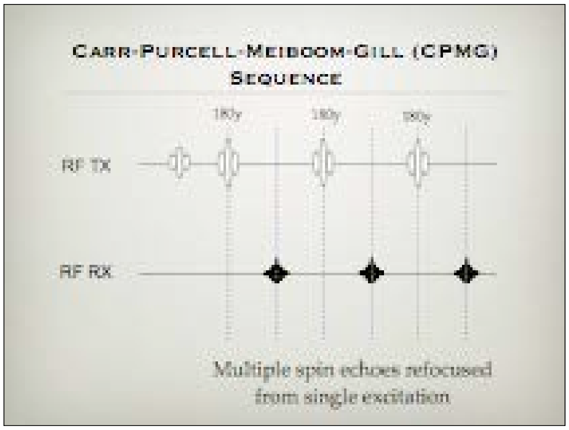
Carr-Purcell-Meiboom-Gill (CPMG) Sequence
180y
180y
180y
RF TX
RF RX
Multiple spin echoes refocused from single excitation

5

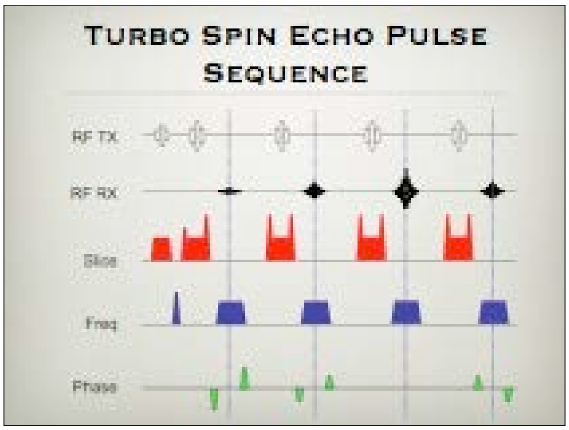
Turbo Spin Echo Pulse Sequence
RF TX
RF RX
Slice
Freq
Phase

6

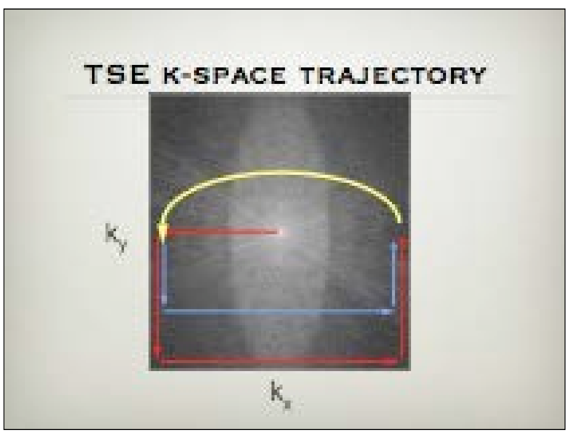
TSE k-space trajectory
k_y
k_x

7

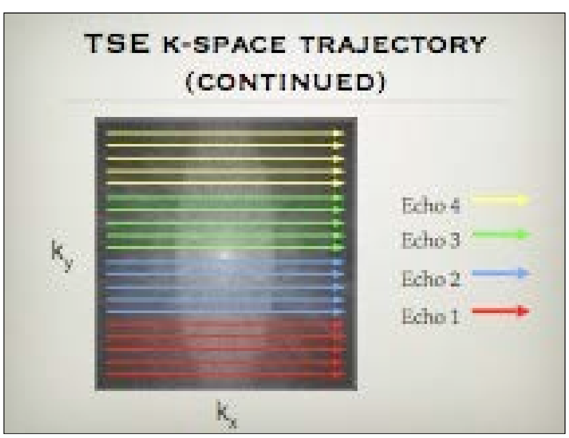
TSE k-space trajectory (continued)
k_y
Echo 4
Echo 3
Echo 2
Echo 1
k_x

8

Turbo Spin Echo

- Key Parameters
  - TR : Typically long (seconds)
  - TE : Typically long (10s to 100s ms)
  - Echo Train Length : Speed factor with side-effects
  - Typically T_2-weighted (T_1-weighted possible)
- Primary Applications
  - Rapid T2-weighted 2D multislice imaging
- Artifacts
  - Motion sensitive (single-shot less sensitive)
  - Blurring from short T_2 tissues

9

T_2-weighted RARE

10

Single-shot RARE

Quail Embryo *in ovo*

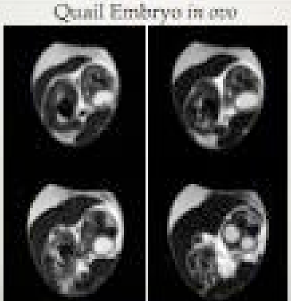

11

Propeller

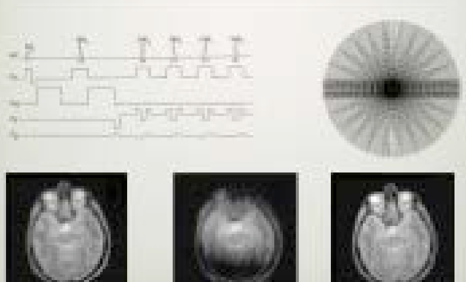

No Motion   Motion   Motion Corrected

12

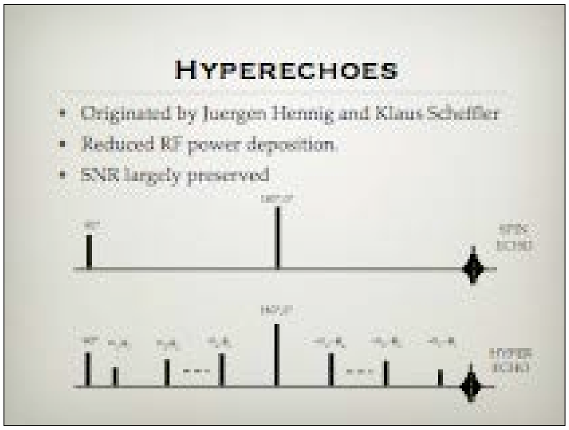
HYPERECHOES
Originated by Juergen Hennig and Klaus Scheffler
Reduced RF power deposition.
SNR largely preserved
SPIN ECHO
HYPER ECHO

13

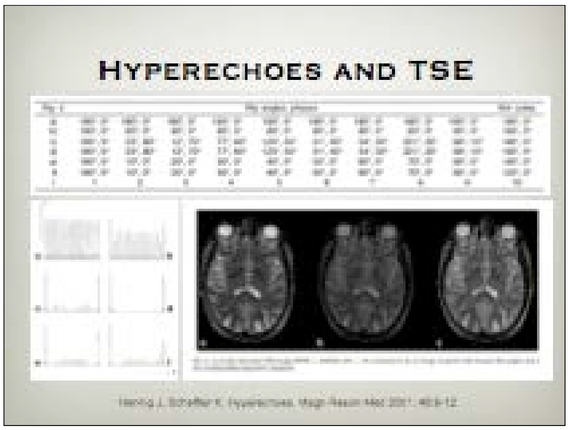
HYPERECHOES AND TSE

14


RARE SYNONYMS
RARE : Rapid Acquisition with Relaxation Enhancement
TSE : Turbo Spin Echo
FSE : Fast Spin Echo
ssRARE : Single-shot RARE
HASTE : Half-Fourier Acquisition Single-shot TSE

15


STIMULATED ECHO MRI

16

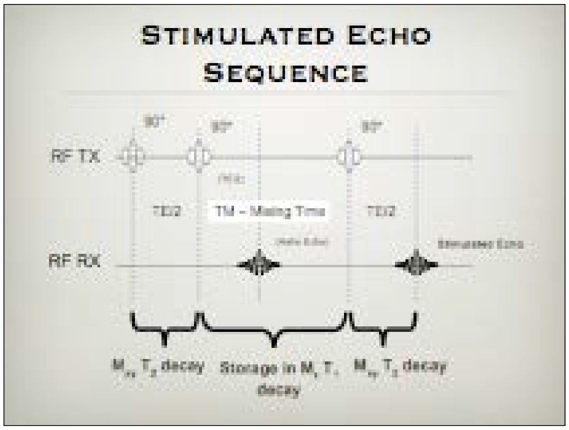

STIMULATED ECHO SEQUENCE
90°
90°
90°
RF TX
TE/2
TM – Mixing Time
TE/2
Stimulated Echo
RF RX
M_{xy} T_2 decay
Storage in M_z T_1 decay
M_{xy} T_2 decay

17

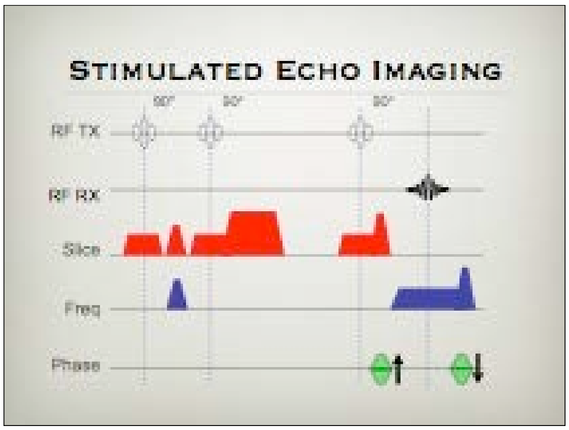

STIMULATED ECHO IMAGING
90°
90°
90°
RF TX
RF RX
Slice
Freq
Phase

18

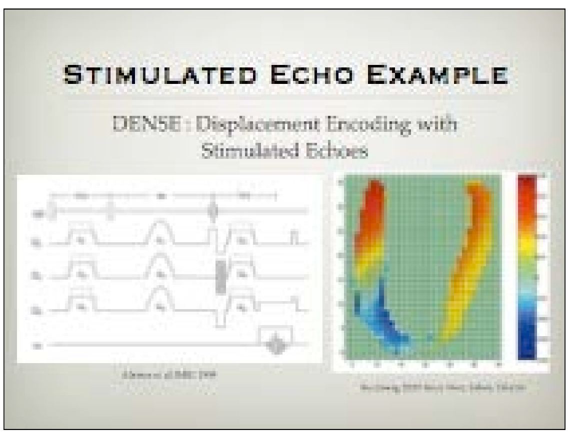

STIMULATED ECHO EXAMPLE
DENSE : Displacement Encoding with Stimulated Echoes

19

ECHO PLANAR IMAGING

20

Echo-planar Imaging

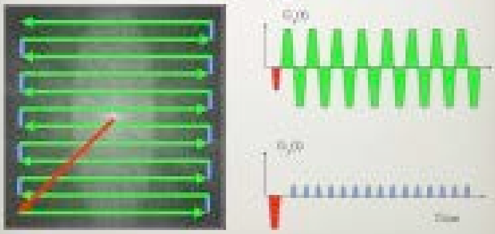

21

EPI Pulse Sequences

- Any transverse magnetization preparation can be imaged using an EPI k-space traversal.
- Gradient echo and spin echo most common preparation methods.
- Other popular sequences:
  - Inversion Recovery Spin-echo EPI
  - Diffusion-weighted Spin-echo EPI

22

FID EPI

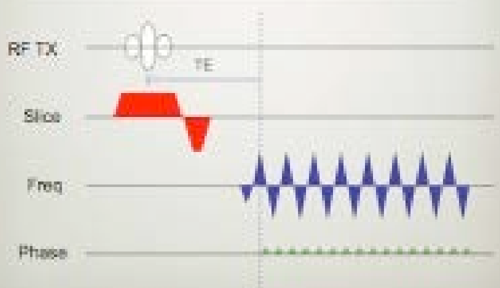

23

FID-EPI

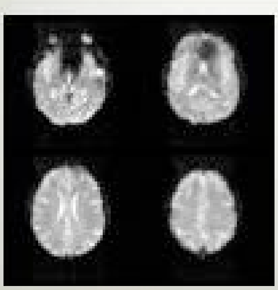

FID-EPI
Shots :1
TR :3000ms
TE :60ms
Slice :5mm/2.5mm (15)
Matrix :128 x 128
FOV :24cm x 24cm
Time :6s
NEX :1

24

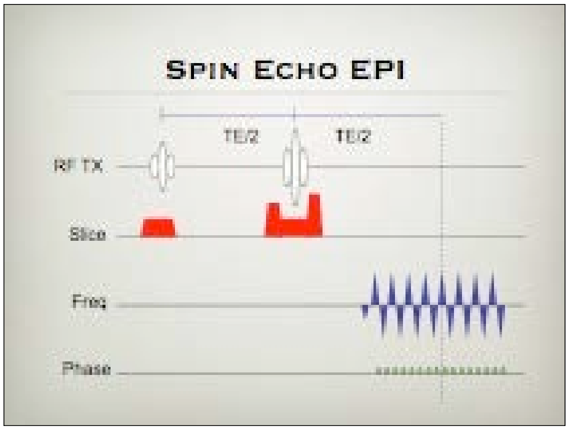
Spin Echo EPI
TE/2
TE/2
RF TX
Slice
Freq
Phase

25

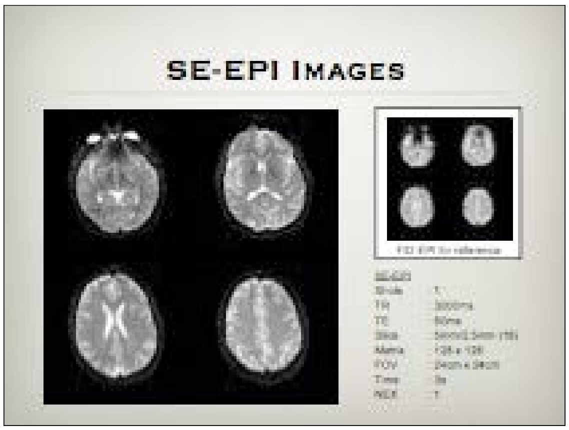
SE-EPI Images

26

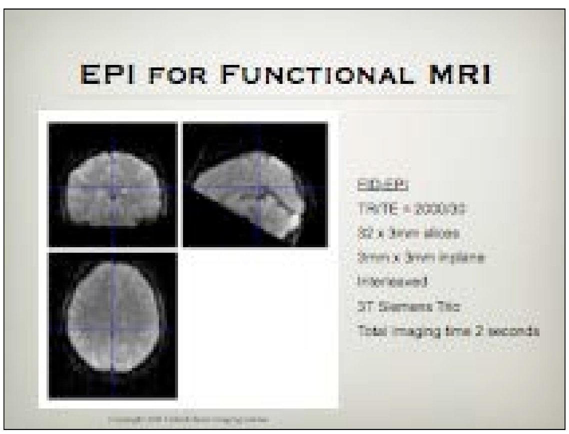
EPI for Functional MRI
FID-EPI
TR/TE = 2000/30
32 x 3mm slices
3mm x 3mm inplane
Interleaved
3T Siemens Trio
Total imaging time 2 seconds

27

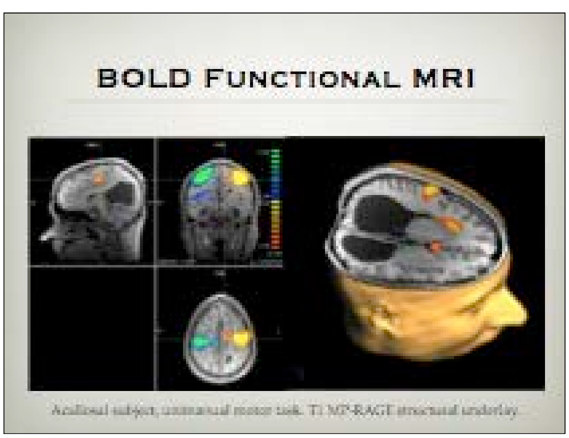
BOLD Functional MRI
Acallosal subject, unimanual motor task. T1 MP-RAGE structural underlay.

28


ACHILLES' HEEL OF EPI

29

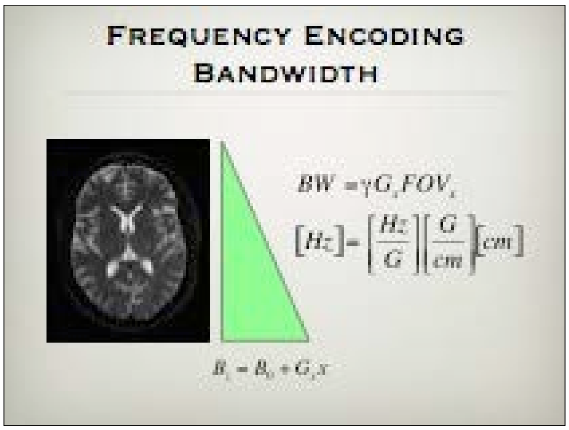
FREQUENCY ENCODING BANDWIDTH
$BW = \gamma G_x FOV_x$
$[Hz] = \left[\frac{Hz}{G}\right]\left[\frac{G}{cm}\right][cm]$
$B_x = B_0 + G_x x$

30

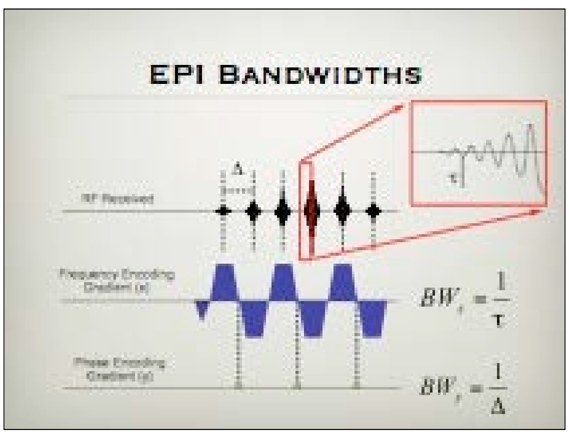
EPI BANDWIDTHS
RF Received
Frequency Encoding Gradient (x)
Phase Encoding Gradient (y)
Δ
τ
$BW_x = \frac{1}{\tau}$
$BW_y = \frac{1}{\Delta}$

31

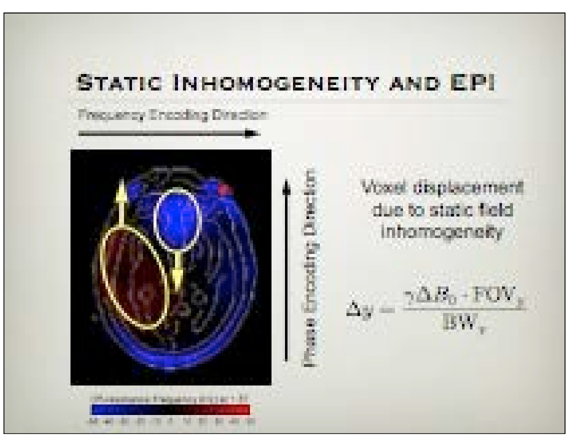
STATIC INHOMOGENEITY AND EPI
Frequency Encoding Direction
Phase Encoding Direction
Voxel displacement due to static field inhomogeneity
$\Delta y = \frac{\gamma \Delta B_0 \cdot FOV_y}{BW_y}$

32

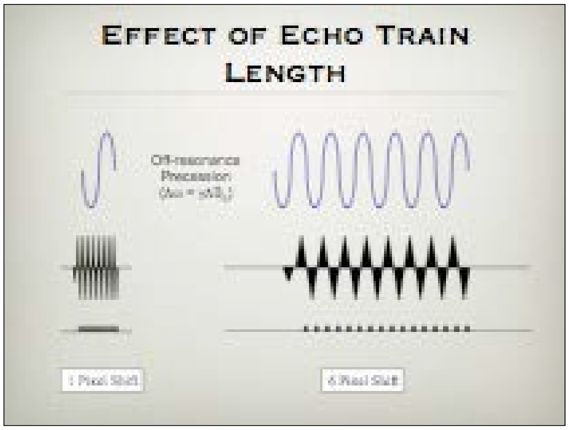
Effect of Echo Train Length
Off-resonance Precession

33

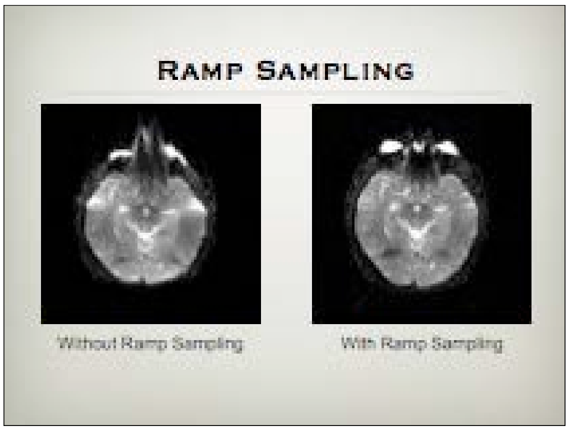
Ramp Sampling
Without Ramp Sampling
With Ramp Sampling

34

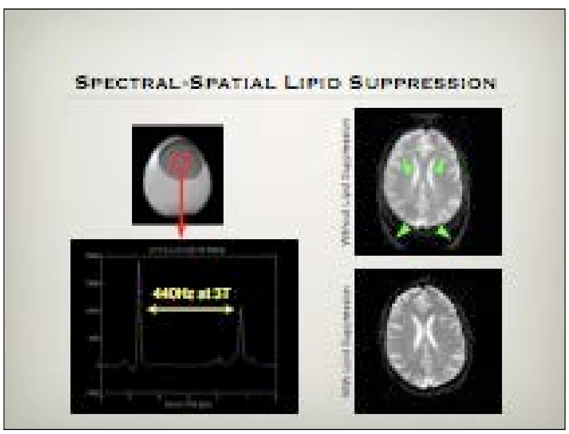
Spectral-Spatial Lipid Suppression
440Hz at 3T

35

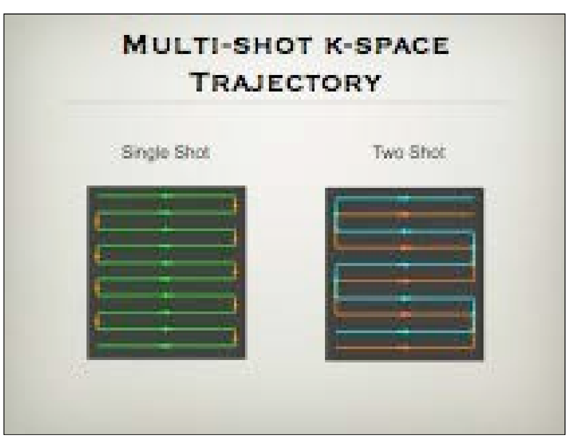
Multi-shot K-space Trajectory
Single Shot
Two Shot

36

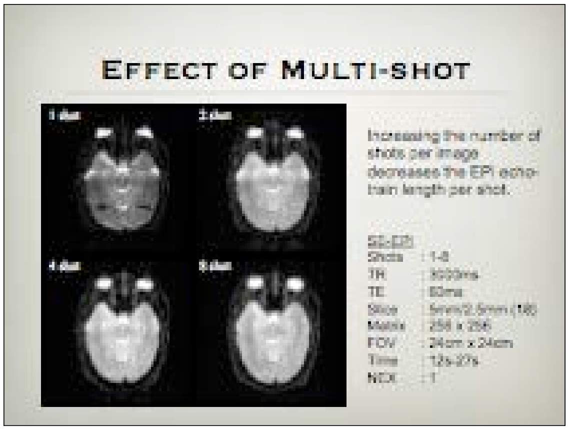
EFFECT OF MULTI-SHOT
Increasing the number of shots per image decreases the EPI echo-train length per shot.
Shots : 1-8
TR : 3000ms
TE : 60ms
Slice : 5mm/2.5mm (18)
Matrix : 256 x 256
FOV : 24cm x 24cm
Time : 12s-27s
NEX : 1

37

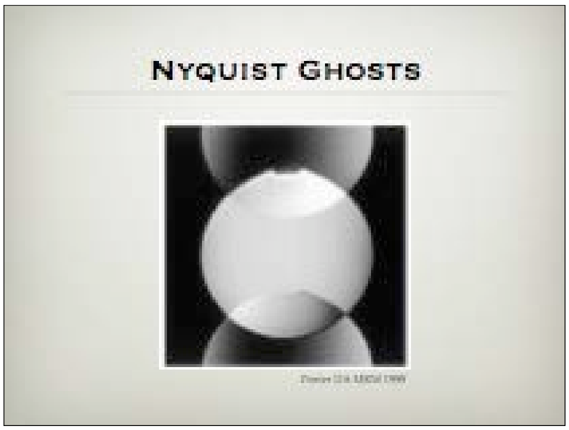
NYQUIST GHOSTS

38

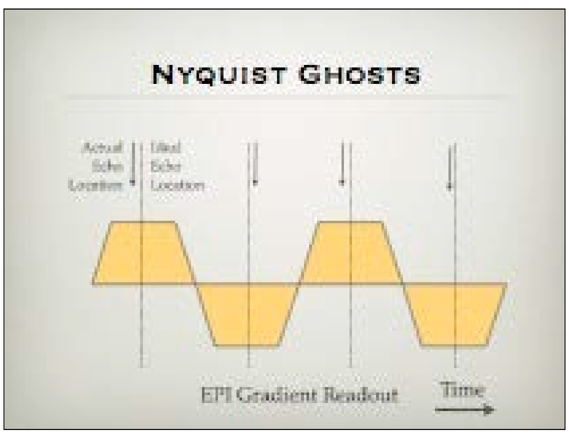
NYQUIST GHOSTS
Actual Echo Location
Ideal Echo Location
EPI Gradient Readout
Time

39

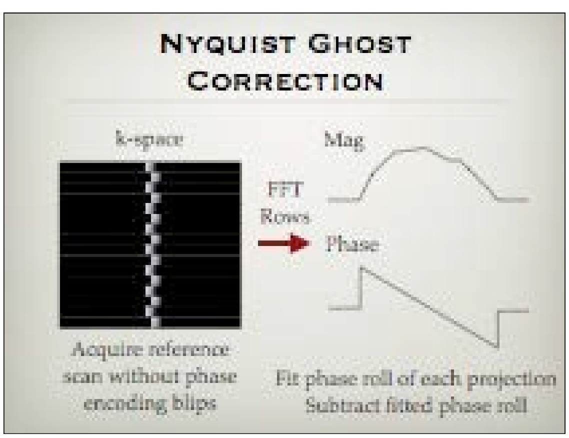
NYQUIST GHOST CORRECTION
k-space
Mag
FFT Rows
Phase
Acquire reference scan without phase encoding blips
Fit phase roll of each projection
Subtract fitted phase roll

40

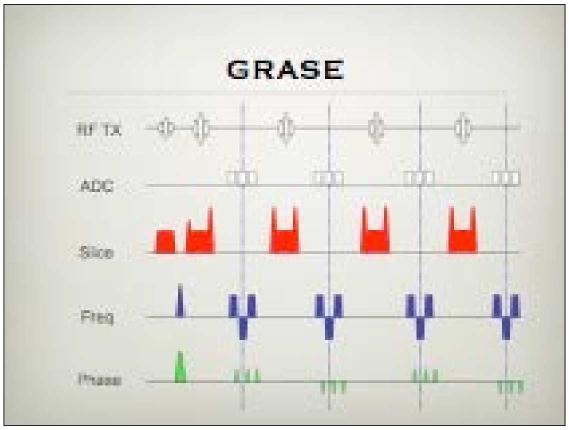
GRASE
RF TX
ADC
Slice
Freq
Phase

41

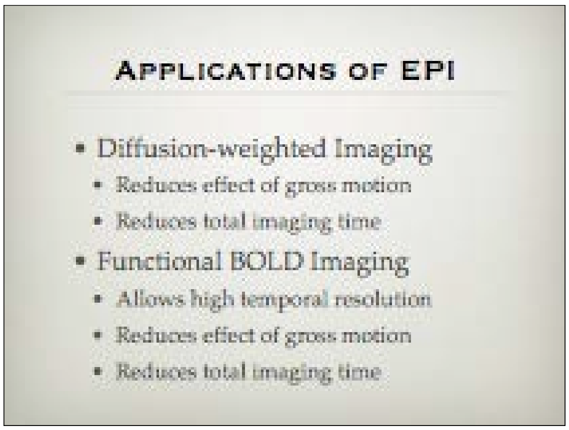
Applications of EPI
• Diffusion-weighted Imaging
• Reduces effect of gross motion
• Reduces total imaging time
• Functional BOLD Imaging
• Allows high temporal resolution
• Reduces effect of gross motion
• Reduces total imaging time

42


Spiral MRI

43

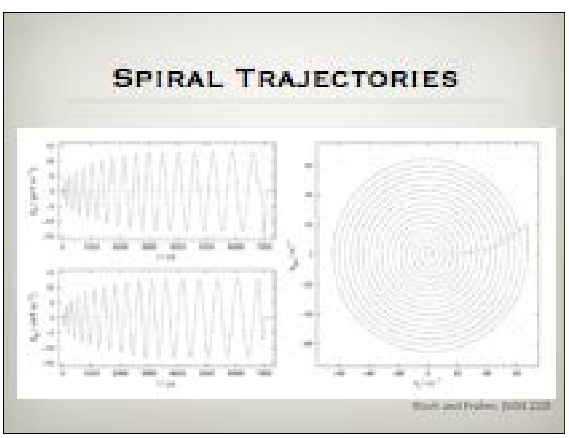
Spiral Trajectories

44

Spiral Artifacts

Imperfections in actual trajectory cause artifacts in both EPI and Spiral MRI

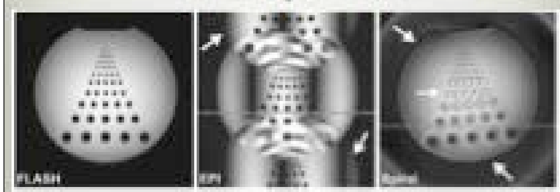

45

Spiral Features

- Spiral trajectory less sensitive to motion (periodic first order moment nulling).
- Artifacts are more diffuse and peripheral than for Cartesian trajectories.
- Image reconstruction requires regridding to Cartesian grid for FFT.

46

Spiral Applications: MR Coronary Angiography

47

Spiral for BOLD FMRI

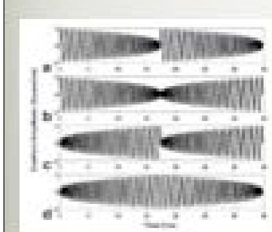

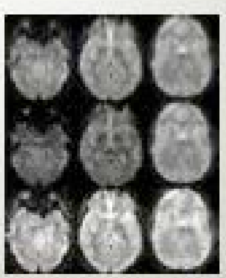

DSPIN Trajectory

48


MAGNETIZATION
PREPARATION

49

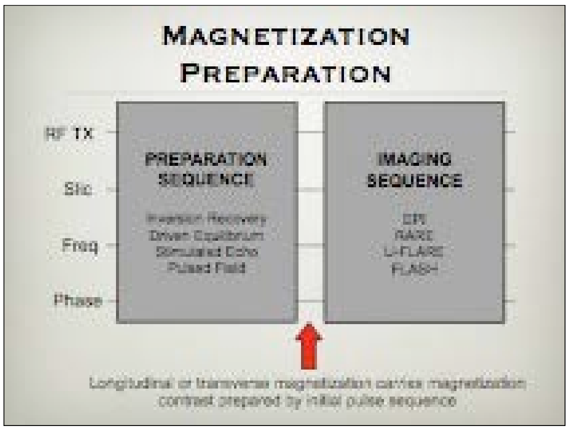
MAGNETIZATION
PREPARATION
RF TX
Slic
Freq
Phase
PREPARATION
SEQUENCE
Inversion Recovery
Driven Equilibrium
Stimulated Echo
Pulsed Field
IMAGING
SEQUENCE
EPI
RARE
U-FLARE
FLASH
Longitudinal or transverse magnetization carries magnetization
contrast prepared by initial pulse sequence

50

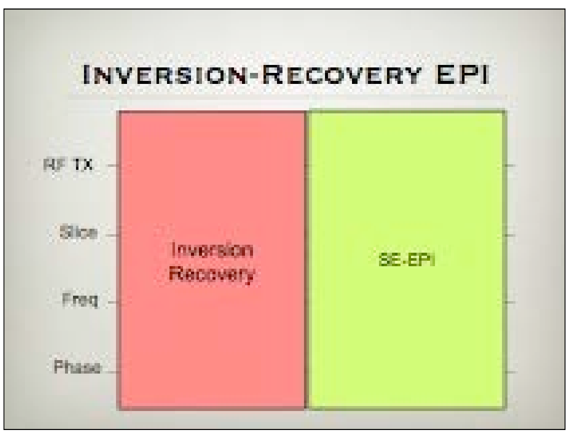
INVERSION-RECOVERY EPI
RF TX
Slice
Freq
Phase
Inversion
Recovery
SE-EPI

51

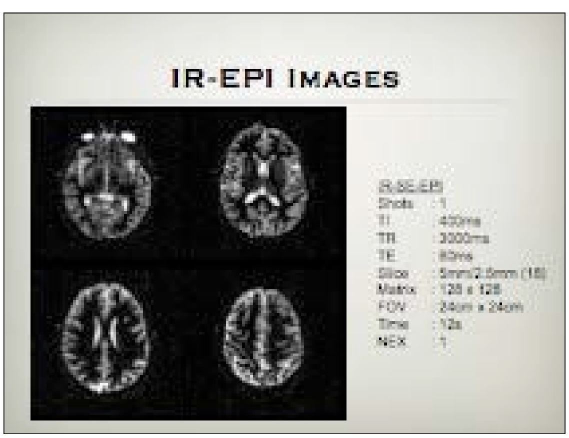
IR-EPI IMAGES
IR-SE-EPI
Shots : 1
TI : 400ms
TR : 3000ms
TE : 80ms
Slice : 5mm/2.5mm (16)
Matrix : 128 x 128
FOV : 24cm x 24cm
Time : 12s
NEX : 1

52

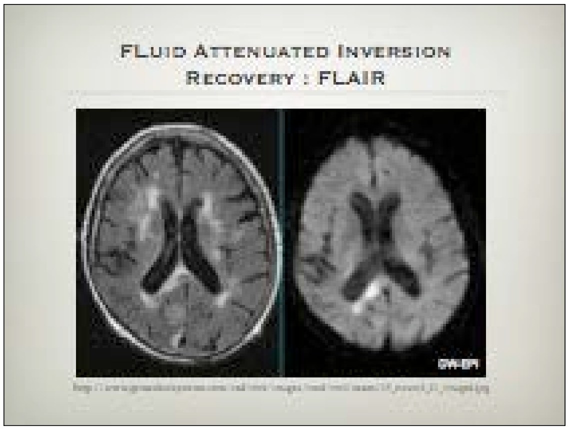
FLUID ATTENUATED INVERSION
RECOVERY : FLAIR

53

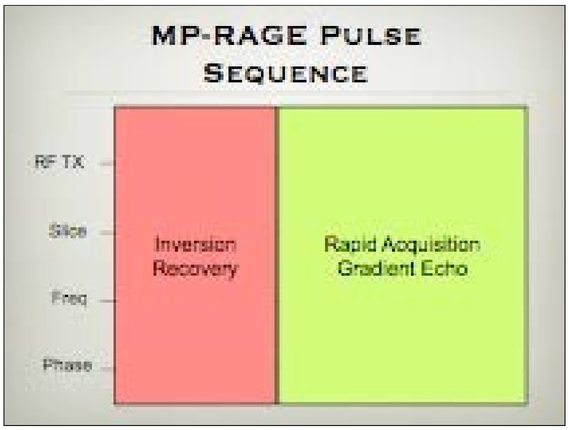
MP-RAGE PULSE
SEQUENCE
RF TX
Slice
Freq
Phase
Inversion
Recovery
Rapid Acquisition
Gradient Echo

54

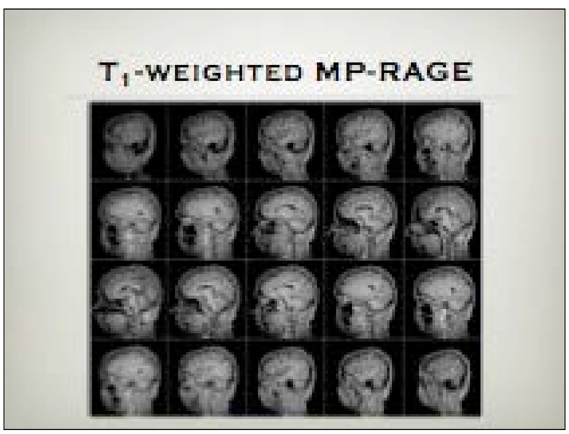
T1-WEIGHTED MP-RAGE

55

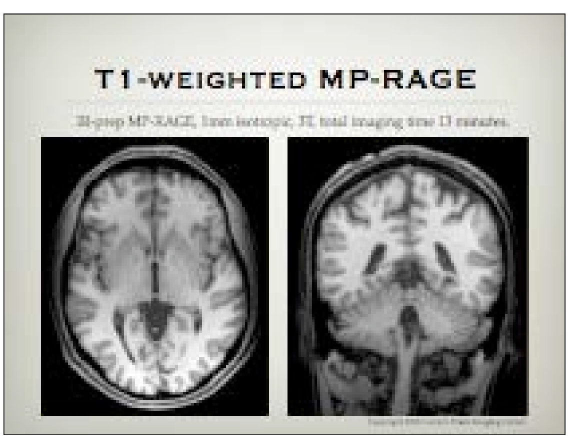
T1-WEIGHTED MP-RAGE

56

57

Next Lecture

- MR Image Formation II
  - Steady-state MRI

58

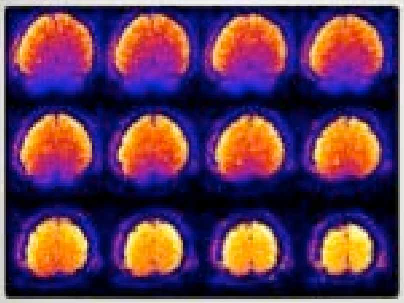

BE/CNS 248
3.1 Imaging Motion

1

Lecture Summary

- 3.1 MRI of Motion
  - Dynamic MRI
  - Physiological synchronization
  - ECG, pulse oximetry and respiration
  - Prospective and retrospective gating
  - Navigation and wireless Gating
  - Myocardial Tagging
  - Time-of-Flight MRI

2

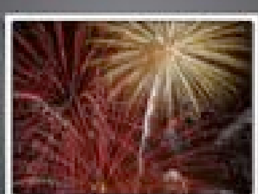

Dynamic MRI

3

Physiological Motion

Periodic	Aperiodic
Myocardial Motion	Development
Respiration	Musculoskeletal Motion
Cardiovascular Flow	Gut Peristalsis
CSF Flow	

4

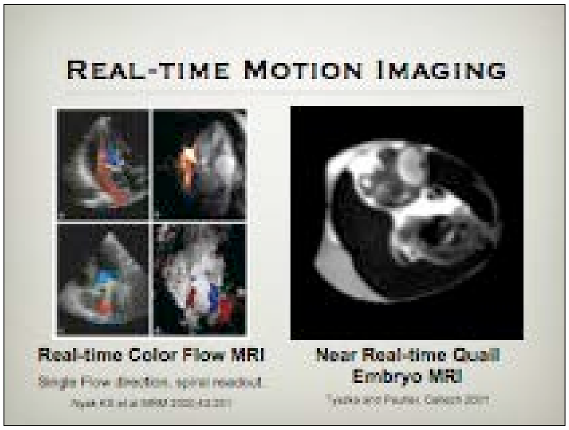
REAL-TIME MOTION IMAGING
Real-time Color Flow MRI
Near Real-time Quail
Embryo MRI

5


GROWTH AND DEVELOPMENT

6

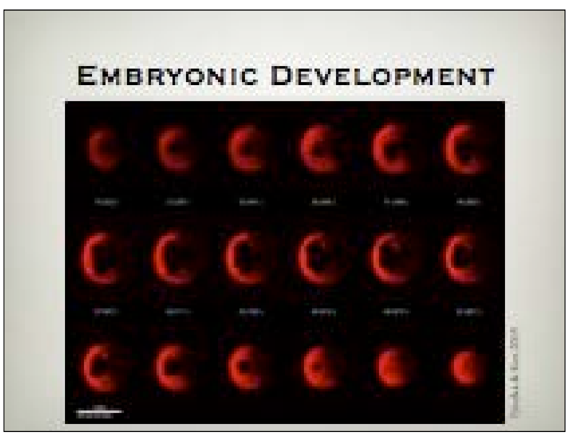
EMBRYONIC DEVELOPMENT

7

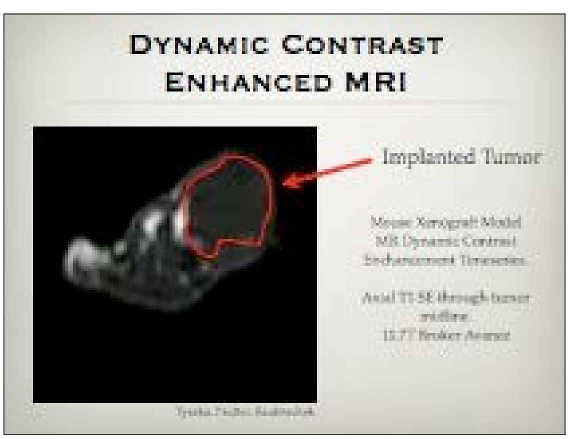
DYNAMIC CONTRAST
ENHANCED MRI
Implanted Tumor

8


Gut Peristalsis
Mouse Xenograft Model
MR DCE bolus passage.
Axial T1-weighted SE
through kidneys.
11.7 Bruker Avance

9

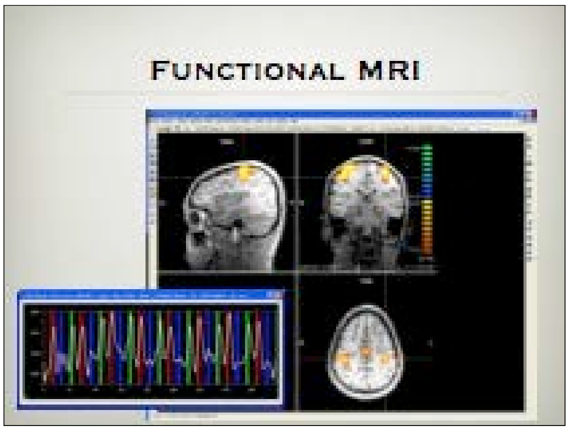
Functional MRI

10

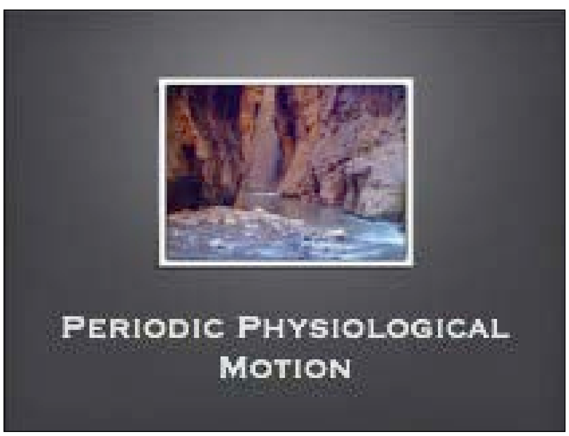
Periodic Physiological
Motion

11

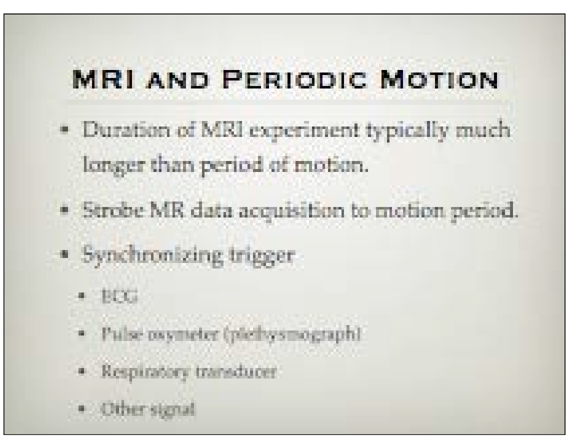
MRI and Periodic Motion
• Duration of MRI experiment typically much longer than period of motion.
• Strobe MR data acquisition to motion period.
• Synchronizing trigger
• ECG
• Pulse oxymeter (plethysmograph)
• Respiratory transducer
• Other signal

12

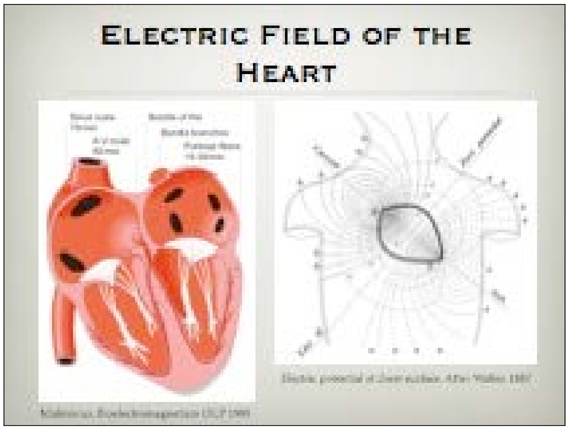
Electric Field of the Heart

13

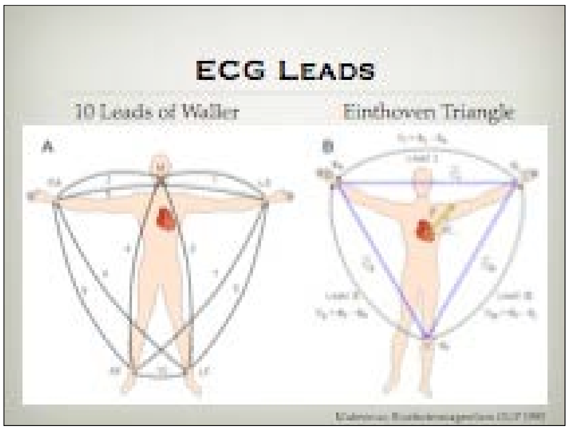
ECG Leads
10 Leads of Waller
Einthoven Triangle

14

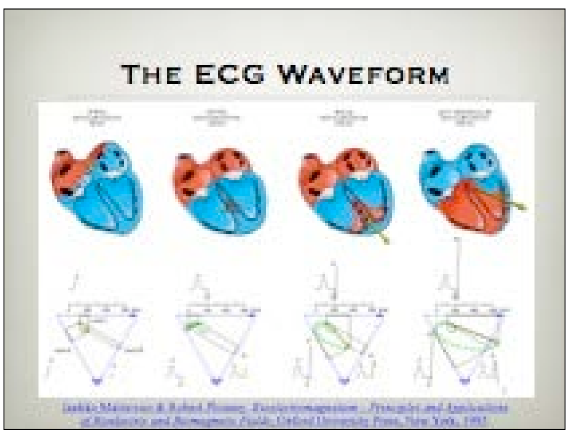
The ECG Waveform

15

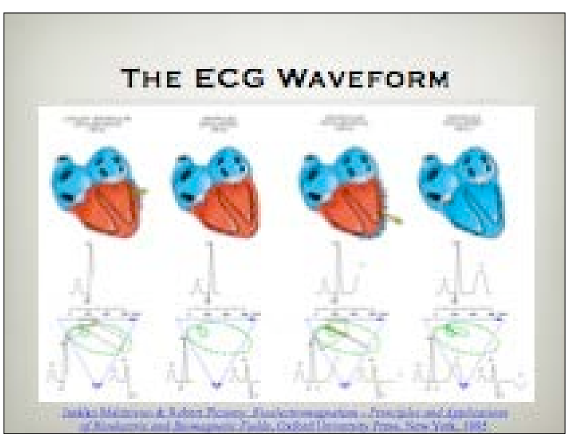
The ECG Waveform

16

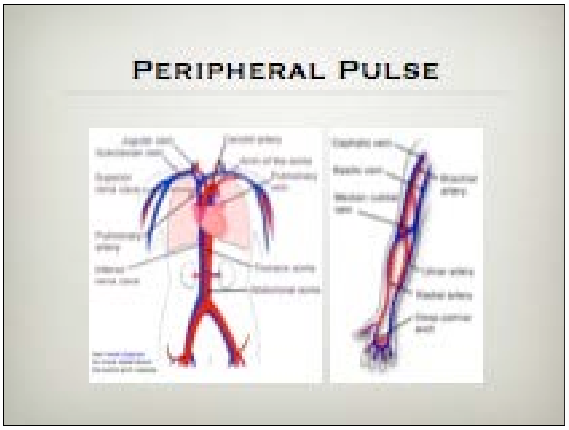
Peripheral Pulse

17

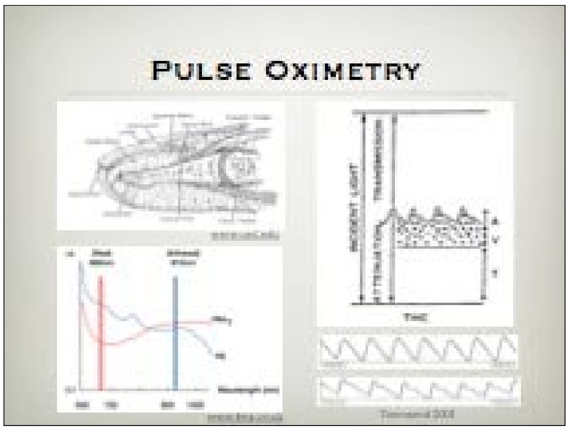
Pulse Oximetry

18

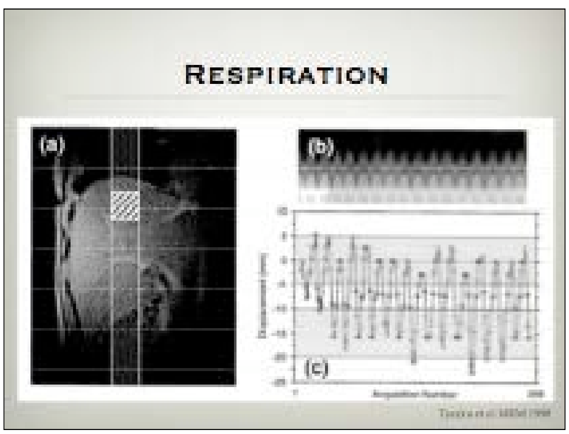
Respiration
(a)
(b)
(c)

19


Prospective Gating

20

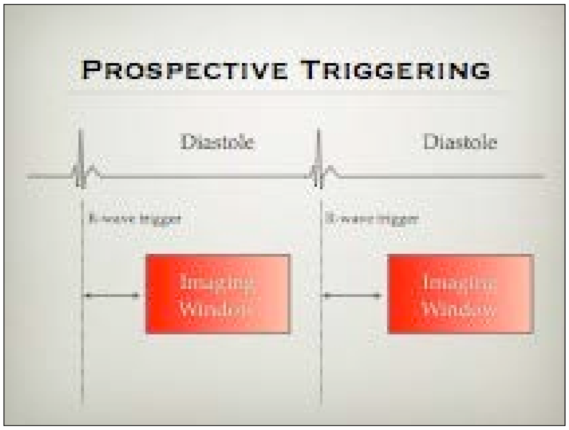
PROSPECTIVE TRIGGERING
Diastole
Diastole
Imaging Window
Imaging Window

21

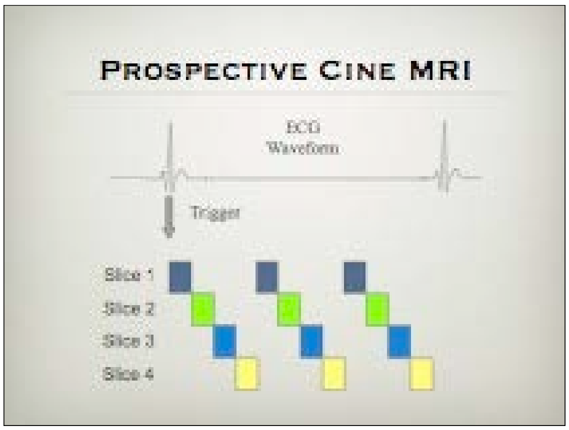
PROSPECTIVE CINE MRI
ECG Waveform
Trigger
Slice 1
Slice 2
Slice 3
Slice 4

22

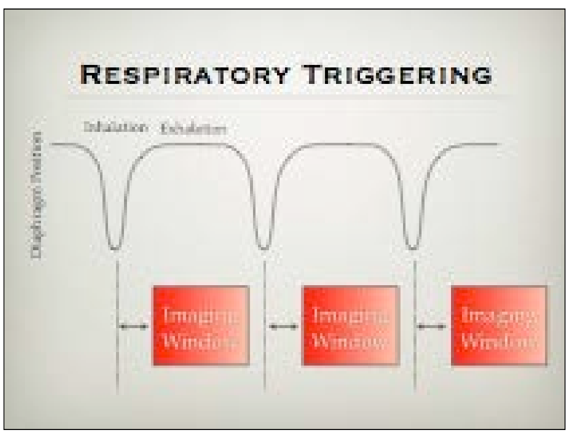
RESPIRATORY TRIGGERING
Inhalation
Exhalation
Imaging Window
Imaging Window
Imaging Window

23


RETROSPECTIVE GATING

24

Retrospective Gating

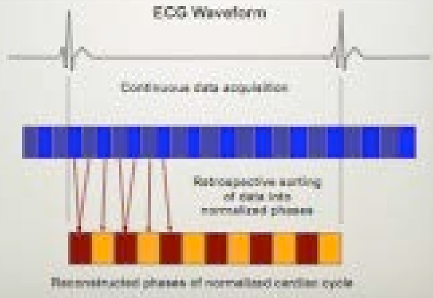

25

Retrospective Gating Rationale

- Prospective gating not a good match for steady-state imaging.
- Can we preserve steady-state but still obtain cardiac cycle resolved images?
- Acquire continuous MRI and simultaneously record ECG for reference.
- Sort out the mess retrospectively.

26

Arrhythmia in Retrospective gating

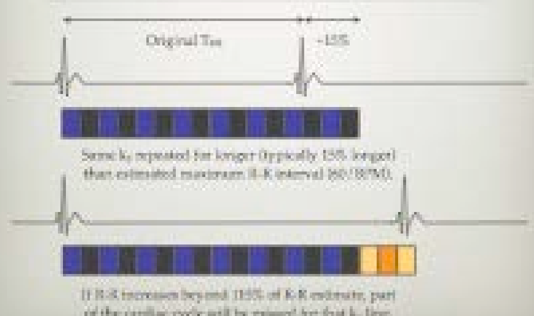

27

Gated or Triggered Motion Imaging

Short Axis Adult Human Heart.
Retrospectively gated.

28

Other Trigger Sources

29

Image-based Gating

- Detect onset of an event from the image data stream or navigation.
- Volume selective excitation tracks signal in a key region such as the aorta or diaphragm.
- Also called "wireless" gating.

30

Physiological Modulation

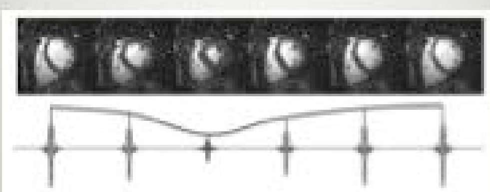

31

Navigation

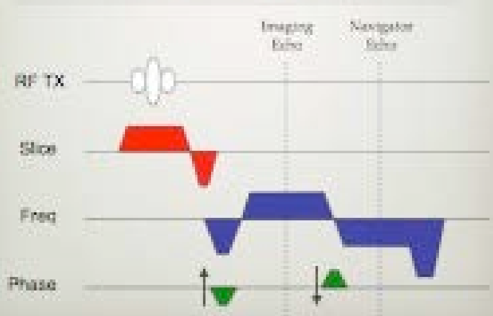

32

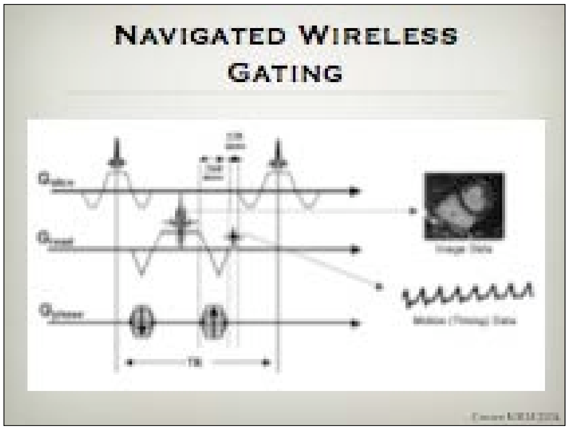
NAVIGATED WIRELESS GATING

33

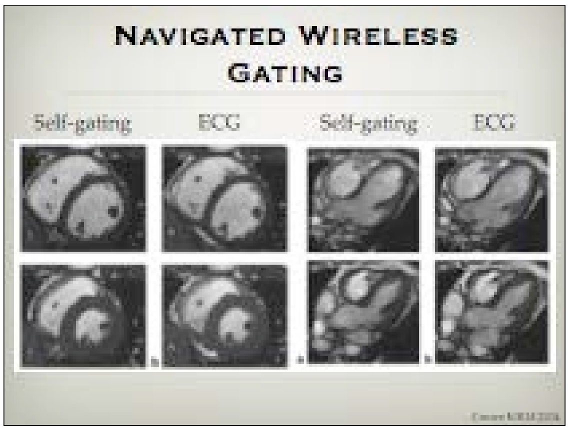
NAVIGATED WIRELESS GATING
Self-gating
ECG
Self-gating
ECG

34

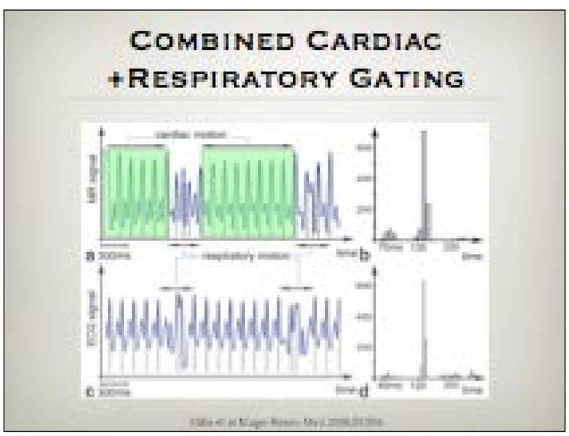
COMBINED CARDIAC +RESPIRATORY GATING
a
b
c
d

35

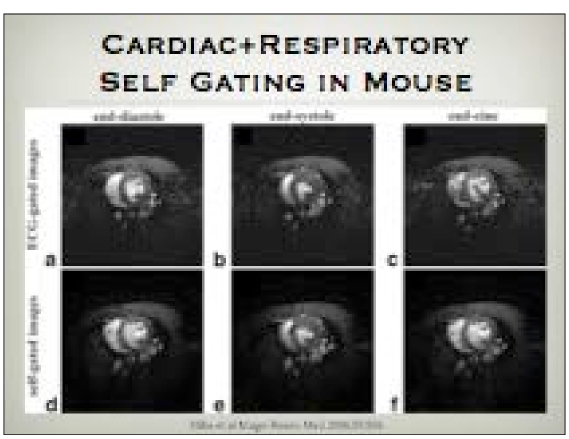
CARDIAC+RESPIRATORY SELF GATING IN MOUSE
a
b
c
d
e
f

36


MYOCARDIAL TAGGING

37

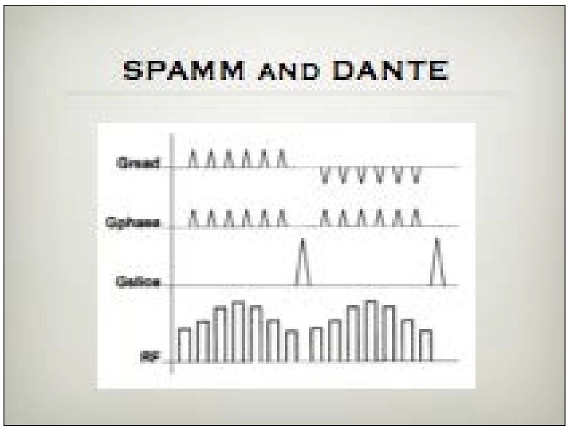
SPAMM AND DANTE
Gread
Gphase
Gslice
RF

38


MAGNETIZATION TAGGING
• Longitudinal magnetization tagging at end-diastole
• Image at subsequent phases of cardiac cycle to follow myocardial motion

39

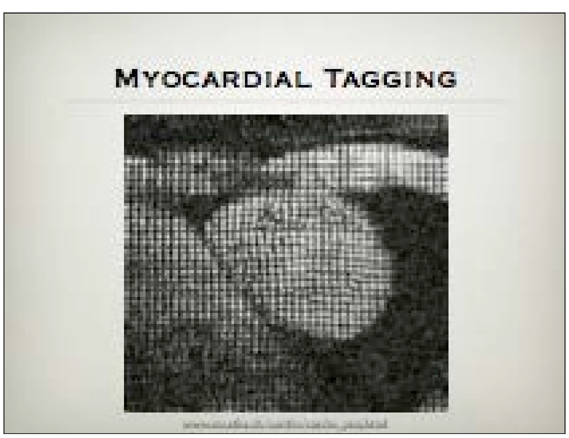
MYOCARDIAL TAGGING

40

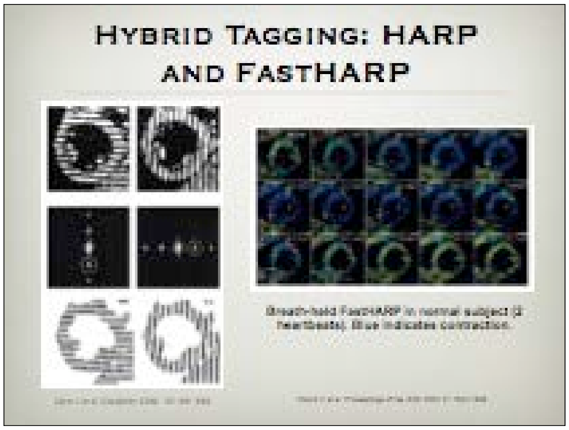
Hybrid Tagging: HARP and FastHARP
Breath-hold FastHARP in normal subject (2 heartbeats). Blue indicates contraction.

41

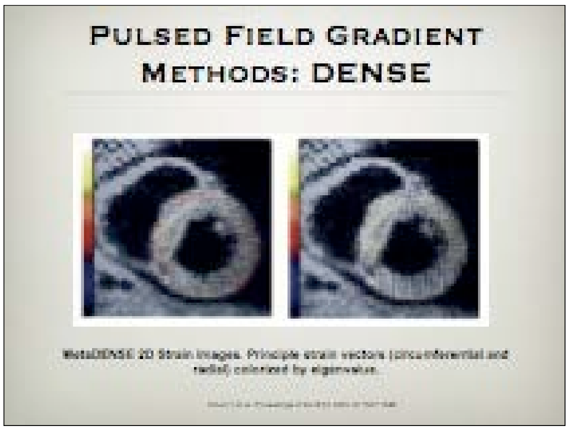
Pulsed Field Gradient Methods: DENSE
MetaDENSE 2D Strain images. Principle strain vectors (circumferential and radial) colorized by eigenvalue.

42


Time-of-Flight MRI

43

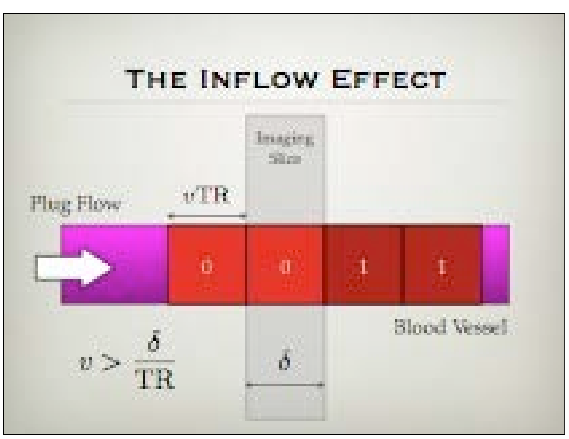
The Inflow Effect
Imaging Slice
Plug Flow
vTR
0
0
1
1
Blood Vessel
$v > \frac{\delta}{TR}$
δ

44

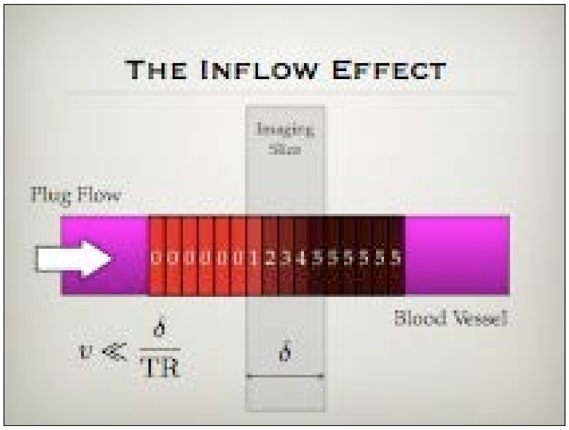
THE INFLOW EFFECT
Imaging Slice
Plug Flow
0 0 0 0 0 0 1 2 3 4 5 5 5 5 5 5
Blood Vessel
$v \ll \frac{\delta}{\mathrm{TR}}$
δ

45

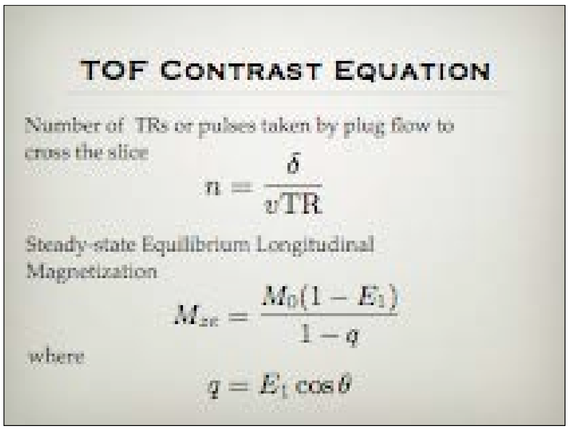
TOF CONTRAST EQUATION
Number of TRs or pulses taken by plug flow to cross the slice
$n = \frac{\delta}{v\mathrm{TR}}$
Steady-state Equilibrium Longitudinal Magnetization
$M_{ze} = \frac{M_0(1-E_1)}{1-q}$
where
$q = E_1 \cos\theta$

46

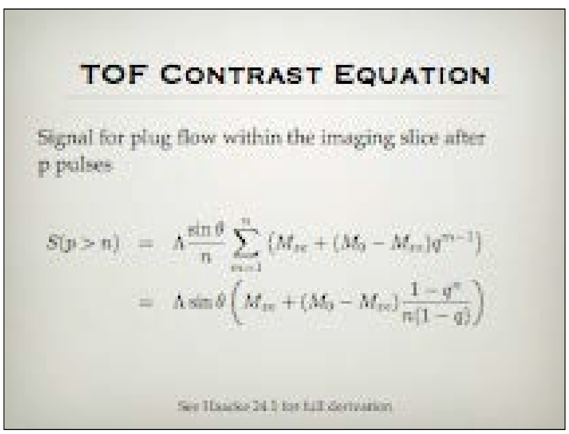
TOF CONTRAST EQUATION
Signal for plug flow within the imaging slice after p pulses
$S(p>n) = \Lambda \frac{\sin\theta}{n} \sum_{m=1}^{n} \left(M_{ze} + (M_0 - M_{ze}) q^{m-1}\right)$
$= \Lambda \sin\theta \left(M_{ze} + (M_0 - M_{ze}) \frac{1-q^n}{n(1-q)} \right)$
See Haacke 24.3 for full derivation

47

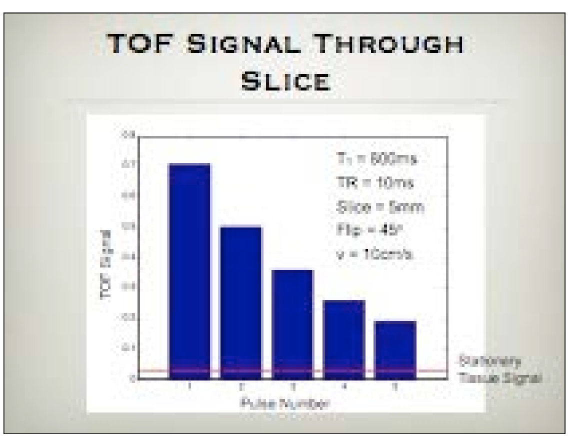
TOF SIGNAL THROUGH SLICE
T_1 = 600ms
TR = 10ms
Slice = 5mm
Flip = 45°
v = 10cm/s
TOF Signal
Pulse Number
Stationary Tissue Signal

48

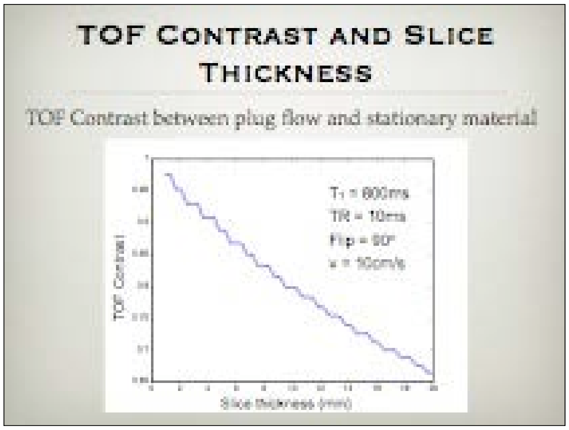
TOF Contrast and Slice Thickness
TOF Contrast between plug flow and stationary material
T_1 = 800ms
TR = 10ms
Flip = 90°
v = 10cm/s
TOF Contrast
Slice thickness (mm)

49

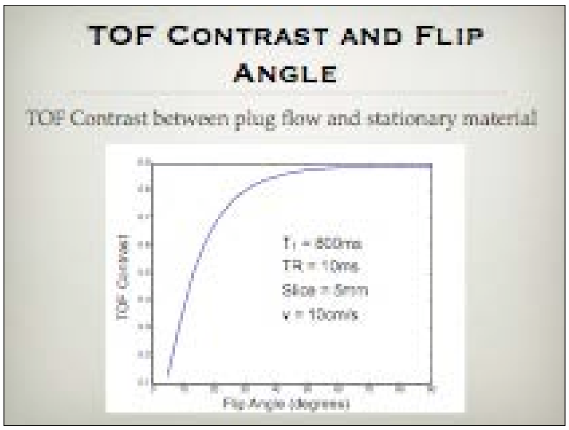
TOF Contrast and Flip Angle
TOF Contrast between plug flow and stationary material
T_1 = 800ms
TR = 10ms
Slice = 5mm
v = 10cm/s
TOF Contrast
Flip Angle (degrees)

50

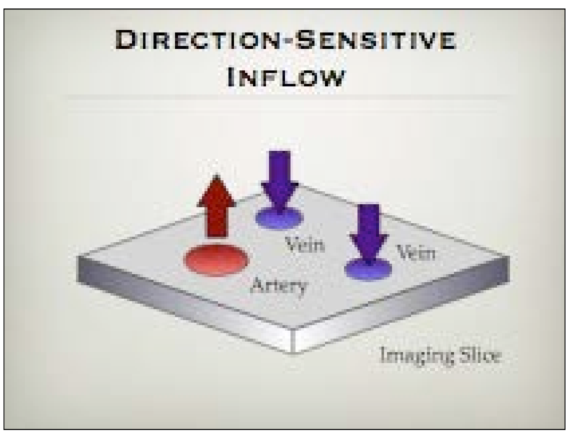
Direction-Sensitive Inflow
Vein
Vein
Artery
Imaging Slice

51

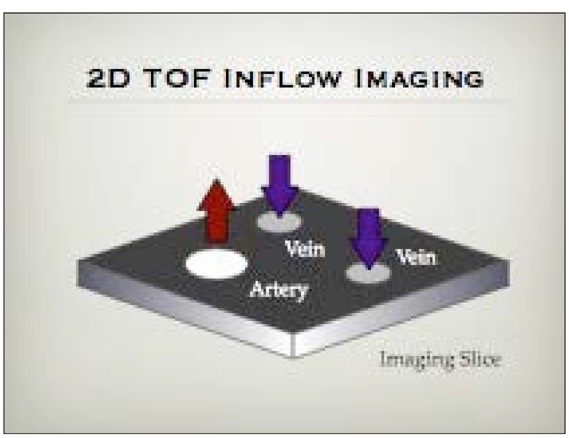
2D TOF Inflow Imaging
Vein
Vein
Artery
Imaging Slice

52

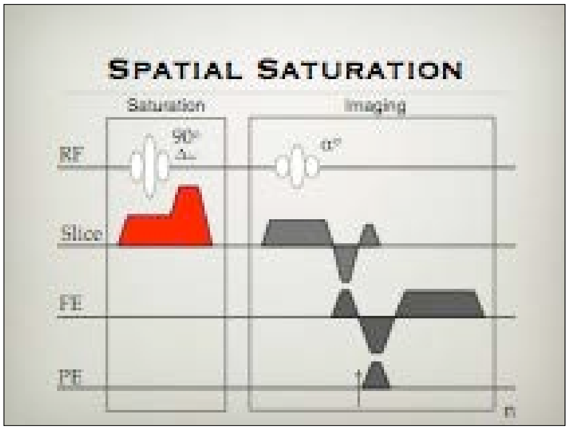
Spatial Saturation
Saturation
Imaging
90°
α°
RF
Slice
FE
PE

53

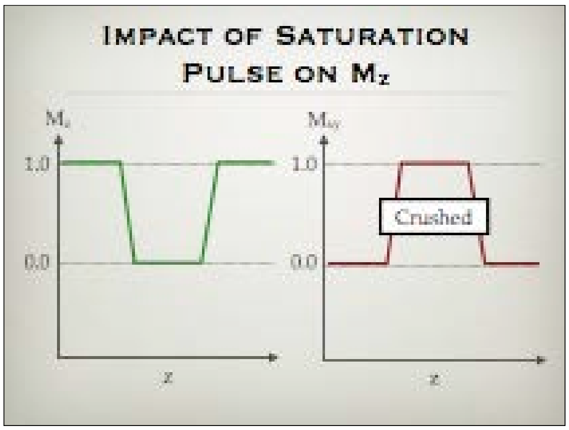
Impact of Saturation Pulse on Mz
1.0
0.0
Crushed
z

54

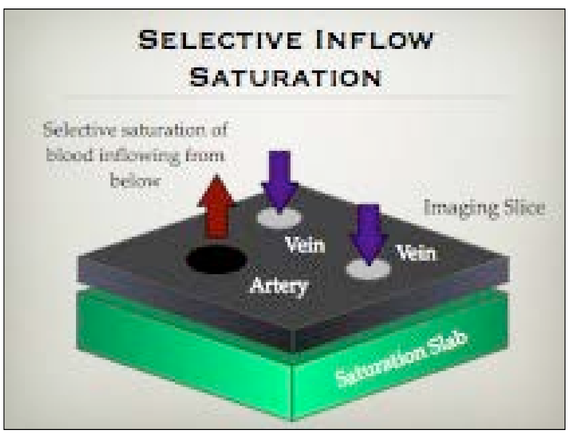
Selective Inflow Saturation
Selective saturation of blood inflowing from below
Imaging Slice
Vein
Vein
Artery
Saturation Slab

55

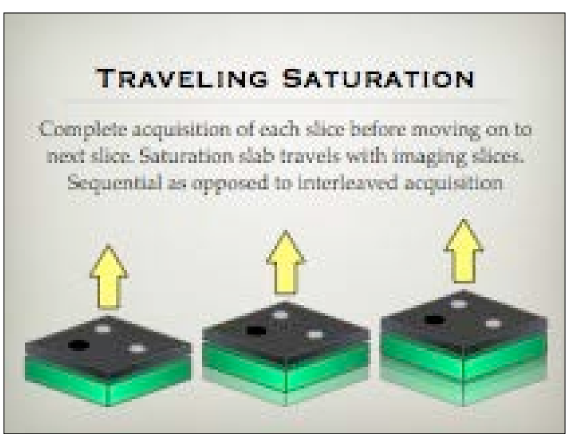
Traveling Saturation
Complete acquisition of each slice before moving on to next slice. Saturation slab travels with imaging slices. Sequential as opposed to interleaved acquisition

56

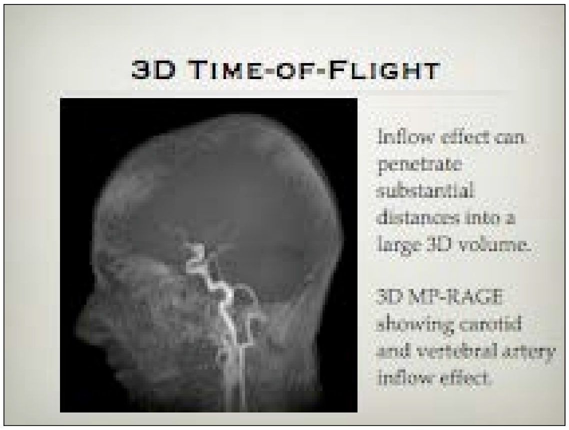
3D Time-of-Flight
Inflow effect can penetrate substantial distances into a large 3D volume.
3D MP-RAGE showing carotid and vertebral artery inflow effect.

57

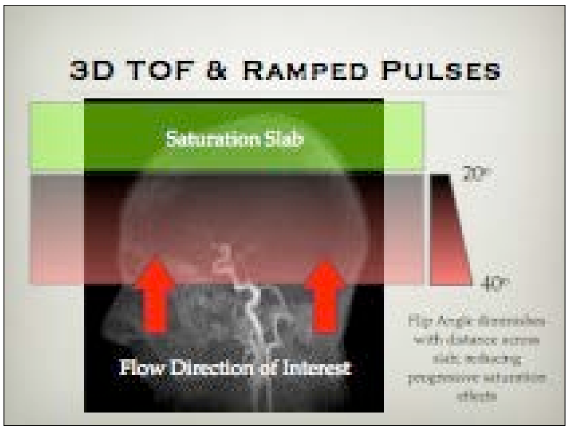
3D TOF & Ramped Pulses
Saturation Slab
20°
40°
Flow Direction of Interest

58

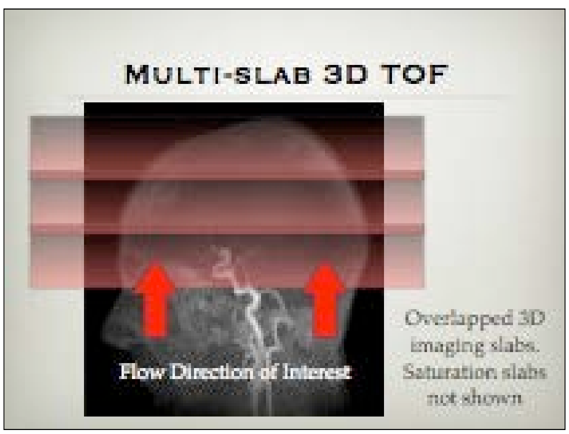
Multi-slab 3D TOF
Flow Direction of Interest
Overlapped 3D imaging slabs. Saturation slabs not shown

59

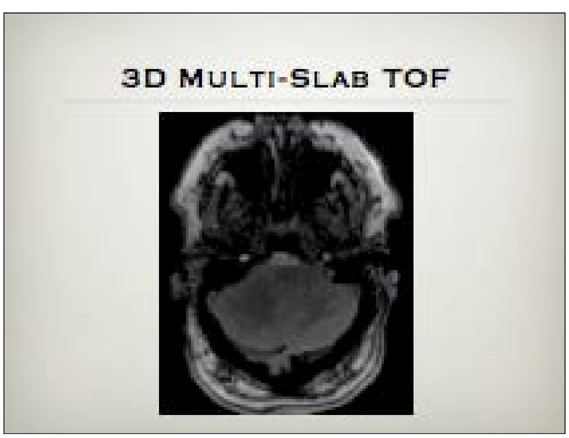
3D Multi-Slab TOF

60

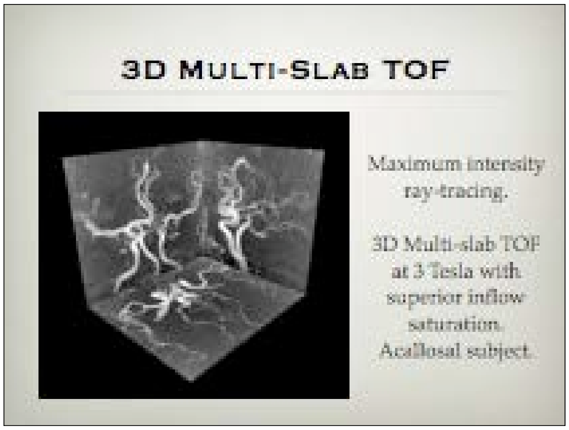
3D Multi-Slab TOF
Maximum intensity ray-tracing.
3D Multi-slab TOF at 3 Tesla with superior inflow saturation. Acallosal subject.

61

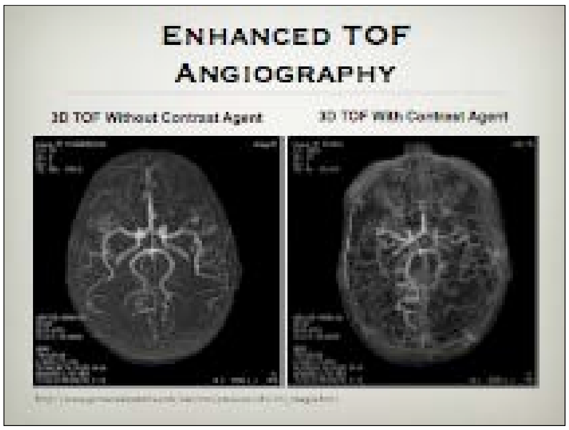
Enhanced TOF Angiography
3D TOF Without Contrast Agent
3D TOF With Contrast Agent

62

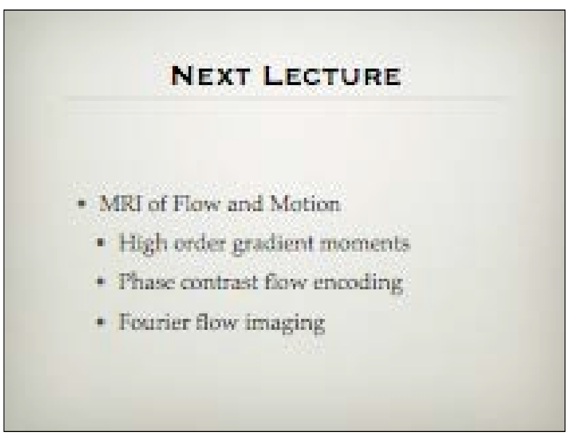
Next Lecture
MRI of Flow and Motion
High order gradient moments
Phase contrast flow encoding
Fourier flow imaging

63

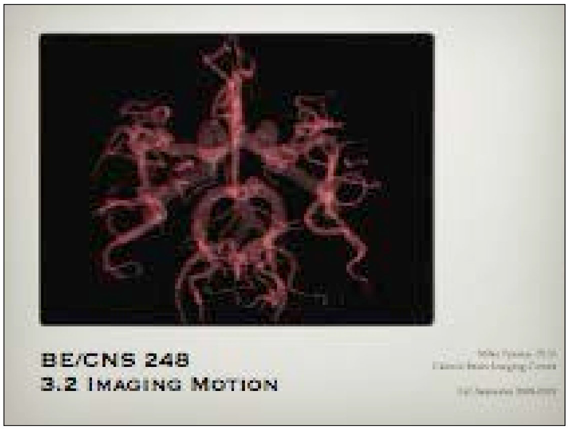
BE/CNS 248
3.2 Imaging Motion

1

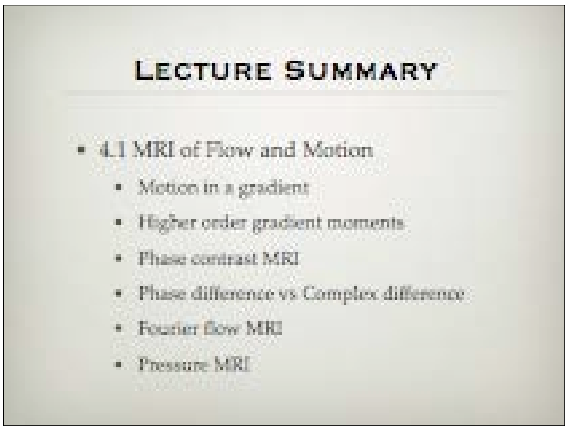
Lecture Summary
4.1 MRI of Flow and Motion
Motion in a gradient
Higher order gradient moments
Phase contrast MRI
Phase difference vs Complex difference
Fourier flow MRI
Pressure MRI

2


Motion in a Field Gradient

3

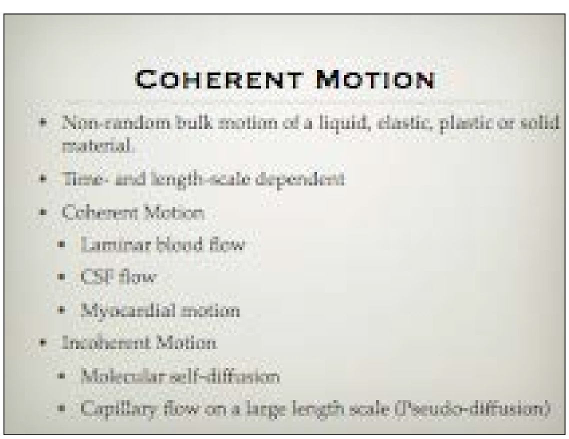
Coherent Motion
Non-random bulk motion of a liquid, elastic, plastic or solid material.
Time- and length-scale dependent
Coherent Motion
Laminar blood flow
CSF flow
Myocardial motion
Incoherent Motion
Molecular self-diffusion
Capillary flow on a large length scale (Pseudo-diffusion)

4

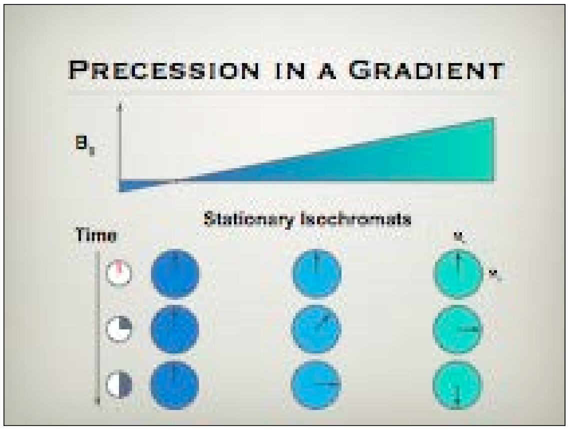

PRECESSION IN A GRADIENT
B_0
Stationary Isochromats
Time

5

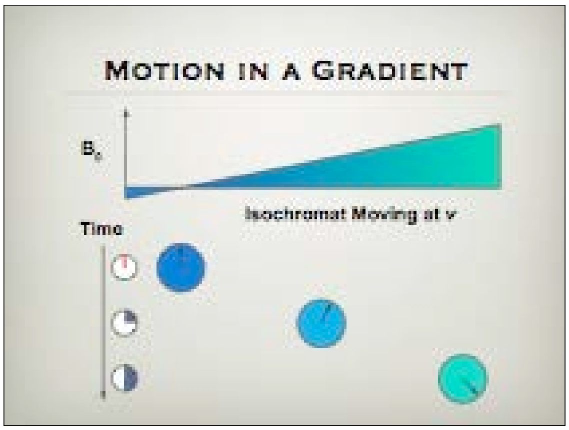

MOTION IN A GRADIENT
B_0
Isochromat Moving at v
Time

6

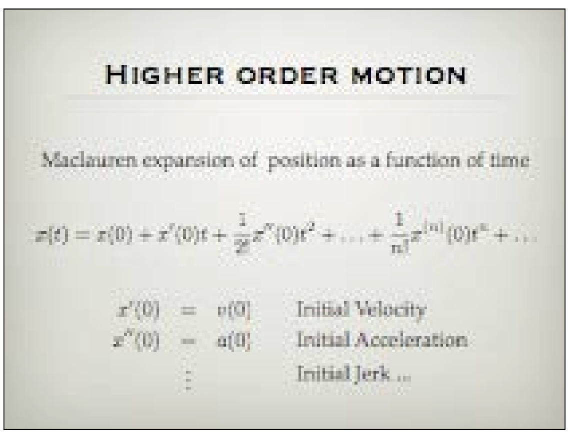

HIGHER ORDER MOTION
Maclauren expansion of position as a function of time
$x(t) = x(0) + x'(0)t + \frac{1}{2!}x''(0)t^2 + \ldots + \frac{1}{n!}x^{(n)}(0)t^n + \ldots$
$x'(0) = v(0)$ Initial Velocity
$x''(0) = a(0)$ Initial Acceleration
$\vdots$ Initial Jerk ...

7

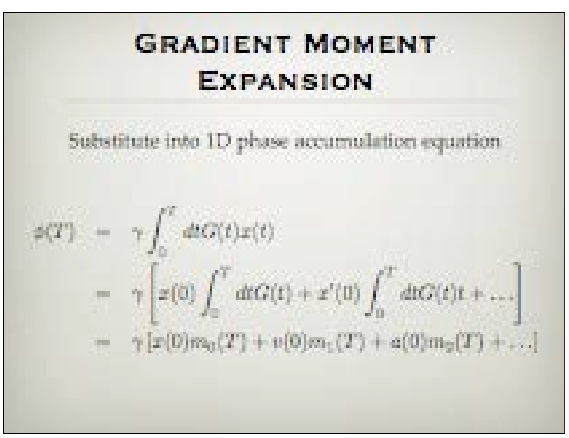

GRADIENT MOMENT EXPANSION
Substitute into 1D phase accumulation equation
$\phi(T) = \gamma \int_0^T dt G(t) x(t)$
$= \gamma \left[x(0) \int_0^T dt G(t) + x'(0) \int_0^T dt G(t) t + \ldots \right]$
$= \gamma [x(0) m_0(T) + v(0) m_1(T) + a(0) m_2(T) + \ldots]$

8

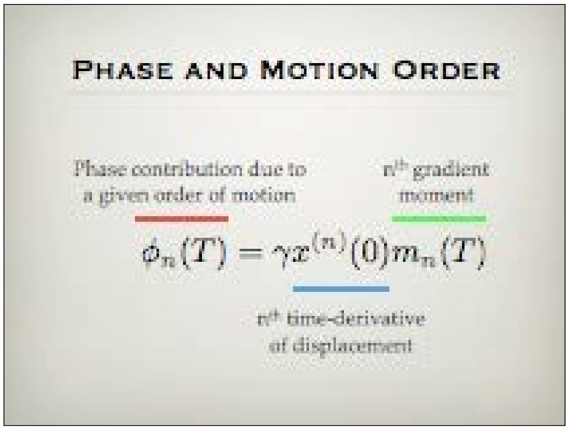

Phase and Motion Order
Phase contribution due to a given order of motion
n^{th} gradient moment
$\phi_n(T) = \gamma x^{(n)}(0) m_n(T)$
n^{th} time-derivative of displacement

9

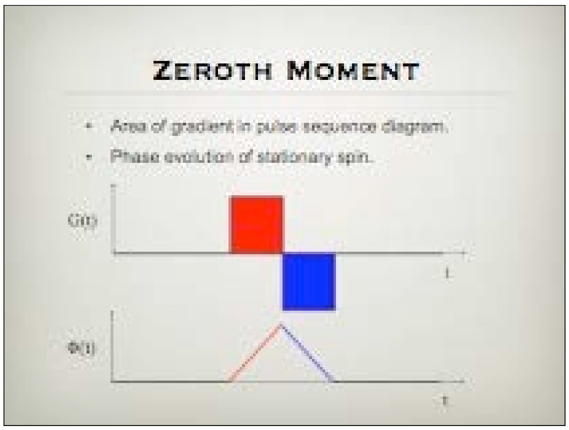

Zeroth Moment
• Area of gradient in pulse sequence diagram.
• Phase evolution of stationary spin.
G(t)
t
Φ(t)
t

10

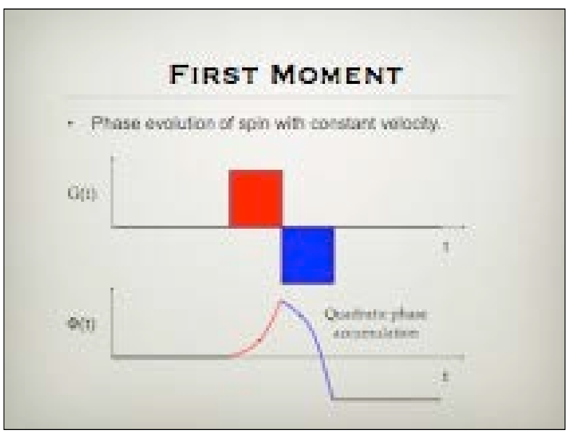

First Moment
• Phase evolution of spin with constant velocity.
G(t)
t
Φ(t)
Quadratic phase accumulation
t

11

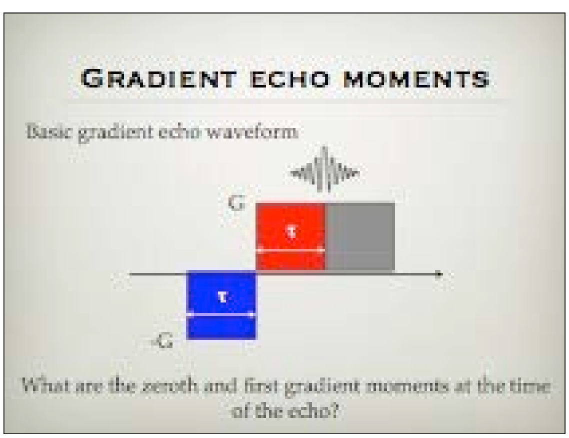

Gradient echo moments
Basic gradient echo waveform
G
τ
τ
-G
What are the zeroth and first gradient moments at the time of the echo?

12

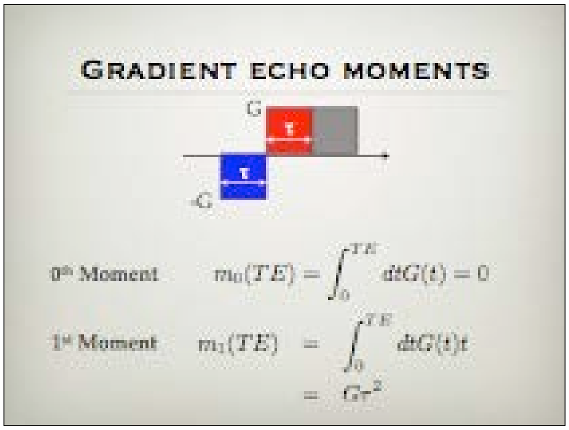
Gradient echo moments
G
τ
τ
-G
0th Moment $m_0(TE) = \int_0^{TE} dtG(t) = 0$
1st Moment $m_1(TE) = \int_0^{TE} dtG(t)t$
$= G\tau^2$

13


Flow Compensation

14

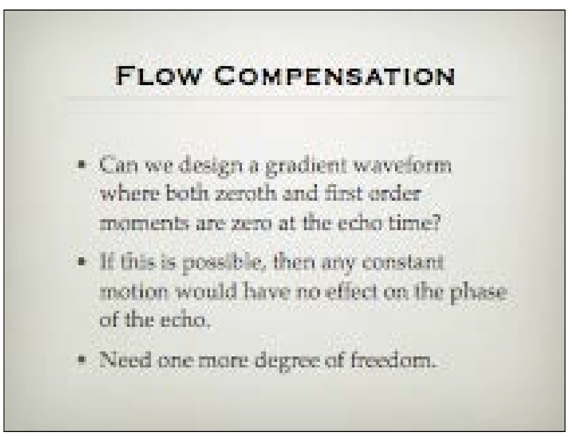
Flow Compensation
• Can we design a gradient waveform where both zeroth and first order moments are zero at the echo time?
• If this is possible, then any constant motion would have no effect on the phase of the echo.
• Need one more degree of freedom.

15

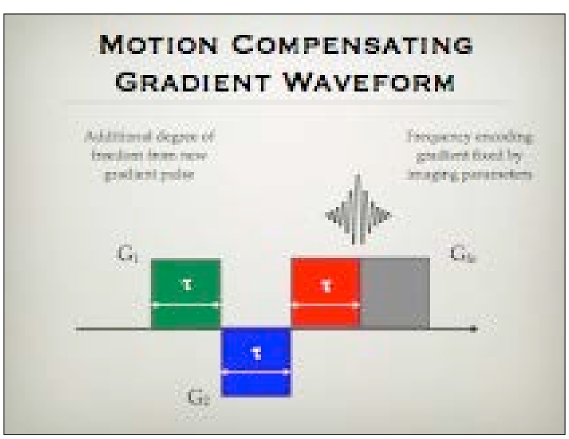
Motion Compensating Gradient Waveform
Additional degree of freedom from new gradient pulse
Frequency encoding gradient fixed by imaging parameters
G_1
G_2
τ
τ
τ

16

Moment Equations

Gradient echo with equal duration gradient pulses

$$
\begin{aligned}
m_0(TE) &= \tau(G_1 + G_2 + G_{fe}) \\
m_1(TE) &= \frac{1}{2}\tau^2(G_1 + 3G_2 + 5G_{fe})
\end{aligned}
$$

17

Motion Compensation Solution

$m_0(TE) = m_1(TE) = 0$

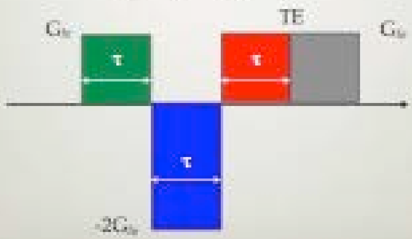

18

Even Echo Flow Compensation

First moment nulled intrinsically for even echos in both gradient and spin echo trains

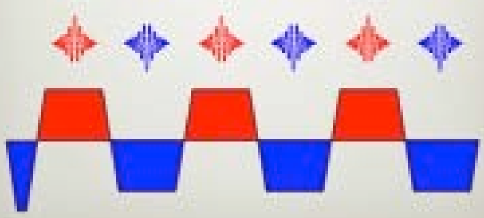

19

Flow Compensated Slice Selection and Phase Encoding

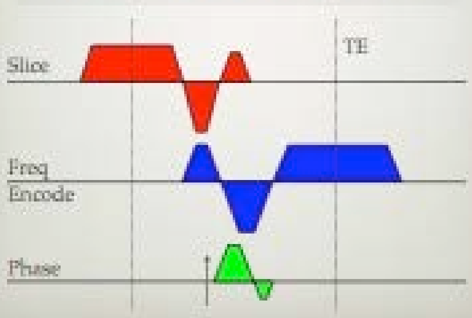

20

Flow Encoding

21

Phase Encoding of Flow

- Can a gradient waveform be designed that gives the echo a phase proportional to velocity in a given direction?
- Requires that zeroth moment is zero and first moment is finite at the echo time.
- More convenient still to have independent control over first moment.

22

Biopolar Flow Encoding Pulses

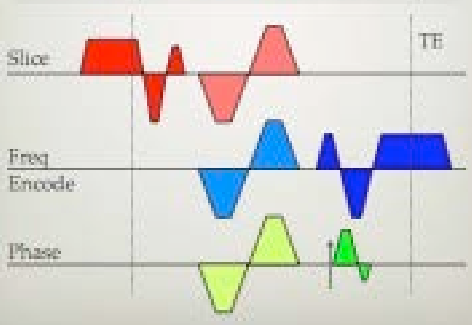

23

Background Phase

- The voxel phase without velocity encoding cannot be assumed to be zero.
- Many contributions to background phase:
  - B_0 inhomogeneity
  - Gradient eddy currents
  - Other orders of motion
  - Deliberate offsetting of echo position
  - ...

24

Removing Background Phase

General velocity encoded magnetization

$$\tilde{\rho} = \rho_0 e^{i(\phi_b + \phi_v)}$$

Acquire two images with opposite sign bipolar gradient pulses

$$\tilde{\rho}_\pm = \rho_0 e^{i(\phi_b \pm \phi_v)}$$

$$\phi_v = \frac{1}{2}(\angle\tilde{\rho}_+ - \angle\tilde{\rho}_-)$$

25

Phase Difference

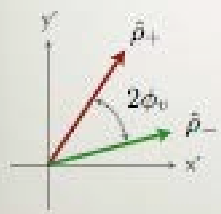

Difference in phase of transverse magnetization between positive and negative velocity encoded acquisitions.

26

Principle of Phase Contrast

Background phase arises from B_0 inhomogeneities, echo timing offsets, eddy currents, Maxwell terms, ...

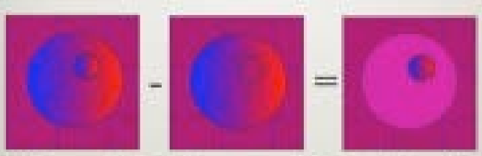

Velocity encoded through plane | Velocity compensated reference | Corrected phase velocity image

27

Encoding Schemes

6 Point Scheme | 4 Point Scheme

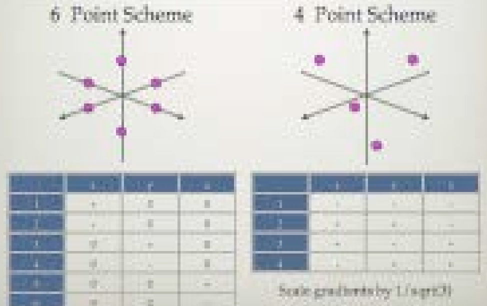

Scale gradients by 1/sqrt(3)

28

Recovering Velocity from 4-point Encoding

Use linear combinations of the voxel phase from each acquisition. For example, for the phase encoded z-component of velocity:

$$\phi_z = \frac{1}{2}\left[(\phi_3 + \phi_4) - (\phi_1 + \phi_2)\right]$$

29

Aliasing Velocity : VENC

Phase is modulo 2π so we expect to see phase aliasing if the velocity exceeds a certain value.
This critical velocity is called the encoding velocity or V_{enc}

$$V_{enc} = \frac{\pi}{\gamma m_1(TE)}$$

30

Phase Unwrapping

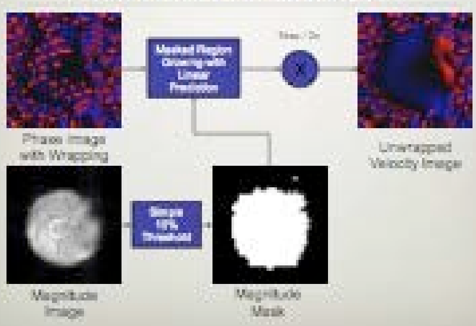

31

Velocity Imaging

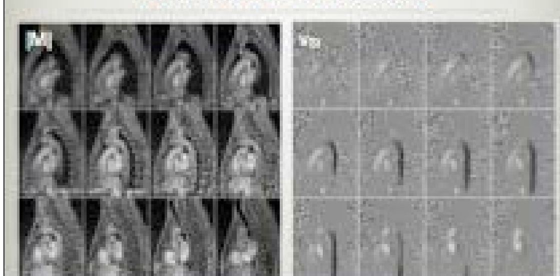

32

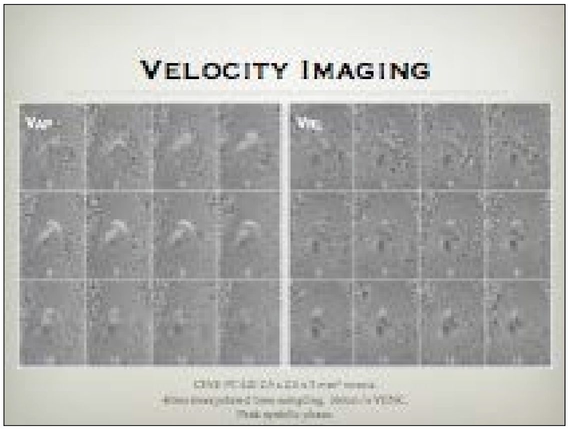

VELOCITY IMAGING

33

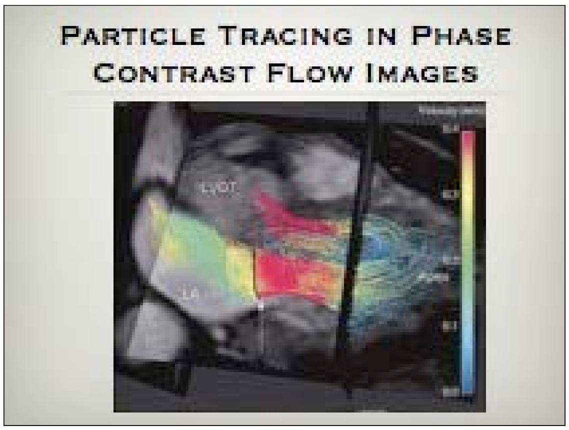

PARTICLE TRACING IN PHASE CONTRAST FLOW IMAGES
LVOT
LA

34

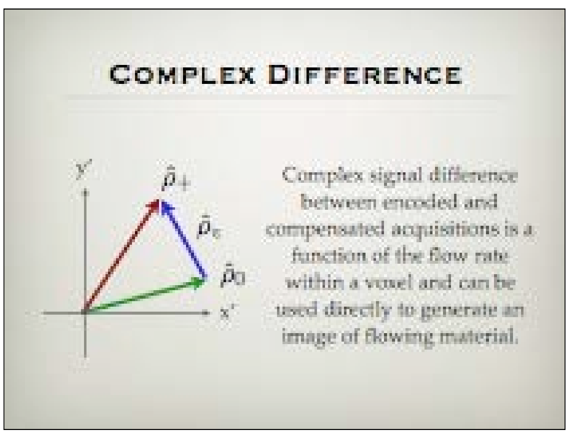

COMPLEX DIFFERENCE
y'
x'
Complex signal difference between encoded and compensated acquisitions is a function of the flow rate within a voxel and can be used directly to generate an image of flowing material.

35

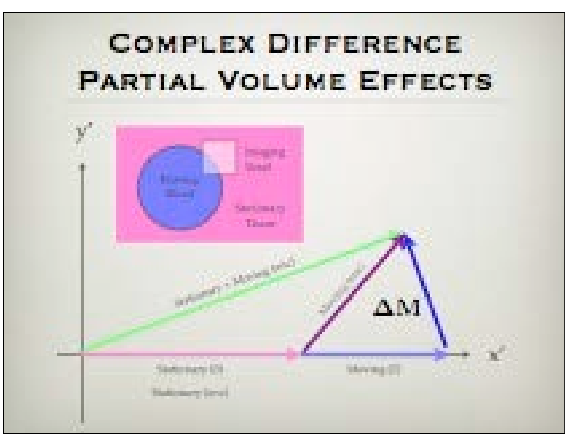

COMPLEX DIFFERENCE
PARTIAL VOLUME EFFECTS
y'
ΔM
x'

36

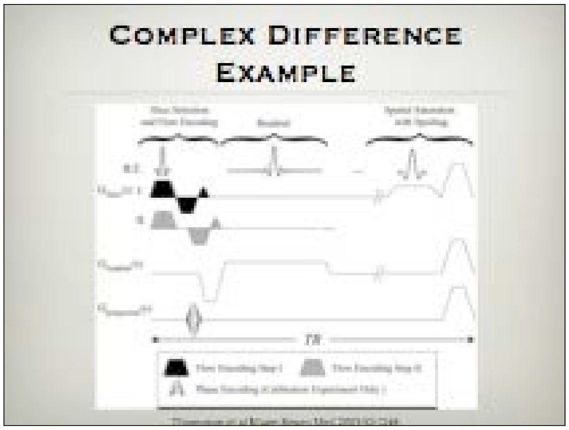
COMPLEX DIFFERENCE EXAMPLE

37

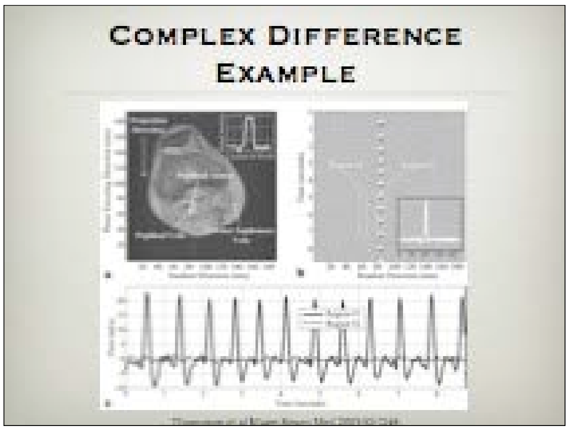
COMPLEX DIFFERENCE EXAMPLE

38


TIME-RESOLVED FLOW MEASUREMENT

39

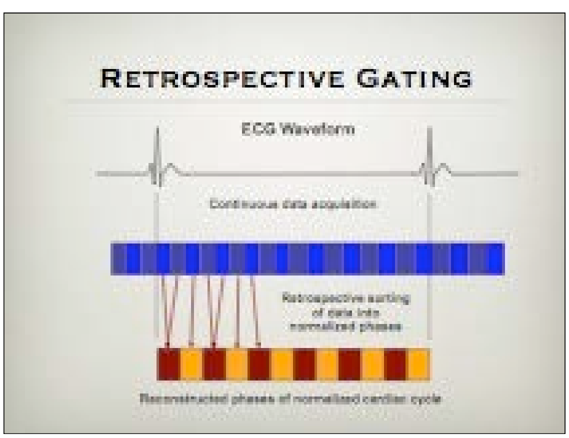
RETROSPECTIVE GATING
ECG Waveform
Continuous data acquisition
Retrospective sorting of data into normalized phases
Reconstructed phases of normalized cardiac cycle

40

Retrospectively Gated Phase Contrast MRI

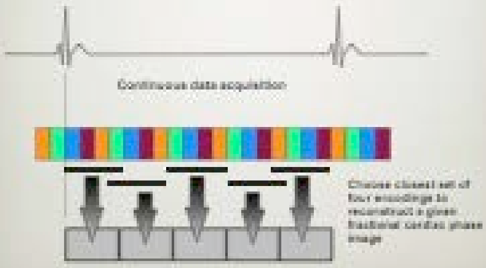

41

3D Phase Contrast CINE

SI Flow AP Flow

42

Real-time Velocity MRI

Spiral MRI with compensated and encoded acquisitions at 18 fps

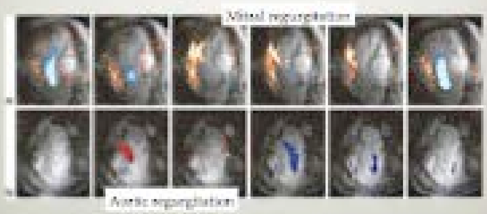

43

New velocity Dimension

Compare phase encoding of displacement

$$S(x) = \int_{-\infty}^{\infty} dt S(0) e^{-ik_x x}$$

with phase encoding of velocity

$$S(v) = \int_{-\infty}^{\infty} dt S(0) e^{-iq_z v_z}$$

44

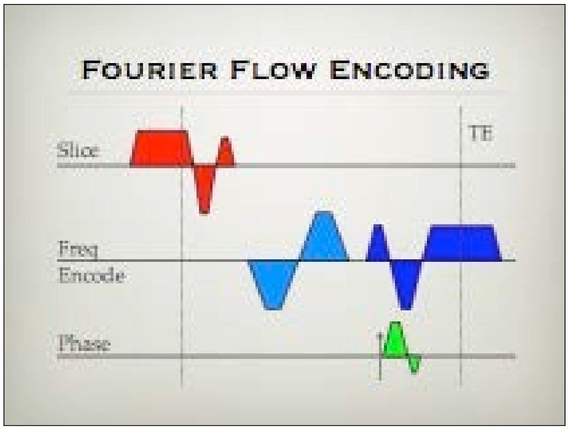
Fourier Flow Encoding
Slice
TE
Freq
Encode
Phase

45

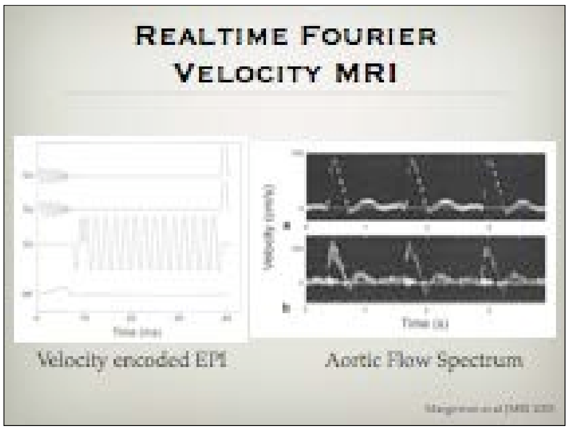
Realtime Fourier
Velocity MRI
Velocity (cm/s)
Time (s)
Velocity encoded EPI
Aortic Flow Spectrum

46

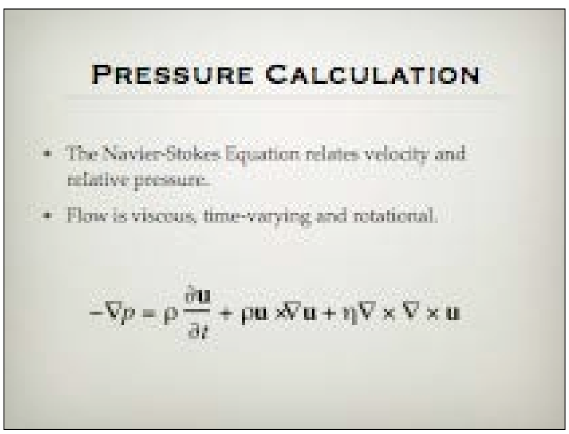
Pressure Calculation
The Navier-Stokes Equation relates velocity and relative pressure.
Flow is viscous, time-varying and rotational.
$-\nabla p = \rho \frac{\partial \mathbf{u}}{\partial t} + \rho \mathbf{u} \cdot \nabla \mathbf{u} + \eta \nabla \times \nabla \times \mathbf{u}$

47

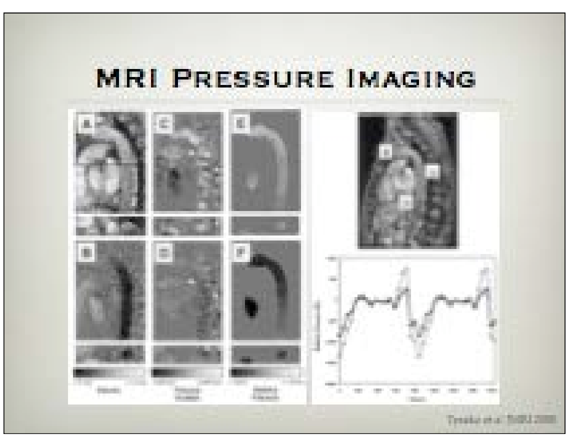
MRI Pressure Imaging

48

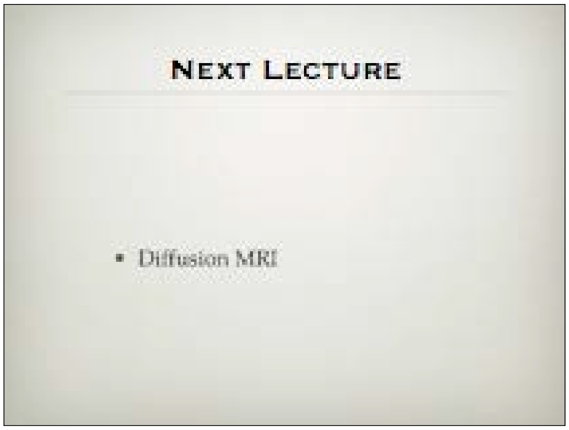

49

BE/CNS 248
4.1 DIFFUSION MRI

1

LECTURE SUMMARY

- 5.1 Diffusion MRI
  - Molecular Self-Diffusion
  - Random-walk and the Einstein Equation
  - Stejskal-Tanner Experiment
  - Apparent Diffusion Coefficient
  - Restricted and Hindered Diffusion
  - The Diffusion Tensor Model
  - Diffusion Tensor Imaging

2

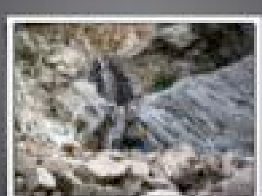

MOLECULAR SELF-DIFFUSION

3

DIFFUSION

4

Einstein Diffusion Equation

1D Diffusion

Diffusion Coefficient, Concentration

$$\frac{\partial C}{\partial t} = D\frac{\partial^2 C}{\partial x^2}$$

3D Diffusion

$$\frac{\partial C}{\partial t} = D\nabla^2 C$$

5

Diffusion Equation Solutions

The 1D spatial concentration distribution is a time-evolving normalized Gaussian

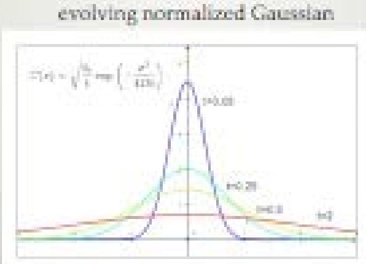

6

Mean Square Displacement

RMS displacement of a molecule

$$\langle x \rangle = 0$$

1D Diffusion $\langle x^2 \rangle = 2Dt$

3D Diffusion $\langle x^2 \rangle = 6Dt$

7

Stejskal-Tanner (PGSE) Experiment

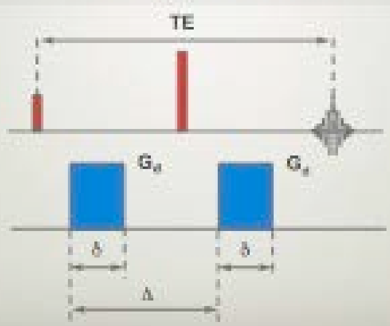

8

Signal Attenuation by Diffusion

Incoherent molecular self-diffusion in a gradient causes dephasing of transverse magnetization

1D Gaussian Diffusion

$$S(b) = S(0)e^{-bD}$$

Where b is a measure of the diffusion weighting generated by the balanced gradient pulses

Ideal Diffusion Attenuation

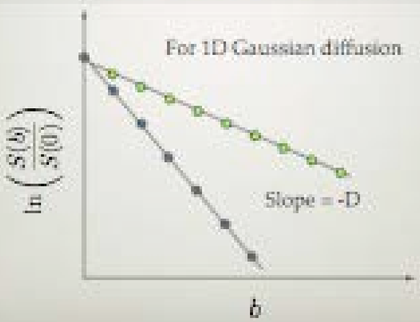

The b-factor

The b-factor can be calculated from the k-space trajectory:

$$b_x(T) = \int_0^T dt\,|\gamma k_x(t)|^2$$

b-factor for Stejskal-Tanner

$$b(TE) = (\gamma G\delta)^2\left(\Delta - \frac{\delta}{3}\right)$$

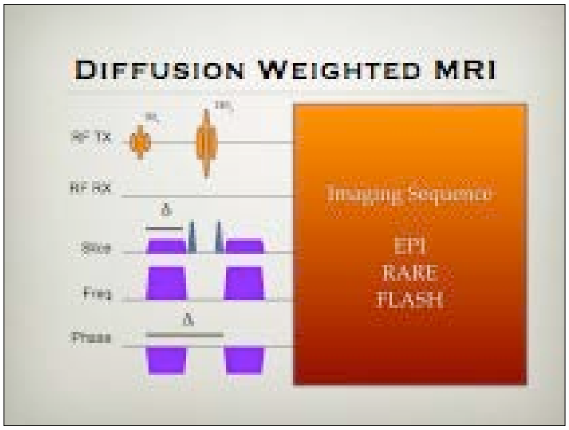
DIFFUSION WEIGHTED MRI
RF TX
RF RX
δ
Slice
Freq
Δ
Phase
Imaging Sequence
EPI
RARE
FLASH

13

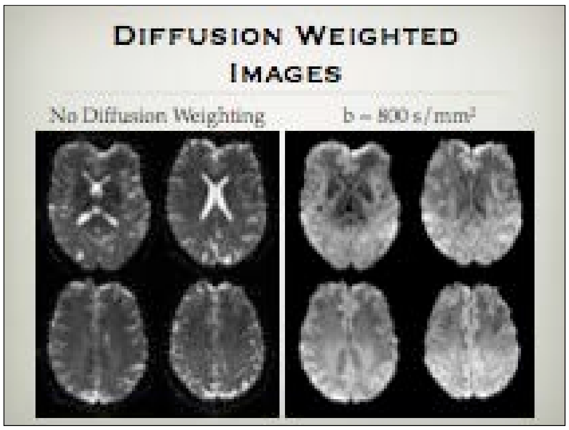
DIFFUSION WEIGHTED IMAGES
No Diffusion Weighting
b = 800 s/mm²

14

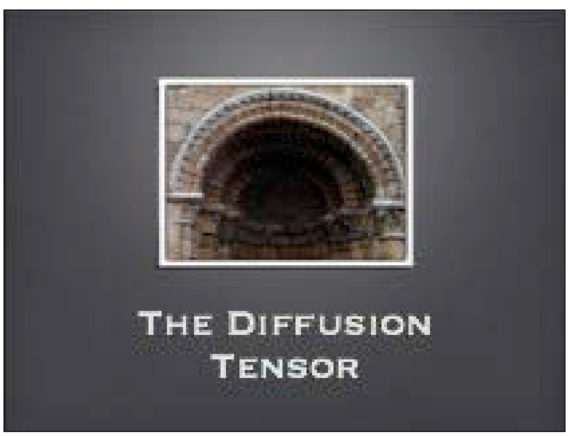
THE DIFFUSION TENSOR

15

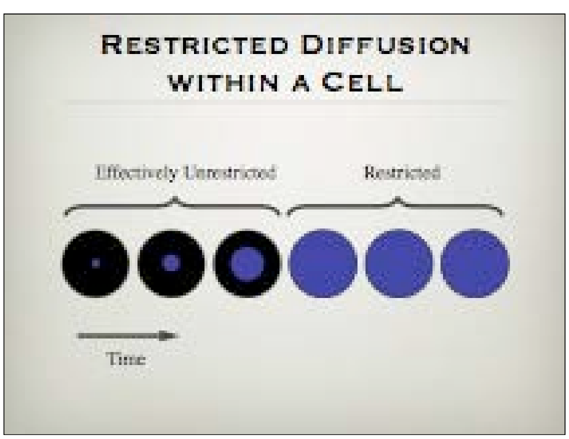
RESTRICTED DIFFUSION WITHIN A CELL
Effectively Unrestricted
Restricted
Time

16

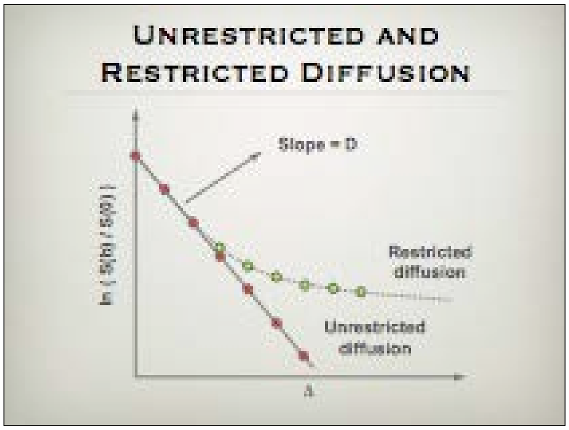

Unrestricted and Restricted Diffusion
Slope = D
ln (S(b) / S(0))
Restricted diffusion
Unrestricted diffusion
Δ

17

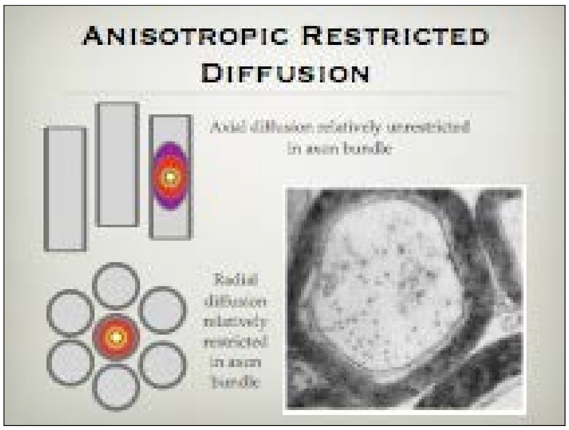

Anisotropic Restricted Diffusion
Axial diffusion relatively unrestricted in axon bundle
Radial diffusion relatively restricted in axon bundle

18

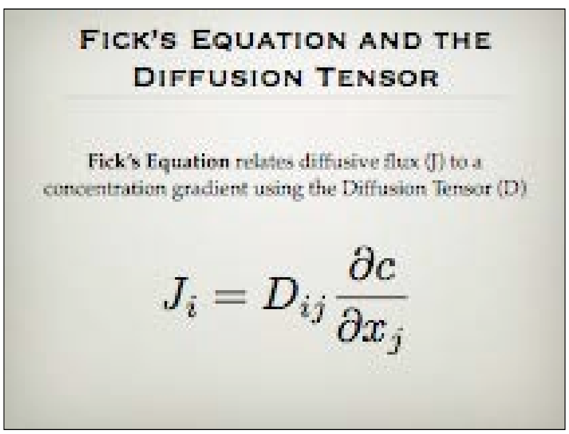

Fick's Equation and the Diffusion Tensor
Fick's Equation relates diffusive flux (J) to a concentration gradient using the Diffusion Tensor (D)
$$J_i = D_{ij} \frac{\partial c}{\partial x_j}$$

19

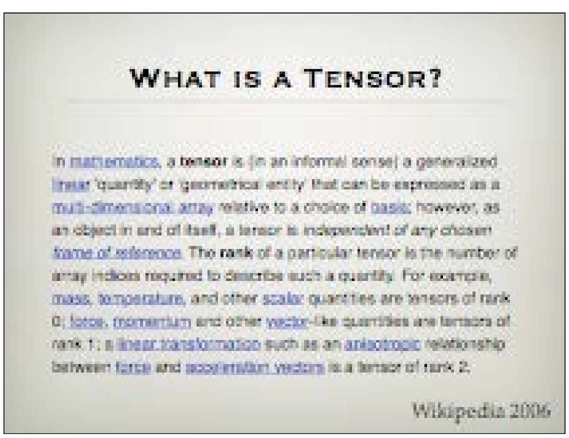

What is a Tensor?
In mathematics, a tensor is (in an informal sense) a generalized linear 'quantity' or 'geometrical entity' that can be expressed as a multi-dimensional array relative to a choice of basis; however, as an object in and of itself, a tensor is independent of any chosen frame of reference. The rank of a particular tensor is the number of array indices required to describe such a quantity. For example, mass, temperature, and other scalar quantities are tensors of rank 0; force, momentum and other vector-like quantities are tensors of rank 1; a linear transformation such as an anisotropic relationship between force and acceleration vectors is a tensor of rank 2.
Wikipedia 2006

20

Properties of the Diffusion tensor

D is an upper triangle symmetric, positive definite second rank tensor ⇒ six unknowns

$$\mathbf{D} = \begin{pmatrix} D_{11} & D_{12} & D_{13} \\ D_{12} & D_{22} & D_{23} \\ D_{13} & D_{23} & D_{33} \end{pmatrix}$$

D has three orthogonal positive eigenvectors with corresponding eigenvalues

$$\mathbf{D}e_i = \lambda_i e_i \qquad i = 1, 2, 3$$

21

Diffusion Weighted Images for DTI

- Diffusion tensor has six unknowns
- At least six diffusion weighted images
- Diffusion gradient directions sample directional space
- Encoding directions cannot be co-linear
- Additional image with minimal b-value used to eliminate all other weightings (T1, T2, ...)

22

The b-matrix

More generally, for DTI we need to calculate the b-matrix which includes cross terms between the gradient axes.

$$b_{ij}(T) = \gamma^2 \int_0^T dt\, k_i(t) k_j(t)$$

$$S(b_{ij}) = S(0) \exp\left(- \sum_{i=1}^{3} \sum_{j=1}^{3} b_{ij} D_{ij} \right)$$

23

Analytical b-Matrices

Ideal rectangular pulses

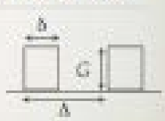

$$b_{ij} = \gamma^2 G_i G_j \delta^2 \left(\Delta - \frac{1}{3}\delta \right)$$

Trapezoidal pulses

$$b_{ij} = \gamma^2 G_i G_j \left[\delta^2 \left(\Delta - \frac{1}{3}\delta \right) + \frac{1}{30}\epsilon^3 - \frac{1}{6}\delta\epsilon^2 \right]$$

24

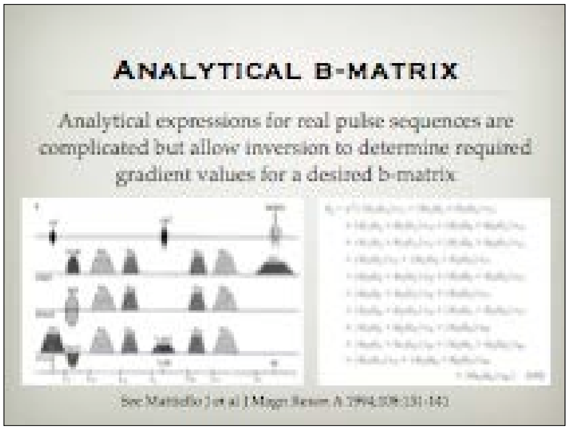
ANALYTICAL B-MATRIX
Analytical expressions for real pulse sequences are complicated but allow inversion to determine required gradient values for a desired b-matrix
See Mattiello J et al J Magn Reson A 1994;108:131-141

25

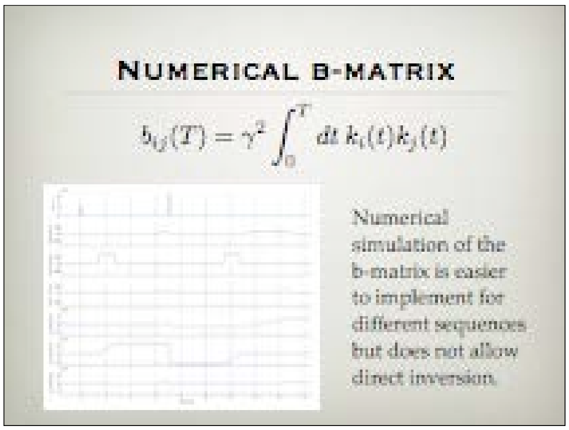
NUMERICAL B-MATRIX
$b_{ij}(T) = \gamma^2 \int_0^T dt\, k_i(t) k_j(t)$
Numerical simulation of the b-matrix is easier to implement for different sequences but does not allow direct inversion.

26

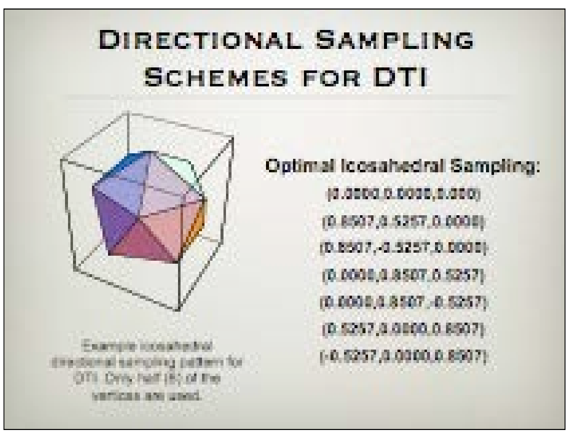
DIRECTIONAL SAMPLING SCHEMES FOR DTI
Optimal Icosahedral Sampling:
(0.0000,0.0000,0.000)
(0.8507,0.5257,0.0000)
(0.8507,-0.5257,0.0000)
(0.0000,0.8507,0.5257)
(0.0000,0.8507,-0.5257)
(0.5257,0.0000,0.8507)
(-0.5257,0.0000,0.8507)
Example icosahedral directional sampling pattern for DTI. Only half (6) of the vertices are used.

27

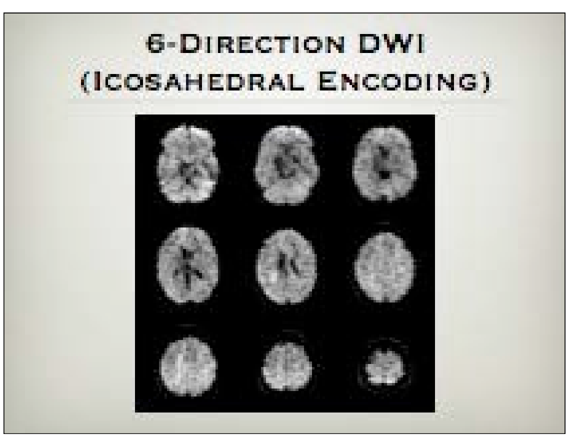
6-DIRECTION DWI (ICOSAHEDRAL ENCODING)

28

From DWIs to DTI

Reference image (no DW) $S(0)$

Diffusion weighted images $S(b_{ij})$

$$\log\left(\frac{S(b_{ij})}{S(0)}\right) = \sum_{i=1}^{3}\sum_{j=1}^{3} b_{ij} D_{ij}$$

29

Solving for the Tensor

Recast as a matrix equation

$$\mathbf{s} = \mathbf{B}\mathbf{d}$$

$$-\begin{pmatrix} \log S(\mathbf{b}_1) \\ \log S(\mathbf{b}_2) \\ \vdots \\ \log S(\mathbf{b}_n) \end{pmatrix} = \begin{pmatrix} b_{11,1} & b_{12,1} & b_{13,1} & b_{22,1} & b_{23,1} & b_{33,1} & 1 \\ b_{11,2} & b_{12,2} & b_{13,2} & b_{22,2} & b_{23,2} & b_{33,2} & 1 \\ & & & \vdots & & & \\ b_{11,n} & b_{12,n} & b_{13,n} & b_{22,n} & b_{23,n} & b_{33,n} & 1 \end{pmatrix} \begin{pmatrix} D_{11} \\ D_{12} \\ D_{13} \\ D_{22} \\ D_{23} \\ D_{33} \\ -\log S(0) \end{pmatrix}$$

Solve using the Moore-Penrose pseudo inverse

$$\mathbf{d} = \mathbf{B}^{+}\mathbf{s}$$

30

DT Model of Restricted, Anisotropic Diffusion

Actual Diffusion Restriction

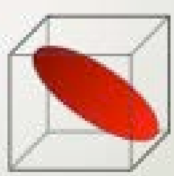

Tensor Model

31

Diffusion Tensor Ellipsoids

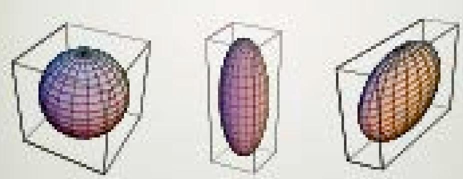

Orientation and length of ellipsoid axes correspond to eigenvectors and eigenvalues of the diffusion tensor.

32

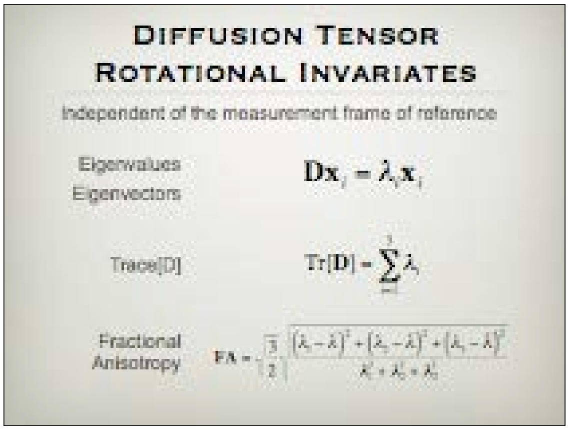

DIFFUSION TENSOR ROTATIONAL INVARIATES
Independent of the measurement frame of reference
Eigenvalues
Eigenvectors
$\mathbf{D}\mathbf{x}_i = \lambda_i \mathbf{x}_i$
Trace[D]
$\mathrm{Tr}[\mathbf{D}] = \sum_{i=1}^{3} \lambda_i$
Fractional Anisotropy
$\mathrm{FA} = \sqrt{\frac{3}{2}} \sqrt{\frac{(\lambda_1-\bar{\lambda})^2+(\lambda_2-\bar{\lambda})^2+(\lambda_3-\bar{\lambda})^2}{\lambda_1^2+\lambda_2^2+\lambda_3^2}}$

33

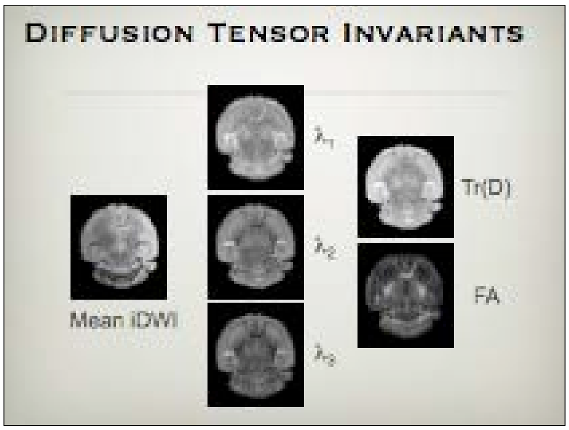

DIFFUSION TENSOR INVARIANTS
λ_1
λ_2
λ_3
Tr(D)
FA
Mean iDWI

34

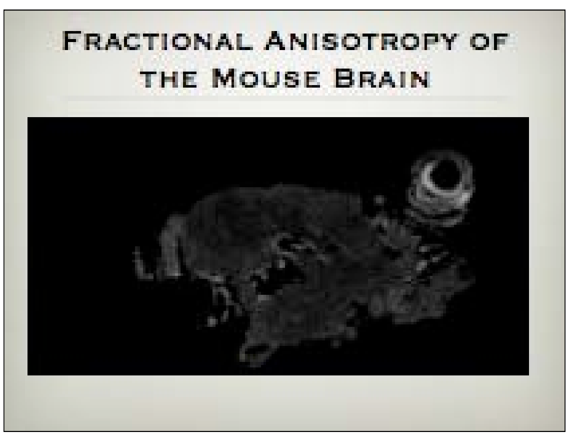

FRACTIONAL ANISOTROPY OF THE MOUSE BRAIN

35

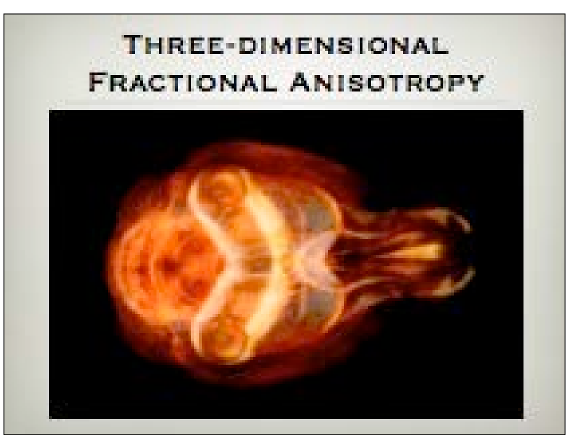

THREE-DIMENSIONAL FRACTIONAL ANISOTROPY

36

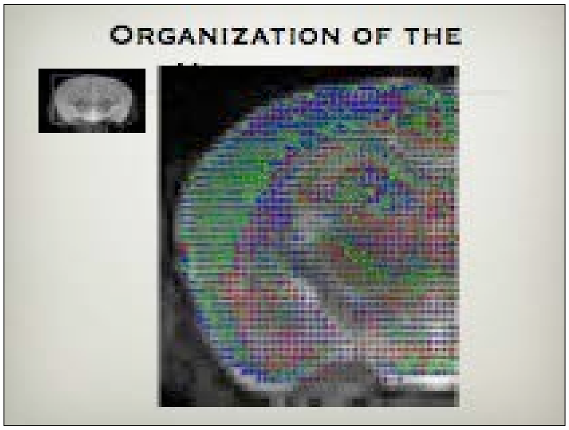
ORGANIZATION OF THE

37

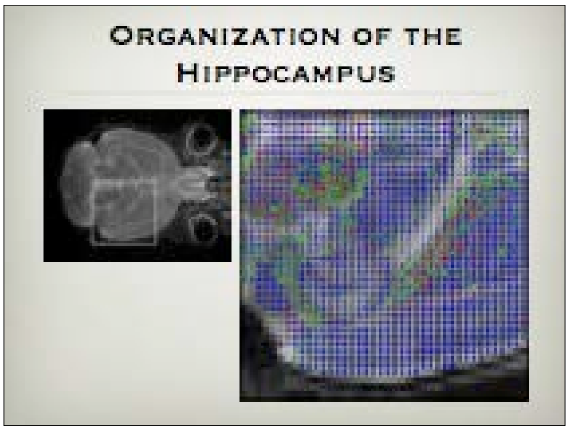
ORGANIZATION OF THE
HIPPOCAMPUS

38

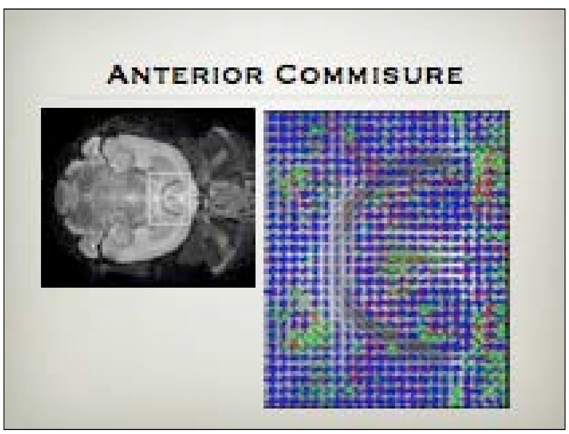
ANTERIOR COMMISURE

39

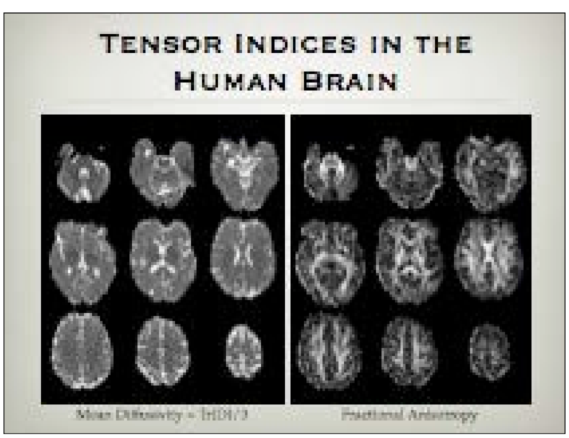
TENSOR INDICES IN THE
HUMAN BRAIN

40

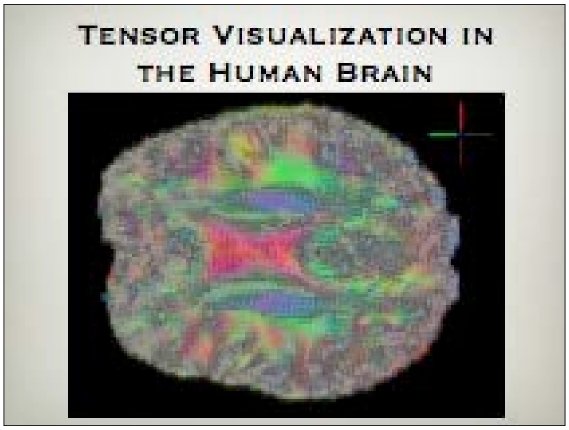
TENSOR VISUALIZATION IN
THE HUMAN BRAIN

41

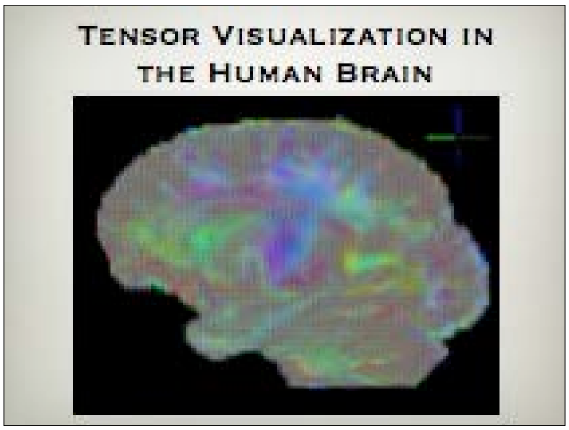
TENSOR VISUALIZATION IN
THE HUMAN BRAIN

42

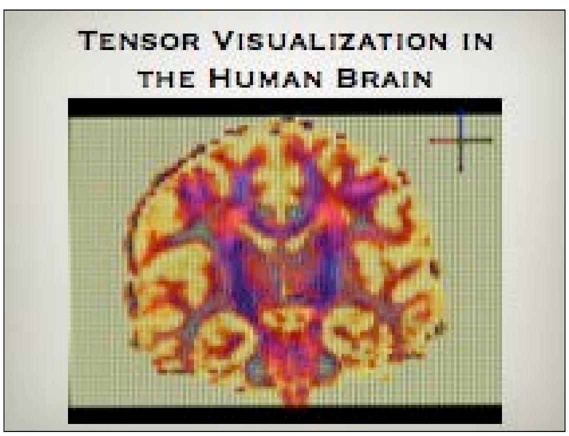
TENSOR VISUALIZATION IN
THE HUMAN BRAIN

43

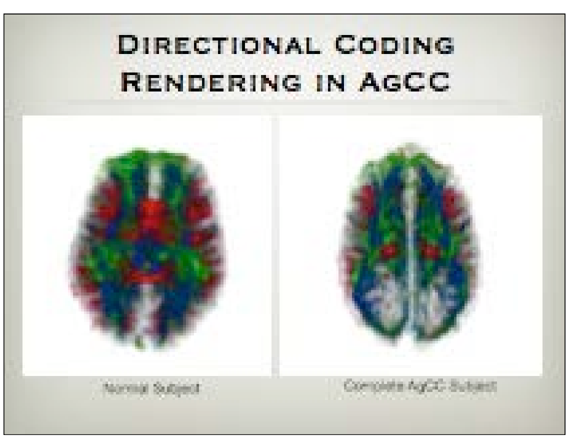
DIRECTIONAL CODING
RENDERING IN AGCC
Normal Subject
Complete AgCC Subject

44

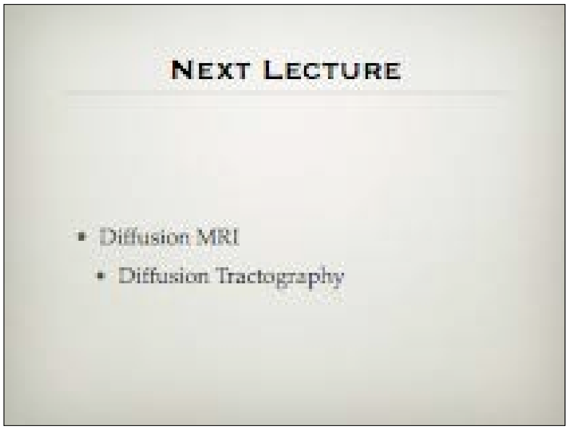

45

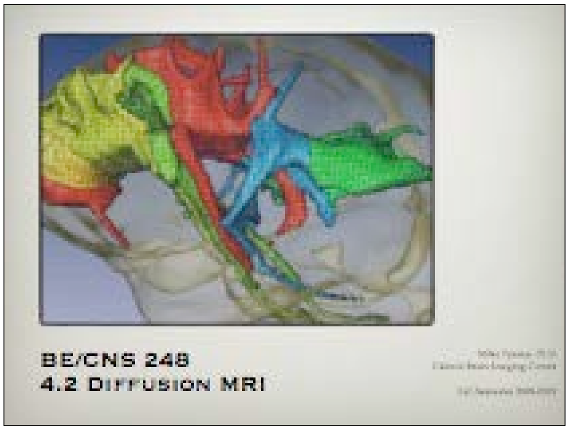
BE/CNS 248
4.2 Diffusion MRI

1


Lecture Summary
5.2 Diffusion MRI
Clinical Applications of DTI
DTI Tract Tracing Methods
Limitations of Deterministic Fiber Tracking
Probabilistic Fiber Tracking
HARDI and the ODF
Q-space
Q-ball Imaging

2

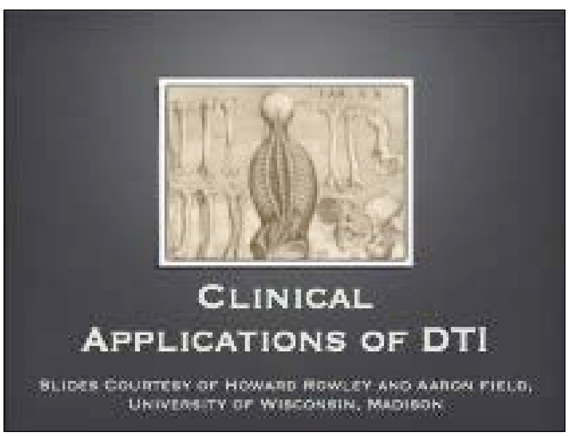
Clinical Applications of DTI
Slides courtesy of Howard Rowley and Aaron Field, University of Wisconsin, Madison

3

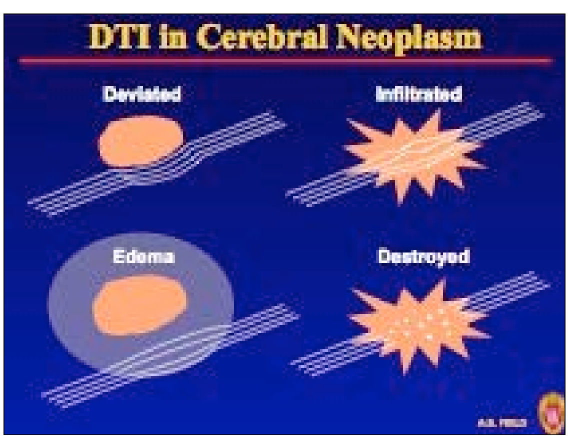
DTI in Cerebral Neoplasm
Deviated
Infiltrated
Edema
Destroyed

4

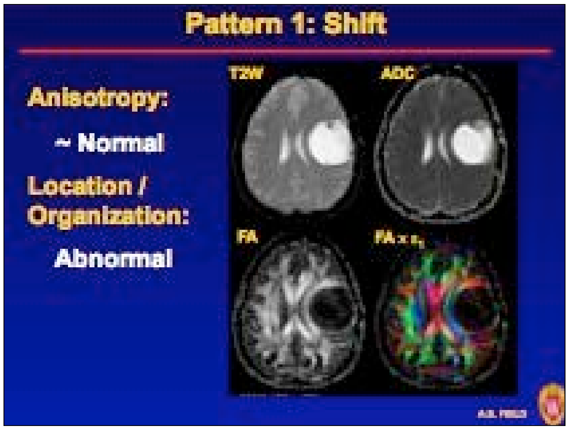

Pattern 1: Shift
Anisotropy:
~ Normal
Location / Organization:
Abnormal
T2W
ADC
FA

5

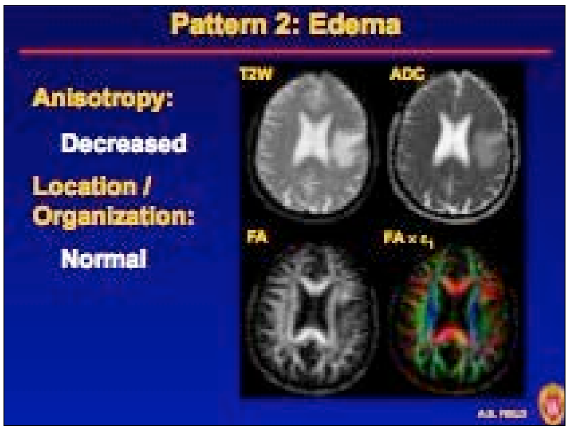

Pattern 2: Edema
Anisotropy:
Decreased
Location / Organization:
Normal
T2W
ADC
FA

6

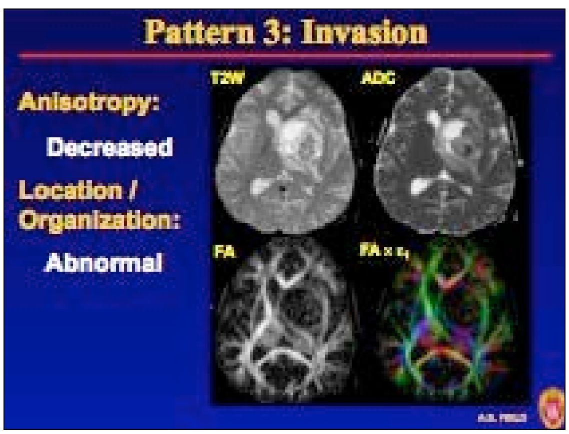

Pattern 3: Invasion
Anisotropy:
Decreased
Location / Organization:
Abnormal
T2W
ADC
FA

7

Pattern 4: Destruction
T2W
ADC
FA
Anisotropy: ~ 0
Location / Organization: ??

8

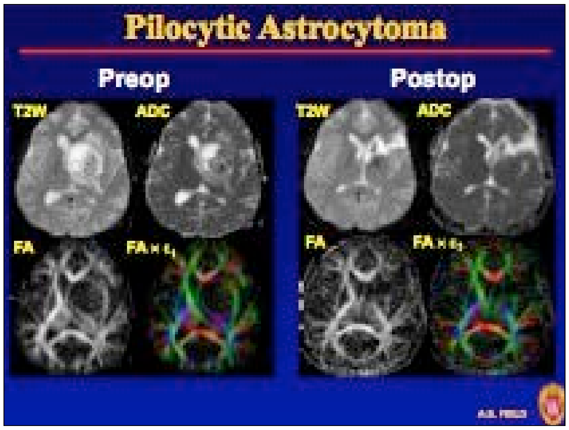

Pilocytic Astrocytoma
Preop
Postop
T2W
ADC
FA

9

TRACT TRACING

10

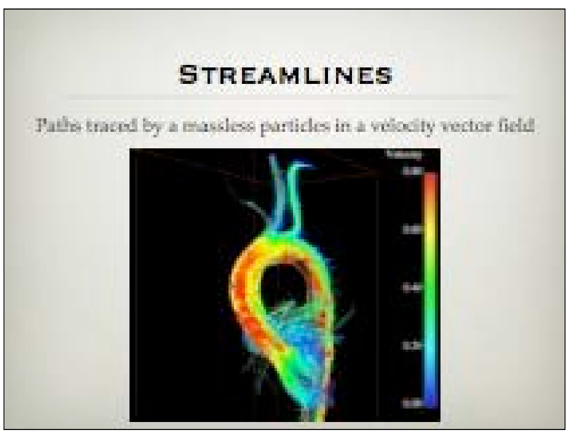

STREAMLINES
Paths traced by a massless particles in a velocity vector field

11

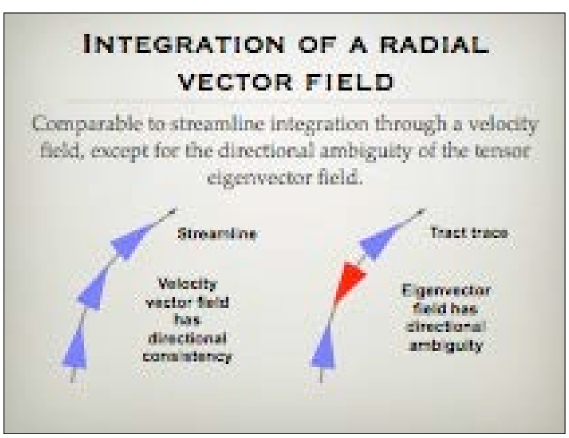

INTEGRATION OF A RADIAL VECTOR FIELD
Comparable to streamline integration through a velocity field, except for the directional ambiguity of the tensor eigenvector field.
Streamline
Velocity vector field has directional consistency
Tract trace
Eigenvector field has directional ambiguity

12

Fiber Tracking Algorithms

- Wide variety of deterministic fiber tracking algorithms
- Most based on finite difference integration of the principle eigenvector or equivalent estimate of maximum diffusion direction
- Not specific to axons - can be performed in any fibrous tissue, including skeletal muscle and myocardium.

13

Streamline Tract Tracing (STT)

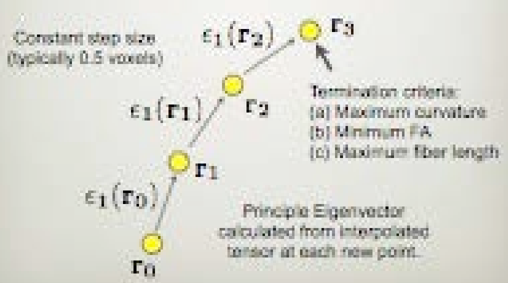

14

Streamline Tract Tracing (STT)

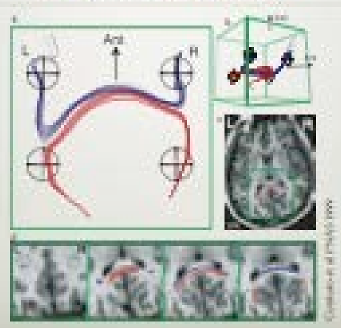

15

Fiber Assignment by Continuous Tracking (FACT)

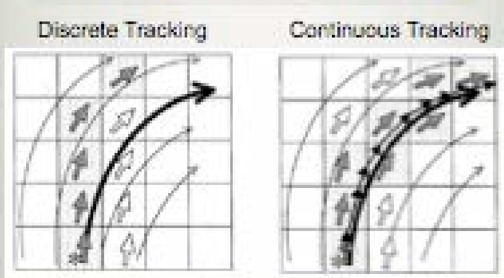

16

Fiber Assignment by Continuous Tracking (FACT)

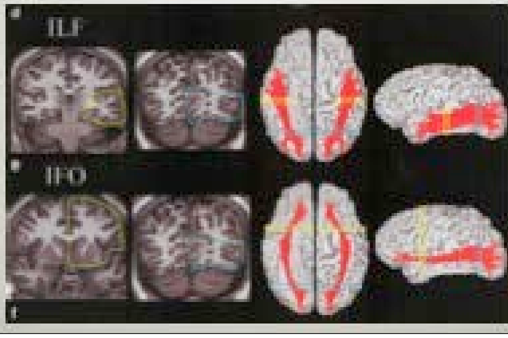

17

Tensor Deflection

Addresses propagation difficulties in areas of low fractional anisotropy.

$$\mathbf{v}_{out} = \mathbf{D}\mathbf{v}_{in}$$

Tensor deflects fiber vector towards principle eigenvector.

18

Tensorline Algorithm

Weighted combination of STT and Tensor Deflection proposed by Weinstein et al

$$\mathbf{v}_{out} = (f\mathbf{e}_1) + (1-f)((1-g)\mathbf{v}_{in} + g\mathbf{D}\mathbf{v}_{in})$$

f and g are user defined in range 0..1

19

Tensorline Visualization

20

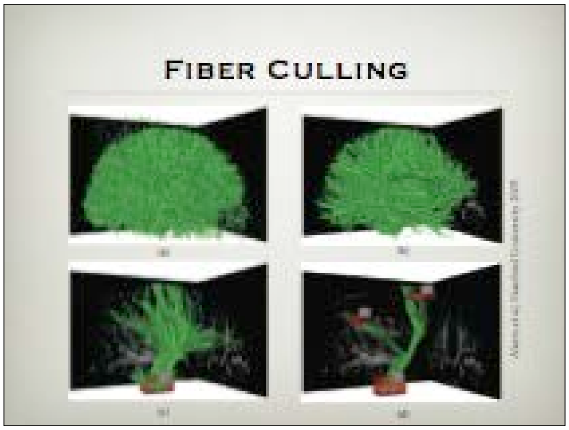
FIBER CULLING

21

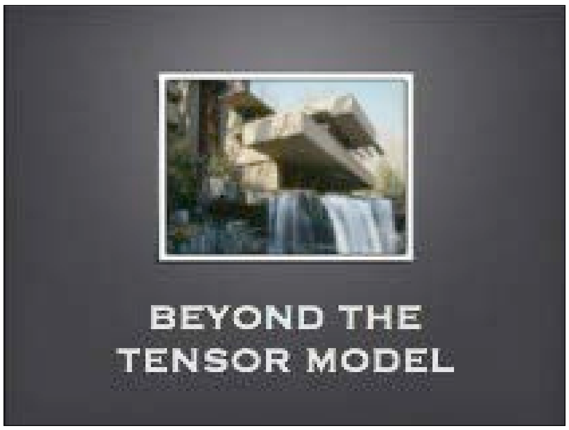
BEYOND THE
TENSOR MODEL

22

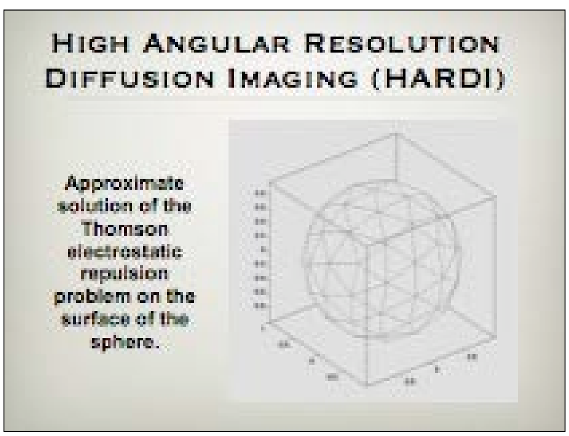
HIGH ANGULAR RESOLUTION
DIFFUSION IMAGING (HARDI)
Approximate solution of the Thomson electrostatic repulsion problem on the surface of the sphere.

23

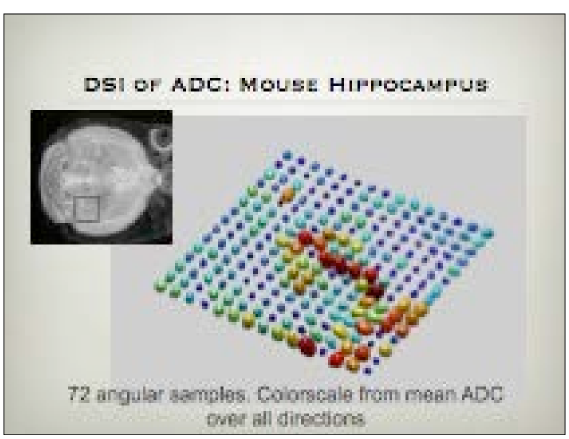
DSI OF ADC: MOUSE HIPPOCAMPUS
72 angular samples. Colorscale from mean ADC over all directions

24

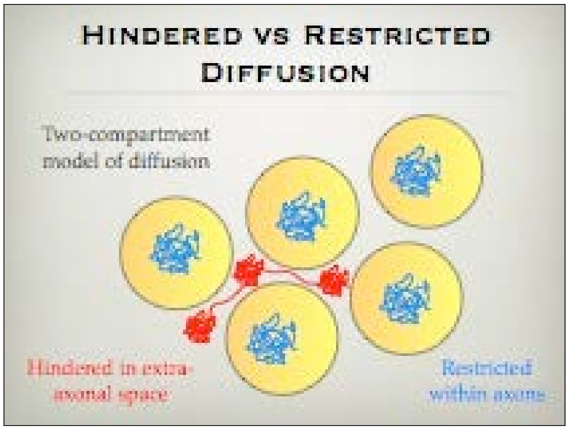
HINDERED VS RESTRICTED DIFFUSION
Two-compartment model of diffusion
Hindered in extra-axonal space
Restricted within axons

25

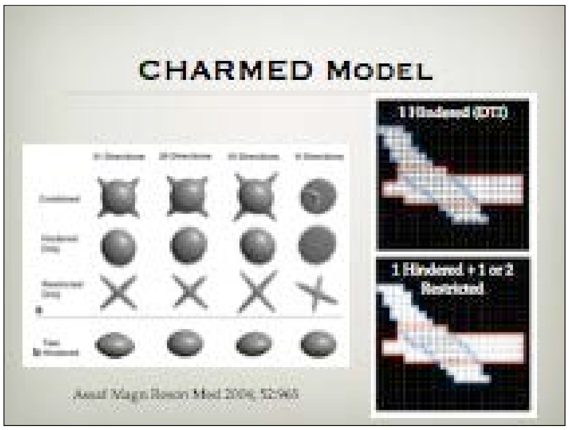
CHARMED MODEL
1 Hindered (DTI)
1 Hindered + 1 or 2 Restricted
Assaf Magn Reson Med 2004; 52:965

26

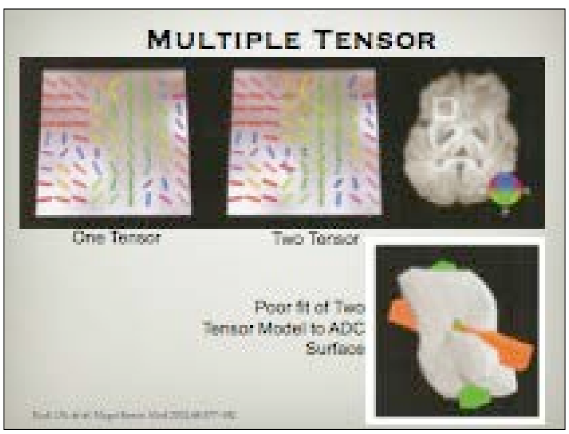
MULTIPLE TENSOR
One Tensor
Two Tensor
Poor fit of Two Tensor Model to ADC Surface

27

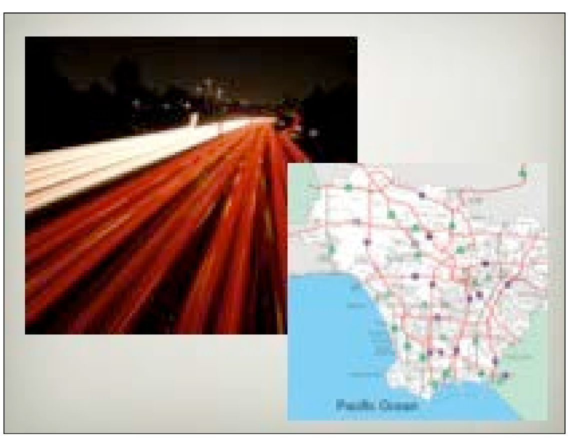
Pacific Ocean

28

29

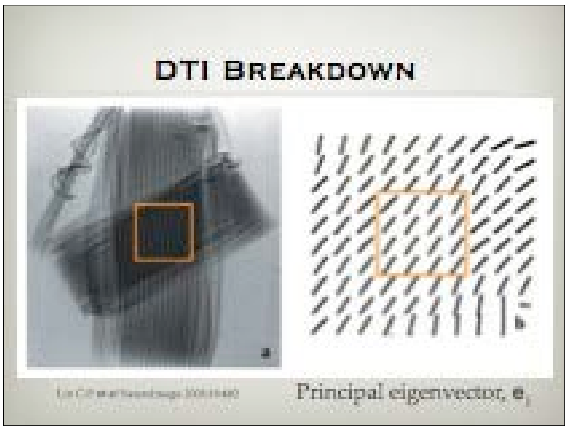
DTI Breakdown
Principal eigenvector, e_1

30

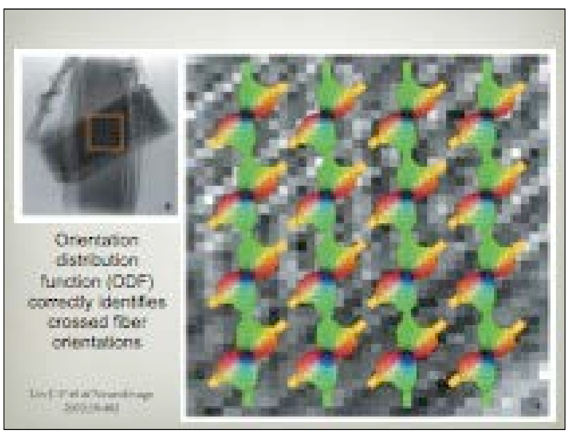
Orientation distribution function (ODF) correctly identifies crossed fiber orientations

31


Other Fiber Tracking Methods

32

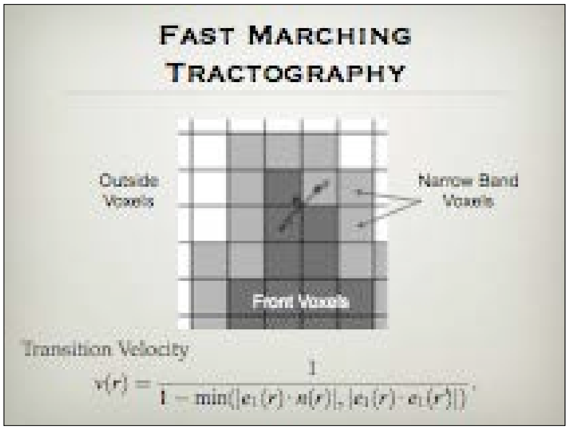
FAST MARCHING TRACTOGRAPHY
Outside Voxels
Narrow Band Voxels
Front Voxels
Transition Velocity
$v(r) = \frac{1}{1 - \min(|e_1(r) \cdot n(r)|, |e_1(r) \cdot e_1(r')|)}$

33

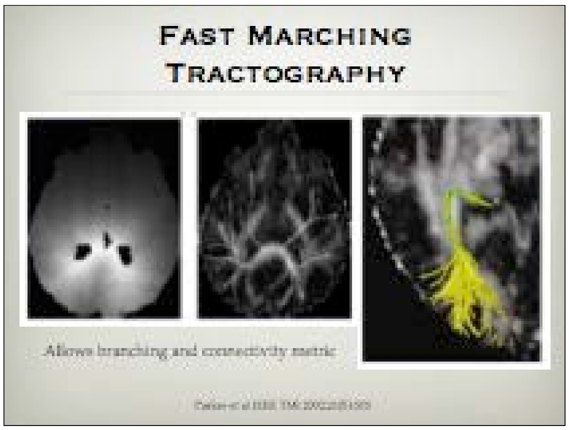
FAST MARCHING TRACTOGRAPHY
Allows branching and connectivity metric

34

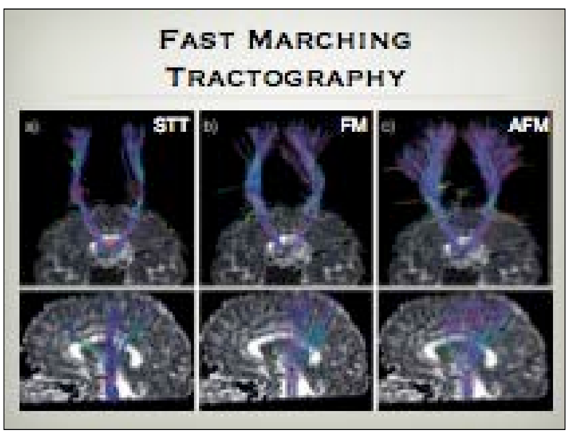
FAST MARCHING TRACTOGRAPHY
a) STT
b) FM
c) AFM

35

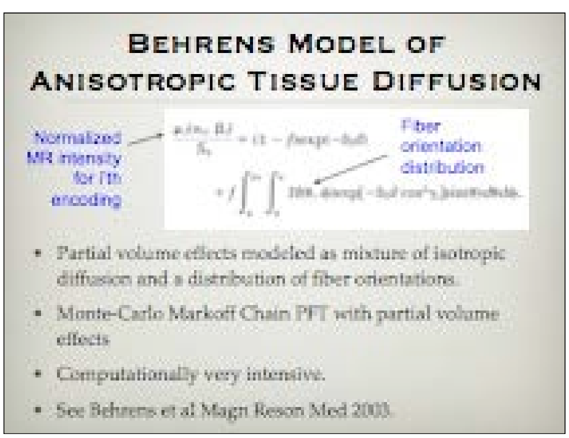
BEHRENS MODEL OF ANISOTROPIC TISSUE DIFFUSION
Normalized MR intensity for i'th encoding
Fiber orientation distribution
Partial volume effects modeled as mixture of isotropic diffusion and a distribution of fiber orientations.
Monte-Carlo Markoff Chain PFT with partial volume effects
Computationally very intensive.
See Behrens et al Magn Reson Med 2003.

36

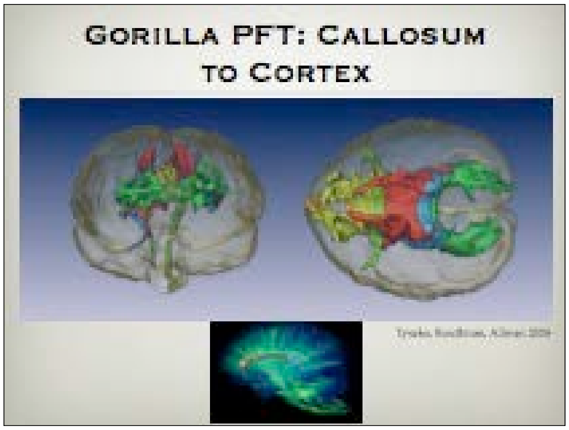
GORILLA PFT: CALLOSUM TO CORTEX

37

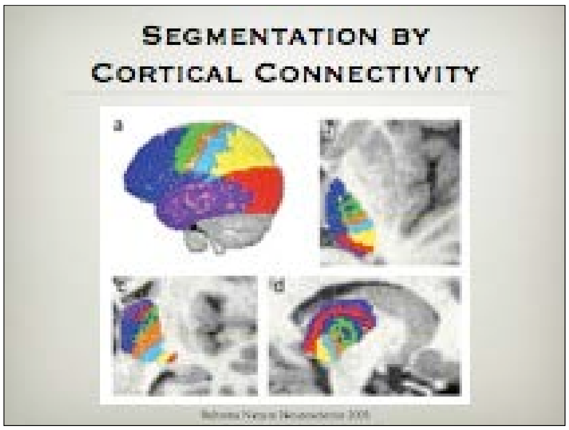
SEGMENTATION BY CORTICAL CONNECTIVITY
a
d

38


Q-SPACE

39

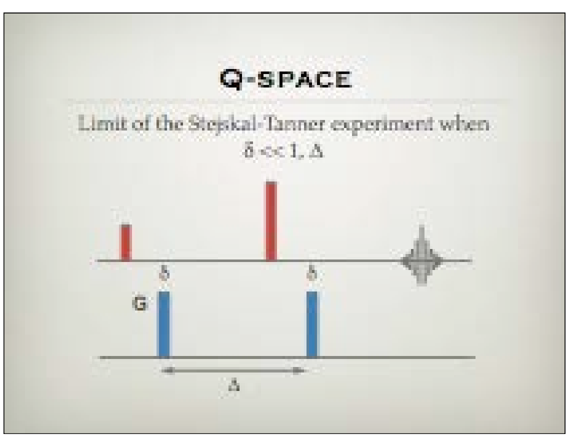
Q-SPACE
Limit of the Stejskal-Tanner experiment when δ << 1, Δ
δ
δ
G
Δ

40

Q: The Diffusion Wavenumber

For the Stejskal-Tanner, aka the Pulsed Field Gradient (PFG), sequence we define a new inverse space coordinate:

$$\mathbf{q}(T) = \frac{\gamma}{2\pi}\int_0^T dt\mathbf{G}(t) = \frac{1}{2\pi}\gamma\mathbf{G}\delta$$

Note that q is a function of G and δ only. Displacement during the gradient pulse is assumed to be negligible.

41

Displacement Probability and Q-space

We can relate the normalized attenuation to the conditional probability density of a molecule moving from one position to another during Δ

$$E(\mathbf{q},\Delta) = \int_{-\infty}^{\infty}\int_{-\infty}^{\infty} P(\mathbf{r}_2,\Delta|\mathbf{r}_1,0)P(\mathbf{r}_1)e^{i\mathbf{q}(\mathbf{r}_2-\mathbf{r}_1)}d^3\mathbf{r}_2 d^3\mathbf{r}_1$$

$$E(\mathbf{q},\Delta) = \frac{S(\mathbf{q},\Delta)}{S(\mathbf{0},\Delta)}$$

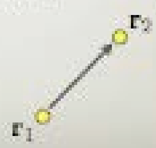

42

Displacement Propagator

If we assume local homogeneity, then the probability density function depends only on the relative displacement, r

$$P(\mathbf{r},\Delta|\mathbf{0},0) = P(\mathbf{r}_2,\Delta|\mathbf{r}_1,0)$$

Easy to show that this PDF can be calculated by inverse FT of the normalized attenuation

$$P(\mathbf{r},\Delta|\mathbf{0},0) = \int_{-\infty}^{\infty} d^3\mathbf{q}\ E(\mathbf{q},\Delta)e^{-i\mathbf{q}\cdot\mathbf{r}}$$

43

Q-space Propagators in Practice

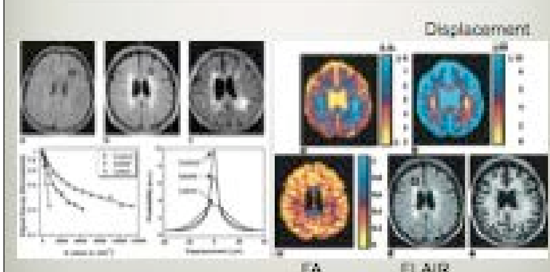

44

Properties of Q-Space Propagator

- No diffusion model assumed.
- Measures probability density of a molecule displacing by a given amount in a given time.
- Time-consuming to acquire data in more than one q-space dimension

45

Q-Ball Imaging

46

Orientational Distribution Function

Radial projection of the 3D displacement probability function

$$\psi(\mathbf{u}) = \int_0^\infty P(r\mathbf{u})dr$$

47

Funk-Radon Transform

Tuch showed that the diffusion weighted signal on a shell in q-space is closely related to the ODF by the Funk-Radon transform.

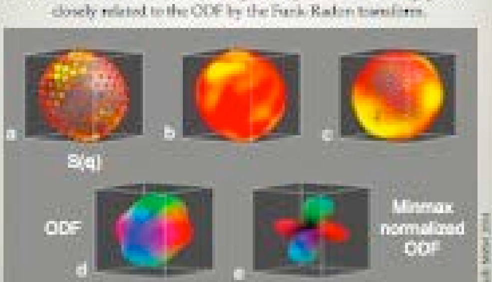

48

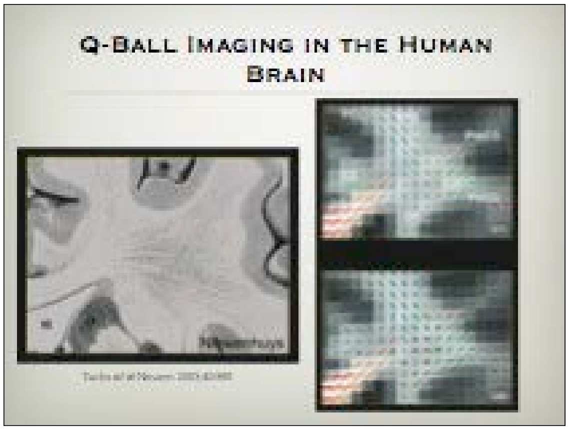
Q-Ball Imaging in the Human Brain

49


QBI of the Midbrain

50

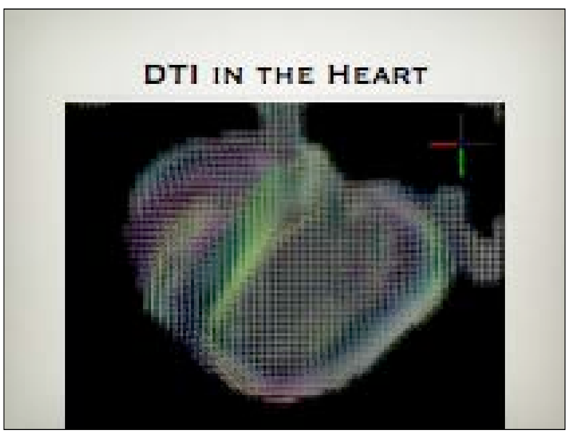
DTI in the Heart

51

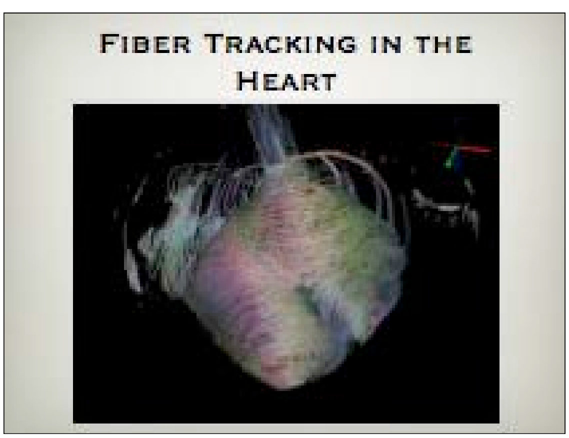
Fiber Tracking in the Heart

52

53

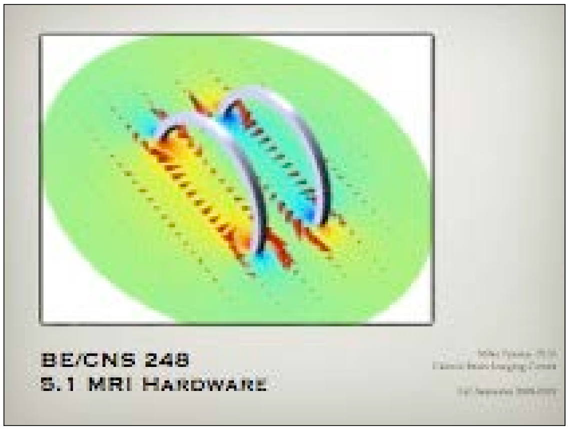

1

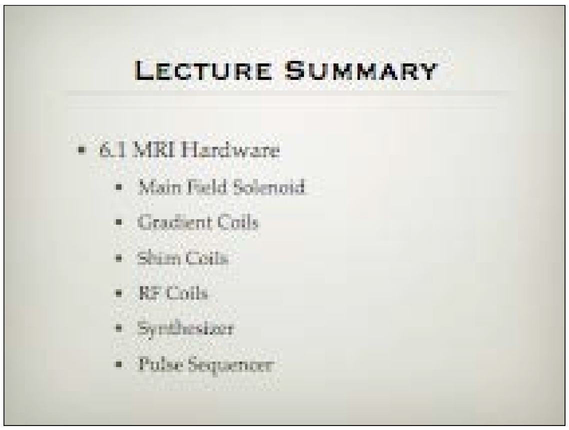

2

3

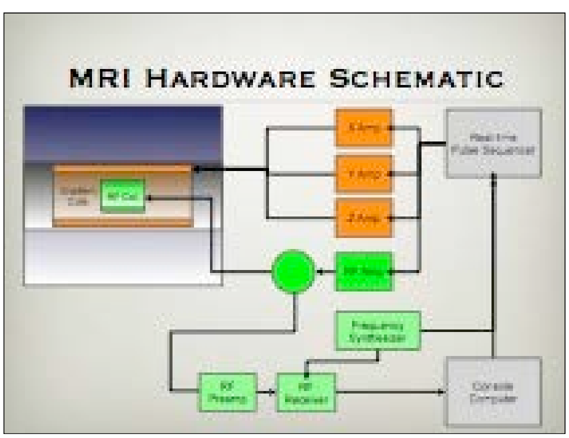

4

Tuesday, October 28, 2008

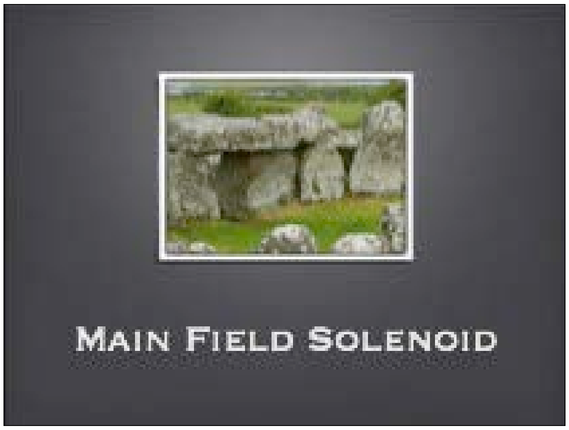
MAIN FIELD SOLENOID

5


MAGNET SOLENOID

6


NMR SOLENOID CUTAWAY

7


HELMHOLTZ PAIR
a
a
z

8

Helmholtz Field on axis

Axial magnetic field

$$B_z = \frac{\mu_0 I}{2a}\left[\frac{1}{(\gamma^2+\gamma+5/4)^{3/2}} + \frac{1}{(\gamma^2-\gamma+5/4)^{3/2}}\right]$$

where $\gamma = \frac{z}{a}$

9

Helmholtz Field Uniformity

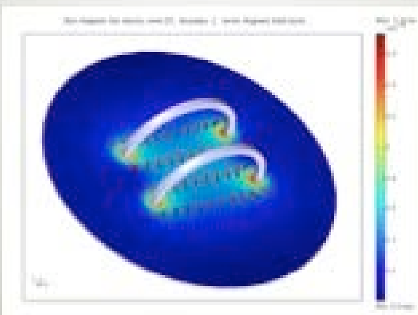

10

Helmholtz Field Uniformity

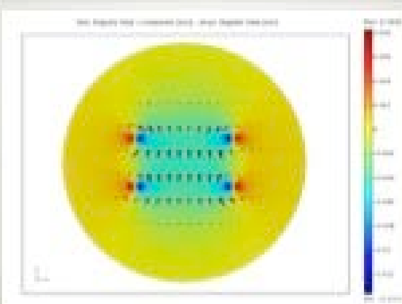

11

Helmholtz Pair Sets

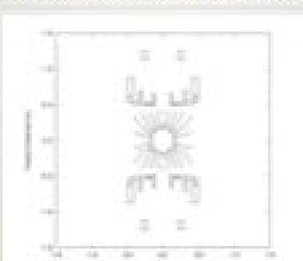

Figure 1. The coil configuration of the magnet design. Also shown are the +/- 0.5ppm contour lines in the central region of the magnet.

12

Superconductors for MRI

850um diameter wire

Niobium-Titanium

Class II Superconductor
Transition temperature : 10K
Critical field : 15T

Material of choice for high-field superconducting magnets due to mechanical and magnetic performance advantages.

13

Dual Skin Cryostats

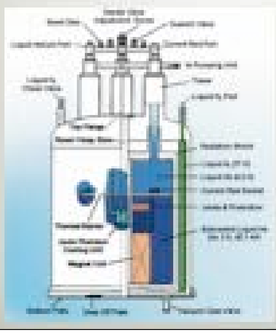

Liquid N_2 boils off preferentially (sacrificial cryogen) in order to reduce liquid He boil off.

Typical MRI cryostat will need N_2 fills weekly to monthly with He fills monthly to quarterly.

14

High-field Magnets

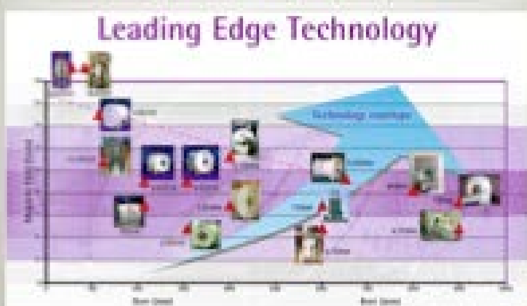

15

Quenching

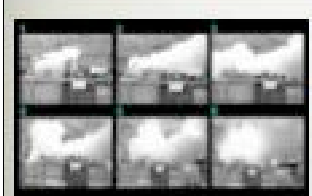

Catastrophic breakdown of superconductivity causes collapse of magnetic field. Stored energy dumped as heat into cryogens. Huge volume of gas released.

16

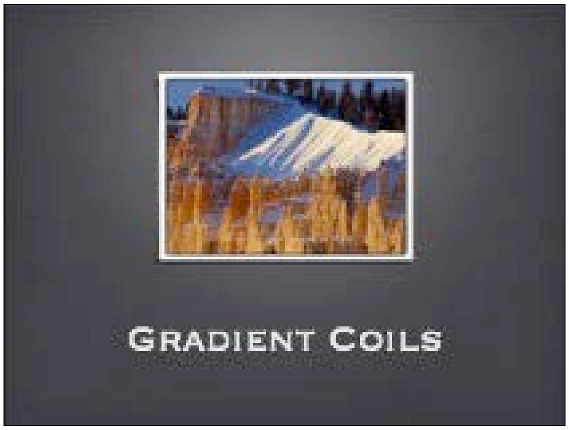
GRADIENT COILS

17

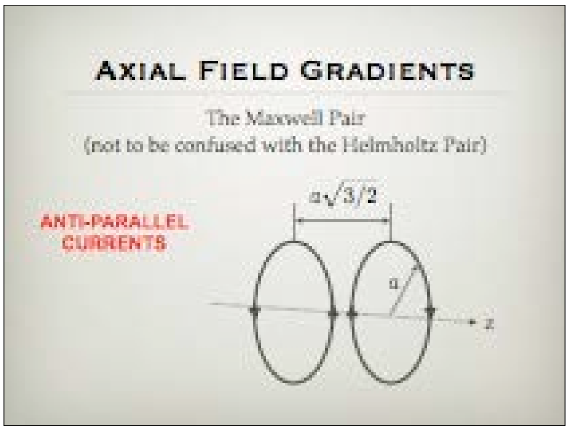
AXIAL FIELD GRADIENTS
The Maxwell Pair
(not to be confused with the Helmholtz Pair)
ANTI-PARALLEL CURRENTS
$a\sqrt{3}/2$
a
z

18

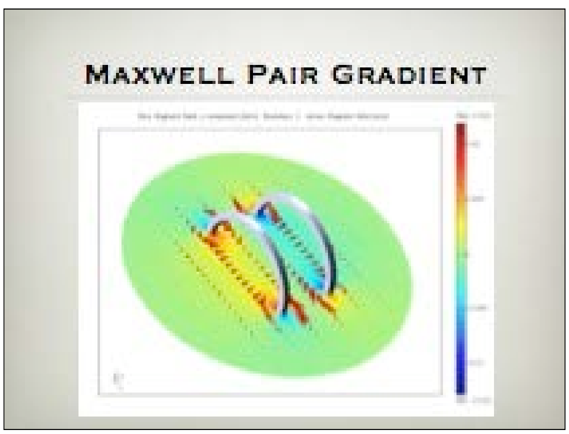
MAXWELL PAIR GRADIENT

19

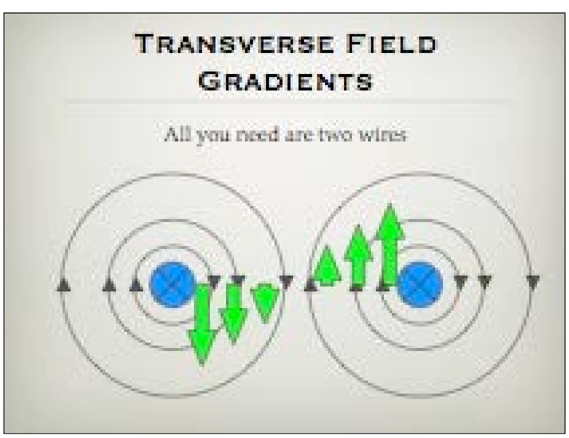
TRANSVERSE FIELD GRADIENTS
All you need are two wires

20

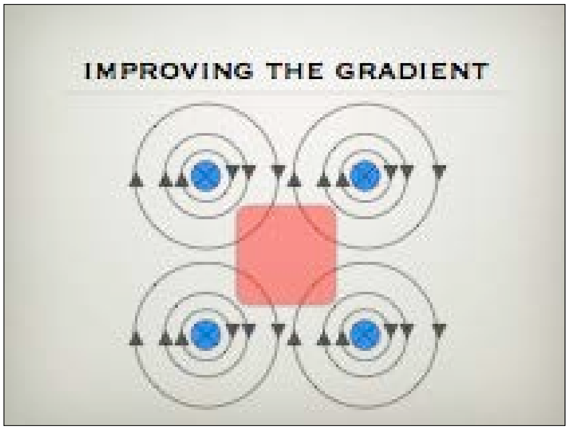
IMPROVING THE GRADIENT

21

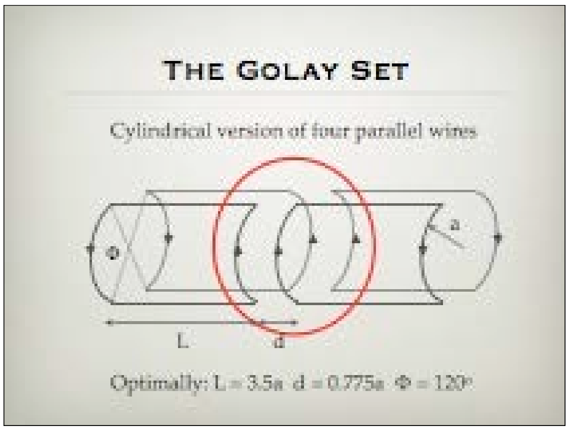
THE GOLAY SET
Cylindrical version of four parallel wires
L
d
a
Φ
Optimally: L = 3.5a d = 0.775a Φ = 120°

22


SHIM HARDWARE
Y Golay
Z Maxwell
X Golay

23


THREE-AXIS GRADIENTS
11mm Maxwell-Golay Design and Fabrication

24

The Target-Field Method

Solve for the current density, $J(z,\theta)$ on the surface of a cylinder of radius a, which generates the required $B_z(z, \theta)$ on the surface of a target cylinder, radius $c < a$.

Integrate current density to determine contours of current density along which windings can be wrapped

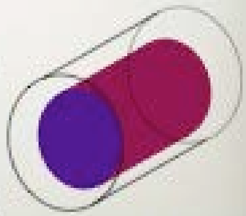

Turner R. Target Field Method. J Phys D 1986;19:L147 for full method.

25

The Target-Field Method

Quadrant of winding pattern for TFM transverse coil winding

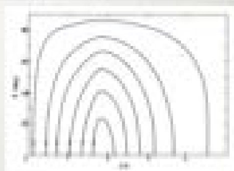

Longitudinal gradient TFM winding pattern

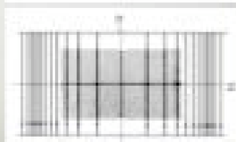

26

Target Field Designs

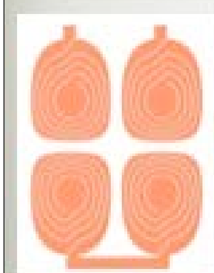

27

Minimum Inductance Designs

28

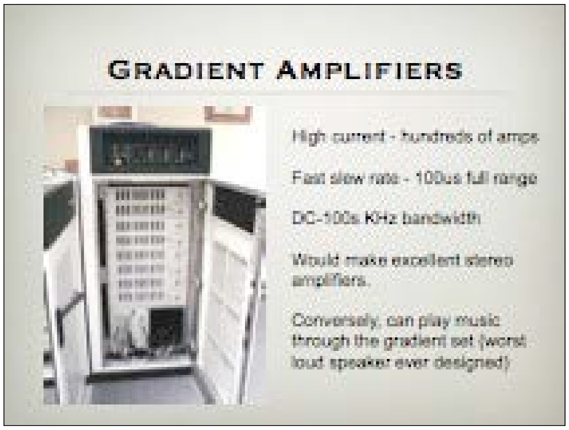
GRADIENT AMPLIFIERS
High current - hundreds of amps
Fast slew rate - 100us full range
DC-100s KHz bandwidth
Would make excellent stereo amplifiers.
Conversely, can play music through the gradient set (worst loud speaker ever designed)

29

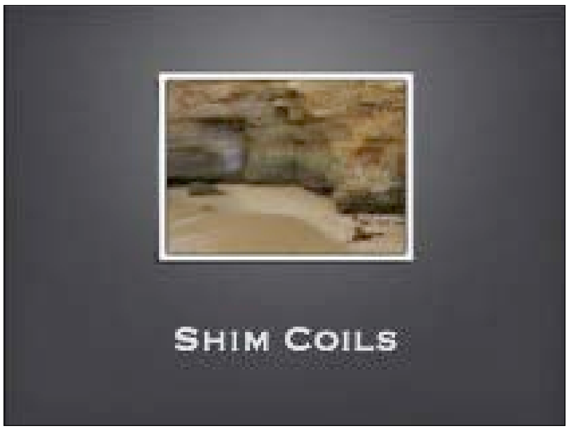
SHIM COILS

30

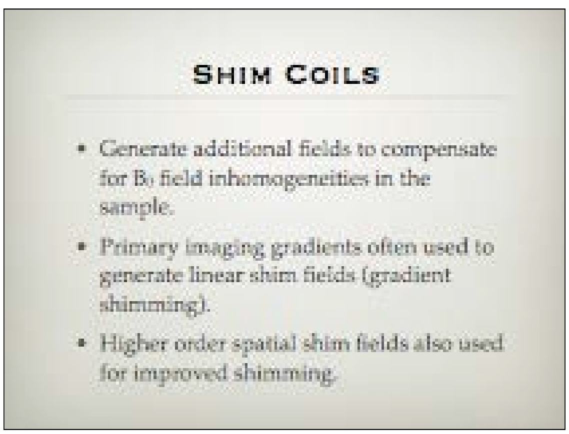
SHIM COILS
• Generate additional fields to compensate for B_0 field inhomogeneities in the sample.
• Primary imaging gradients often used to generate linear shim fields (gradient shimming).
• Higher order spatial shim fields also used for improved shimming.

31


SHIMMING
Zero shims
$sd(B_0) = 100Hz$
Optimized shims
$sd(B_0) = 25Hz$

32

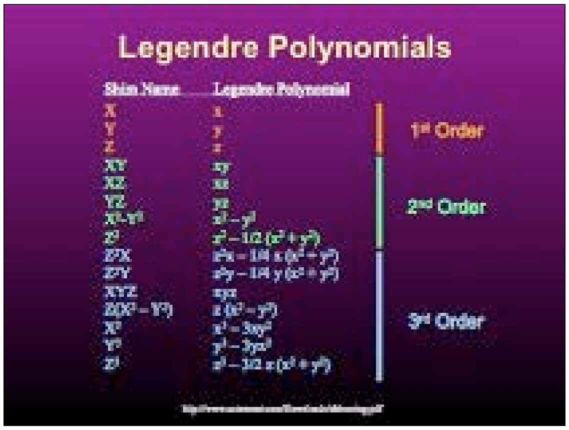
Legendre Polynomials
Shim Name Legendre Polynomial
X x
Y y
Z z
1st Order
XY xy
XZ xz
YZ yz
X²-Y² x² – y²
Z² z² – 1/2 (x² + y²)
2nd Order
Z²X z²x – 1/4 x (x² + y²)
Z²Y z²y – 1/4 y (x² + y²)
XYZ xyz
Z(X² – Y²) z (x² – y²)
X³ x³ – 3xy²
Y³ y³ – 3yx²
Z³ z³ – 3/2 z (x² + y²)
3rd Order

33


TFM Shim Coils
Y
Z(X2-Y2)
Use stream function approach to generate winding patterns for high order shim fields

34


Radiofrequency Coils

35


RF Coil Designs

36

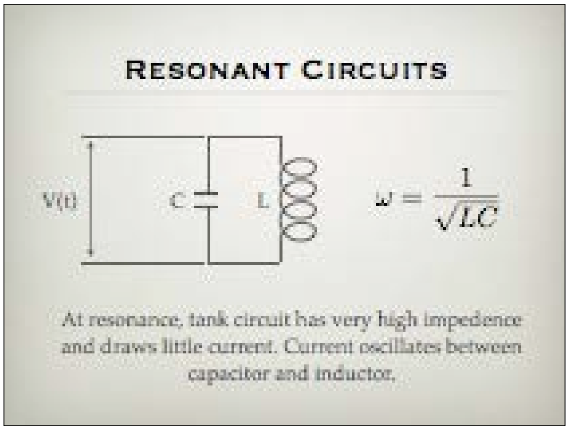
RESONANT CIRCUITS
V(t)
C
L
$\omega = \frac{1}{\sqrt{LC}}$
At resonance, tank circuit has very high impedence and draws little current. Current oscillates between capacitor and inductor.

37

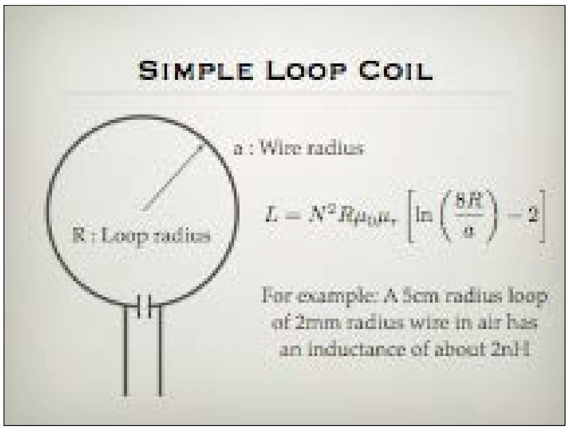
SIMPLE LOOP COIL
a : Wire radius
R : Loop radius
$L = N^2 R \mu_0 \mu_r \left[\ln\left(\frac{8R}{a}\right) - 2 \right]$
For example: A 5cm radius loop of 2mm radius wire in air has an inductance of about 2nH

38

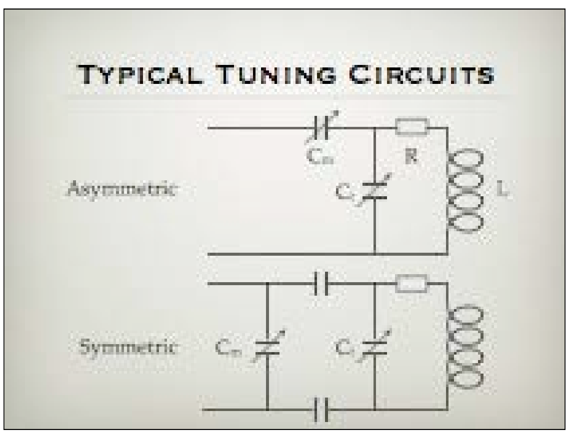
TYPICAL TUNING CIRCUITS
Asymmetric
C_m
R
C_t
L
Symmetric
C_m
C_t

39

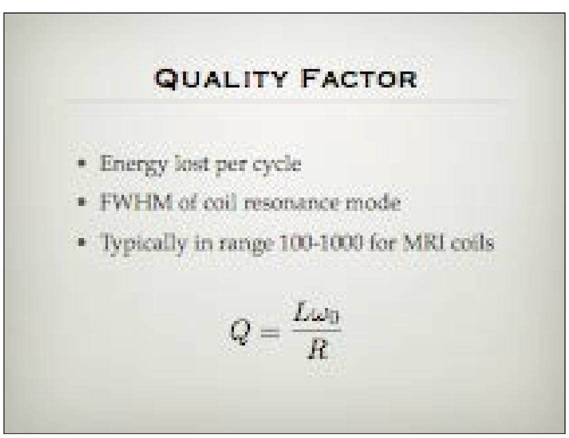
QUALITY FACTOR
• Energy lost per cycle
• FWHM of coil resonance mode
• Typically in range 100-1000 for MRI coils
$Q = \frac{L\omega_0}{R}$

40

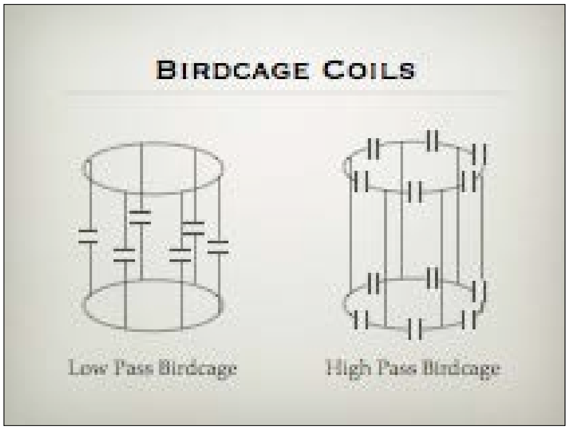
BIRDCAGE COILS
Low Pass Birdcage
High Pass Birdcage

41

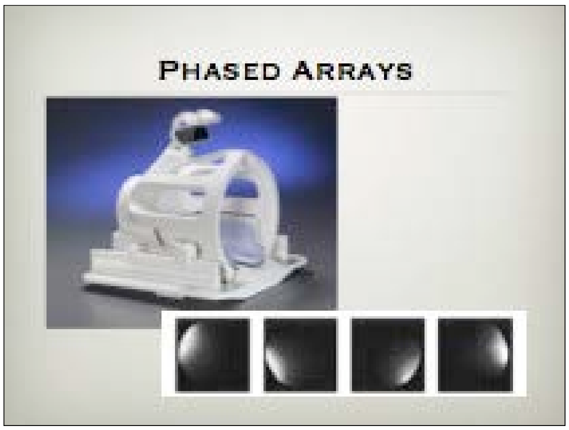
PHASED ARRAYS

42

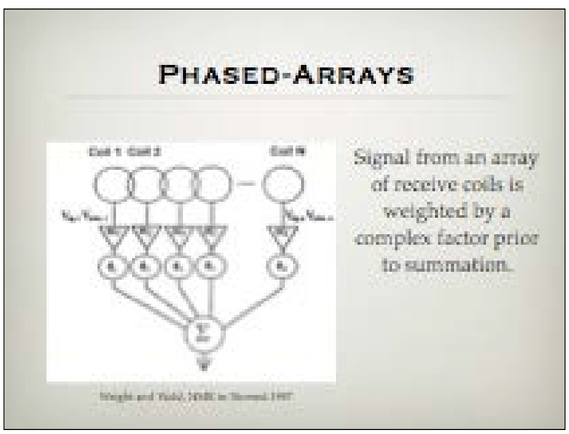
PHASED-ARRAYS
Signal from an array of receive coils is weighted by a complex factor prior to summation.

43

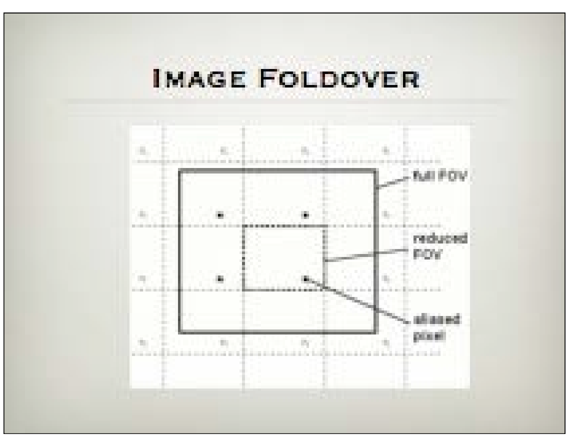
IMAGE FOLDOVER
full FOV
reduced FOV
aliased pixel

44

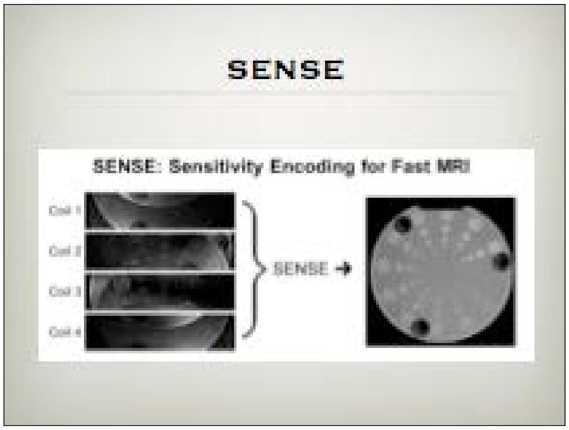
SENSE
SENSE: Sensitivity Encoding for Fast MRI
Coil 1
Coil 2
Coil 3
Coil 4
SENSE

45

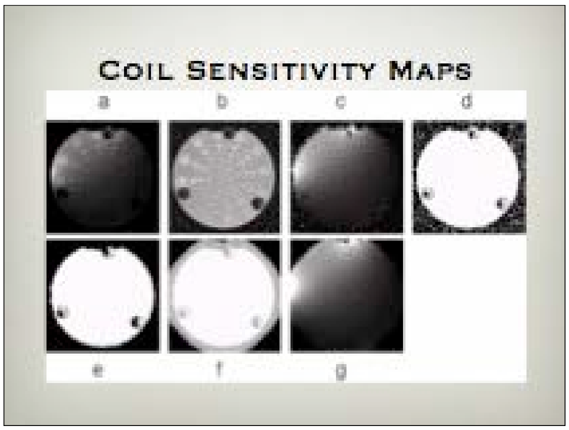
Coil Sensitivity Maps
a
b
c
d
e
f
g

46

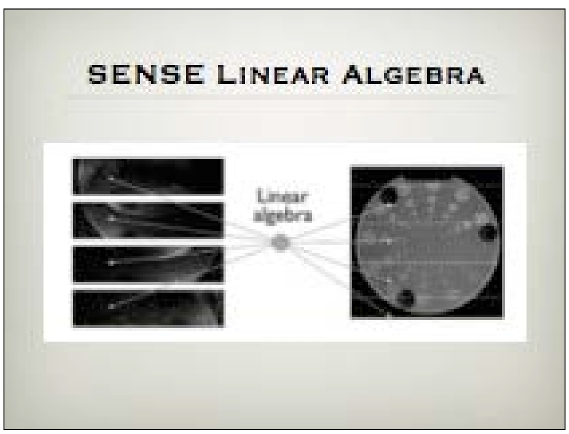
SENSE Linear Algebra
Linear algebra

47

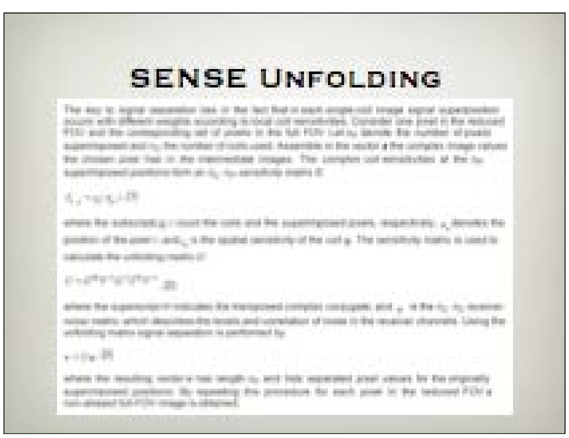
SENSE Unfolding

48

SENSE Limitations

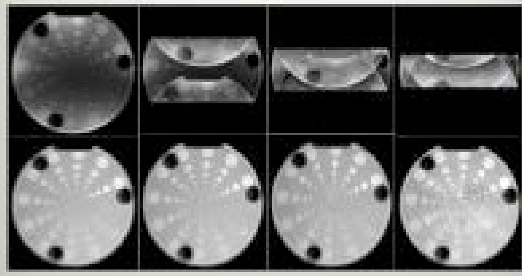

49

EPI and SENSE

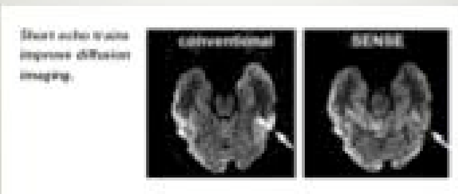

50

Brain Imaging

51

Next Lecture

- MRI Bioeffects and Safety
  - Static magnetic field
  - Gradient switching
  - RF heating
  - Other effects

52

BE/CNS 248
6.2 MRI Bioeffects

1

Lecture Summary

- 6.2 MRI Bioeffects and Safety
  - Static field effects
  - Forces on ferromagnetic materials
  - Rapid gradient switching
  - Peripheral nerve stimulation
  - Acoustic noise
  - Claustrophobia
  - Screening questionnaires
  - Human Subjects Protection

2

Static Magnetic Fields

3

Franz Anton Mesmer
1734-1815

- German physician practiced in Vienna
- Therapeutic system based on manipulation of magnetic fluids in the body.
- "Animal Magnetism"
- Early attempt to exploit magnetic bioeffects.

4

Static Magnetic Field

- Main cause of MRI accidents
- 3 Tesla = 30,000 Gauss
- Forces and torques on ferromagnetic objects.
- Eddy current effects in non-ferromagnetic conductors.
- Induced potential differences in moving conductive fluids such as blood.

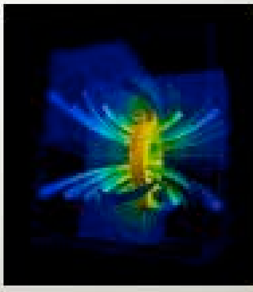

5

Magnetic Susceptibility

$$\mathbf{M} = \chi \mathbf{H}$$

$$\mathbf{B} = \mu_0 (\mathbf{H} + \mathbf{M}) = \mu_0 \mathbf{H} (1 + \chi)$$

6

Susceptibility Spectrum

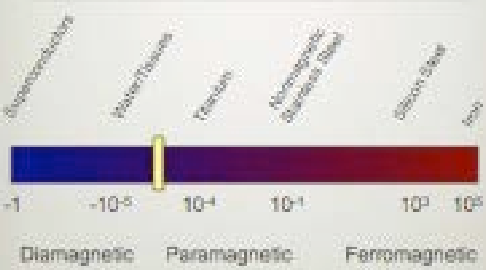

7

Ferromagnetic Metals

- Distinguish between ferro-magnetic and non-ferromagnetic metals
- Ferromagnetic:
  - Mild, Tool, HSS Steel
  - Staples, Paper Clips
  - Iron Filings
- Non-ferromagnetic:
  - Gold, platinum, silver
  - Copper, brass, aluminum
  - Many, but not all stainless steels

8

Forces in a Magnetic Field

In general, the force on an object is equal to the gradient of the magnetic potential energy

$$\mathbf{F} = -\nabla U$$

If we can determine U then we can derive the force on a magnetized object in a field.

9

Magnetic Potential Energy

For a permanent magnetic dipole brought into a field B

$$U = -\mathbf{m} \cdot \mathbf{B}$$

For a magnetizable object brought into a field B

$$U = -\frac{1}{2}\mathbf{m} \cdot \mathbf{B}$$

10

Magnetic Force in a Field Gradient

For an isotropic object with volume V and field-induced magnetization

$$F_z = \frac{V}{2\mu_0}\chi B_z \frac{\partial B_z}{\partial z} \quad \chi \ll 1$$

$$F_z = \frac{V}{2\alpha\mu_0} B_z \frac{\partial B_z}{\partial z} \quad \chi \gg 1$$

11

Torque in a Magnetic Field

For a small, weakly susceptible object

$$\begin{aligned} \mathbf{T} &= -\frac{\partial U}{\partial \theta}\mathbf{u} \\ &= \mathbf{M} \times \mathbf{B} \end{aligned}$$

12

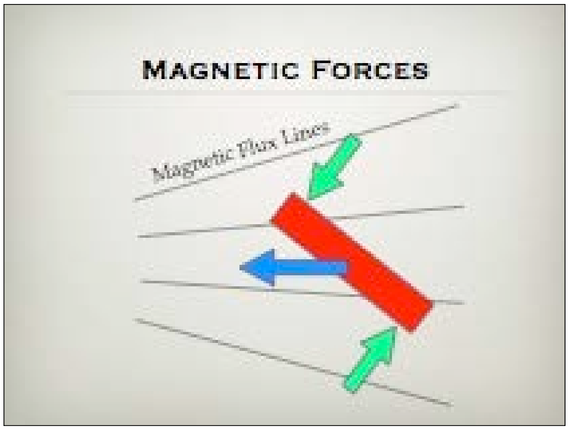
Magnetic Forces
Magnetic Flux Lines

13

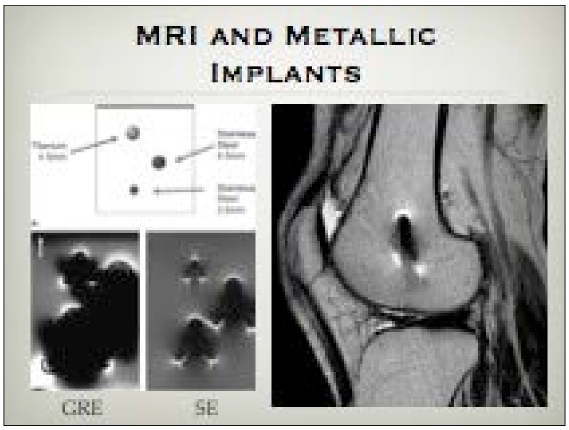
MRI and Metallic Implants
GRE
SE

14


MR Accidents

15


IV Pole

16

...

17

MRI Fatalities

The New York Times

Hospital Details Failures Leading to M.R.I. Fatality

A poorly trained staff, technical malfunctions and lapses in communication among workers contributed to the death of a 6-year-old boy last month who was struck by an oxygen canister drawn into a magnetic resonance imaging machine at Westchester Medical Center, according to a report by the hospital released today.

The review, required by the state after medical fatalities, was conducted after the death of the boy, Michael Colombini of Croton-on-Hudson, who was struck by a 5.5-pound metal oxygen tank that was pulled into the machine by its magnetic field as he underwent a test.

By RANDAL C. ARCHIBOLD
Published: August 22, 2001

18

Radiofrequency Fields

19

Radiofrequency Field

- 128 MHz RF Electromagnetic Field at 3T
- Tissue heating by current induction
- Specific Absorption of Radiation (SAR)
- 1-3W/kg limited
- RF arcing possible, but very rare.

20

Specific Absorption Ratio (SAR)

- SAR is defined as the power absorbed per unit mass.
- SAR is the primary focus of RF heating safety limits in MRI.
- Can be simulated by numerical methods.
- Common limit for RF-heavy pulse sequences.

21

Analytical SAR

Conductivity

Electric Field

Equivalent rect RF pulse duration

$$\mathrm{SAR} = \frac{\sigma|\mathbf{E}|^2}{2\rho}\,\frac{\tau}{\mathrm{TR}}$$

Density

Repetition time

22

Tissue Properties for Simulation

TABLE 1
Tissue Properties

		64 MHz		128 MHz		171 MHz		256 MHz	
Tissue type	ρ (g/cm³)	ϵ_r	σ (S/m)	ϵ_r	σ (S/m)	ϵ_r	σ (S/m)	ϵ_r	σ (S/m)
CSF	[illegible]	[illegible]	[illegible]	[illegible]	[illegible]	[illegible]	[illegible]	[illegible]	[illegible]
air		1	0	1	0	1	0	1	0
[illegible]	[illegible]	[illegible]	[illegible]	[illegible]	[illegible]	[illegible]	[illegible]	[illegible]	[illegible]
[illegible]	[illegible]	[illegible]	[illegible]	[illegible]	[illegible]	[illegible]	[illegible]	[illegible]	[illegible]
[illegible]	[illegible]	[illegible]	[illegible]	[illegible]	[illegible]	[illegible]	[illegible]	[illegible]	[illegible]
[illegible]	[illegible]	[illegible]	[illegible]	[illegible]	[illegible]	[illegible]	[illegible]	[illegible]	[illegible]
[illegible]	[illegible]	[illegible]	[illegible]	[illegible]	[illegible]	[illegible]	[illegible]	[illegible]	[illegible]
[illegible]	[illegible]	[illegible]	[illegible]	[illegible]	[illegible]	[illegible]	[illegible]	[illegible]	[illegible]
[illegible]	[illegible]	[illegible]	[illegible]	[illegible]	[illegible]	[illegible]	[illegible]	[illegible]	[illegible]

ϵ_r = relative permittivity σ = electrical conductivity

From: Chen IEEE TMI 1998

23

FDTD Simulations

Solve Maxwell's equations for E and H on a mesh

$$\begin{aligned} \nabla \times \mathbf{E} &= -\mu_0 \frac{\partial \mathbf{H}}{\partial t} \\ \nabla \times \mathbf{H} &= \epsilon \frac{\partial \mathbf{E}}{\partial t} + \sigma \mathbf{E} + \mathbf{J}^{ex} \end{aligned}$$

24

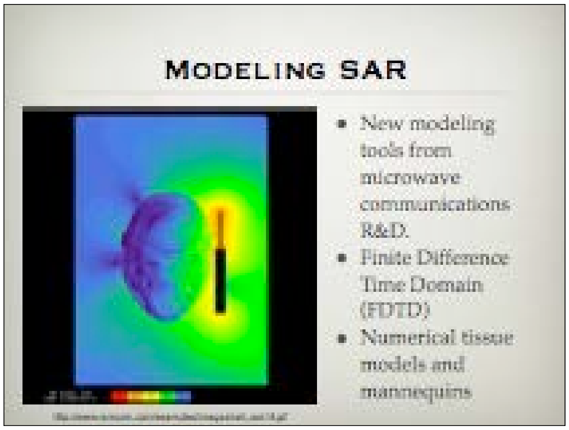
MODELING SAR
New modeling tools from microwave communications R&D.
Finite Difference Time Domain (FDTD)
Numerical tissue models and mannequins

25

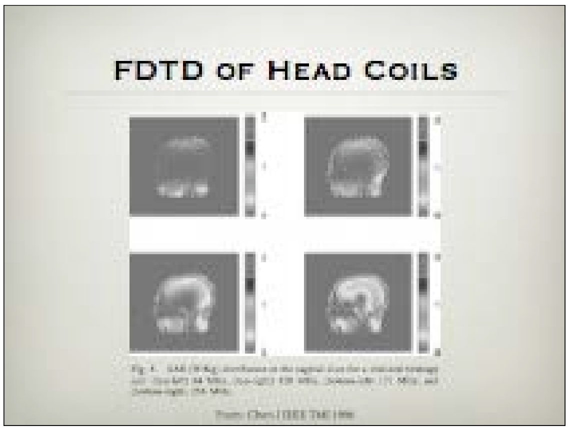
FDTD OF HEAD COILS

26

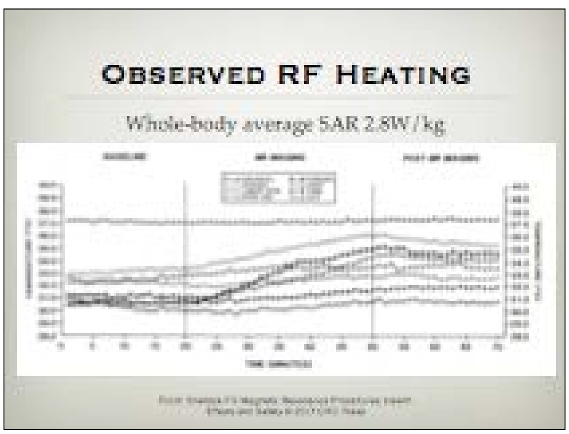
OBSERVED RF HEATING
Whole-body average SAR 2.8W/kg

27


SAR STANDARDS
US FDA Mean SAR Maxima
4W/kg over whole body over any 15 minute period
3W/kg over head over any 10 minute period
8W/kg in any gram (head and torso) over any 5 minute period
12W/kg in any gram (extremities) over any 5 minute period
IEC
NORMAL OPERATING MODE
FIRST LEVEL CONTROLLED OPERATING MODE
SECOND LEVEL CONTROLLED OPERATING MODE

28

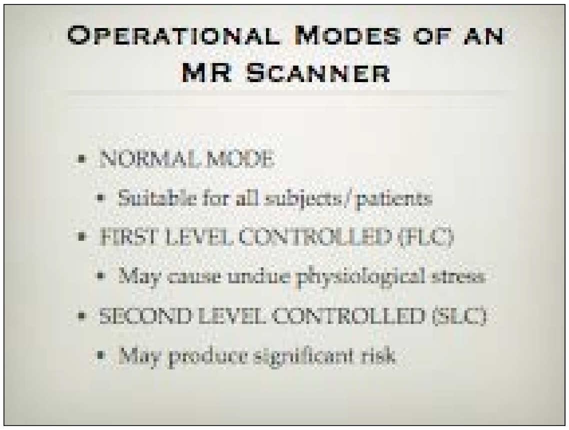
OPERATIONAL MODES OF AN MR SCANNER
NORMAL MODE
Suitable for all subjects/patients
FIRST LEVEL CONTROLLED (FLC)
May cause undue physiological stress
SECOND LEVEL CONTROLLED (SLC)
May produce significant risk

29


MRI AND TATOOS
Second-degree burns (arrows) following 1.5T MRI

30

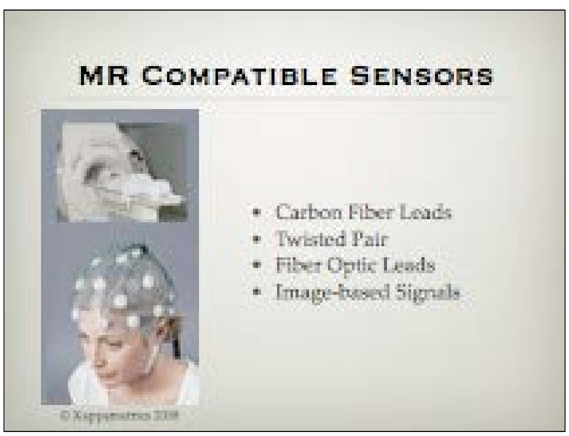
MR COMPATIBLE SENSORS
Carbon Fiber Leads
Twisted Pair
Fiber Optic Leads
Image-based Signals

31


FIELD GRADIENT SWITCHING

32

Rapidly Varying Field Gradients

- Causes rapid change in B (dB/dt)
- dB/dt increases linearly with distance from gradient isocenter
- dB/dt induces currents
- Peripheral nerve stimulation

33

Empirical Determination of PNS Threshold

- Volunteer subjects exposed to gradient pulsing.
- Slew durations from 50us to 1000us.
- Subjective rating from 0 (not felt) to 10 (intolerable)

34

PNS Testing

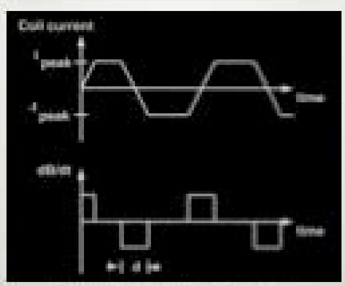

35

PNS Stimulation Curve

Median responses from 84 subjects

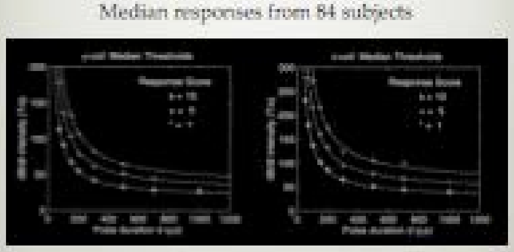

36

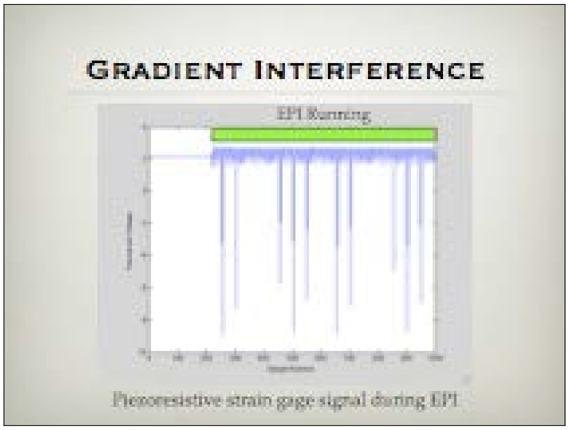
GRADIENT INTERFERENCE
EPI Running
Piezoresistive strain gage signal during EPI

37


OTHER EFFECTS

38

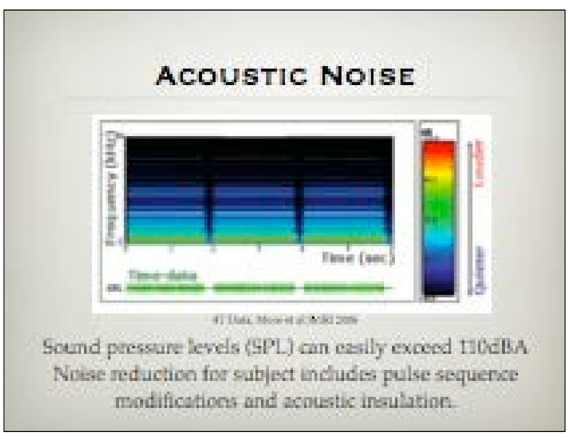
ACOUSTIC NOISE
Frequency (kHz)
Time (sec)
Time-data
Sound pressure levels (SPL) can easily exceed 110dBA
Noise reduction for subject includes pulse sequence
modifications and acoustic insulation.

39

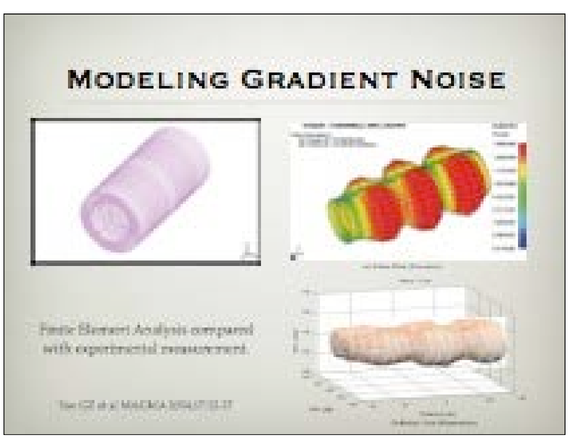
MODELING GRADIENT NOISE
Finite Element Analysis compared
with experimental measurement.

40

Claustrophobia

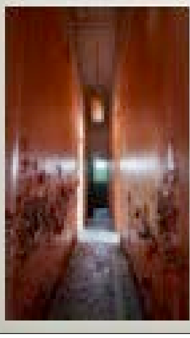

- Reported incidence at clinical sites highly variable: 0.7% to 20%
- Much lower incidence in motivated research subjects.
- Many solutions: open magnets, reassurance, sedation ...

41

Recommended Reading

- Shellock FG. *Magnetic Resonance Procedures: Health Effects and Safety*. CRC Press
- Jin JM. *Electromagnetic Analysis and Design in Magnetic Resonance Imaging* CRC Press

42

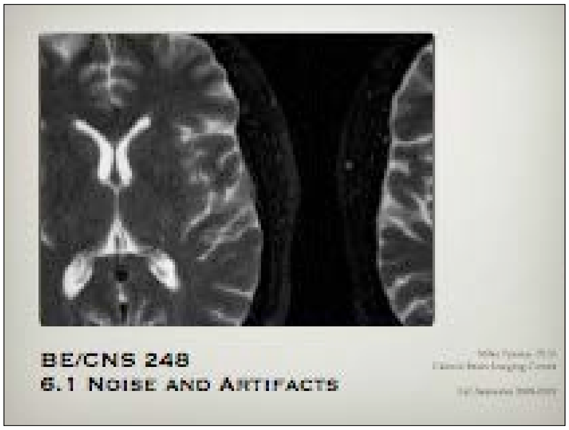
BE/CNS 248
6.1 Noise and Artifacts

1


Lecture Summary
• 6.1 Noise and Artifacts
• Noise sources in MRI
• Noise properties
• Bandwidth and noise
• SNR and CNR
• Field inhomogeneity artifacts
• Other artifacts
• Corrections

2

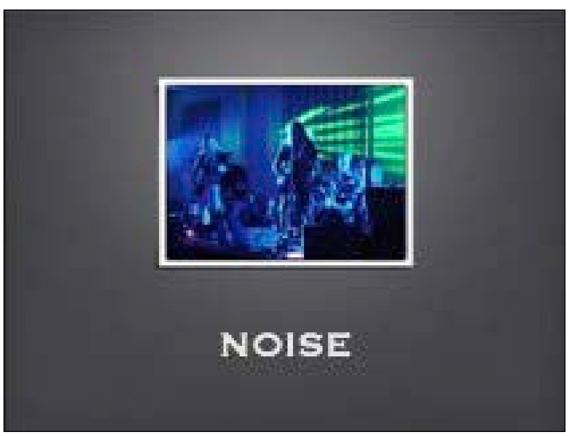
NOISE

3

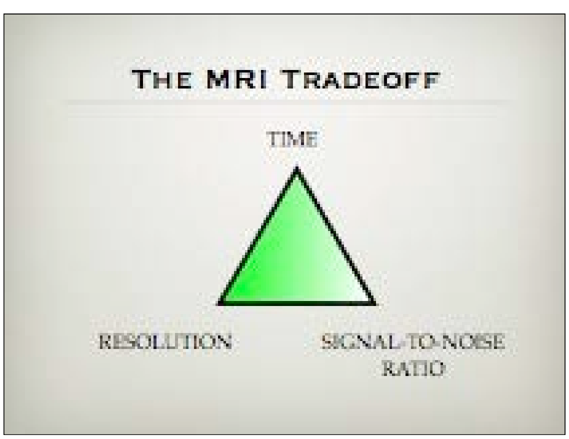
The MRI Tradeoff
TIME
RESOLUTION
SIGNAL-TO-NOISE RATIO

4

Sources of Noise in MRI

- Sample or Subject
  - Important at lower fields/larger subjects
- RF coil
  - Important at higher fields/smaller samples
- RF Preamplifier
- RF Receiver Electronics
- External Sources

5

Sample to Coil Noise Ratio

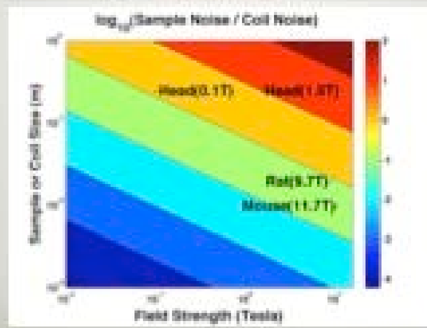

6

Signal and Noise

Total signal from a voxel is proportional to the voxel volume:

$$\frac{S}{N} \propto \Delta x^3 \sqrt{N_{av}}$$

$$N_{av} \propto \frac{1}{\Delta x^6}$$

Total imaging time has an inverse sixth power relation to voxel dimension at constant SNR.

7

Frequency Encoding Bandwidth and Noise

SNR is proportional to the square-root of the total digitizer acquisition time (c.f. SNR proportional to the square root of the number of signal averages).

$$\frac{S}{N} \propto \sqrt{T_{acq}} = \sqrt{N_x \Delta t} = \sqrt{\frac{N_x}{BW}}$$

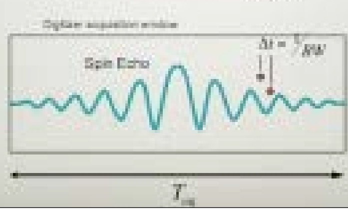

8

SNR per Voxel

$$SNR/voxel \propto \Delta x \Delta y \Delta z \sqrt{\frac{N_{acq} N_x N_y N_z}{BW_{fe}}}$$

9

SNR and CNR

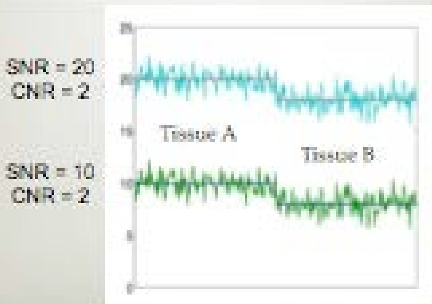

10

*** More on SNR ***

- Full SNR equation (including field strength, etc)
- More on noise spectrum (white, gaussian)
- Prewhitening of NMR noise
- Image example for CNR
- Microscopy vs human MRI SNR
- SNR efficiency

11

Denoising

12

Noise in MRI

- Typically treated as Gaussian White Noise
- Zero mean, standard deviation σ_N
- Magnitude image has a Rician noise distribution.
- Non-zero mean, asymmetric distribution.

13

Gaussian Noise

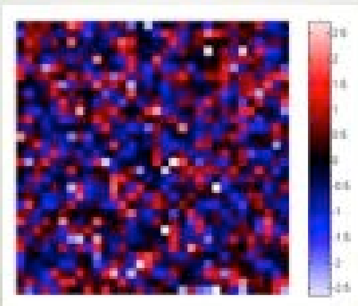

14

Gaussian Noise

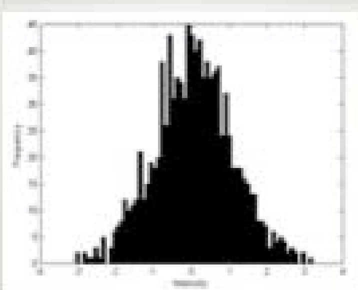

N(0,1)

15

Rician Noise

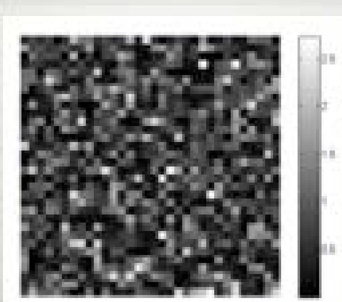

16

Rician Noise

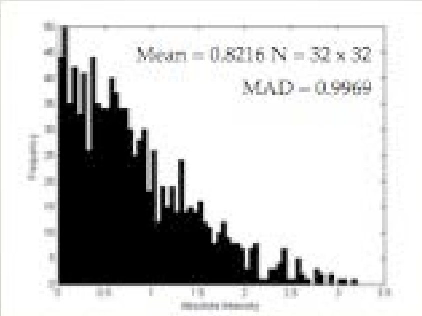

17

Estimating Noise

MAD : Median Absolute Deviation (from the median)

$$\mathrm{MAD}(x_i) = \mathrm{med}(|x_i| - \mathrm{med}(x_i))$$

For Gaussian Noise

$$\hat{\sigma}_N = \frac{MAD(x_i)}{0.6745}$$

18

Synthetic Gaussian Noise

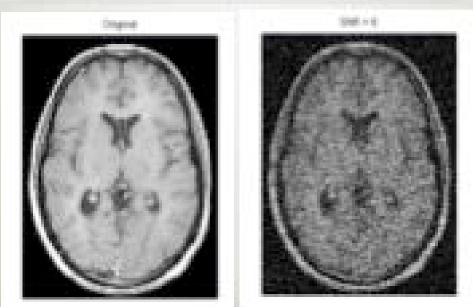

19

Gaussian Filter Denoising

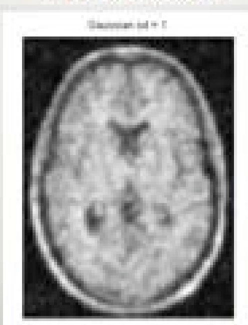

20

Median Filter Denoising

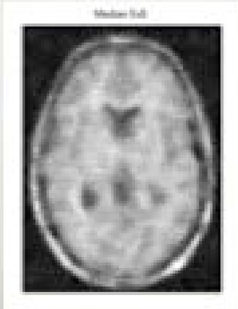

21

Wavelet Denoising

- Wavelet decompose 2D or 3D image.
- Estimate appropriate threshold at each level of decomposition for removing noise components.
- Recompose image from thresholded wavelet decomposition.

22

Example Wavelet Denoising

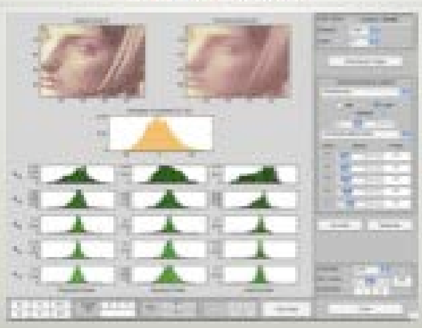

23

Wavelet Decomposition

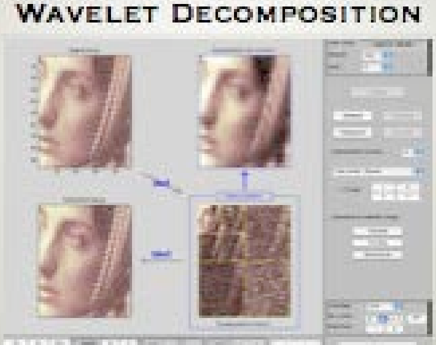

24


ARTIFACTS

25

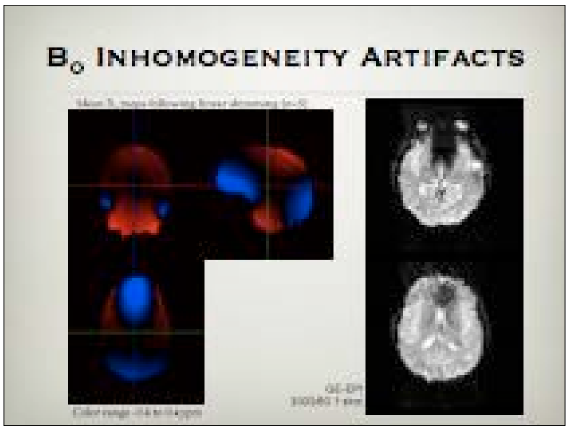
B_0 INHOMOGENEITY ARTIFACTS

26

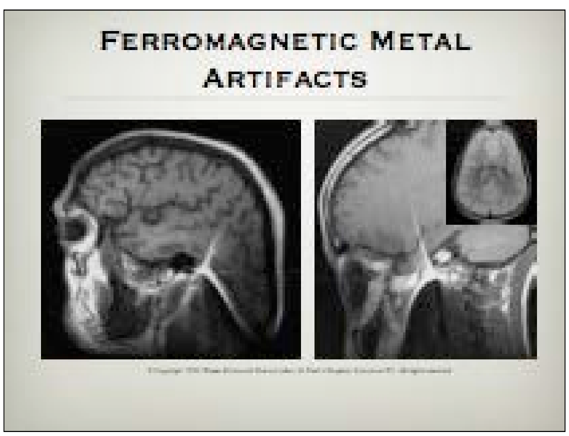
FERROMAGNETIC METAL ARTIFACTS

27

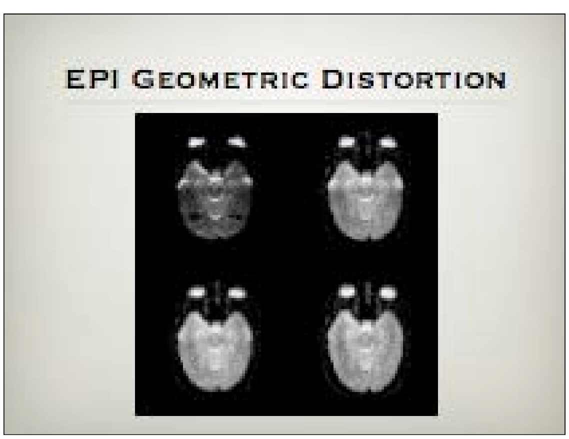
EPI GEOMETRIC DISTORTION

28

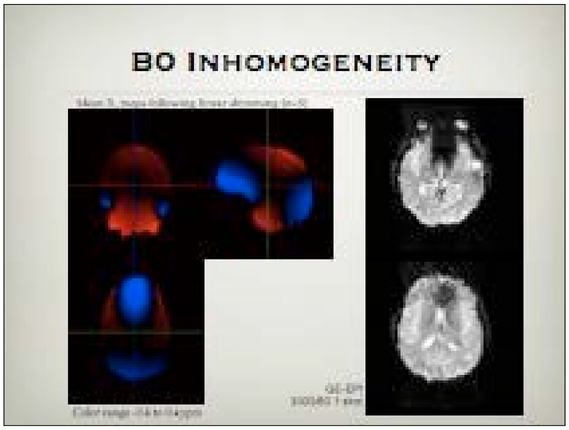
B0 Inhomogeneity

29

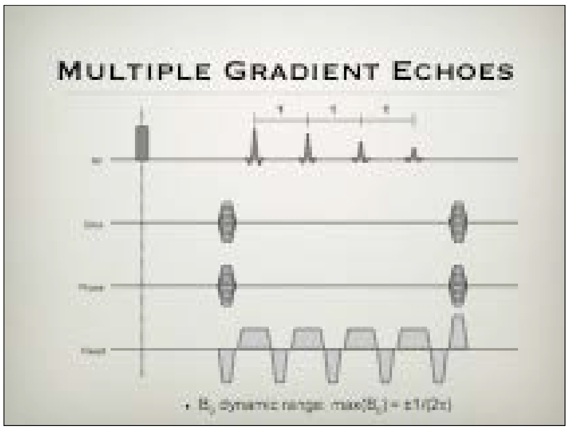
Multiple Gradient Echoes

30

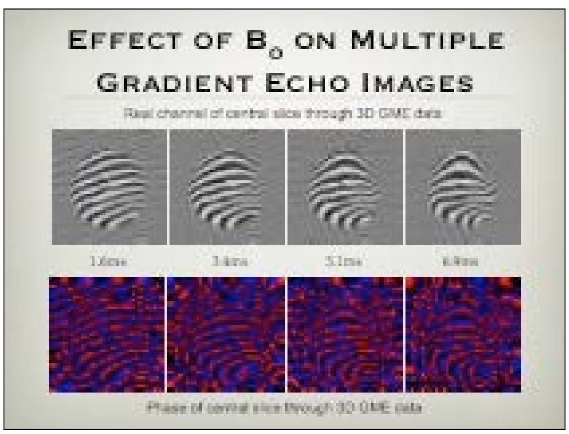
Effect of B0 on Multiple Gradient Echo Images
Real channel of central slice through 3D GME data
Phase of central slice through 3D GME data

31

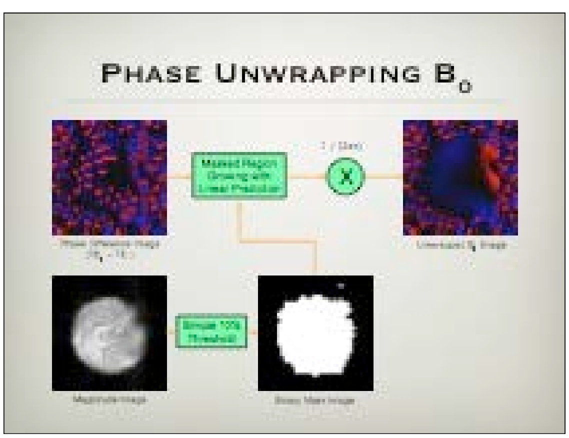
Phase Unwrapping B0

32

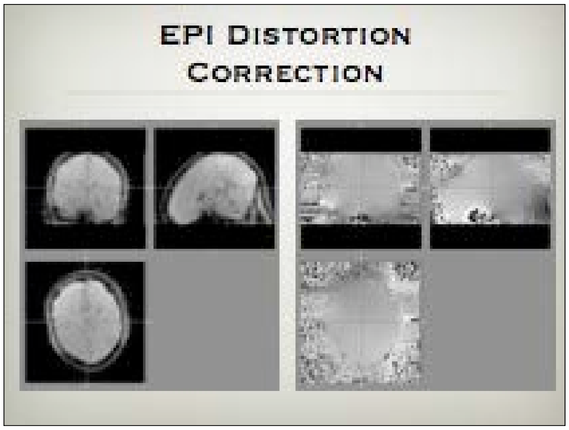
EPI Distortion
Correction

33

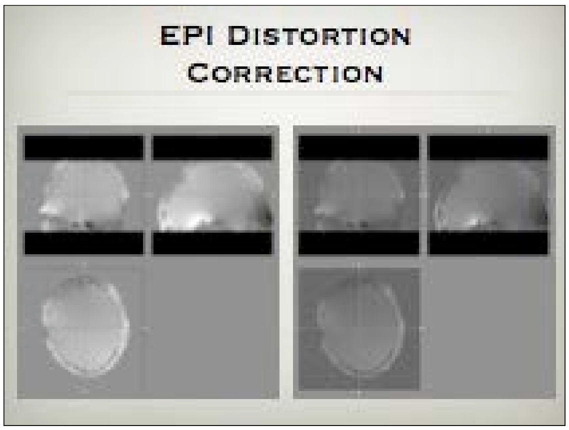
EPI Distortion
Correction

34

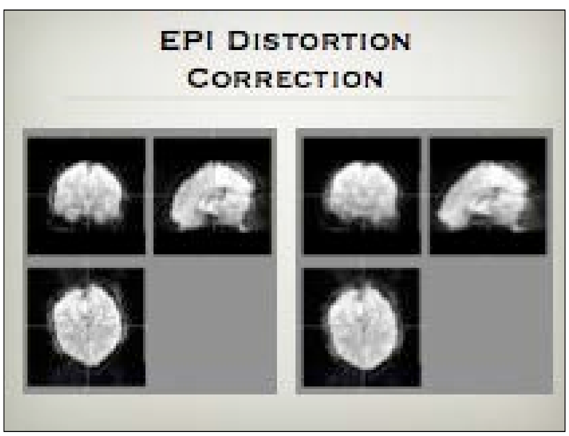
EPI Distortion
Correction

35

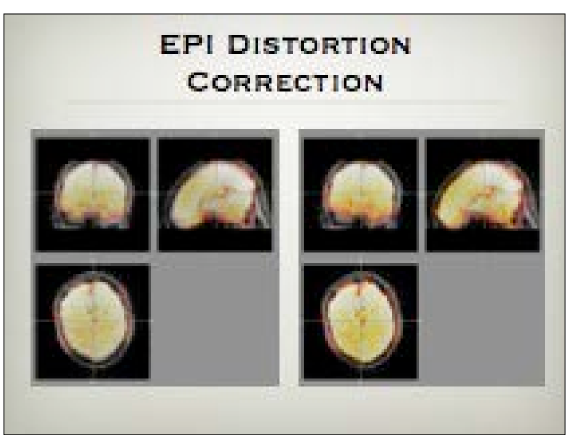
EPI Distortion
Correction

36

Bias Correction

37

B_1 Inhomogeneity

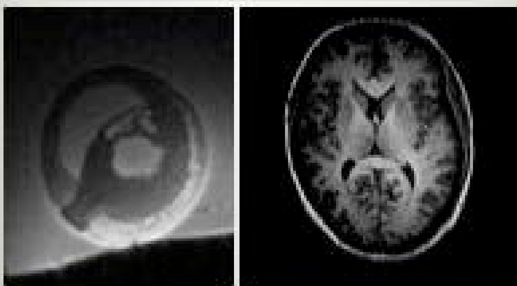

12T 1mm Surface Coil | 3T CP Head Coil

38

Sources of Signal Bias

- B1 inhomogeneity
  - Transmit coil response
  - Receive coil response
  - High field effects
- B0 inhomogeneity
  - Signal dropout (GE and EPI)

39

Appearance of B1 inhomogeneity

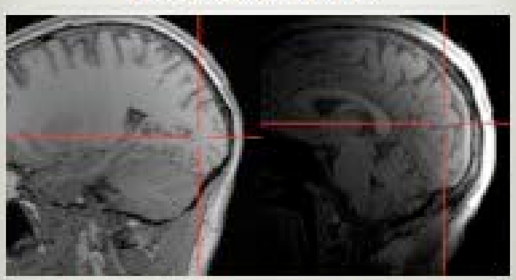

8-channel Whole-head Phased Array | 8-channel Occipital Phased Array

40

Approaches to Bias Correction

- Calibrate spatial response of coil in a phantom.
- Estimate bias from whole image.
- Estimate bias from presumably homogeneous tissue.

41

Smoothness Assumptions

- Assume that bias field has much lower spatial frequency than tissue structures.
- Estimating bias field from naive smoothing of image data generally fails for real MR data.
- Need to combine with segmentation, allowing bias field estimation within presumably homogeneous tissue.

42

Tissue Specific Bias Correction

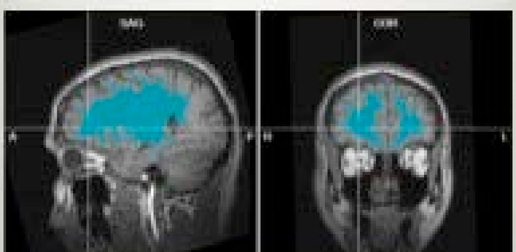

BrainVoyager: Step 1 - flood fill "white matter"

43

Tissue Specific Bias Correction

BrainVoyager: Step 2 - fit multiplicative 3rd order 3D polynomial (bias field estimate). Repeat until happy.

44

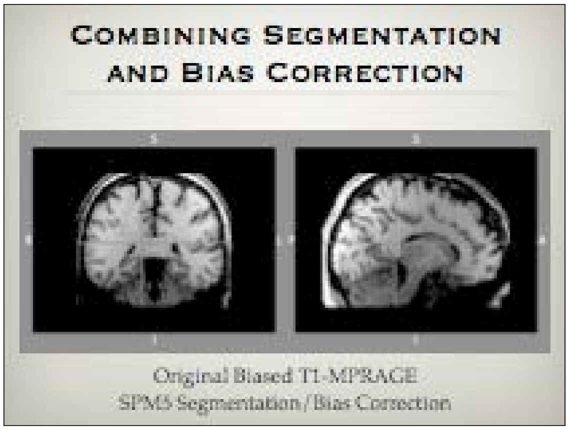
COMBINING SEGMENTATION AND BIAS CORRECTION
Original Biased T1-MPRAGE
SPM5 Segmentation / Bias Correction

45

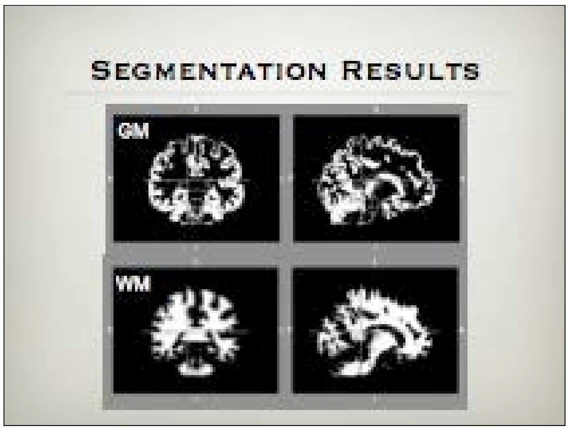
SEGMENTATION RESULTS
GM
WM

46

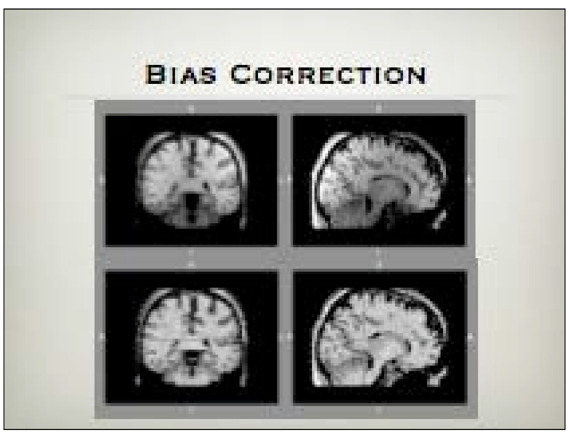
BIAS CORRECTION

47


OTHER ARTIFACTS

48

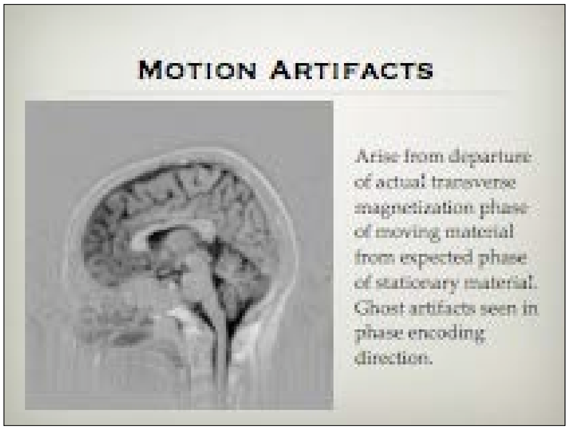
Motion Artifacts
Arise from departure of actual transverse magnetization phase of moving material from expected phase of stationary material. Ghost artifacts seen in phase encoding direction.

49

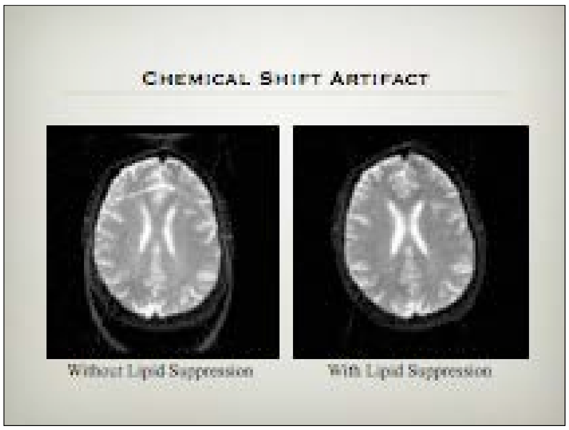
Chemical Shift Artifact
Without Lipid Suppression
With Lipid Suppression

50

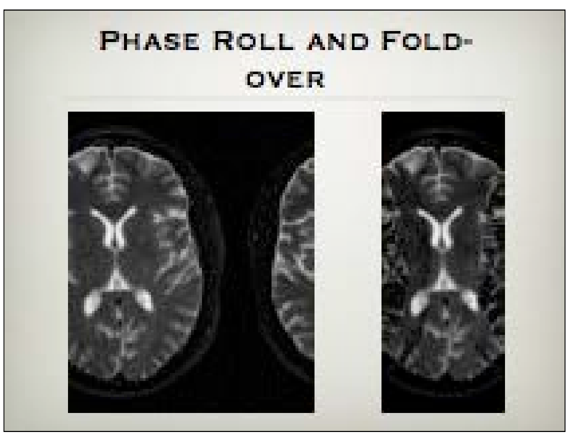
Phase Roll and Fold-over

51

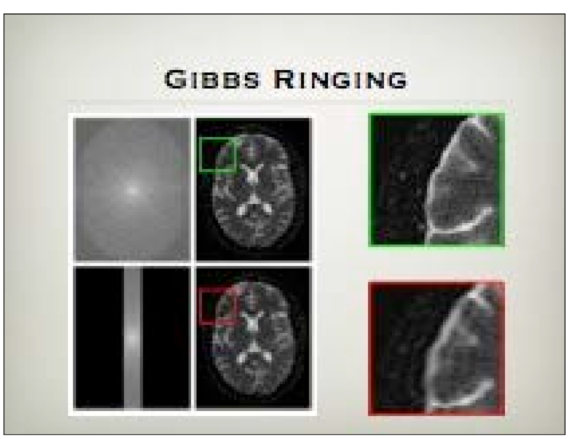
Gibbs Ringing

52

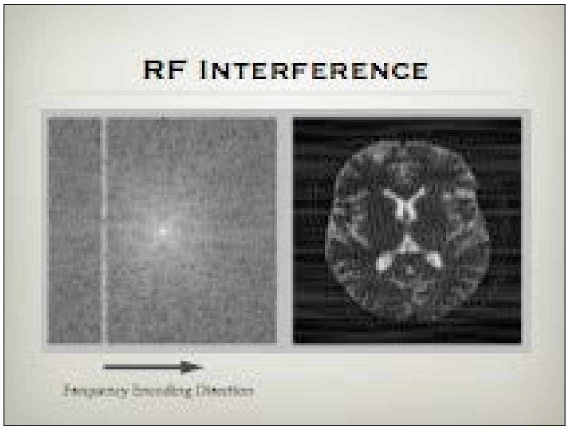
RF Interference
Frequency Encoding Direction

53

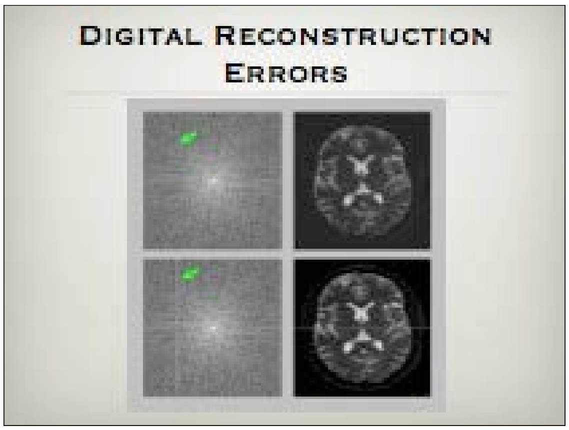
Digital Reconstruction Errors

54

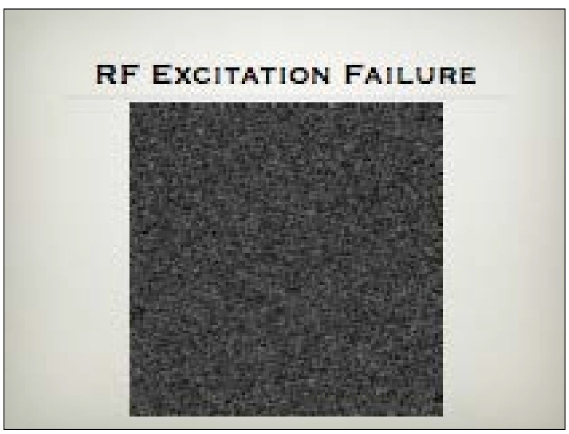
RF Excitation Failure

55

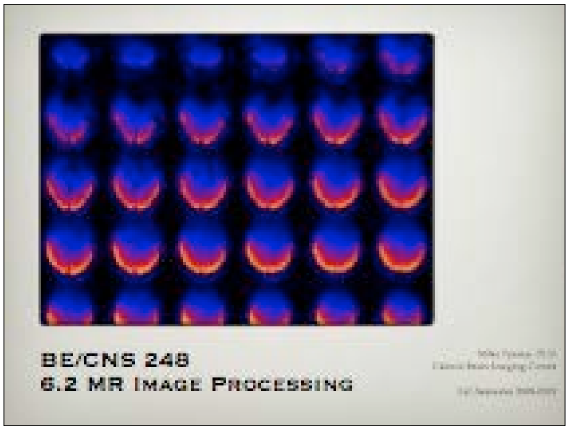

1

Lecture Summary

- 6.2 MR Image Processing
  - Spatial Filtering
  - Binary Operations
  - Spatial Interpolation
  - Quantitative image analysis
  - Image Registration
  - Tissue Segmentation
  - Bias Correction

2

3

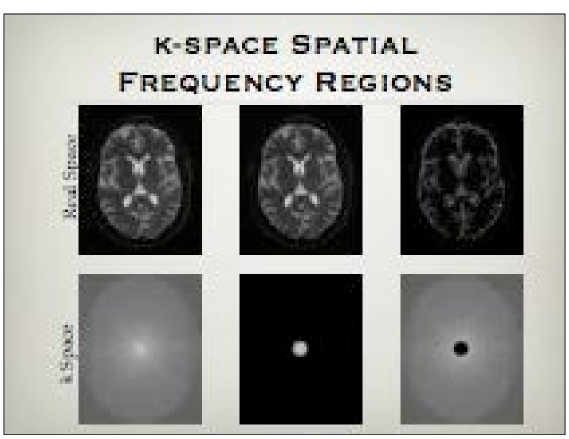

4

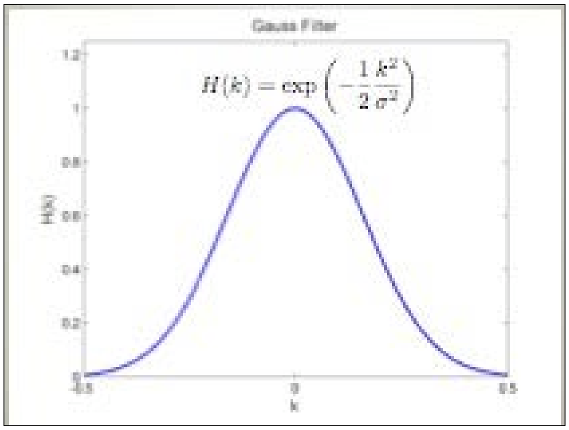

Gauss Filter
$H(k) = \exp\left(-\frac{1}{2}\frac{k^2}{\sigma^2}\right)$
H(k)
k

5

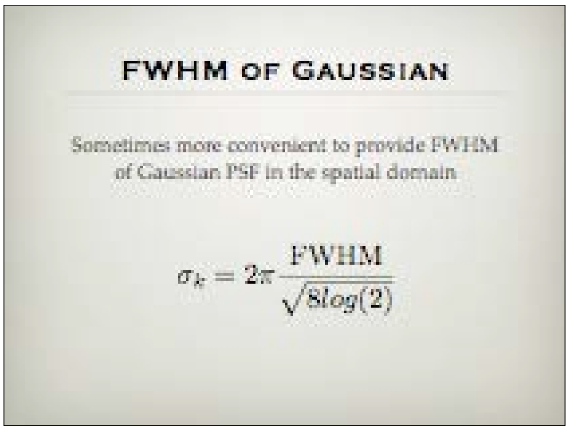

FWHM OF GAUSSIAN
Sometimes more convenient to provide FWHM of Gaussian PSF in the spatial domain
$\sigma_k = 2\pi \frac{\text{FWHM}}{\sqrt{8log(2)}}$

6

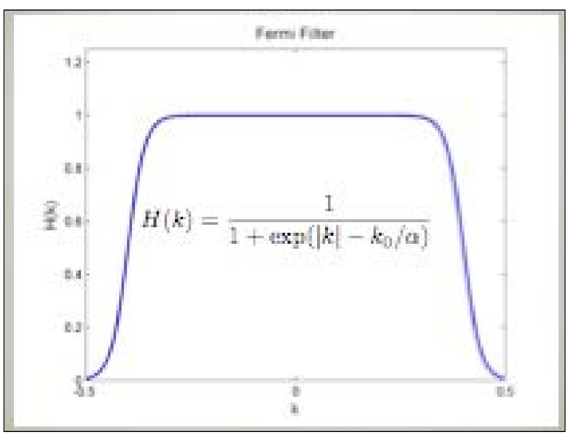

Fermi Filter
$H(k) = \frac{1}{1 + \exp(|k| - k_0/\alpha)}$
H(k)
k

7

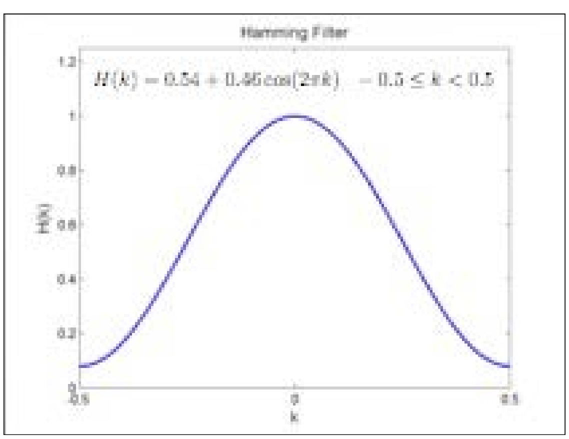

Hamming Filter
$H(k) = 0.54 + 0.46\cos(2\pi k) \quad -0.5 \le k < 0.5$
H(k)
k

8

PSF due to Filtering

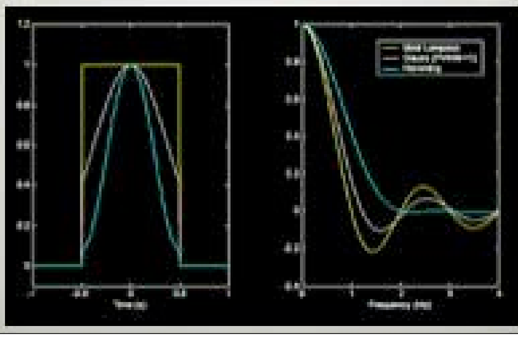

9

Spatial Domain Filtering

- Discrete implementation of convolution filtering in spatial domain.
- 2D or 3D convolution function.
- Linear (eg Gaussian) or non-linear (Median).
- Implemented in a moving mask or kernel.

10

Mask Operations

Mask Kernel * Image = New Image

Mask Kernel				Image				New Image		
0	1	0		8	5	5				
1	2	1	*	6	3	2	=		3.5	
0	1	0		3	2	2				

$$S'(x,y) = \frac{1}{Q}\sum_{k=-m}^{k=m}\sum_{l=-m}^{l=m} H(k,l)S(x+k,y+l)$$

$$Q = \sum_{k=-m}^{k=m}\sum_{l=-m}^{l=m} H(k,l)$$

11

Gaussian Filter

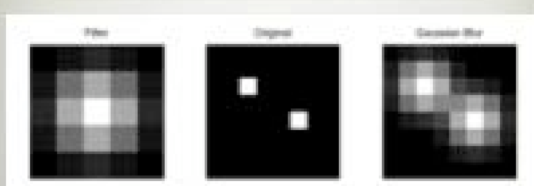

$$H(k,l) = H_0 \exp\left(\frac{-(k^2+l^2)}{2\sigma^2}\right) \quad k,l = -m \ldots m \quad m = 1,2,\ldots$$

Radial Gaussian

12

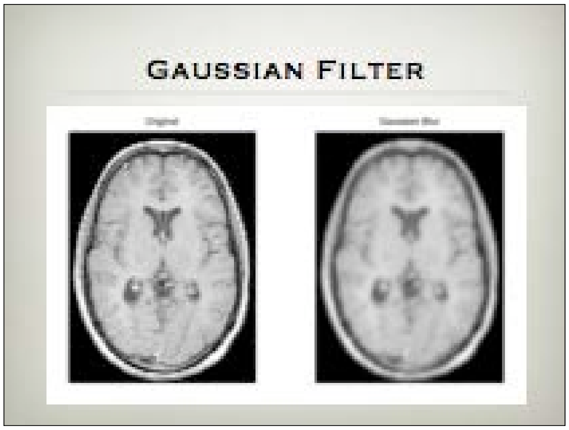
GAUSSIAN FILTER

13

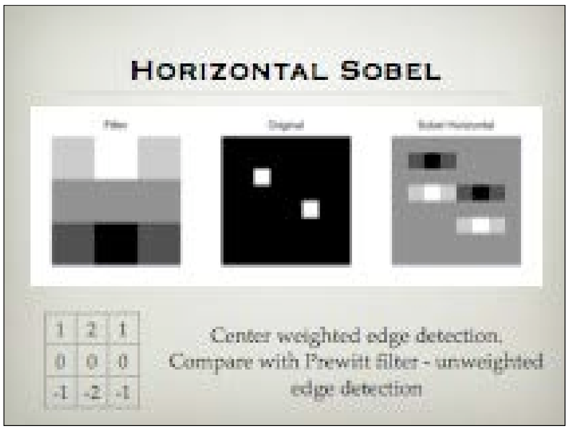
HORIZONTAL SOBEL
1 2 1
0 0 0
-1 -2 -1
Center weighted edge detection.
Compare with Prewitt filter - unweighted edge detection

14

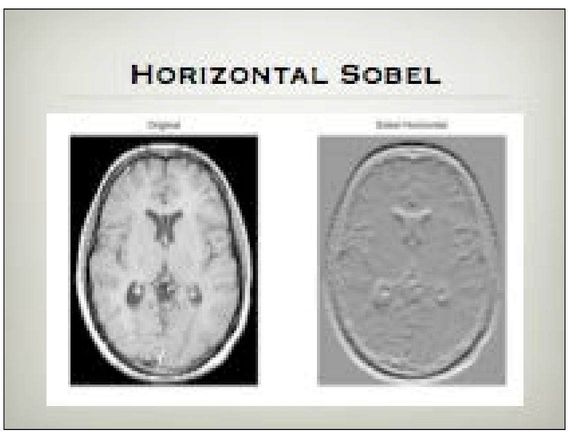
HORIZONTAL SOBEL

15

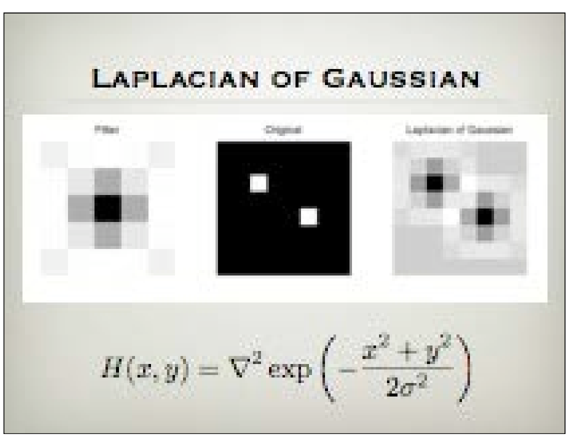
LAPLACIAN OF GAUSSIAN
$H(x,y) = \nabla^2 \exp\left(-\frac{x^2+y^2}{2\sigma^2}\right)$

16

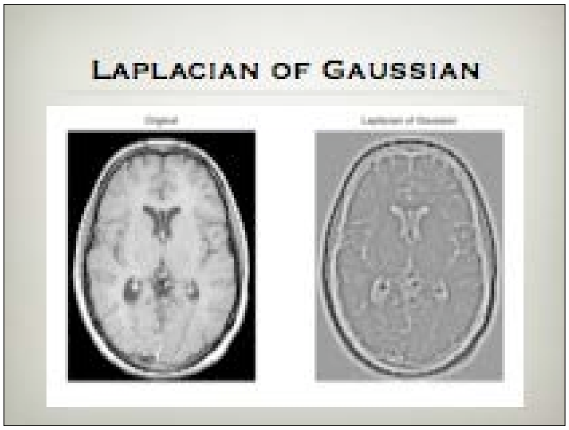
LAPLACIAN OF GAUSSIAN

17

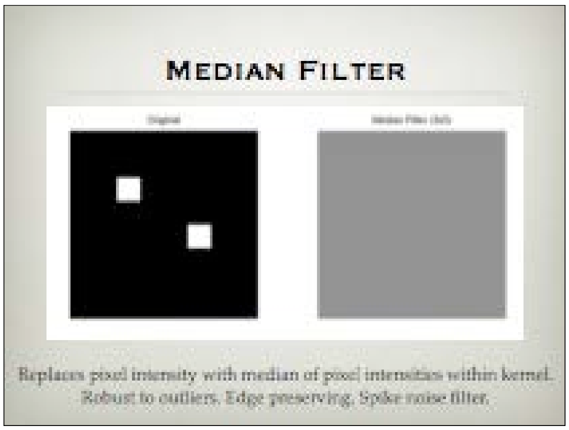
MEDIAN FILTER
Replaces pixel intensity with median of pixel intensities within kernel.
Robust to outliers. Edge preserving. Spike noise filter.

18

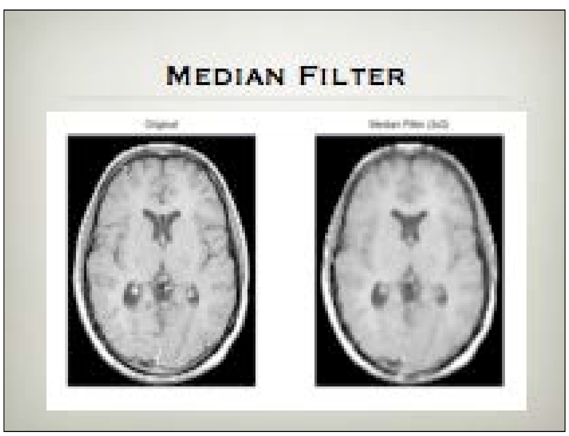
MEDIAN FILTER

19

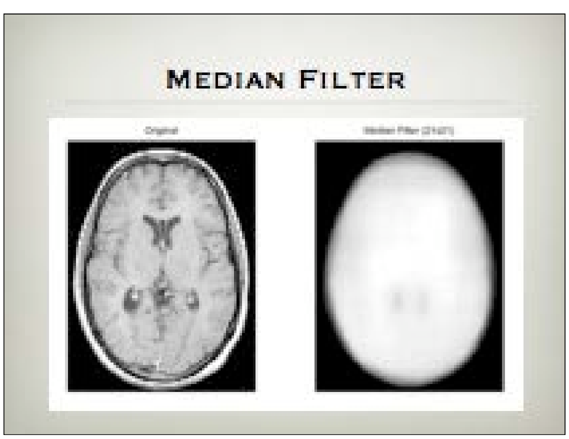
MEDIAN FILTER

20


BINARY OPERATIONS

21

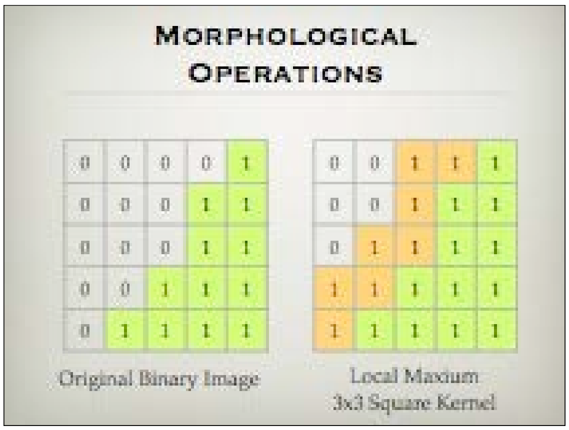
MORPHOLOGICAL OPERATIONS
0 0 0 0 1
0 0 0 1 1
0 0 0 1 1
0 0 1 1 1
0 1 1 1 1
Original Binary Image
0 0 1 1 1
0 0 1 1 1
0 1 1 1 1
1 1 1 1 1
1 1 1 1 1
Local Maxium
3x3 Square Kernel

22

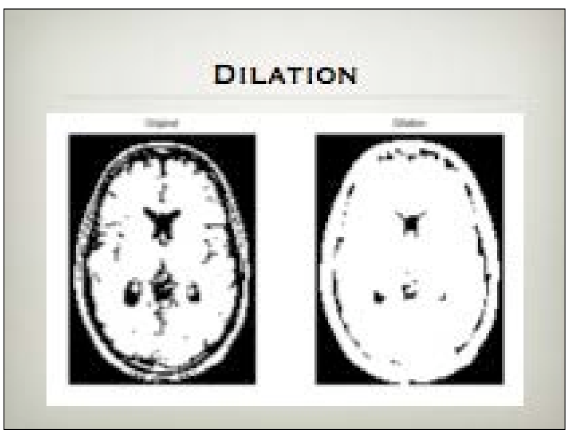
DILATION

23

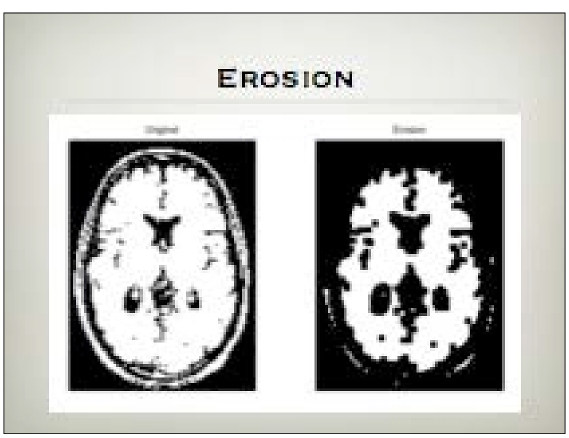
EROSION

24

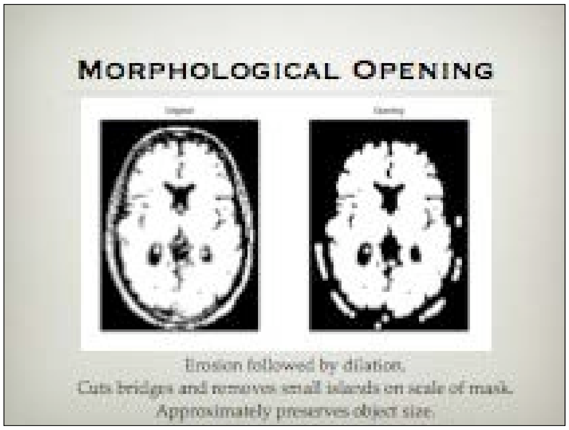
MORPHOLOGICAL OPENING
Erosion followed by dilation.
Cuts bridges and removes small islands on scale of mask.
Approximately preserves object size.

25

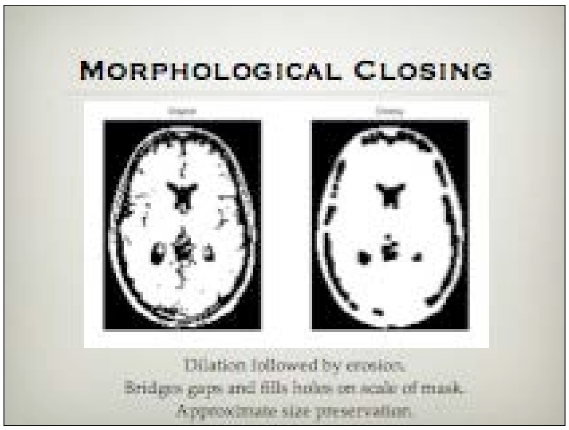
MORPHOLOGICAL CLOSING
Dilation followed by erosion.
Bridges gaps and fills holes on scale of mask.
Approximate size preservation.

26

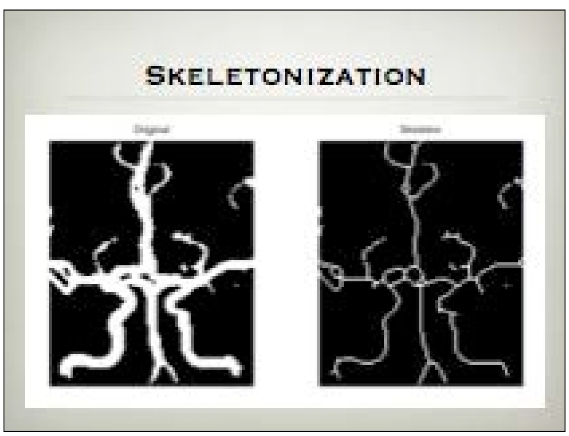
SKELETONIZATION

27

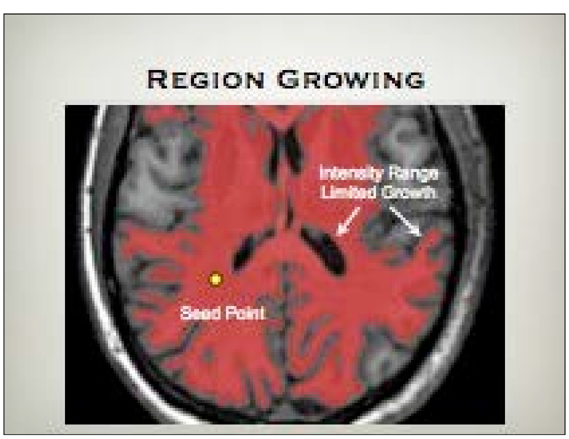
REGION GROWING
Intensity Range
Limited Growth
Seed Point

28


QUANTITATIVE IMAGE ANALYSIS

29

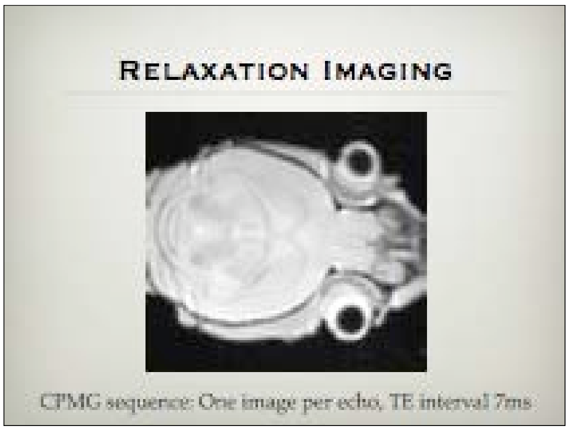
RELAXATION IMAGING
CPMG sequence: One image per echo, TE interval 7ms

30

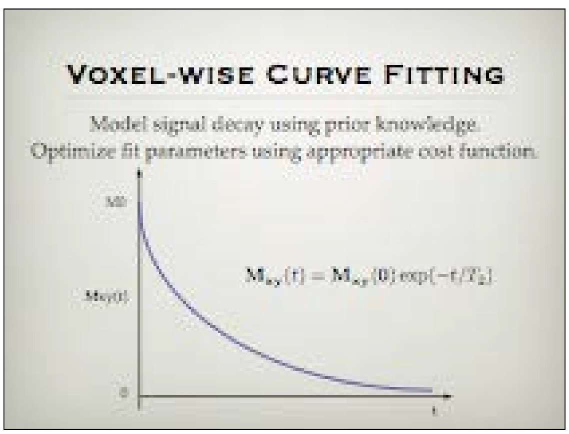
VOXEL-WISE CURVE FITTING
Model signal decay using prior knowledge.
Optimize fit parameters using appropriate cost function.
$M_{xy}(t) = M_{xy}(0)\exp(-t/T_2)$

31

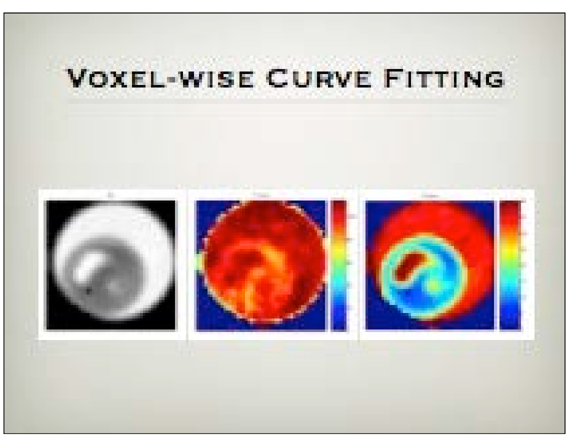
VOXEL-WISE CURVE FITTING

32

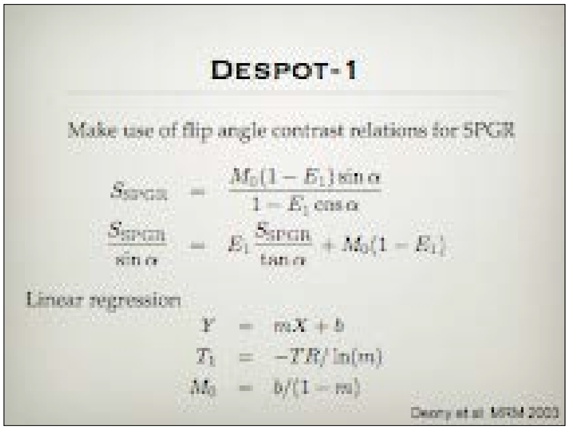

DESPOT-1
Make use of flip angle contrast relations for SPGR
$$S_{\mathrm{SPGR}} = \frac{M_0(1-E_1)\sin\alpha}{1-E_1\cos\alpha}$$
$$\frac{S_{\mathrm{SPGR}}}{\sin\alpha} = E_1\frac{S_{\mathrm{SPGR}}}{\tan\alpha} + M_0(1-E_1)$$
Linear regression
$$Y = mX + b$$
$$T_1 = -TR/\ln(m)$$
$$M_0 = b/(1-m)$$
Deoni et al MRM 2003

33

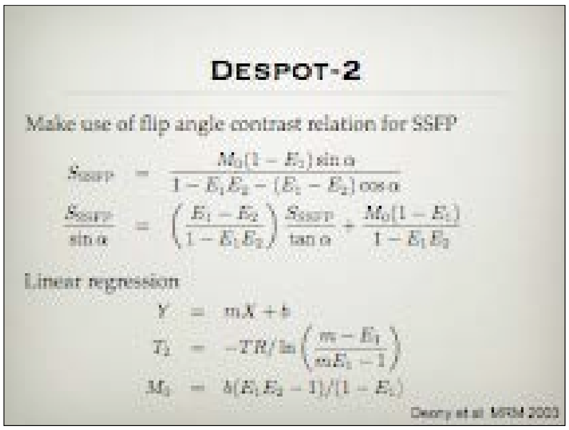

DESPOT-2
Make use of flip angle contrast relation for SSFP
$$S_{\mathrm{SSFP}} = \frac{M_0(1-E_1)\sin\alpha}{1-E_1E_2-(E_1-E_2)\cos\alpha}$$
$$\frac{S_{\mathrm{SSFP}}}{\sin\alpha} = \left(\frac{E_1-E_2}{1-E_1E_2}\right)\frac{S_{\mathrm{SSFP}}}{\tan\alpha} + \frac{M_0(1-E_1)}{1-E_1E_2}$$
Linear regression
$$Y = mX + b$$
$$T_2 = -TR/\ln\left(\frac{m-E_1}{mE_1-1}\right)$$
$$M_0 = b(E_1E_2-1)/(1-E_1)$$
Deoni et al MRM 2003

34

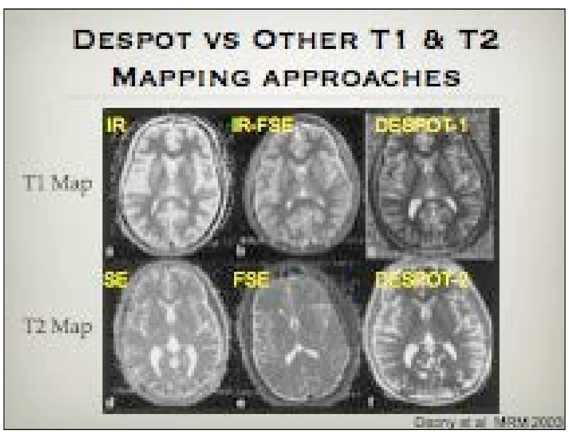

DESPOT VS OTHER T1 & T2 MAPPING APPROACHES
T1 Map
T2 Map
IR
IR-FSE
DESPOT-1
SE
FSE
DESPOT-2
Deoni et al MRM 2003

35

IMAGE REGISTRATION

36

Deformation Fields

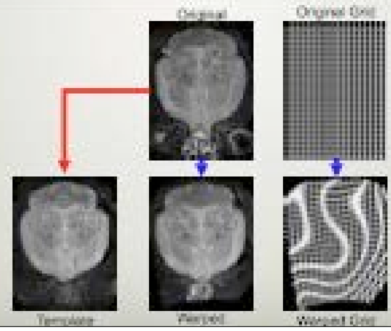

37

Linear Transforms

$$\begin{pmatrix} x' \\ y' \\ z' \\ 1 \end{pmatrix} = \begin{pmatrix} t_{11} & t_{12} & t_{13} & d_x \\ t_{21} & t_{22} & t_{23} & d_y \\ t_{31} & t_{32} & t_{33} & d_z \\ 0 & 0 & 0 & 1 \end{pmatrix} \begin{pmatrix} x \\ y \\ z \\ 1 \end{pmatrix}$$

38

Rigid Body Transforms

- Rigid body transform preserves volume and angles.
- Rotation
- Translation

39

Rotation Matrix

$$\mathbf{R_x}(\theta) = \begin{pmatrix} 1 & 0 & 0 & 0 \\ 0 & \cos\theta & -\sin\theta & 0 \\ 0 & \sin\theta & \cos\theta & 0 \\ 0 & 0 & 0 & 1 \end{pmatrix}$$

40

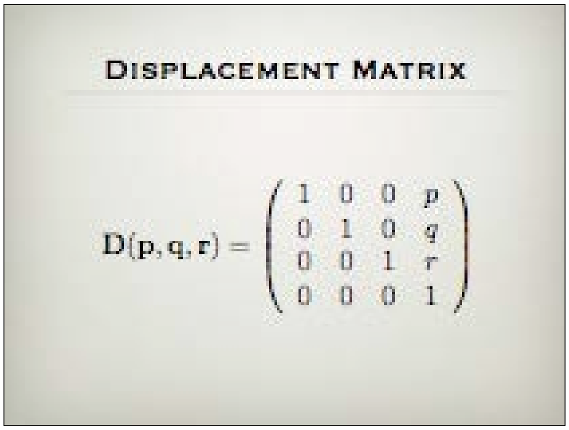
DISPLACEMENT MATRIX
$\mathbf{D}(\mathbf{p},\mathbf{q},\mathbf{r}) = \begin{pmatrix} 1 & 0 & 0 & p \\ 0 & 1 & 0 & q \\ 0 & 0 & 1 & r \\ 0 & 0 & 0 & 1 \end{pmatrix}$

41

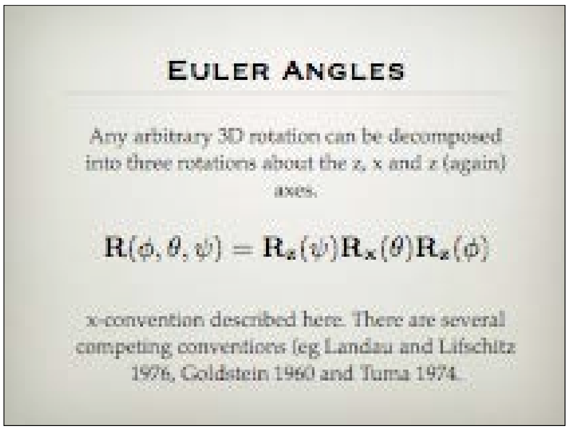
EULER ANGLES
Any arbitrary 3D rotation can be decomposed into three rotations about the z, x and z (again) axes.
$\mathbf{R}(\phi,\theta,\psi) = \mathbf{R_z}(\psi)\mathbf{R_x}(\theta)\mathbf{R_z}(\phi)$
x-convention described here. There are several competing conventions (eg Landau and Lifschitz 1976, Goldstein 1960 and Tuma 1974.

42

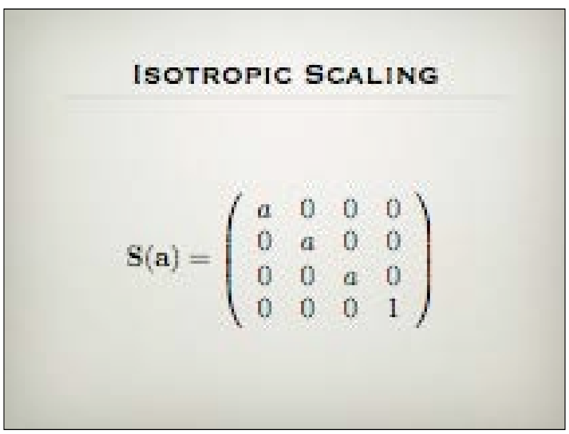
ISOTROPIC SCALING
$\mathbf{S}(\mathbf{a}) = \begin{pmatrix} a & 0 & 0 & 0 \\ 0 & a & 0 & 0 \\ 0 & 0 & a & 0 \\ 0 & 0 & 0 & 1 \end{pmatrix}$

43

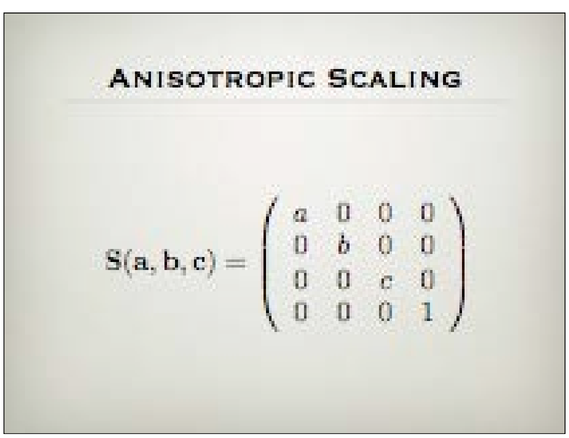
ANISOTROPIC SCALING
$\mathbf{S}(\mathbf{a},\mathbf{b},\mathbf{c}) = \begin{pmatrix} a & 0 & 0 & 0 \\ 0 & b & 0 & 0 \\ 0 & 0 & c & 0 \\ 0 & 0 & 0 & 1 \end{pmatrix}$

44

Shear Transform

$$\mathbf{E}(\sigma_{\mathbf{xy}}, \sigma_{\mathbf{xz}}, \sigma_{\mathbf{yz}}) = \begin{pmatrix} 1 & \sigma_{xy} & \sigma_{xz} & 0 \\ 0 & 1 & \sigma_{yz} & 0 \\ 0 & 0 & 1 & 0 \\ 0 & 0 & 0 & 1 \end{pmatrix}$$

45

Affine Transform

An affine transformation combines rotation, scaling, shear and displacement.

$$\mathbf{T} = \mathbf{D\ E\ S\ R} = \begin{pmatrix} a_{11} & a_{12} & a_{12} & p \\ a_{21} & a_{22} & a_{23} & q \\ a_{31} & a_{32} & a_{33} & r \\ 0 & 0 & 0 & 1 \end{pmatrix}$$

12 independent parameters.
Straight lines and distance ratios are preserved.

46

Non-linear Deformation

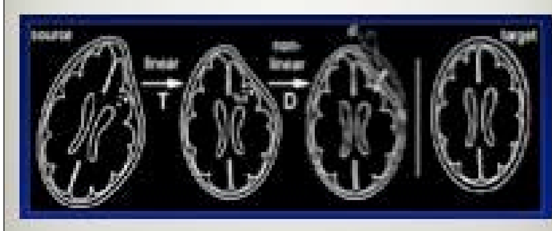

47

Registration Cost Metrics

- Least-squares difference
- Scaled least-squares
- Correlation
- Mutual Information
- Normalized Mutual Information

48

Mutual Information

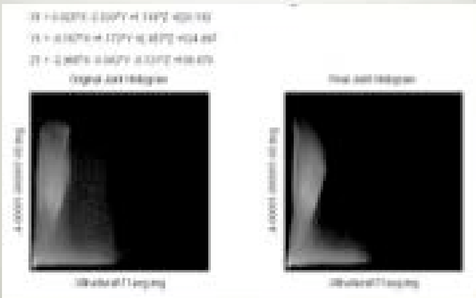

49

Non-linear Registration

50

Non-linear Coregistration

- Inter-subject registration
- Invoked when affine transformation is insufficiently accurate
- Typically extends an affine transformation with a spatially variant but regularized displacement in each dimension
- Registration to normalized brain spaces

51

Normalized Brain Spaces

MNI 305

ICBM 152

PED 175

COLIN 27

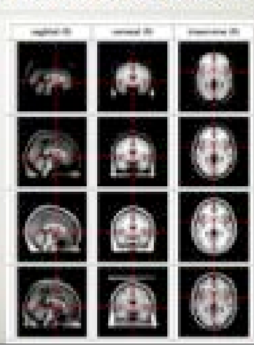

52

Spatial Normalization

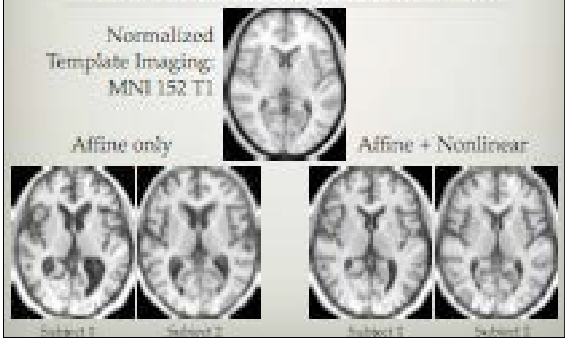

53

Nonlinear Deformation

54

Polynomial Deformation

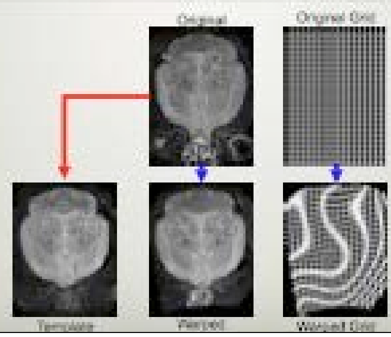

55

Discrete cosine transform deformation

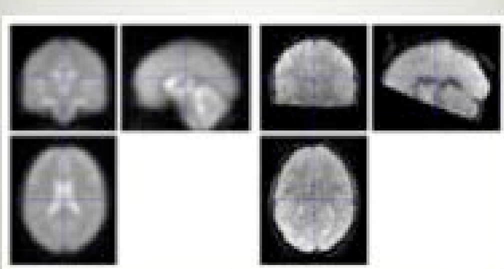

Implemented by SPM5 for spatial normalization

56

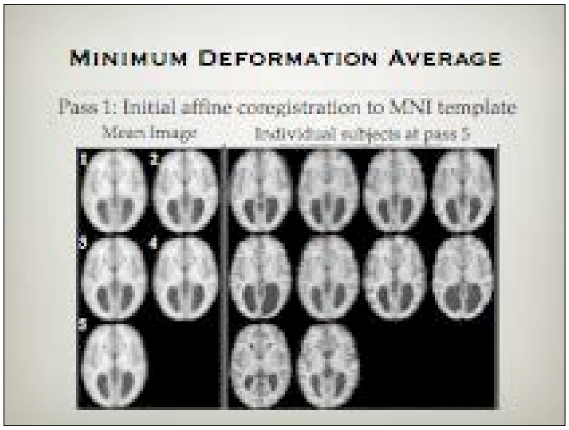
MINIMUM DEFORMATION AVERAGE
Pass 1: Initial affine coregistration to MNI template
Mean Image
Individual subjects at pass 5

57

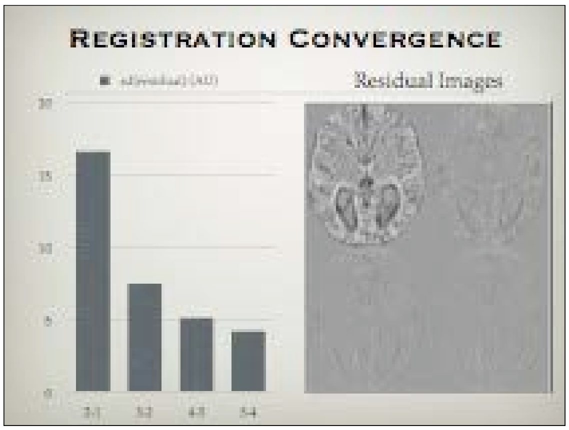
REGISTRATION CONVERGENCE
Residual Images

58

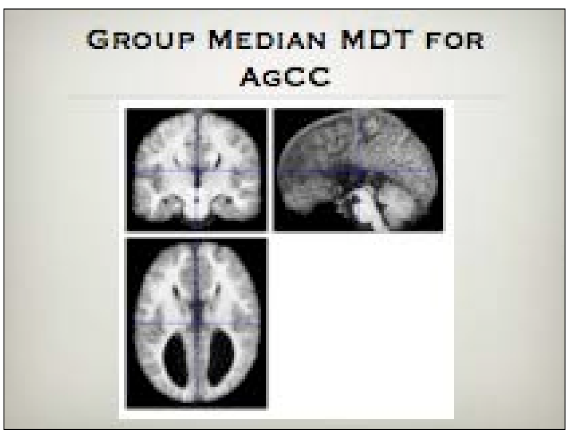
GROUP MEDIAN MDT FOR AGCC

59

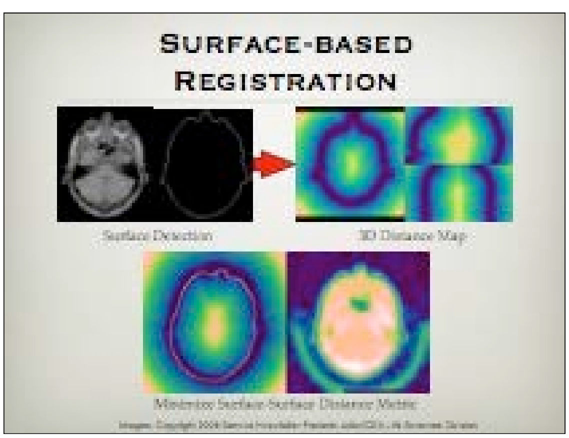
SURFACE-BASED REGISTRATION
Surface Detection
3D Distance Map
Minimize Surface-Surface Distance Metric

60


SPATIAL
INTERPOLATION

61

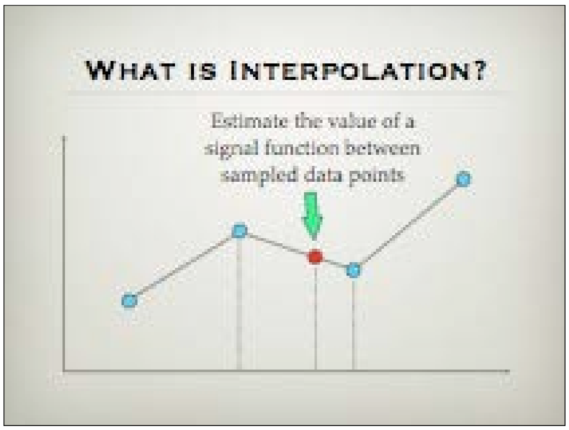
WHAT IS INTERPOLATION?
Estimate the value of a
signal function between
sampled data points

62

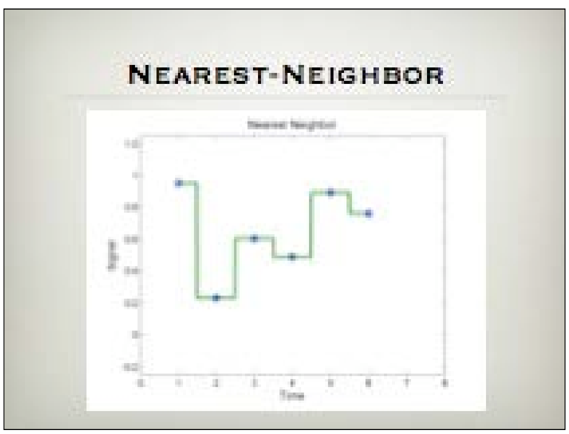
NEAREST-NEIGHBOR

63

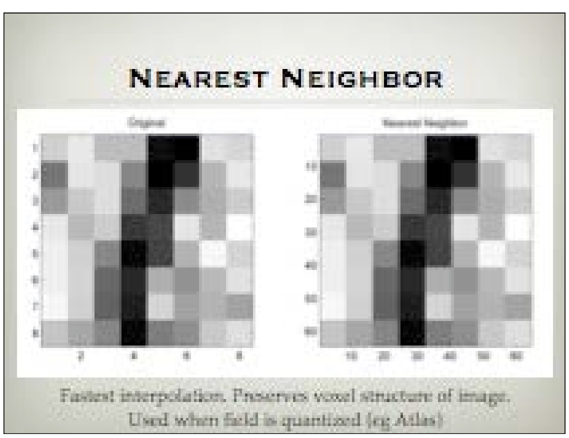
NEAREST NEIGHBOR
Fastest interpolation. Preserves voxel structure of image.
Used when field is quantized (eg Atlas)

64

Linear Interpolation

Assume signal varies linearly between samples

$$S(x) = S(x_0) + \frac{S(x_1) - S(x_0)}{x_1 - x_0}(x - x_0)$$

NOT continuous in the first derivative (C1 continuous)

65

Linear Interpolation

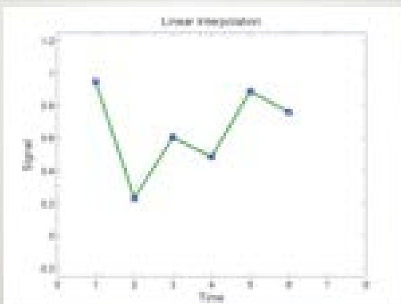

66

Linear Interpolation

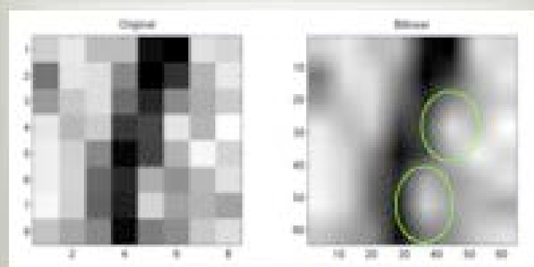

Fast interpolation commonly used for image display ("digital zoom"). "Star artifact" can be distracting at high magnification.

67

Cubic Spline

Specific example of a piecewise polynomial (PP)

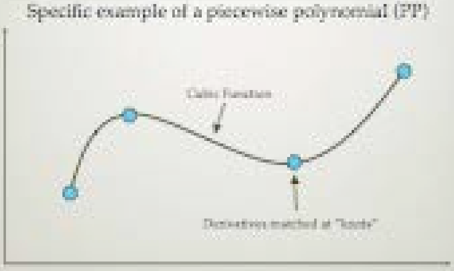

68

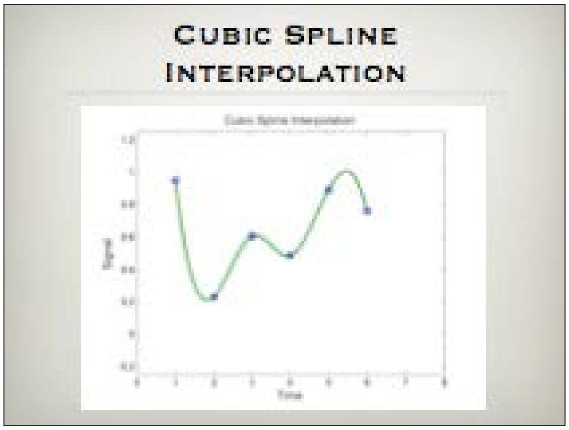
Cubic Spline
Interpolation

69

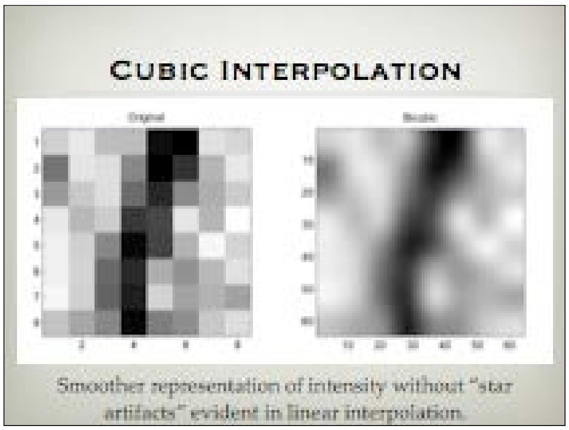
Cubic Interpolation
Smoother representation of intensity without "star artifacts" evident in linear interpolation.

70

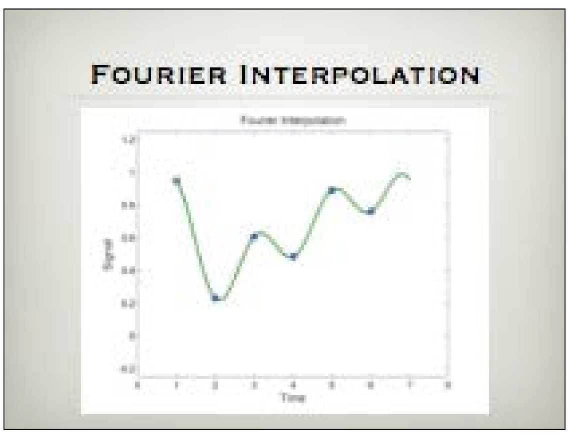
Fourier Interpolation

71

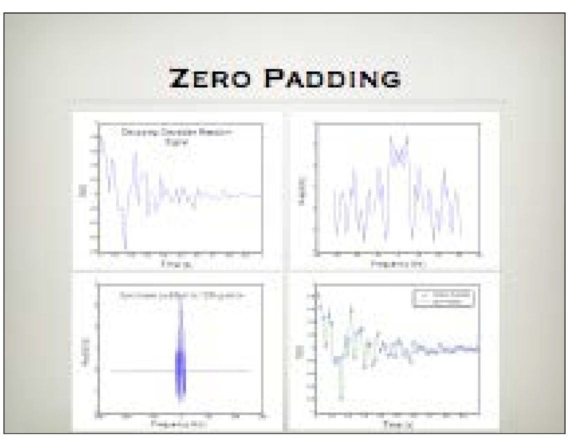
Zero Padding

72


IMAGE SEGMENTATION

73

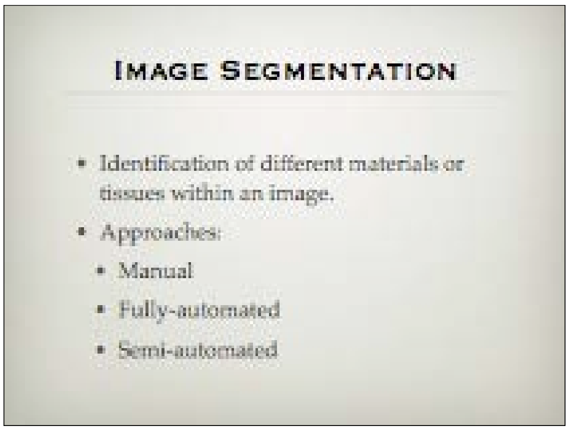
IMAGE SEGMENTATION
• Identification of different materials or tissues within an image.
• Approaches:
• Manual
• Fully-automated
• Semi-automated

74

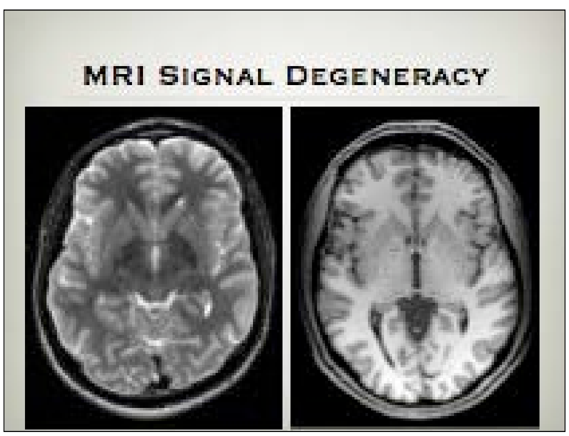
MRI SIGNAL DEGENERACY

75

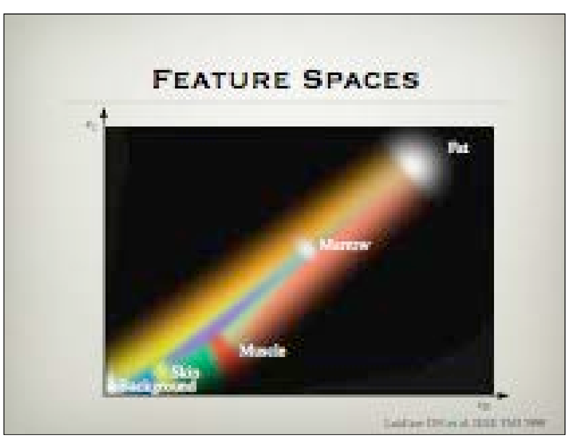
FEATURE SPACES
Fat
Marrow
Muscle
Skin
Background

76

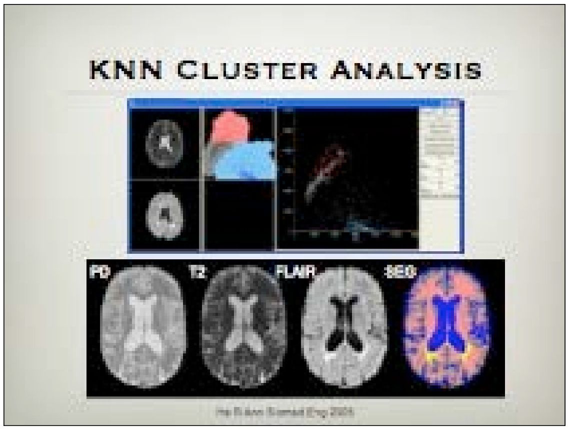
KNN Cluster Analysis
PD
T2
FLAIR
SEG

77

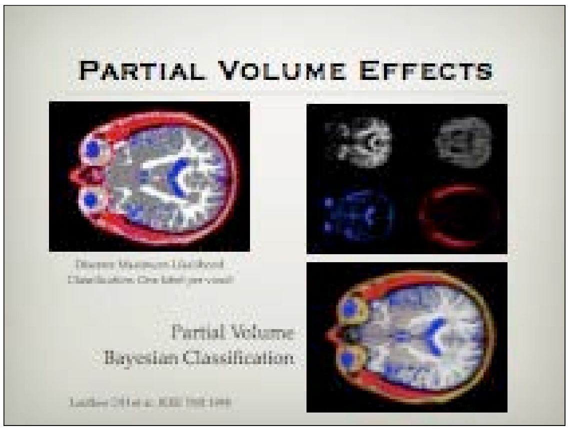
Partial Volume Effects
Partial Volume
Bayesian Classification

78

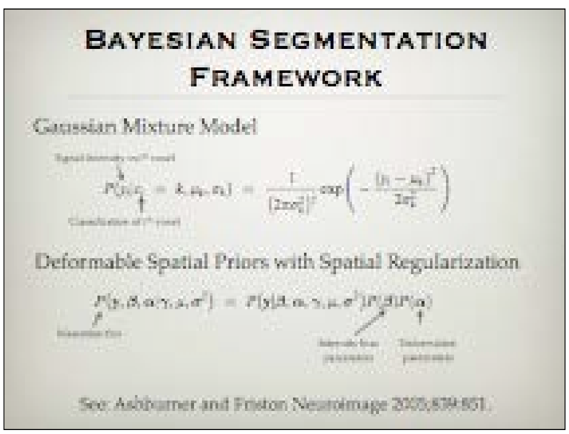
Bayesian Segmentation Framework
Gaussian Mixture Model
Deformable Spatial Priors with Spatial Regularization
See: Ashburner and Friston Neuroimage 2005;839-851.

79

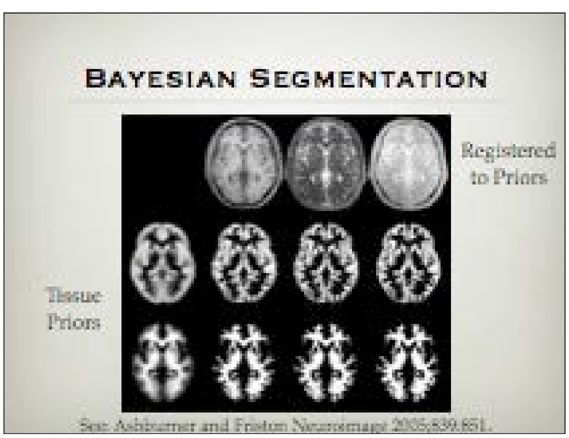
Bayesian Segmentation
Registered
to Priors
Tissue
Priors
See: Ashburner and Friston Neuroimage 2005;839-851.

80

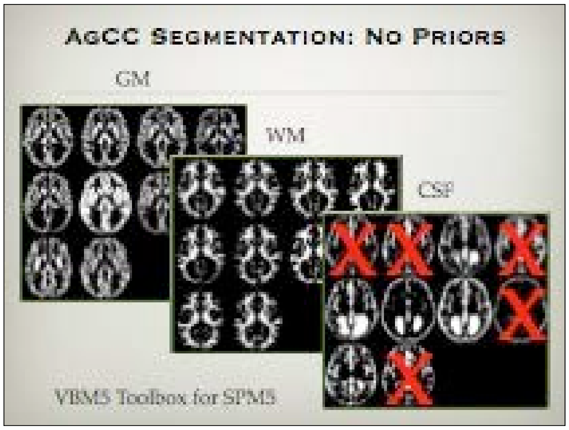
AgCC Segmentation: No Priors
GM
WM
CSF
VBM5 Toolbox for SPM5

81

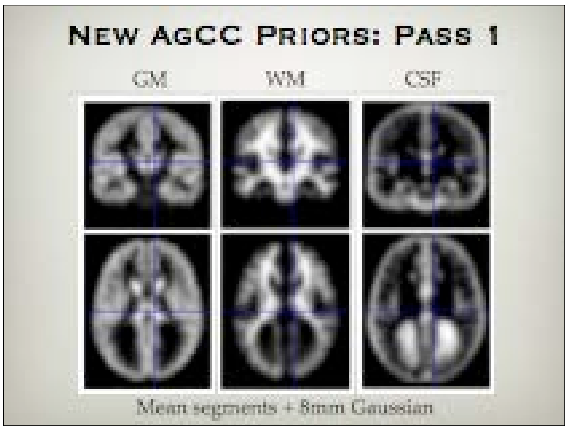
New AgCC Priors: Pass 1
GM
WM
CSF
Mean segments + 8mm Gaussian

82

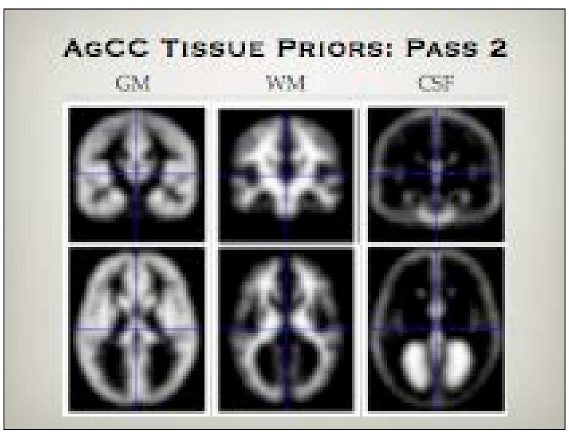
AgCC Tissue Priors: Pass 2
GM
WM
CSF

83

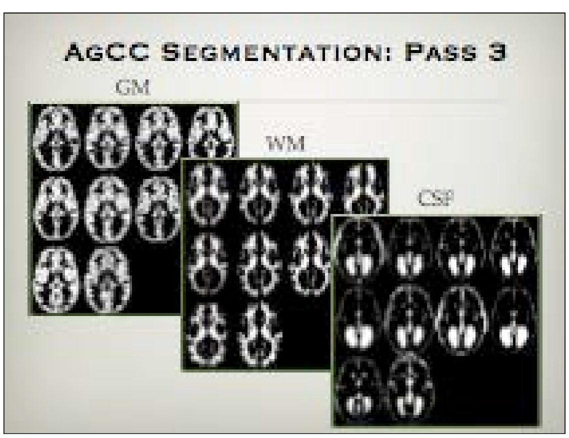
AgCC Segmentation: Pass 3
GM
WM
CSF

84

Atlas-Based Segmentation

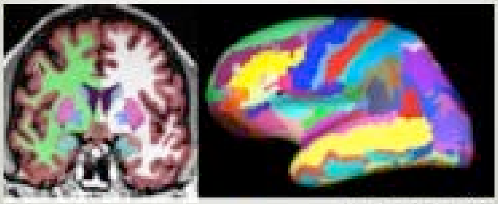

Coregister subject image with template image in standard space (MNI, Talairach).
Allow for variations when segmenting cortex.

85

Cortical Parcellation

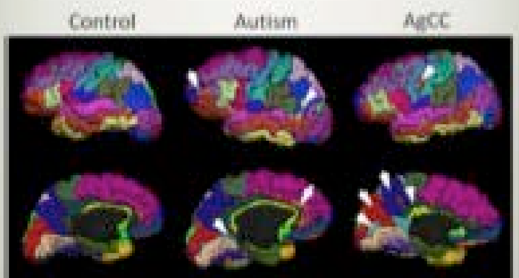

86

Next Lecture

- 7T MRI Demonstrations
  - Bring food samples
  - Meet outside CBIC at 1:30pm

87

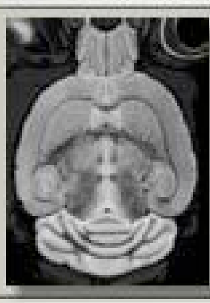

BE/CNS 248

7.1 MR Microscopy

1

Lecture Summary

- 7.1 MR Microscopy
  - Spatial resolution limits
  - MR microscopy achievements
  - MR microscopy hardware
  - Applications examples
    - Diffusion histology
    - Embryonic development
    - Myocardial fiber tracking

2

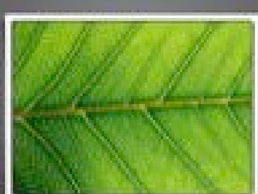

MR Microscopy

3

MR Microscopy

- Roughly defined as MRI with a spatial resolution less than 100um.
- Application areas:
  - Small animal imaging
  - Developmental biology
  - Plant biology
  - MR histology
  - Porous media
  - Chemical Engineering
  - ...

4

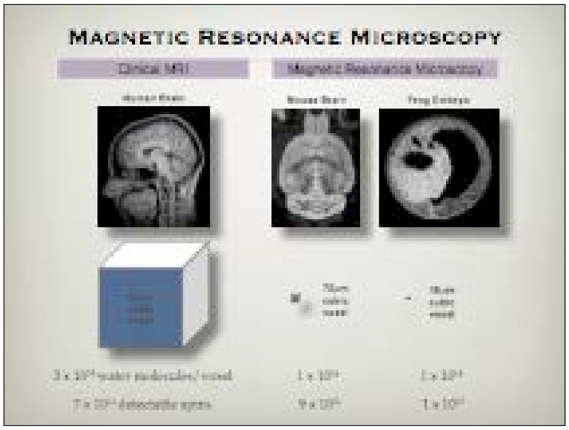

5

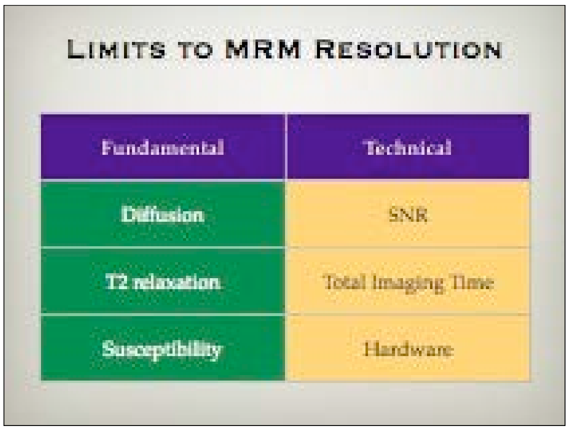

LIMITS TO MRM RESOLUTION

Fundamental	Technical
Diffusion	SNR
T2 relaxation	Total Imaging Time
Susceptibility	Hardware

6

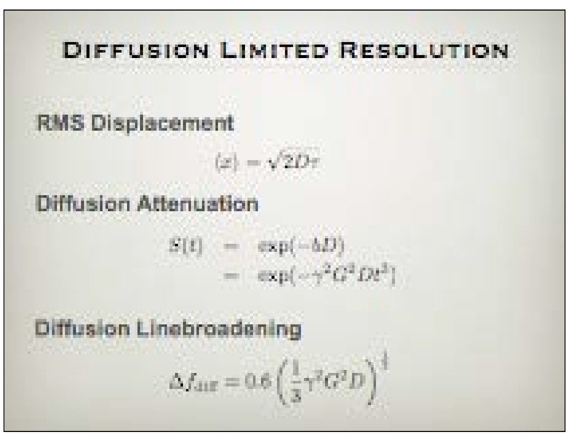

7

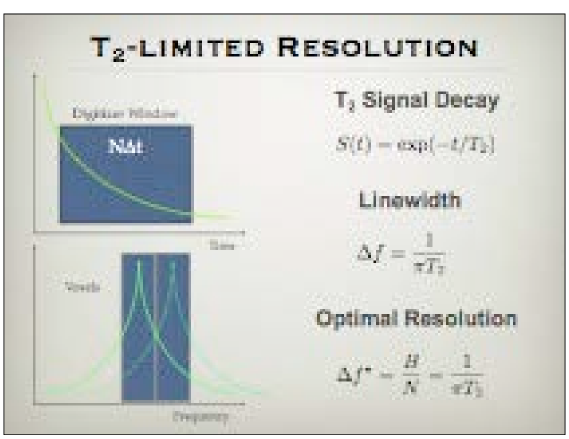

8

Resolution Limits

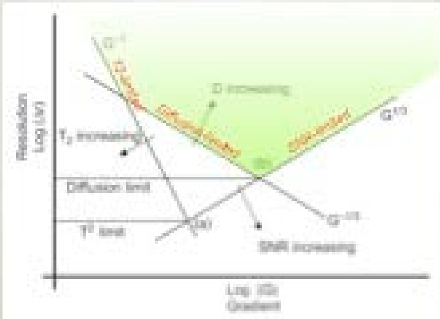

9

Increasing Signal

- Higher field
  - More polarization
  - Greater signal induction
  - Shorter T_2 (bad)
- Smaller coil-sample distances
- Hyperpolarization

10

Reduction of Noise in MRI

- Sample or Subject Noise
  - Important at lower fields/larger subjects
  - Can't cool subject
- RF coil
  - Important at higher fields/smaller samples
  - Can cool coil
- Improve RF preamplifier
- Improve RF receiver electronics
- Minimize external noise sources (EMI)

11

MRM SNR

Signal-to-noise ratio as a function of imaging parameters

$$\frac{S}{\sigma_N} = K\left(\Delta x \cdot \Delta y \cdot \Delta z\right)\sqrt{\frac{N_{av}}{\Delta f}}$$

Total imaging time proportional to N_{av}

$$N_{av} \propto \frac{1}{\Delta x^6}$$

Total imaging time has an inverse sixth power relation to voxel dimension at constant SNR.

12

All MR Microscopy is Diffusion Weighted

- At high spatial resolutions, the gradient pulses associated with image acquisition have comparable moments to diffusion-weighted pulses.
- All MR microscopy must be considered to be intrinsically diffusion weighted.
- b-matrix calculation must account for cross-terms between imaging and diffusion-weighting gradient pulses.

$$b_{ij}(T) = \gamma^2 \int_0^T dt\, k_i(t) k_j(t)$$

13

MRM Resolution Records

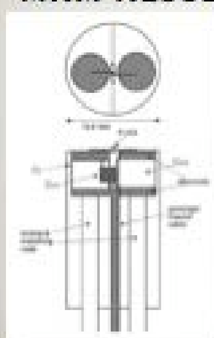

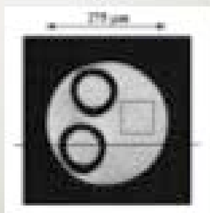

14

MRM Resolution Records

Ciobanu, L. & Pennington, C.H. 3D micron-scale MRI of single biological cells. *Solid State Nucl Magn Reson* **25**, 138-41 (2004)

Field Strength: **9.3T**
RF Coil: **75um id solenoid**
Spatial Resolution: **3.7um x 3.3um x 3.3um**

15

MRI of Neurons

3um isotropic resolution

500um thick mouse striatal tissue slice. 200um diameter micro surface coil. Flint *et al* 2007

16


MR Microscopy
Hardware

17


High Field Magnets for MRM
9.4T 300mm
11.7T 89mm
14.1T 89mm

18


MR Microscopy RF Coils

19


Microscopy Gradients
4T/m Cylindrical
12T/m Biplanar
2.5T/m Uniplanar

20

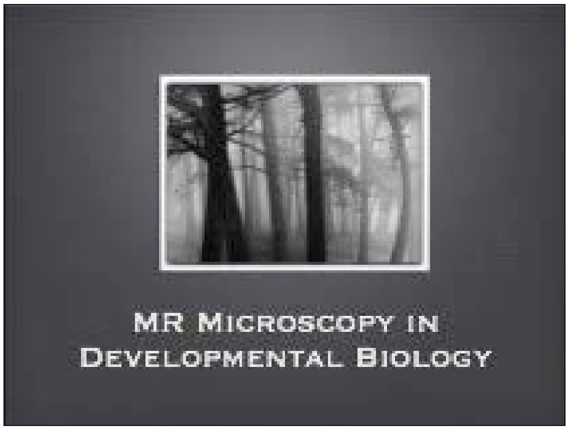
MR Microscopy in
Developmental Biology

21

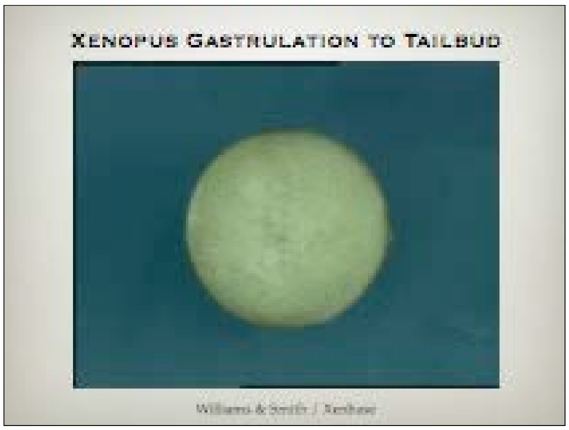
Xenopus Gastrulation to Tailbud

22

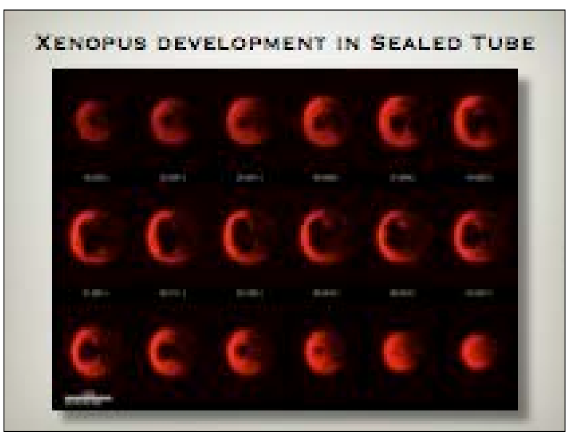
Xenopus development in Sealed Tube

23


From Gastrula to Tail-bud Stage

24

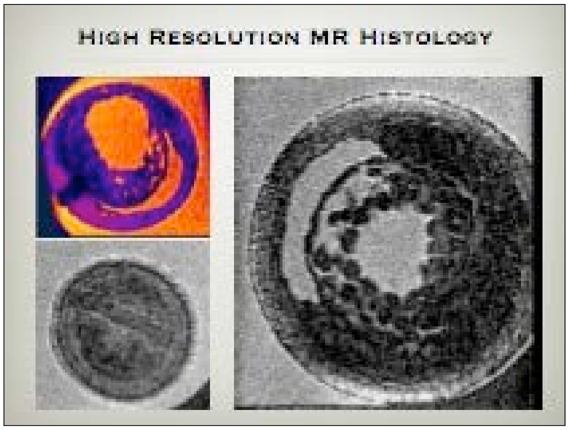
HIGH RESOLUTION MR HISTOLOGY

25

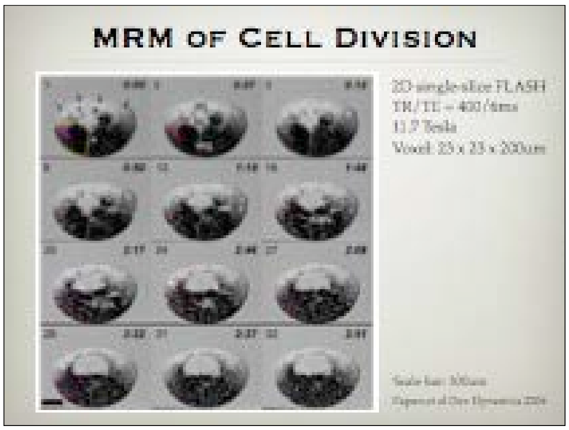
MRM OF CELL DIVISION
2D single-slice FLASH
TR/TE = 400/4ms
11.7 Tesla
Voxel: 23 x 23 x 200um

26

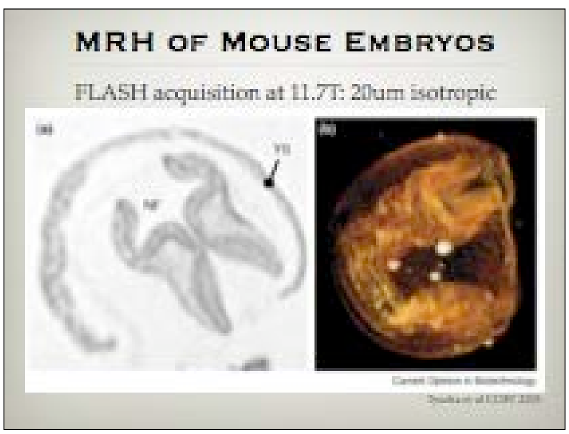
MRH OF MOUSE EMBRYOS
FLASH acquisition at 11.7T: 20um isotropic

27

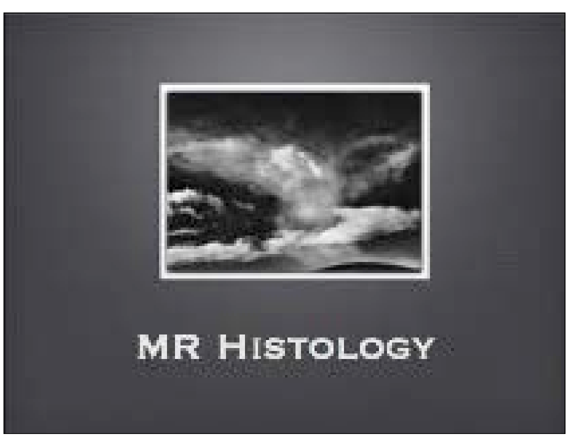
MR HISTOLOGY

28

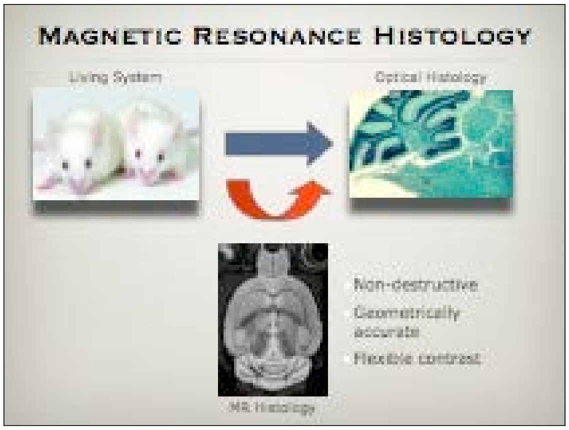

29

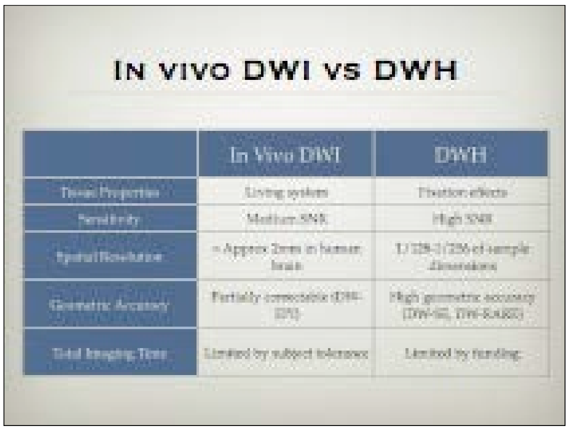

	In Vivo DWI	DWH
Tissue Properties	Living system	Fixation effects
Sensitivity	Medium SNR	High SNR
Spatial Resolution	~ Approx 2mm in human brain	1/128-1/256 of sample dimensions
Geometric Accuracy	Partially correctable (DW-EPI)	High geometric accuracy (DW-SE, DW-RARE)
Total Imaging Time	Limited by subject tolerance	Limited by handling

30

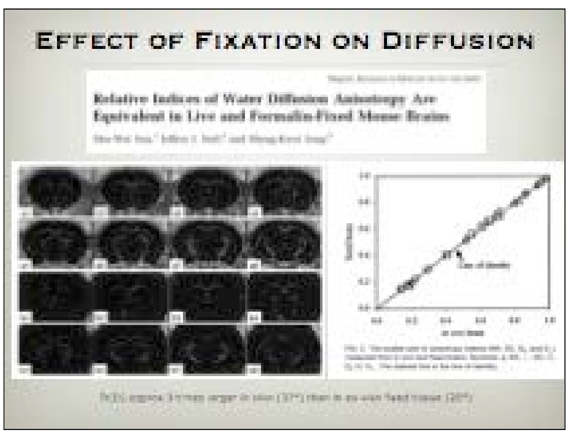

31

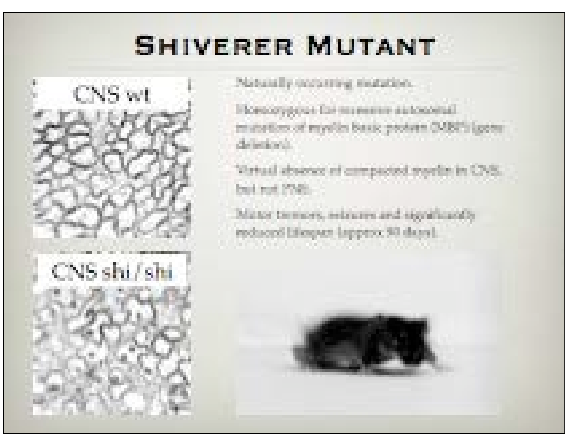

32

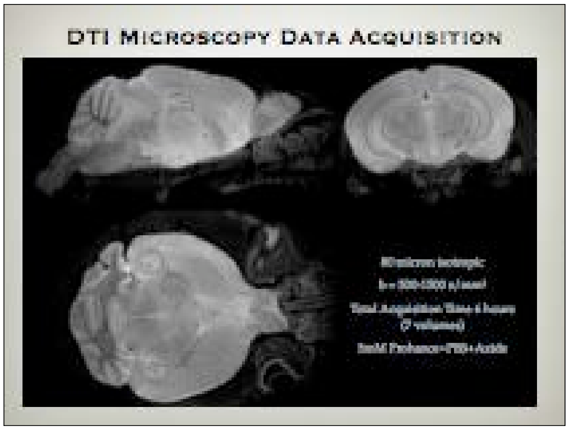
DTI Microscopy Data Acquisition

33

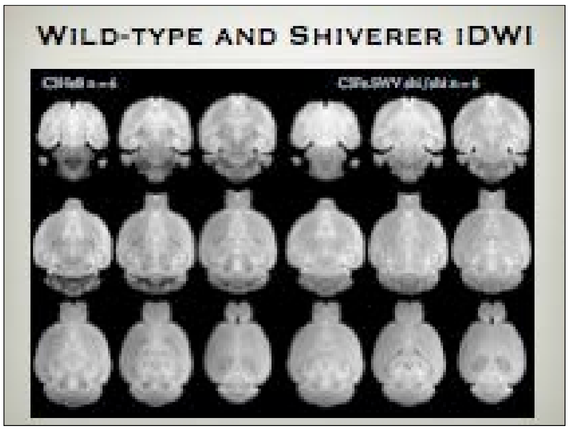
Wild-type and Shiverer iDWI

34

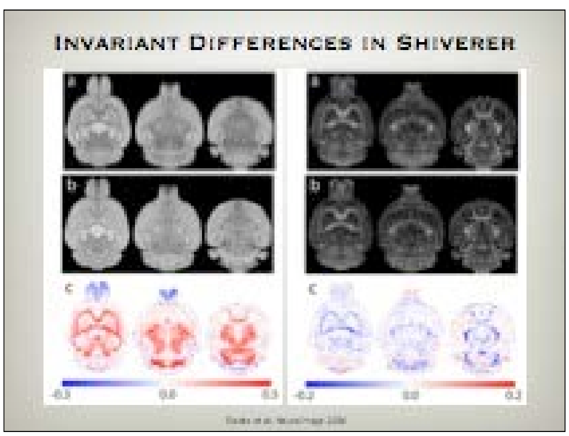
Invariant Differences in Shiverer

35

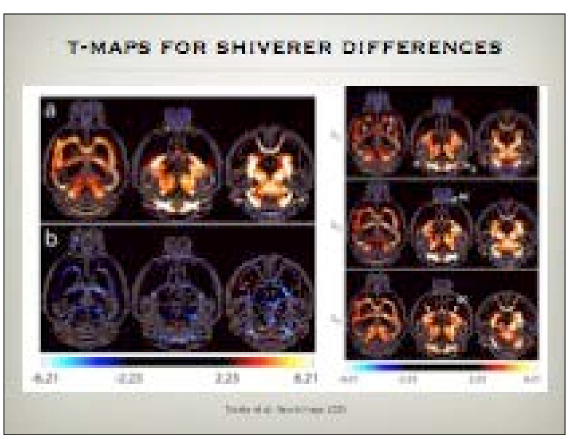
T-maps for Shiverer Differences
a
b
-6.21
-2.23
2.23
6.21

36


SHIVERER HISTOLOGY
Control
Shiverer

37


MR MYOCARDIAL
DIFFUSION MICROSCOPY

38

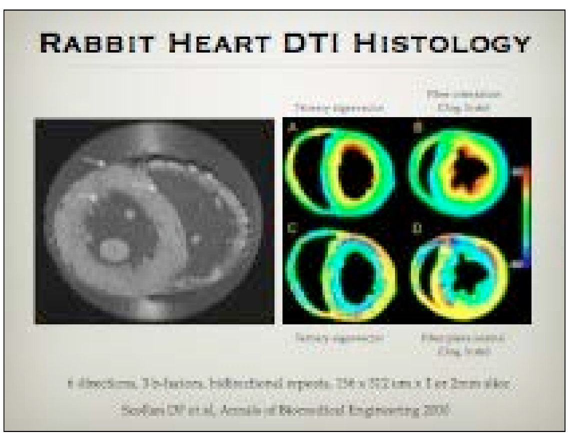
RABBIT HEART DTI HISTOLOGY

39

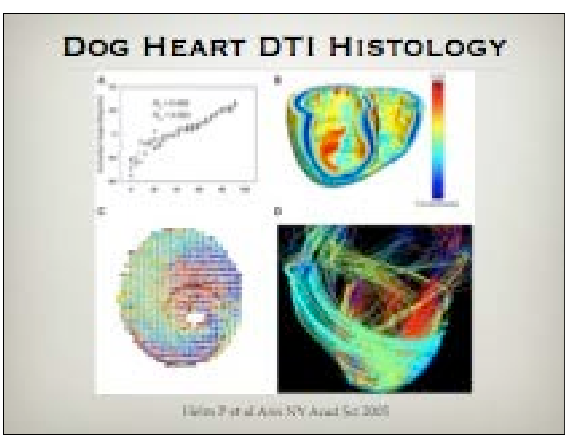
DOG HEART DTI HISTOLOGY

40

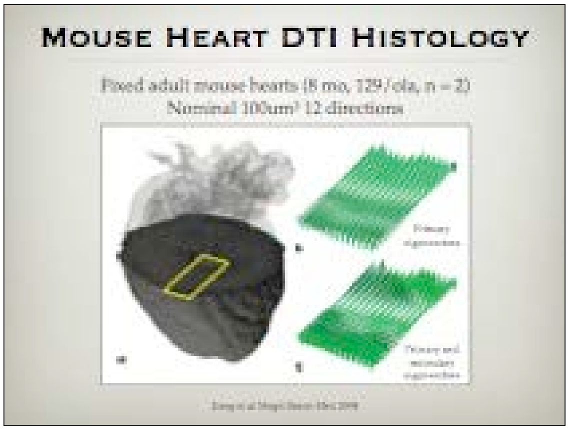
MOUSE HEART DTI HISTOLOGY
Fixed adult mouse hearts (8 mo, 129/ola, n = 2)
Nominal 100um³ 12 directions

41

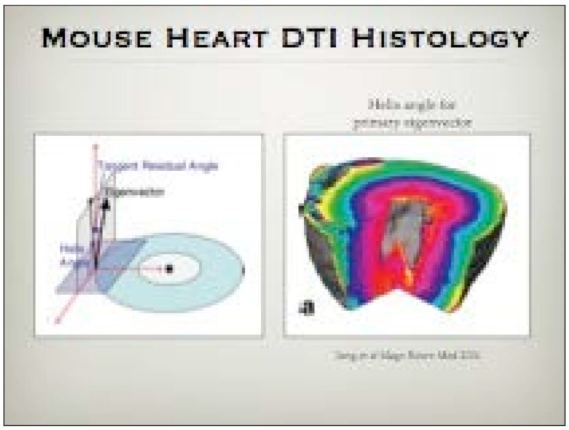
MOUSE HEART DTI HISTOLOGY
Helix angle for
primary eigenvector
Tangent Residual Angle
Eigenvector

42

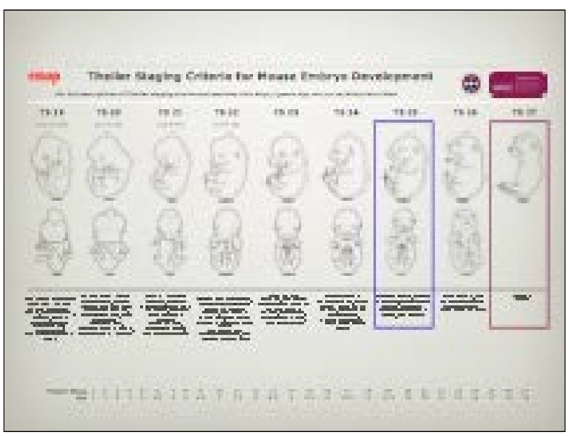
Theiler Staging Criteria for Mouse Embryo Development

43

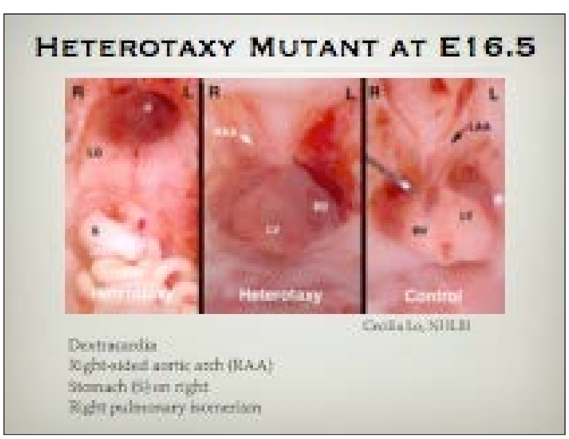
HETEROTAXY MUTANT AT E16.5
R
L
Heterotaxy
Control
Cecilia Lo, NHLBI
Dextrocardia
Right-sided aortic arch (RAA)
Stomach (S) on right
Right pulmonary isomerism

44


SAMPLE PREPARATION
Samples equilibrated in 5mM gadoteridol in PBS and 0.01% sodium azide overnight prior to MRI.
T1 drops to 100-200ms
Two hearts mounted in Teflon holder immersed in Fomblin.

45

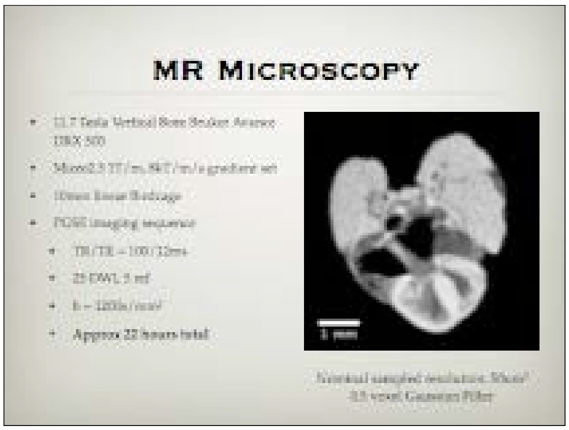
MR MICROSCOPY
Approx 22 hours total

46

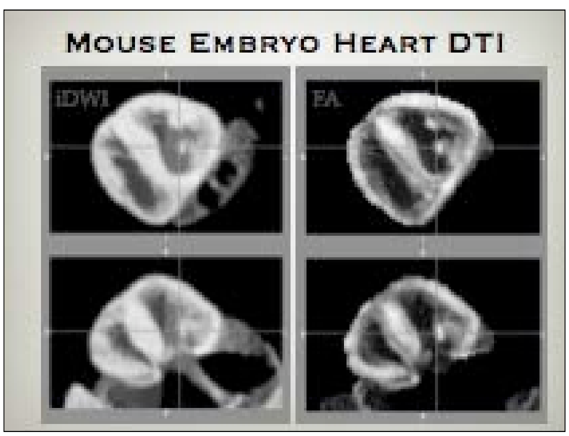
MOUSE EMBRYO HEART DTI
iDWI
FA

47

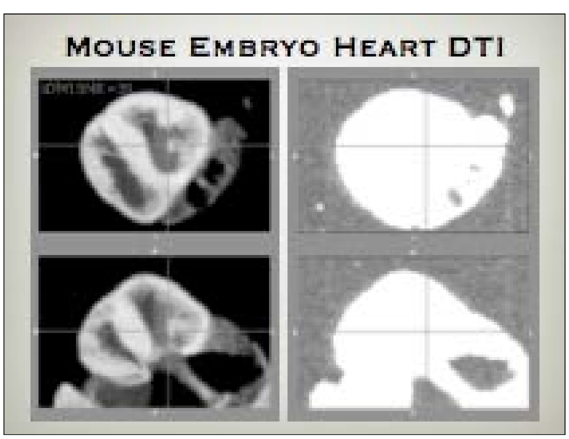
MOUSE EMBRYO HEART DTI

48

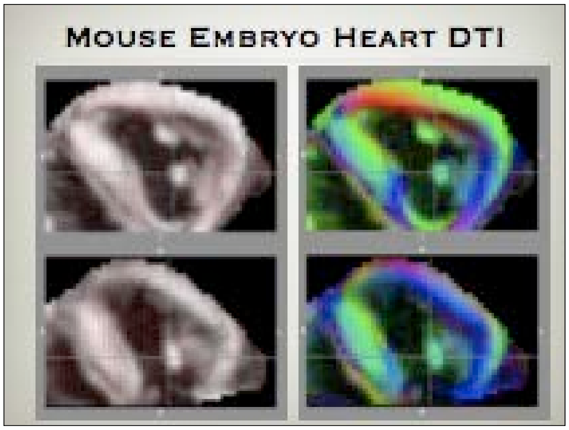
Mouse Embryo Heart DTI

49

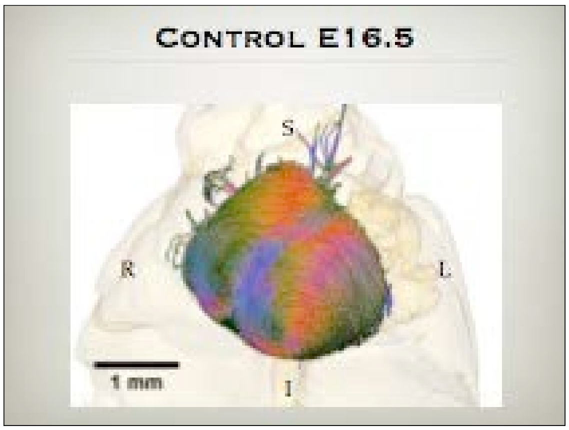
Control E16.5
S
R
L
1 mm
I

50

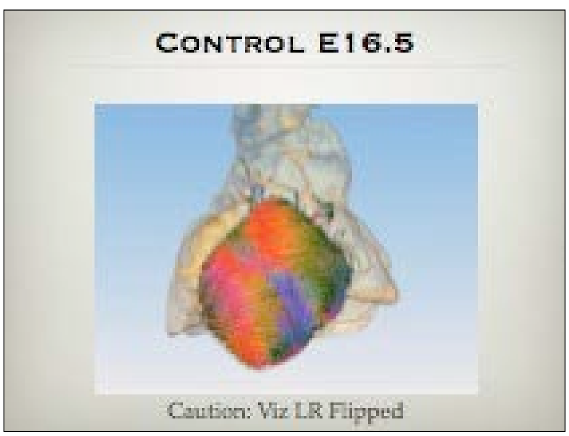
Control E16.5
Caution: Viz LR Flipped

51

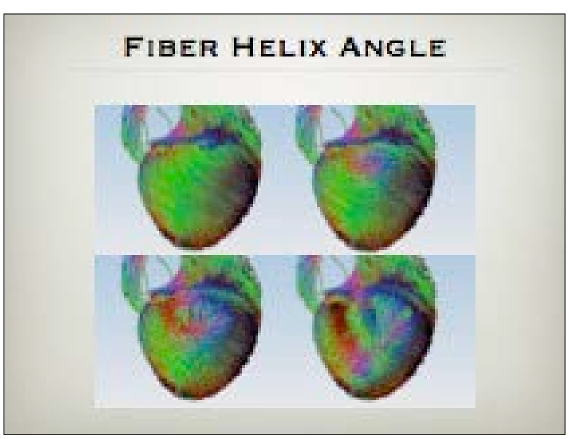
Fiber Helix Angle

52

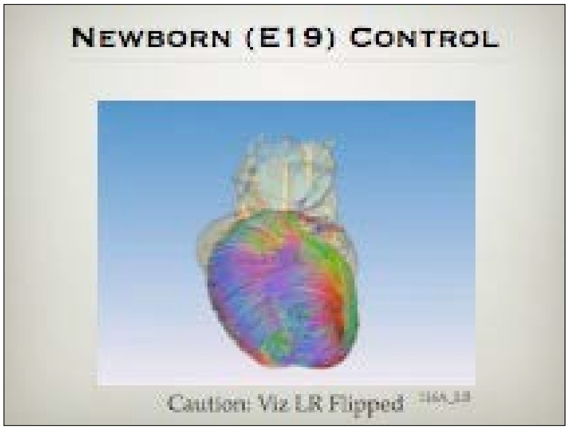
NEWBORN (E19) CONTROL
Caution: Viz LR Flipped

53


HETEROTAXY MUTANT E16.5

54

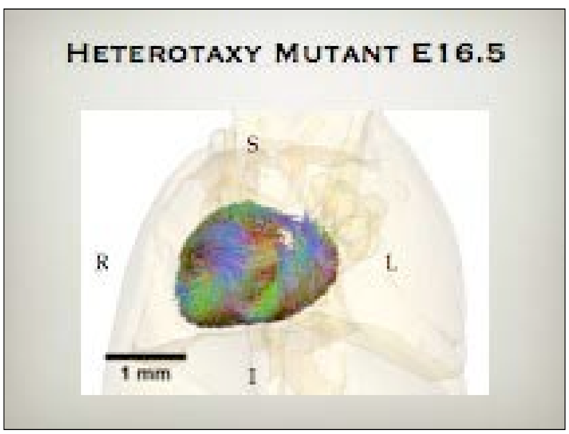
HETEROTAXY MUTANT E16.5
S
R
L
1 mm
I

55

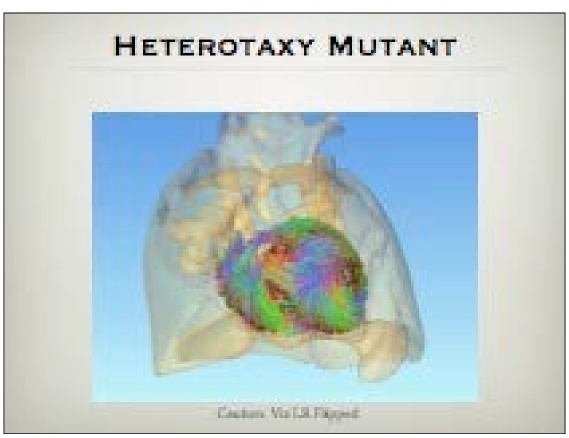
HETEROTAXY MUTANT
Caution: Viz LR Flipped

56

VEGETABLES

57

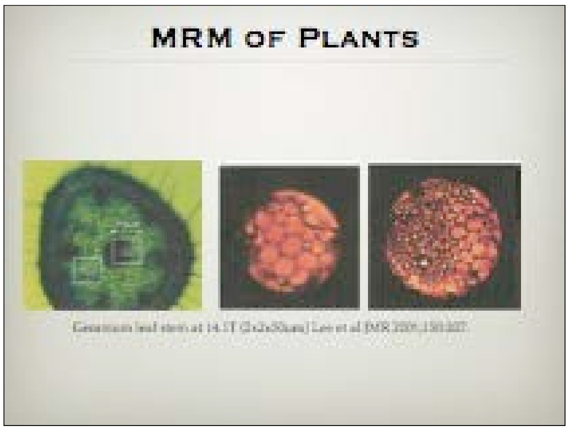

MRM OF PLANTS

58

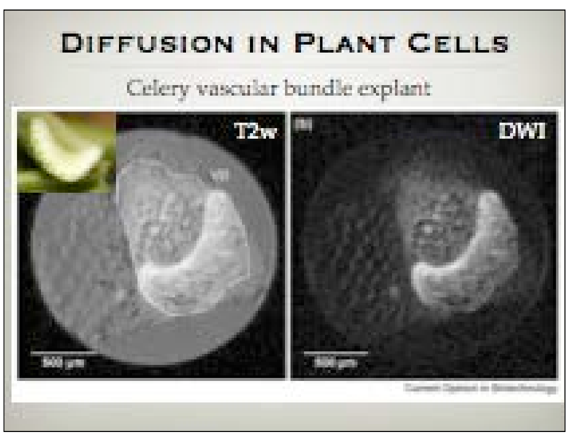

DIFFUSION IN PLANT CELLS
Celery vascular bundle explant
T2w
DWI

59

BE 248 9.1

Functional MRI: Physics and Physiology

Mike Tyszka, Ph.D.

Caltech Brain Imaging Center
Divisions of Bioengineering and Biology
California Institute of Technology

1

Lecture Summary

- 9.1 Functional MRI: Physics and Physiology
  - Neuroanatomy
  - Neurodynamics
  - The BOLD Effect and HDR
  - Neurovascular coupling
  - Nonlinearities in fMRI
  - Spatiotemporal resolution in fMRI

2

Web Resources

- Duke-UNC Brain Imaging and Analysis Center: FMRI Graduate Course
  - http://www.biac.duke.edu/education/courses/fall02/fmri/
- University of Oxford FMRIB FSL and FreeSurfer Courses
  - http://www.fmrib.ox.ac.uk/fslcourse/
- Carnegie Mellon University Computational Analyses of Brain Imaging
  - http://www-2.cs.cmu.edu/afs/cs.cmu.edu/project/theo-20/www/mri/
- Jody Culham - fMRI for Dummies
  - http://defiant.ssc.uwo.ca/Jody_web/fmri4dummies.htm

3

Early "fMRI"

Angelo Mosso
Italian physiologist
(1846-1910)

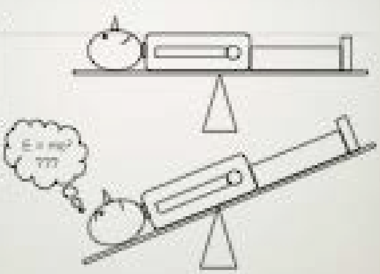

"[In Mosso's experiments] the subject to be observed lay on a delicately balanced table which could tip downward either at the head or at the foot if the weight of either end were increased. The moment emotional or intellectual activity began in the subject, down went the balance at the head-end, in consequence of the redistribution of blood in his system."
– William James, Principles of Psychology (1890)

4

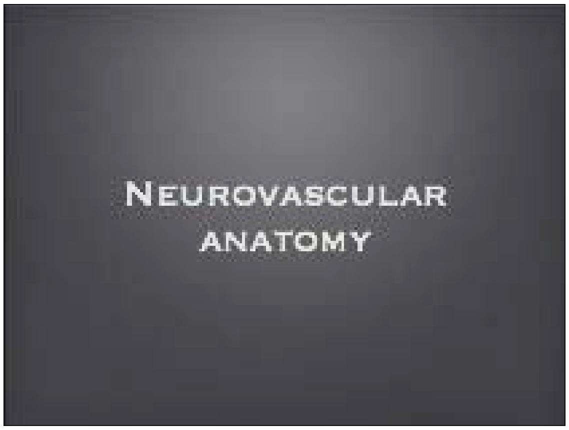
NEUROVASCULAR
ANATOMY

5

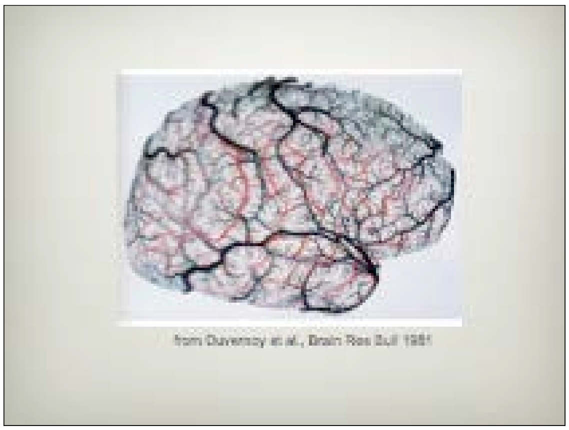
from Duvernoy et al., Brain Res Bull 1981

6

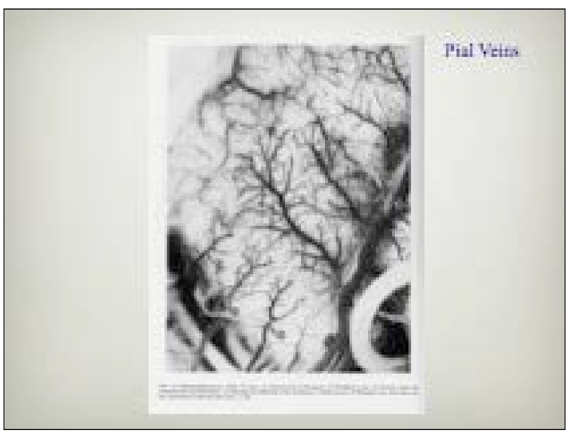
Pial Veins

7

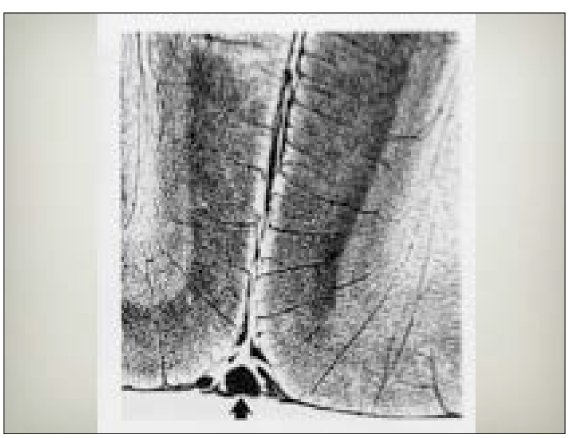

8

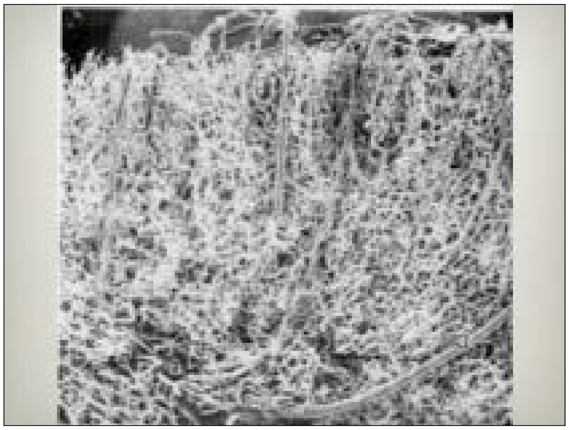

9

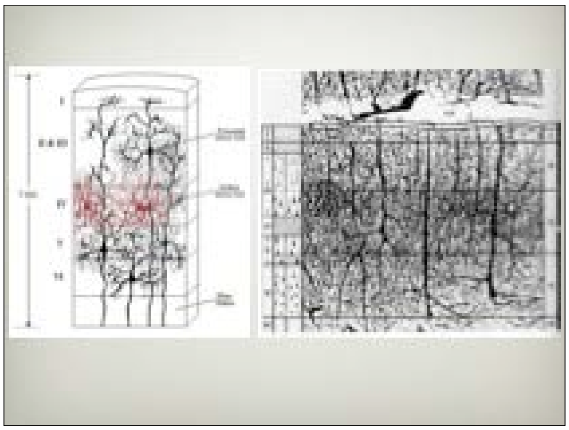

10

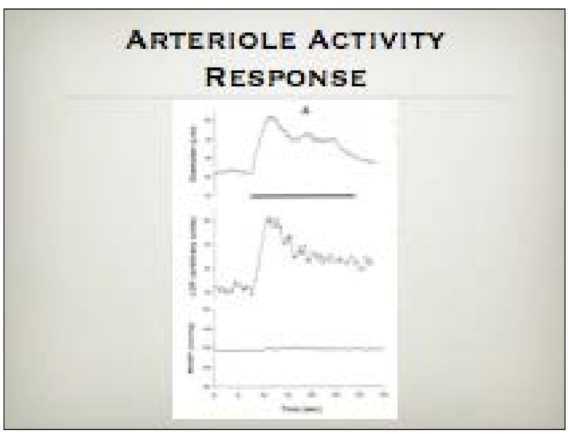

11

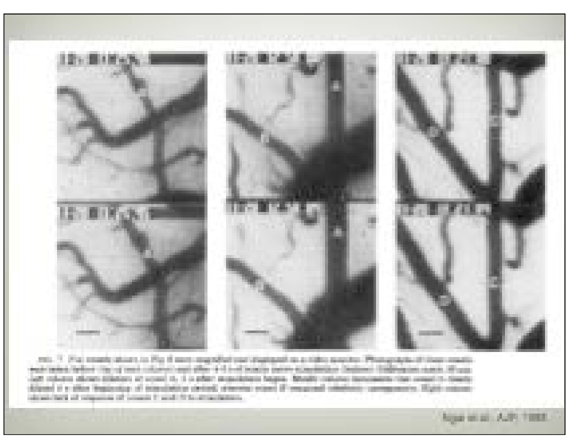

12

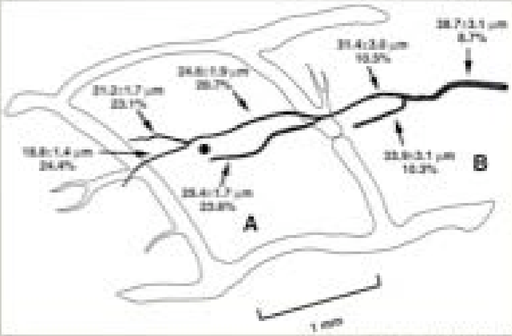

13

THE BOLD EFFECT

14

OGAWA ET AL., 1990A

- Subjects: 1) Mice and Rats, 2) Test tubes
- Equipment: High-field MR (7+ T)
- Results 1:
  - Contrast on gradient-echo images influenced by proportion of oxygen in breathing gas
  - Increasing oxygen content → reduced contrast
  - No vascular contrast seen on spin-echo images
- Results 2:
  - Oxygenated blood in tube leads to little signal change, either on spin- or gradient-echo images
  - Deoxygenated blood leads to large susceptibility effects on gradient-echo images

15

OGAWA ET AL. 1990

HYPEROXIA
Under anesthesia, rats breathing pure oxygen have some BOLD contrast (black lines).

HYPERCAPNIA
Breathing a mix including CO2 results in increased blood flow, in turn increasing blood oxygenation.
There is no increased metabolic load (no task).
Therefore, BOLD contrast is reduced.

16

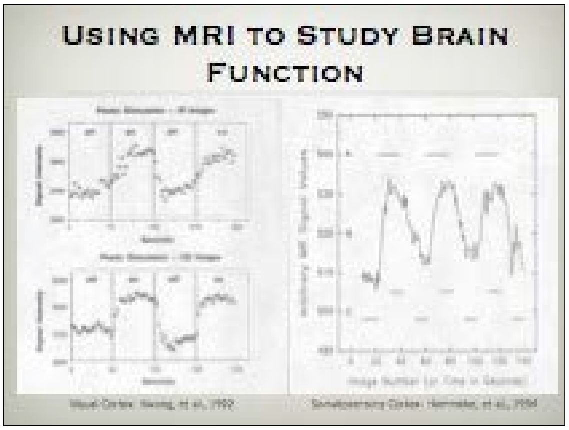
USING MRI TO STUDY BRAIN FUNCTION

17

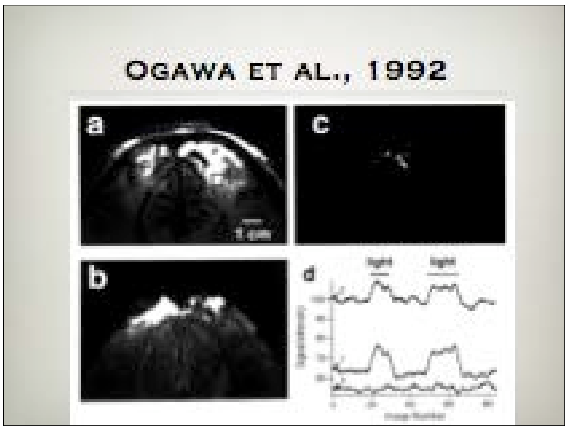
OGAWA ET AL., 1992
a
c
1 cm
b
d
light
light

18

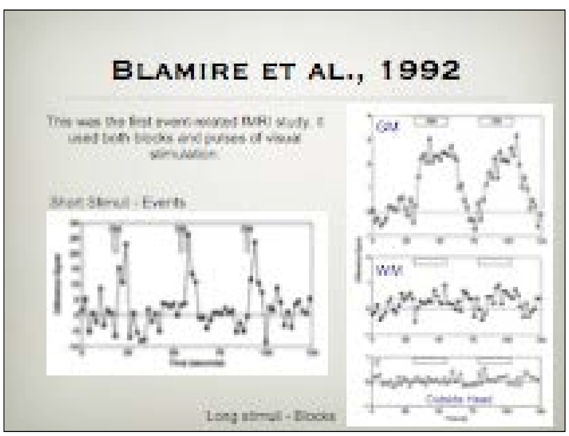
BLAMIRE ET AL., 1992
This was the first event-related fMRI study. It used both blocks and pulses of visual stimulation.
Short Stimuli - Events
GM
WM
Outside Head
Long stimuli - Blocks

19

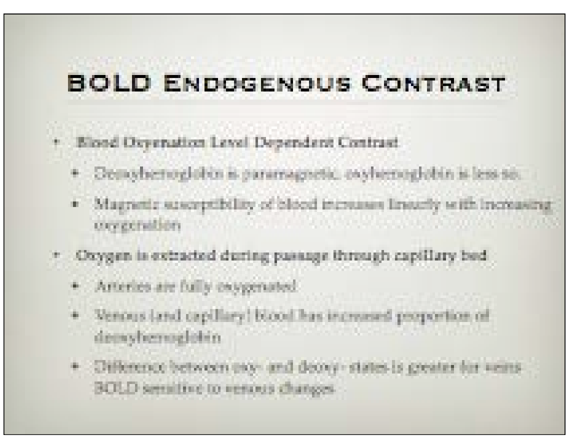
BOLD ENDOGENOUS CONTRAST
Blood Oxygenation Level Dependent Contrast
Deoxyhemoglobin is paramagnetic, oxyhemoglobin is less so
Magnetic susceptibility of blood increases linearly with increasing oxygenation
Oxygen is extracted during passage through capillary bed
Arteries are fully oxygenated
Venous (and capillary) blood has increased proportion of deoxyhemoglobin
Difference between oxy- and deoxy- states is greater for veins
BOLD sensitive to venous changes

20

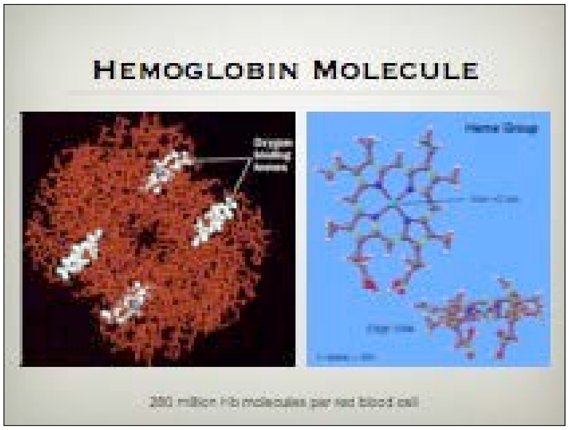

HEMOGLOBIN MOLECULE
Heme Group
280 million Hb molecules per red blood cell

21

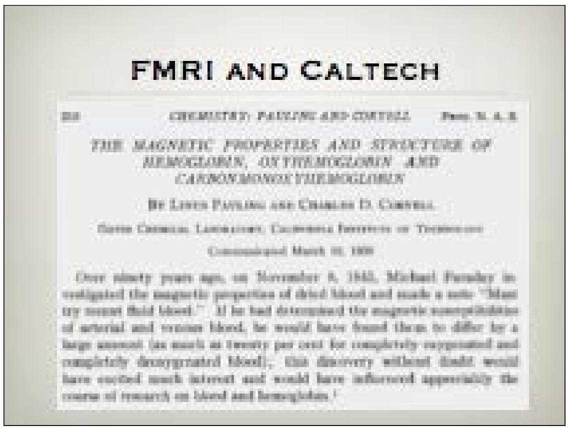

FMRI AND CALTECH
CHEMISTRY: PAULING AND CORYELL
THE MAGNETIC PROPERTIES AND STRUCTURE OF HEMOGLOBIN, OXYHEMOGLOBIN AND CARBONMONOXYHEMOGLOBIN
By Linus Pauling and Charles D. Coryell
Over ninety years ago, on November 8, 1845, Michael Faraday investigated the magnetic properties of dried blood and made a note "Must try recent fluid blood." If he had determined the magnetic susceptibilities of arterial and venous blood, he would have found them to differ by a large amount (as much as twenty per cent for completely oxygenated and completely deoxygenated blood); this discovery without doubt would have excited much interest and would have influenced appreciably the course of research on blood and hemoglobin.

22

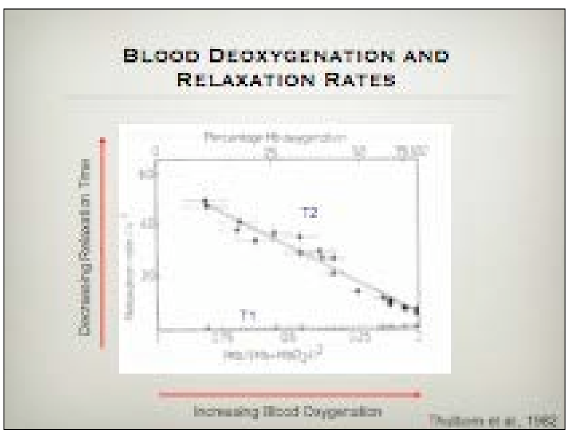

BLOOD DEOXYGENATION AND RELAXATION RATES
Percentage Hb oxygenation
T2
T1
Decreasing Relaxation Time
Increasing Blood Oxygenation
Thulborn et al., 1982

23

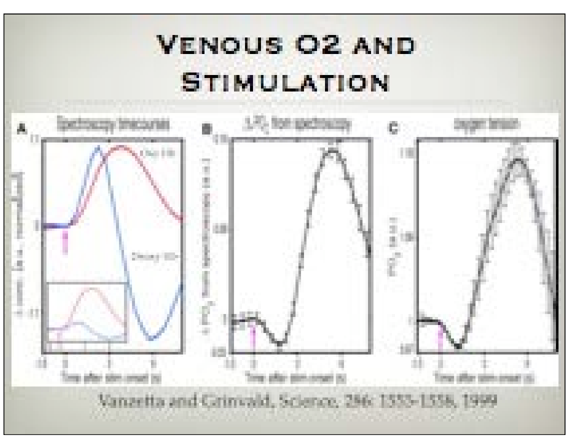

VENOUS O2 AND STIMULATION
A
Spectroscopy timecourses
B
C
oxygen tension
Time after stim onset (s)
Vanzetta and Grinvald, Science, 286: 1555-1558, 1999

24

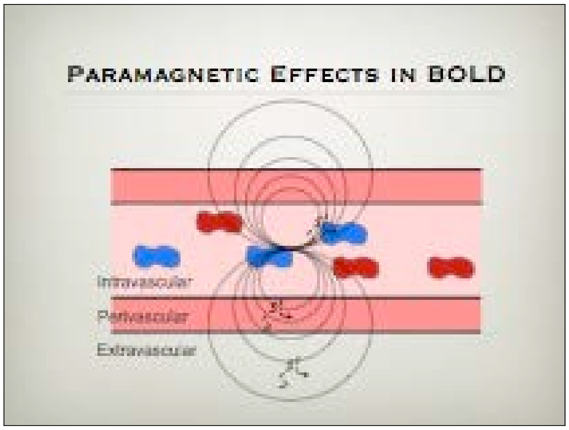
Paramagnetic Effects in BOLD
Intravascular
Perivascular
Extravascular

25

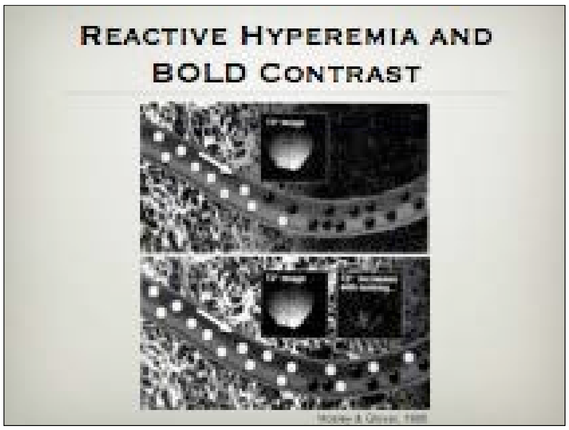
Reactive Hyperemia and BOLD Contrast

26

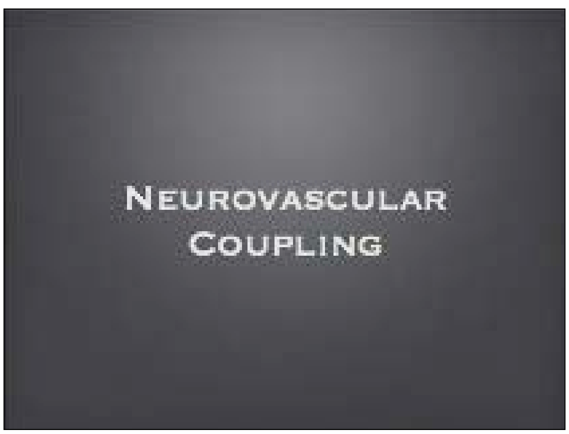
Neurovascular Coupling

27

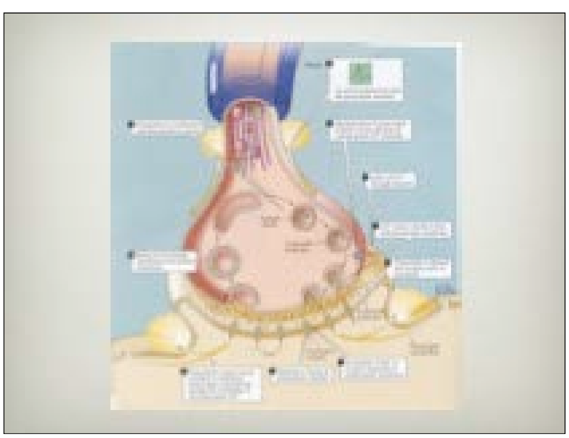

28

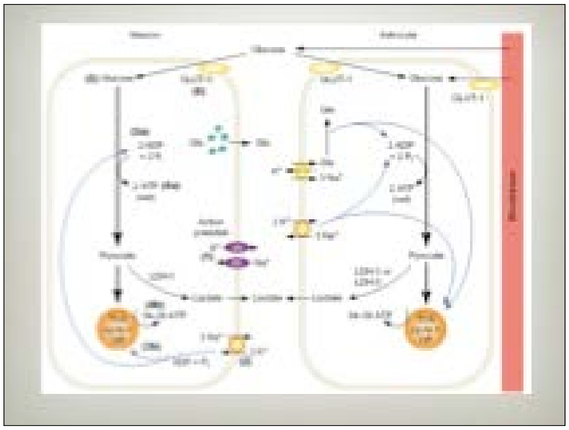

29

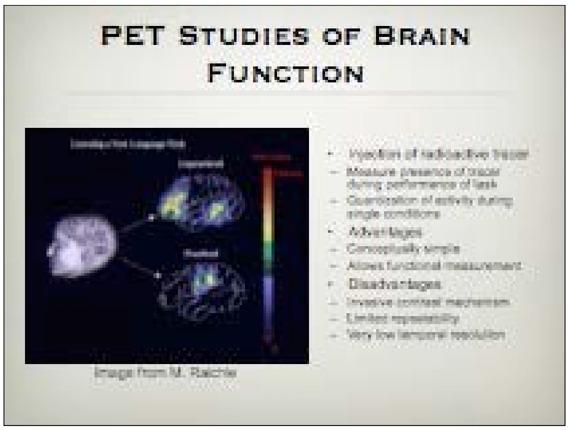
PET Studies of Brain Function
- Injection of radioactive tracer
  - Measure presence of tracer during performance of task
  - Quantization of activity during single conditions
- Advantages
  - Conceptually simple
  - Allows functional measurement
- Disadvantages
  - Invasive contrast mechanism
  - Limited repeatability
  - Very low temporal resolution
Image from M. Raichle

30

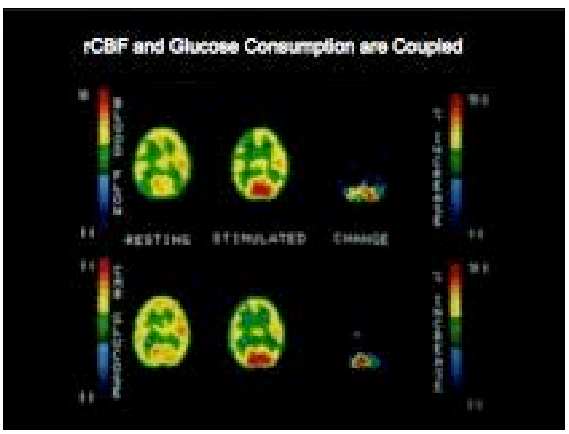
rCBF and Glucose Consumption are Coupled
RESTING
STIMULATED
CHANGE

31

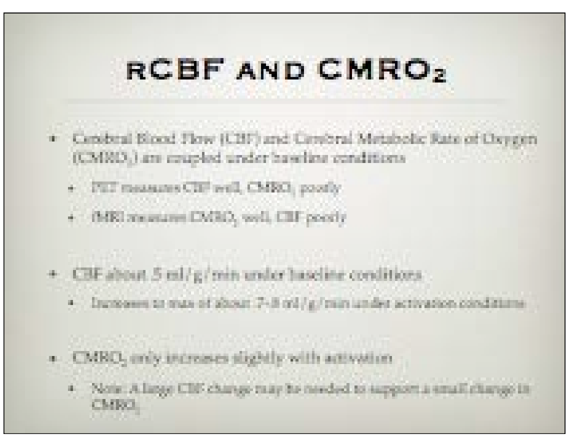
RCBF AND CMRO2
- Cerebral Blood Flow (CBF) and Cerebral Metabolic Rate of Oxygen (CMRO2) are coupled under baseline conditions
  - PET measures CBF well, CMRO2 poorly
  - fMRI measures CMRO2 well, CBF poorly
- CBF about .5 ml/g/min under baseline conditions
  - Increases to max of about .7-.8 ml/g/min under activation conditions
- CMRO2 only increases slightly with activation
  - Note: A large CBF change may be needed to support a small change in CMRO2

32

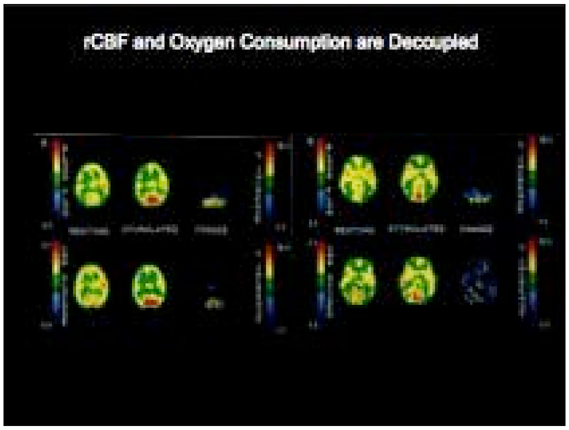
rCBF and Oxygen Consumption are Decoupled

33

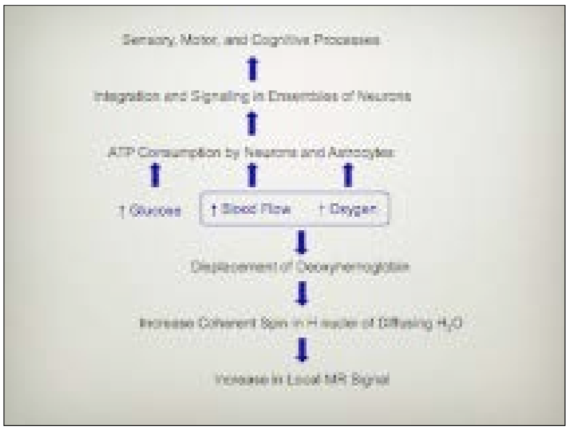
Sensory, Motor, and Cognitive Processes
Integration and Signaling in Ensembles of Neurons
ATP Consumption by Neurons and Astrocytes
↑ Glucose
↑ Blood Flow
↑ Oxygen
Displacement of Deoxyhemoglobin
Increase Coherent Spin in H nuclei of Diffusing H_2O
Increase in Local MR Signal

34

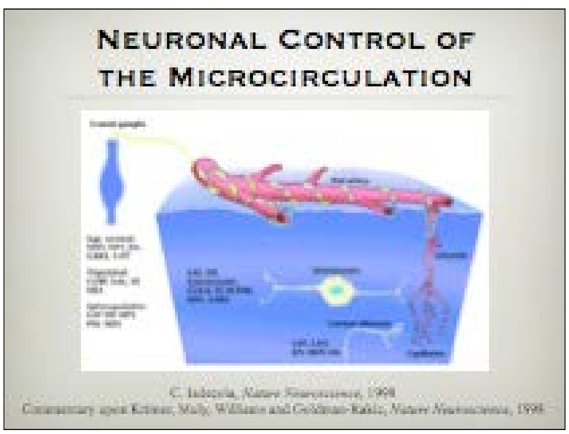
Neuronal Control of the Microcirculation
C. Iadecola, *Nature Neuroscience*, 1998
Commentary upon Krimer, Muly, Williams and Goldman-Rakic, *Nature Neuroscience*, 1998

35

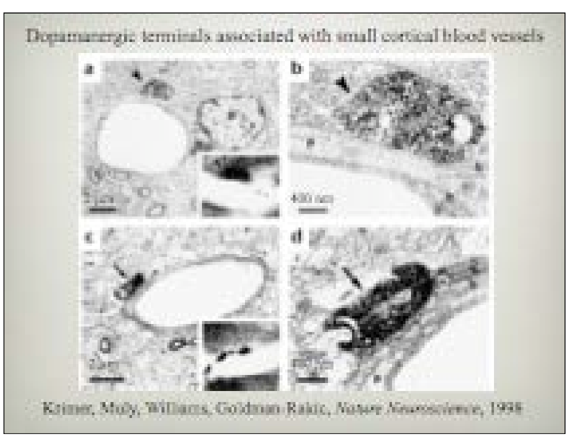
Dopaminergic terminals associated with small cortical blood vessels
a
b
c
d
Krimer, Muly, Williams, Goldman-Rakic, *Nature Neuroscience*, 1998

36

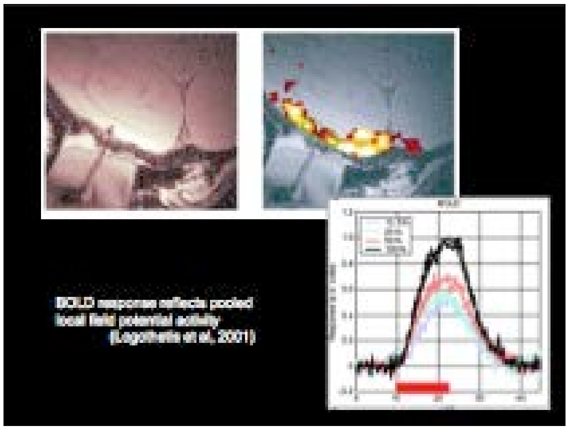

37

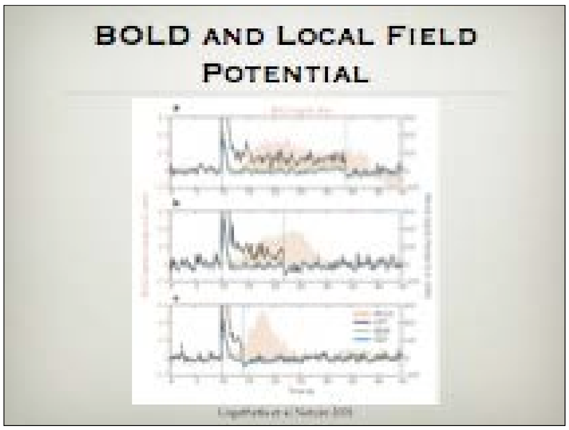

38

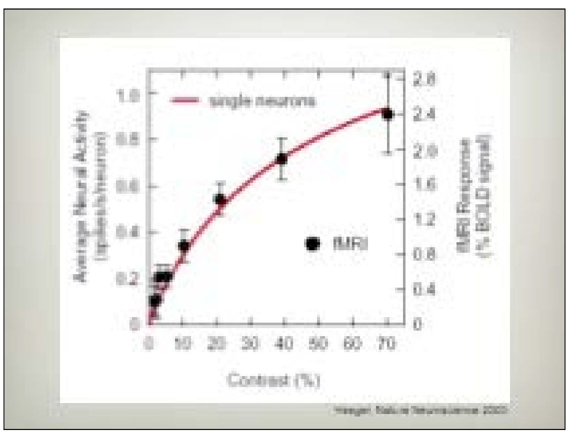

39

The Hemodynamic Response

40

In this period of intense research in the neurosciences, nothing is more promising than functional magnetic resonance imaging (fMRI) and positron emission tomography (PET) methods, which localize brain activities. These functional imaging methodologies map neurophysiological responses to cognitive, emotional, or sensory stimulations. The rapid experimental progress made by using these methods has encouraged widespread optimism about our ability to understand the activities of the mind on a biological basis. However, the relationship between the signal and neurobiological processes related to function is poorly understood, because the functional imaging signal is not a direct measure of neuronal processes related to information transfer, such as action potentials and neurotransmitter release. Rather, the intensity of the imaging signal is related to neurophysiological parameters of energy consumption and blood flow. To relate the imaging signal to specific neuronal processes, two relationships must be established.

The first relationship is between the intensity of the imaging signal and the rate of neurophysiological energy processes, such as the cerebral metabolic rates of glucose (CMRglc) and of oxygen (CMRO2).

The second and previously unavailable relationship is between the neurophysiological processes and the activity of neuronal processes. It is necessary to understand these relationships to directly relate functional imaging studies to neurobiological research that seeks the relationship between the regional activity of specific neuronal processes and mental processes.

41

Basic Form of The Hemodynamic Response

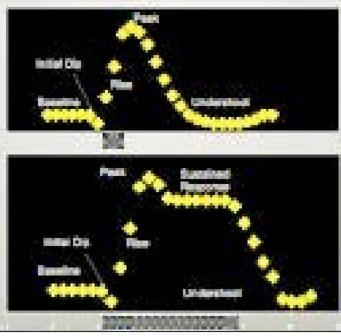

42

Baseline Period

- Why include a baseline period in epoch?
- Corrects for scanner drift across time

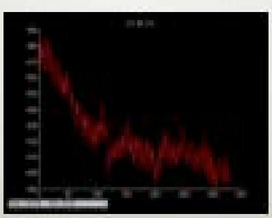

43

BOLD Hemodynamic Response

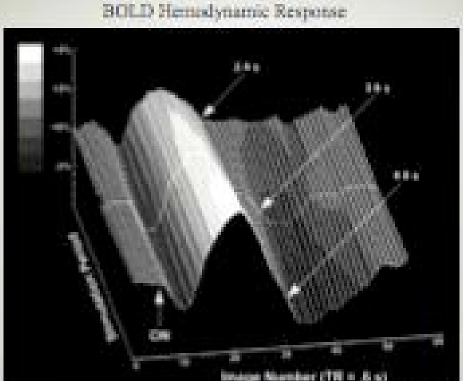

Hu, Le, Ugurbil MRM, 1997

44

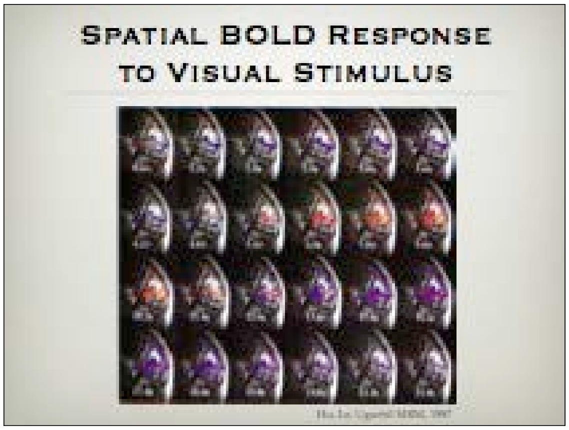
Spatial BOLD Response
to Visual Stimulus

45

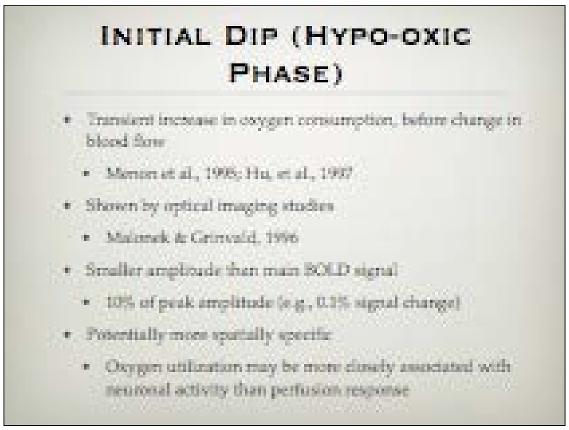
Initial Dip (Hypo-oxic Phase)
• Transient increase in oxygen consumption, before change in blood flow
• Menon et al., 1995; Hu, et al., 1997
• Shown by optical imaging studies
• Malonek & Grinvald, 1996
• Smaller amplitude than main BOLD signal
• 10% of peak amplitude (e.g., 0.1% signal change)
• Potentially more spatially specific
• Oxygen utilization may be more closely associated with neuronal activity than perfusion response

46

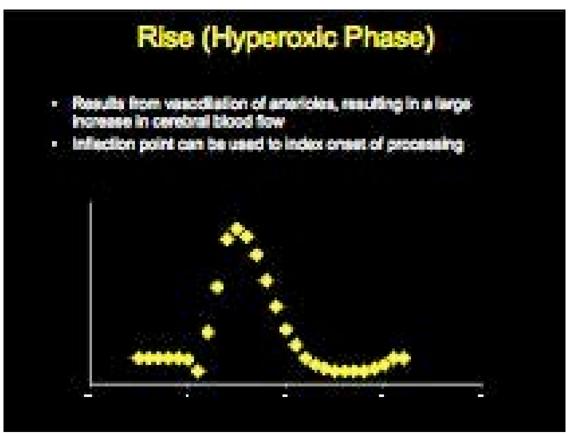
Rise (Hyperoxic Phase)
• Results from vasodilation of arterioles, resulting in a large increase in cerebral blood flow
• Inflection point can be used to index onset of processing

47

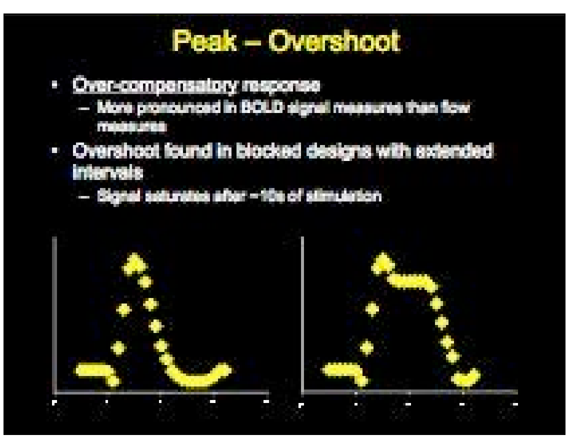
Peak – Overshoot
• Over-compensatory response
– More pronounced in BOLD signal measures than flow measures
• Overshoot found in blocked designs with extended intervals
– Signal saturates after ~10s of stimulation

48

Sustained Response

- Blocked design analyses rest upon presence of sustained response
  - Comparison of sustained activity vs. baseline
  - Statistically simple, powerful
- Problems
  - Difficulty in identifying magnitude of activation
  - Little ability to describe form of hemodynamic response
  - May require detrending of raw time course

49

Undershoot

- CBF more locked to stimuli than CBV
  - Increased blood volume with baseline flow leads to decrease in MR signal
- More frequently observed for longer-duration stimuli (>10s)
  - Short duration stimuli may not evidence
  - May remain for 10s of seconds

50

Issues in HRF Analysis

- Delay in the HRF
  - Hemodynamic activity lags neuronal activity
- Amplitude of the HRF
- Variability in the HRF
- HRF as a relative measure

51

Variability in the Hemodynamic Response

- Across Subjects
- Across Sessions in a Single Subject
- Across Brain Regions
- Across Stimuli

52


Spatial Resolution in fMRI

53


What spatial resolution do we want?
Hemispheric
Lateralization studies
Selective attention studies
Systems / lobes
Relation to lesion data
Centimeter
Identification of active regions
Millimeter
Topographic mapping (e.g., motor, vision)
Sub-millimeter
Ocular Dominance Columns
Cortical Layers

54


What determines Spatial Resolution?
Voxel Size
In-plane Resolution
Slice thickness
Spatial noise
Head motion
Artifacts
Spatial blurring
Smoothing (within subject)
Coregistration (within subject)
Normalization (within subject)
Averaging (across subjects)

55

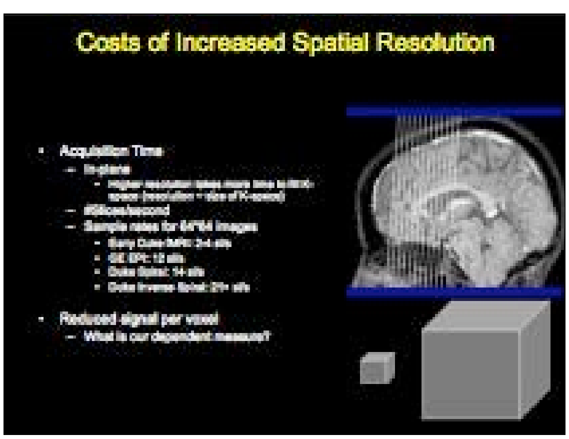
Costs of Increased Spatial Resolution
Acquisition Time
In-plane
#Slices/second
Sample rates for 64*64 images
Reduced signal per voxel
What is our dependent measure?

56

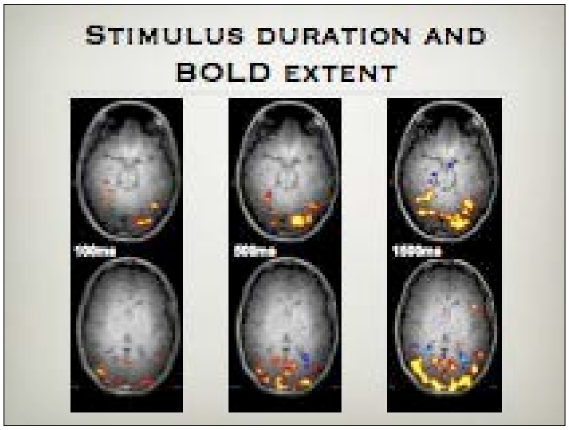

STIMULUS DURATION AND BOLD EXTENT

57

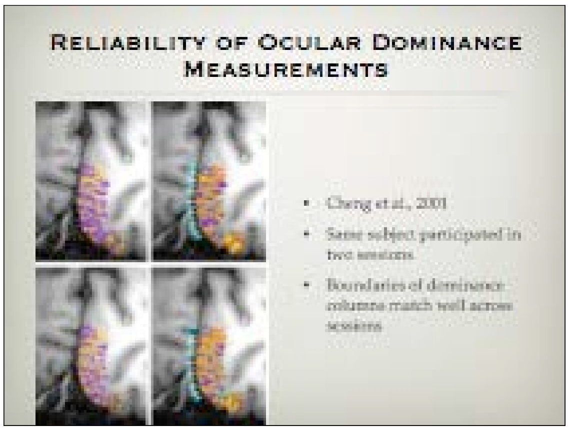

RELIABILITY OF OCULAR DOMINANCE MEASUREMENTS
Cheng et al., 2001
Same subject participated in two sessions
Boundaries of dominance columns match well across sessions

58

TEMPORAL RESOLUTION

59

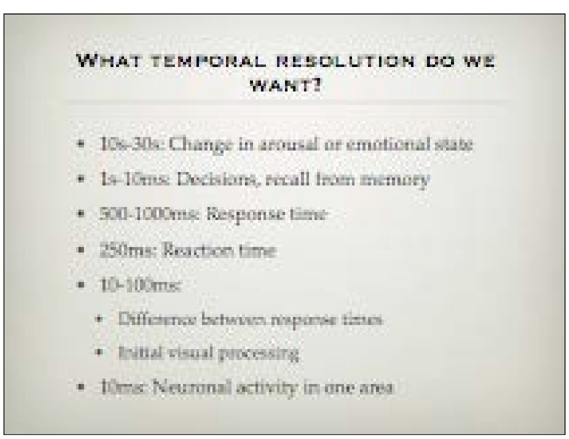

WHAT TEMPORAL RESOLUTION DO WE WANT?
10s-30s: Change in arousal or emotional state
1s-10ms: Decisions, recall from memory
500-1000ms: Response time
250ms: Reaction time
10-100ms:
Difference between response times
Initial visual processing
10ms: Neuronal activity in one area

60

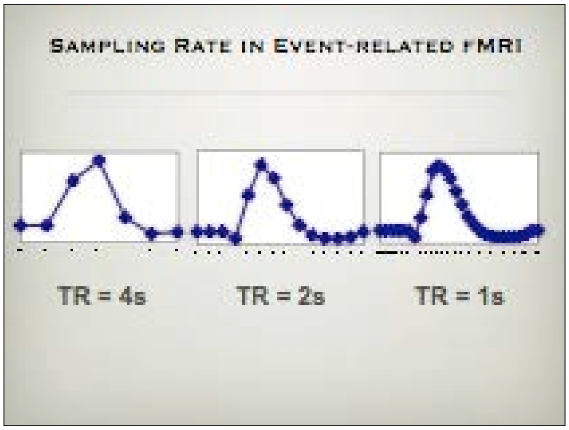
Sampling Rate in Event-related fMRI
TR = 4s
TR = 2s
TR = 1s

61

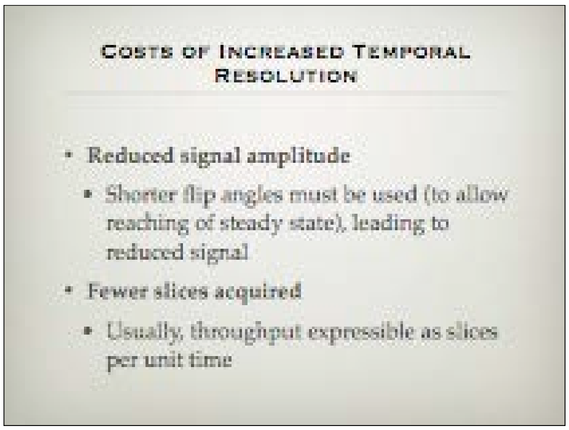
Costs of Increased Temporal Resolution
Reduced signal amplitude
Shorter flip angles must be used (to allow reaching of steady state), leading to reduced signal
Fewer slices acquired
Usually, throughput expressible as slices per unit time

62

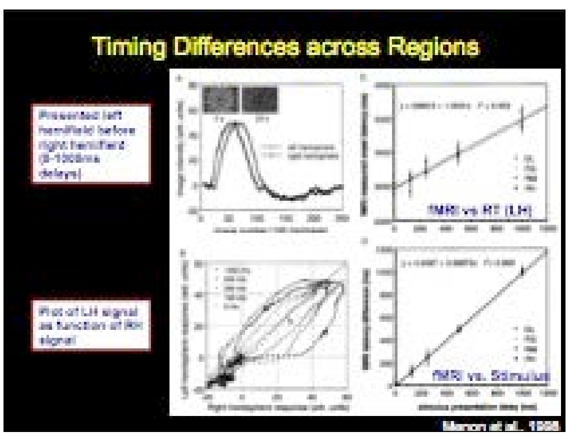
Timing Differences across Regions
Presented left hemifield before right hemifield (0-1000ms delays)
Plot of LH signal as function of RH signal
fMRI vs RT (LH)
fMRI vs. Stimulus
Menon et al. 1998

63

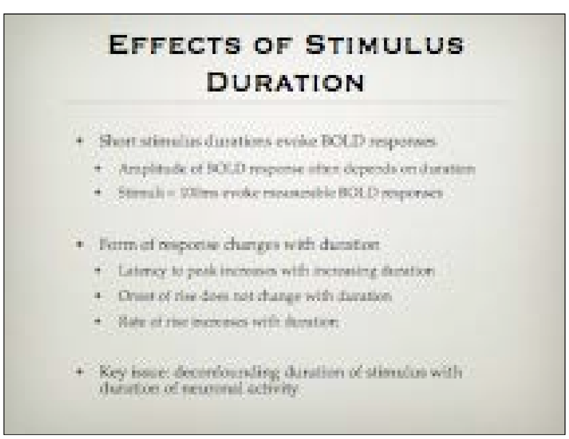
Effects of Stimulus Duration
Short stimulus durations evoke BOLD responses
Amplitude of BOLD response often depends on duration
Form of response changes with duration
Latency to peak increases with increasing duration
Onset of rise does not change with duration
Rate of rise increases with duration
Key issue: deconfounding duration of stimulus with duration of neuronal activity

64

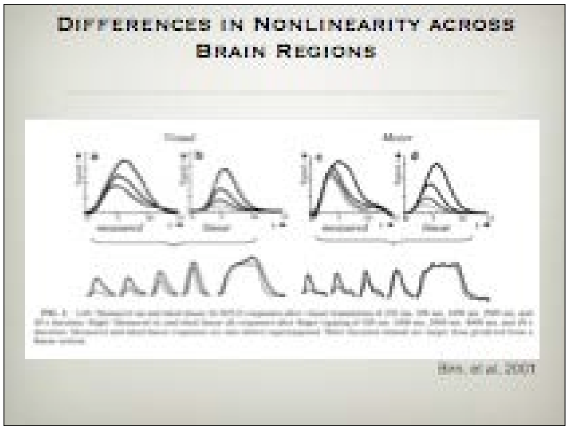

Differences in Nonlinearity across Brain Regions

65

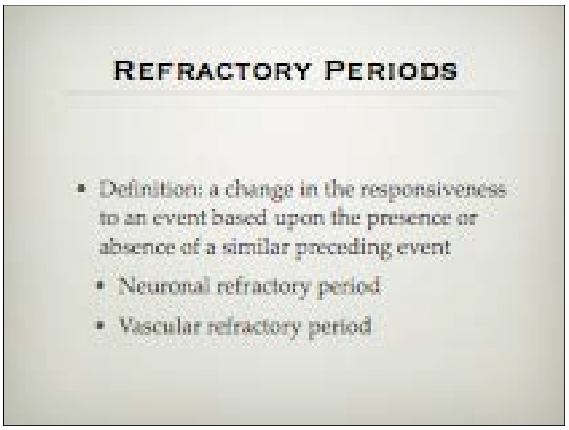

Refractory Periods
• Definition: a change in the responsiveness to an event based upon the presence or absence of a similar preceding event
• Neuronal refractory period
• Vascular refractory period

66

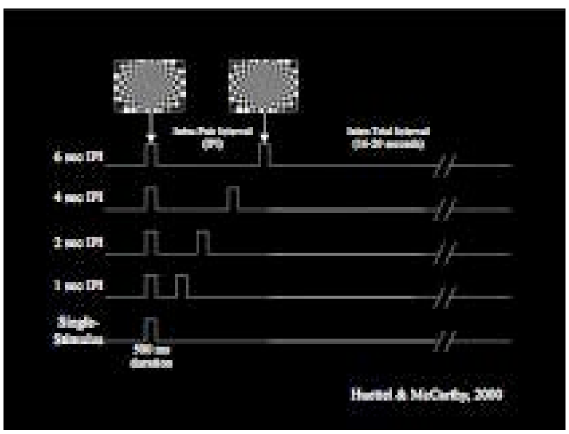

6 sec IPI
4 sec IPI
2 sec IPI
1 sec IPI
Single-Stimulus
Huettel & McCarthy, 2000

67

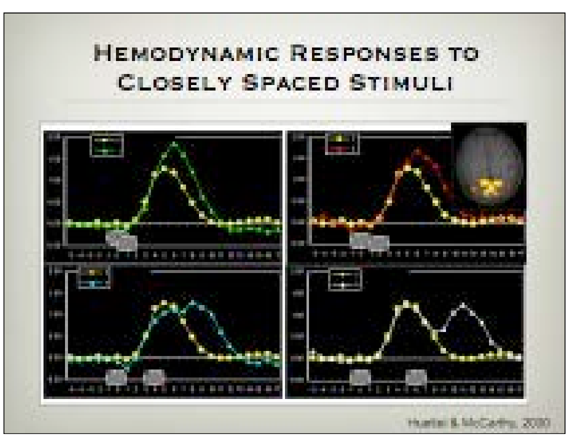

Hemodynamic Responses to Closely Spaced Stimuli
Huettel & McCarthy, 2000

68

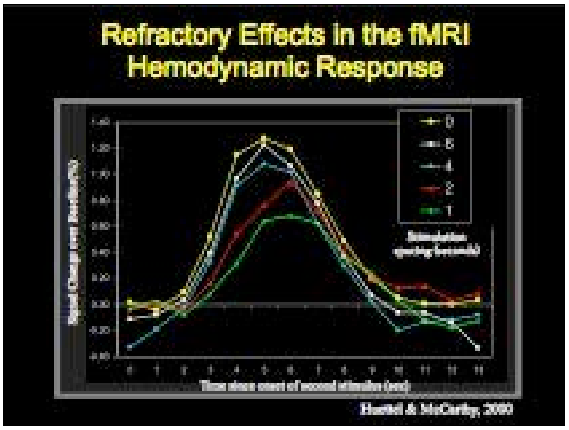
Refractory Effects in the fMRI
Hemodynamic Response
0
6
4
2
1
Stimulation spacing (seconds)
Huettel & McCarthy, 2000

69


Next Lecture
• Data analysis for fMRI
• Preprocessing
• General Linear Model
• Statistical Parametric Mapping

70

BE/CNS 248
9.2 Basic FMRI Analysis

1

Lecture Summary

- 9.2 Functional MRI Processing
  - BOLD data acquisition
  - Preprocessing
  - General Linear Model
  - Statistical Inference

2

Resources

- **SPM for Dummies Course 2006**
  - Functional Imaging Laboratory, University College London, UK
- **fMRI Minicourse 2005**
  - Rik Henson, MRC Cognition and Brain Sciences Unit, Cambridge University, UK

3

Typical BOLD Imaging

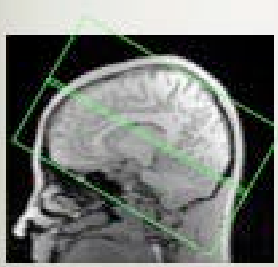

Multislice image volume angled approximately -30° relative to gradient XY plane.

Between 32 and 40 3mm slices covering whole brain.

In-plane resolution approximately 3mm (FOV 64 x 64mm, 64 x 64 matrix)

4

Typical BOLD Imaging

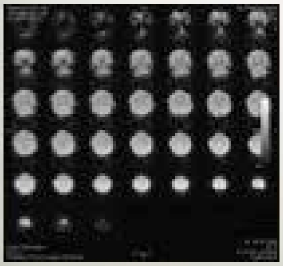

FID-EPI (T2*-weighted)
Single shot
TR/TE: 2000/30ms
Flip angle: 70°
Fat suppression
GRAPPA 2
1 Average

5

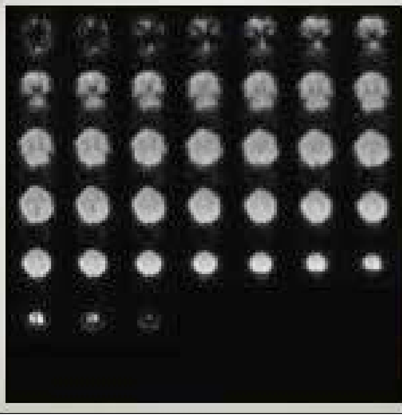

6

FMRI Designs

7

FMRI Design Types

- Blocked Designs
- Event-Related Designs
  - Periodic Single Trial
  - Jittered Single Trial
  - Staggered Single Trial
- Mixed Designs
  - Combination blocked/event-related
  - Variable stimulus probability

8

What are Blocked Designs?

- Blocked designs segregate different cognitive processes into distinct time periods

9

What baseline should you choose?

- Task A vs. Task B
  - Example: Squeezing Right Hand vs. Left Hand
  - Allows you to distinguish differential activation between conditions
  - Does not allow identification of activity common to both tasks
    - Can control for uninteresting activity
- Task A vs. No-task
  - Example: Squeezing Right Hand vs. Rest
  - Shows you activity associated with task
  - Resting state uncontrolled

10

Limitations of Blocked Designs

- Very sensitive to signal drift
  - Sensitive to head motion, especially when only a few blocks are used.
- Poor choice of baseline may preclude meaningful conclusions
- Many tasks cannot be conducted repeatedly
- Difficult to estimate the HDR

11

What are Event-Related Designs?

- Event-related designs associate brain processes with discrete events, which may occur at any point in the scanning session.

12

Why use event-related designs?

- Some experimental tasks are naturally event-related
- Allows studying of trial effects
- Simple analyses
  - Selective averaging
  - No assumptions of linearity required
- Can isolate HRFs associate with different task components

13

Event-Related vs Blocked Designs

Blocked

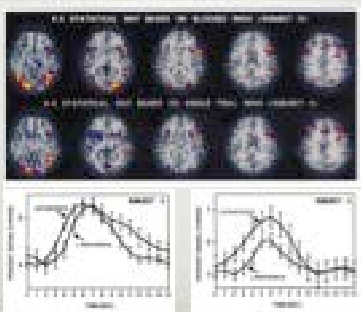

ER

14

Periodic Single-Trial Design

- Stimulus events presented infrequently with a long inter-stimulus interval (ITI)

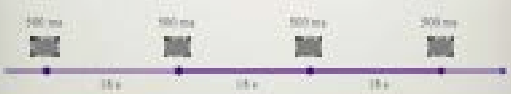

15

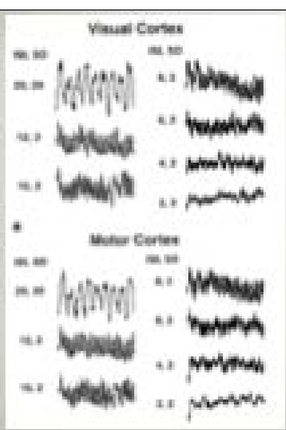

ISI : Interstimulus Interval

SD : Stimulus Duration

From Bandettini and Cox, 2000

16

Jittered Single-Trial Designs

- Varying the timing of trials within a run

17

Extracting different task components

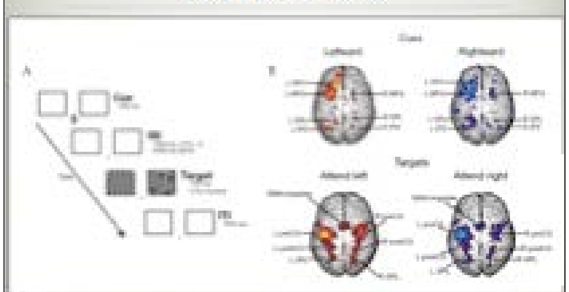

18

Limitations of Event-Related Designs

- Differential effects of ISI
  - Long intervals do not optimally increase stimulus variance
  - Short intervals may result in refractory effects
- Detection ability dependent on form of HDR
- Length of "event" may not be known

19

FMRI ANALYSIS

20

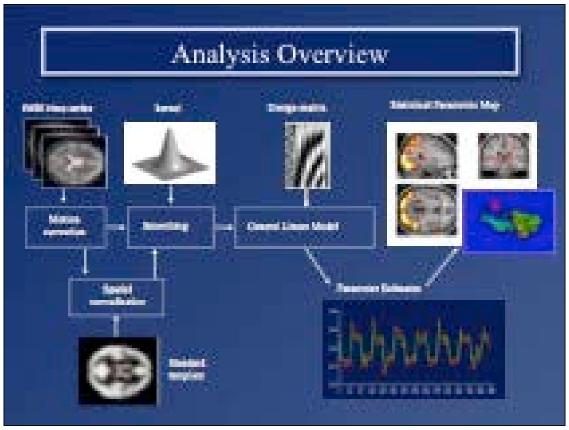
Analysis Overview

21


PREPROCESSING

22

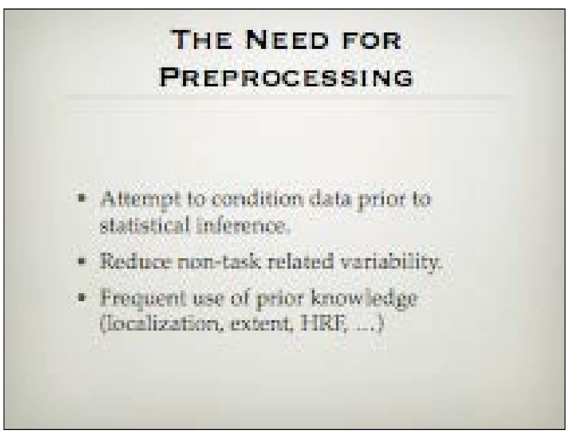
THE NEED FOR PREPROCESSING
• Attempt to condition data prior to statistical inference.
• Reduce non-task related variability.
• Frequent use of prior knowledge (localization, extent, HRF, ...)

23

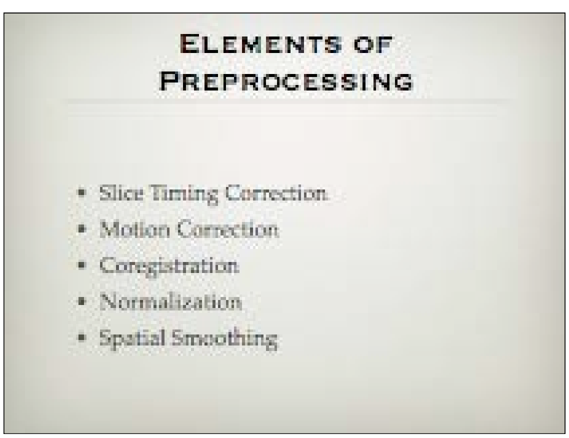
ELEMENTS OF PREPROCESSING
• Slice Timing Correction
• Motion Correction
• Coregistration
• Normalization
• Spatial Smoothing

24

Slice Timing Correction

25

Motivation for Slice Timing Correction

- Most fMRI acquired using 2D multislice EPI
- Individual slices acquired throughout the TR
- TR typically 1-10s
- Slice timing correction attempts to interpolate signal time course at standardized timepoints

26

Volume Timeseries

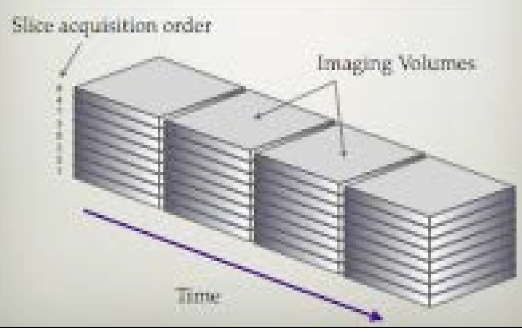

27

Slice timing Delay

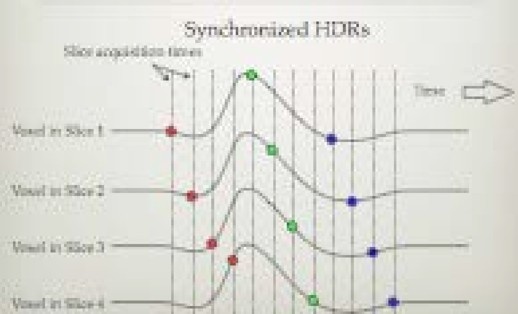

28

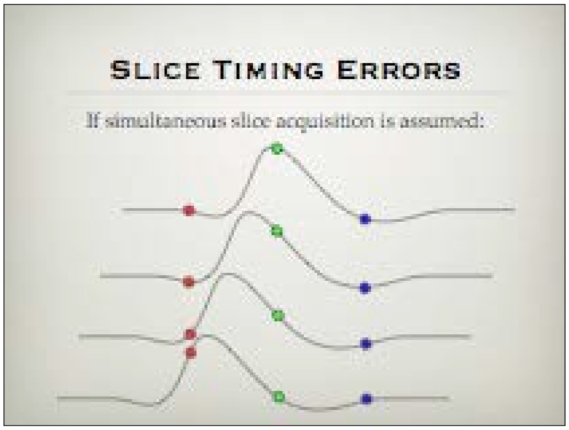
SLICE TIMING ERRORS
If simultaneous slice acquisition is assumed:

29

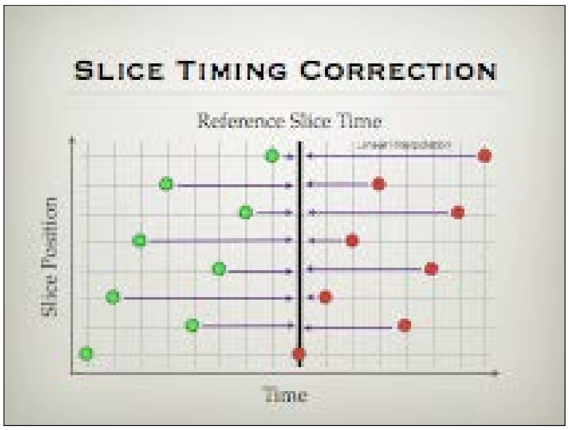
SLICE TIMING CORRECTION
Reference Slice Time
Slice Position
Time

30


MOTION CORRECTION

31

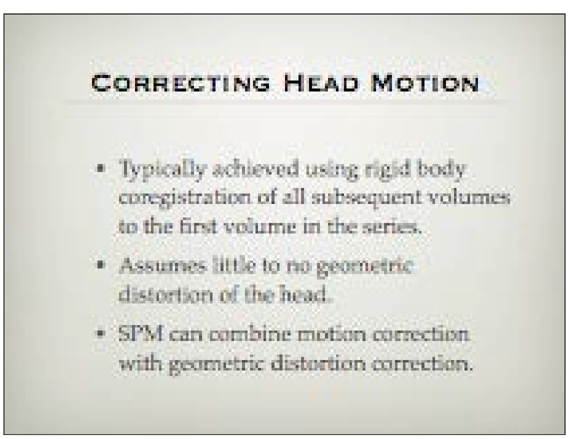
CORRECTING HEAD MOTION
• Typically achieved using rigid body coregistration of all subsequent volumes to the first volume in the series.
• Assumes little to no geometric distortion of the head.
• SPM can combine motion correction with geometric distortion correction.

32

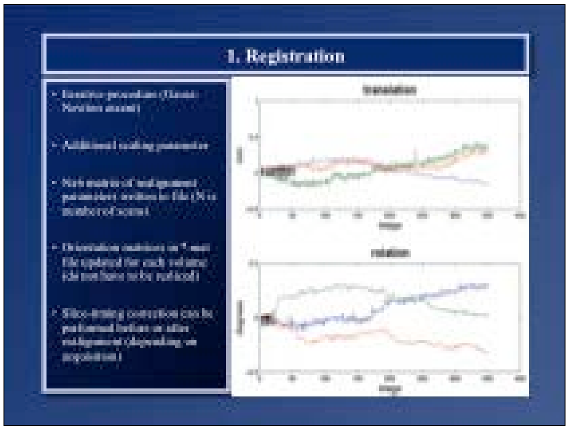

1. Registration
translation
rotation

33

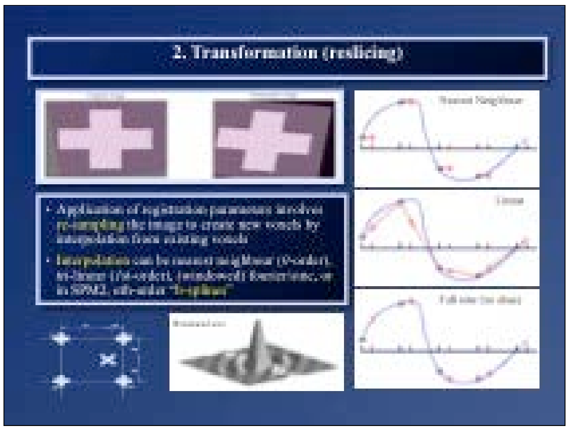

2. Transformation (reslicing)
Application of registration parameters involves re-sampling the image to create new voxels by interpolation from existing voxels
Interpolation can be nearest neighbour (0-order), tri-linear (1st-order), (windowed) fourier/sinc, or in SPM2, nth-order "b-splines"

34

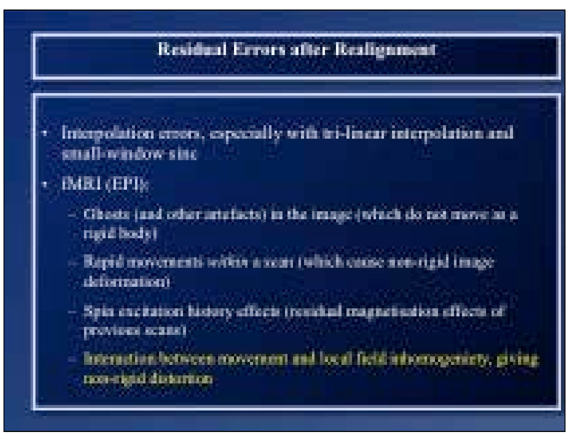

Residual Errors after Realignment
Interpolation errors, especially with tri-linear interpolation and small-window sinc
fMRI (EPI):
Ghosts (and other artefacts) in the image (which do not move as a rigid body)
Rapid movements within a scan (which cause non-rigid image deformation)
Spin excitation history effects (residual magnetisation effects of previous scans)
Interaction between movement and local field inhomogeniety, giving non-rigid distortion

35

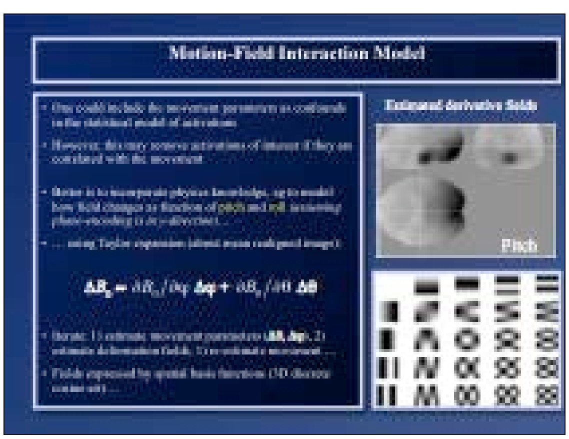

Motion-Field Interaction Model
Pitch

36

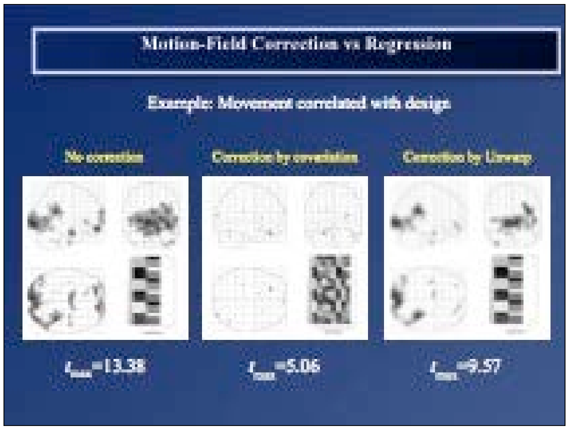

37

SPATIAL NORMALIZATION

38

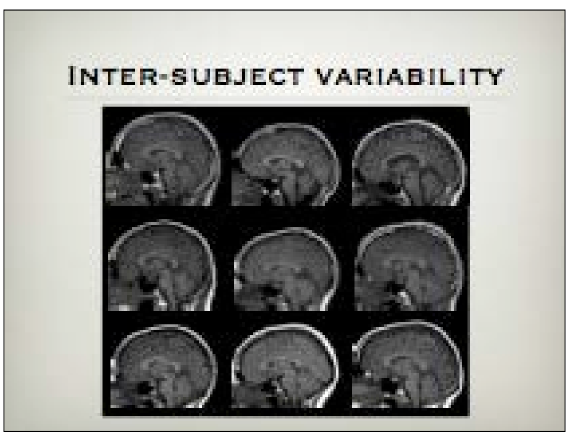

39

Reasons for Normalisation

- Inter-subject averaging
  - extrapolate findings to the population as a whole
  - increase statistical power above that obtained from single subject
- Reporting of activations as co-ordinates within a standard stereotactic space
  - e.g. the space described by Talairach & Tournoux

- Label-based approaches: Warp the images such that defined landmarks (points/lines/surfaces) are aligned
  - but few readily identifiable landmarks (and manually defined?)
- Intensity-based approaches: Warp to images to maximise some voxel-wise similarity measure
  - eg. squared error, assuming intensity correspondence (within-modality)
- Normalisation constrained to correct for only gross differences; residual variability accommodated by subsequent spatial smoothing

40

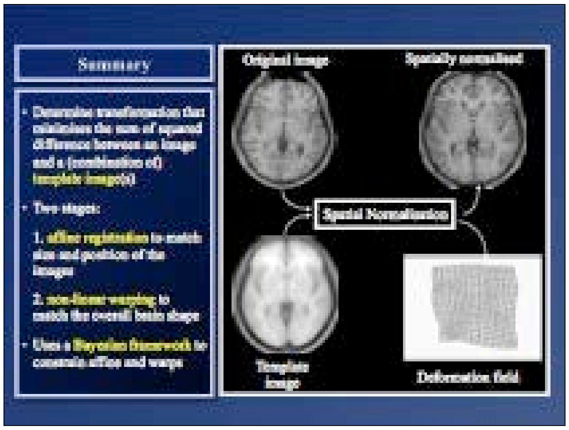
Summary
Determine transformation that minimises the sum of squared difference between an image and a (combination of) template image(s)
Two stages:
1. affine registration to match size and position of the images
2. non-linear warping to match the overall brain shape
Uses a Bayesian framework to constrain affine and warps
Original image
Spatially normalised
Spatial Normalisation
Template image
Deformation field

41

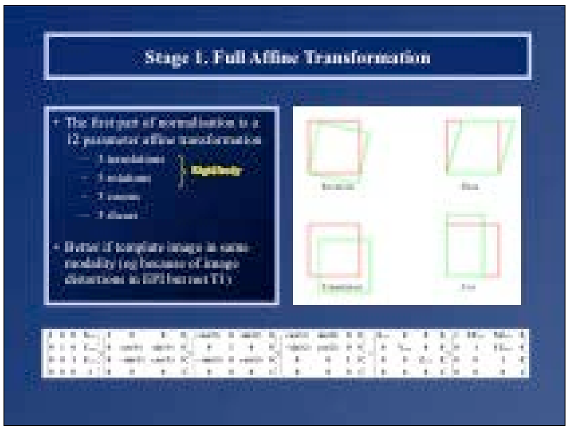
Stage 1. Full Affine Transformation
The first part of normalisation is a 12 parameter affine transformation
3 translations
3 rotations
3 zooms
3 shears
Rigid body
Better if template image in same modality (eg because of image distortions in EPI but not T1)

42

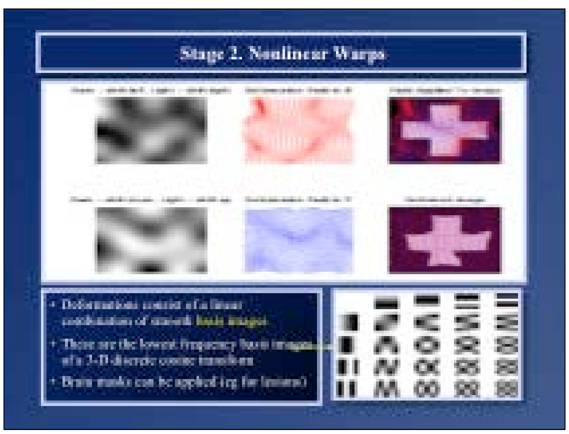
Stage 2. Nonlinear Warps
Deformations consist of a linear combination of smooth basis images
These are the lowest frequency basis images of a 3-D discrete cosine transform
Brain masks can be applied (eg for lesions)

43


Standardized Spaces
Talairach Space (proportional grid system)
From atlas of Talairach and Tournoux (1988)
Based on single subject (60y, Female, Cadaver)
Single hemisphere
Related to Brodmann coordinates
Montreal Neurological Institute Space (MNI and ICBM)
Combination of many MRI scans on normal controls
All right-handed subjects
Approximated to Talairach space
Slightly larger
Taller from AC to top by 5mm; deeper from AC to bottom by 10mm
Used by SPM, National fMRI Database, International Consortium for Brain Mapping

44

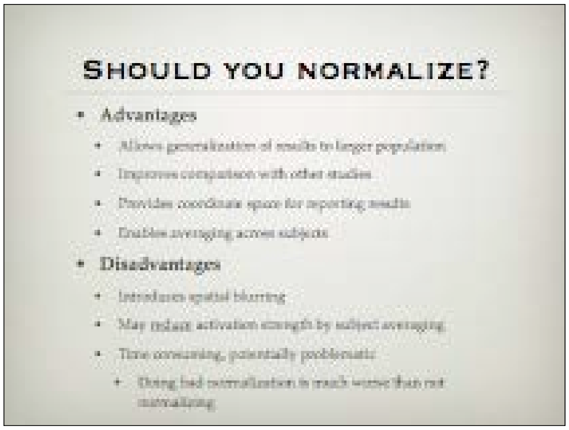
Should you normalize?
Advantages
Allows generalization of results to larger population
Improves comparison with other studies
Provides coordinate space for reporting results
Enables averaging across subjects
Disadvantages
Introduces spatial blurring
May reduce activation strength by subject averaging
Time consuming, potentially problematic
Doing bad normalization is much worse than not normalizing

45


Spatial Smoothing

46

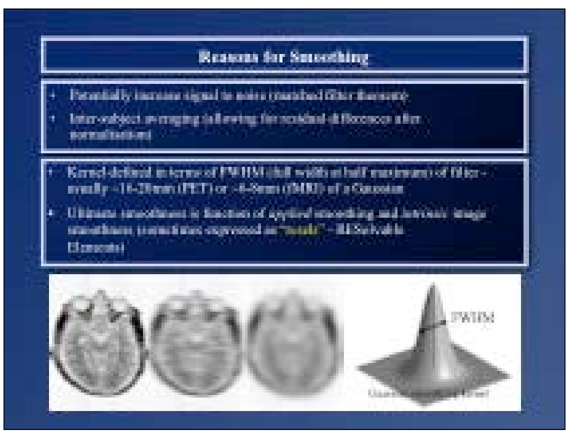
Reasons for Smoothing
FWHM

47

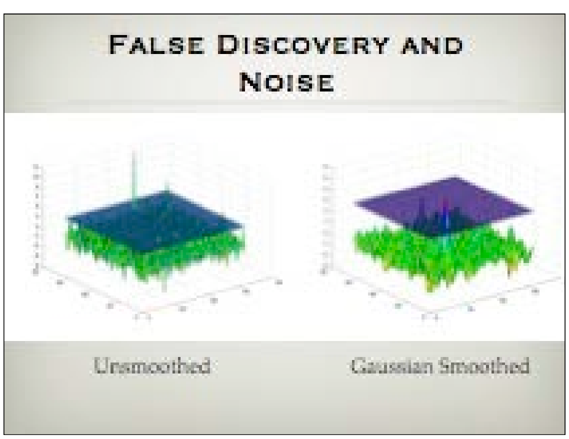
False Discovery and Noise
Unsmoothed
Gaussian Smoothed

48

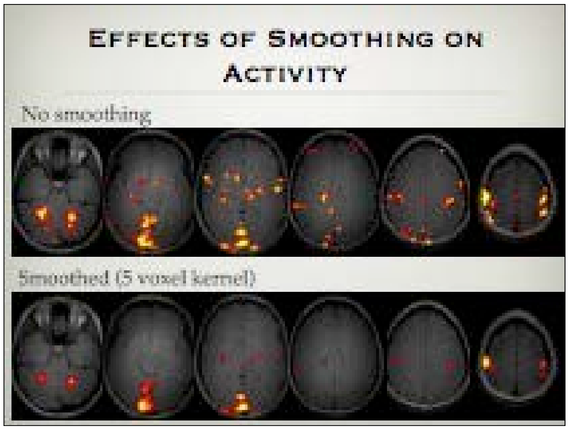
Effects of Smoothing on Activity
No smoothing
Smoothed (5 voxel kernel)

49

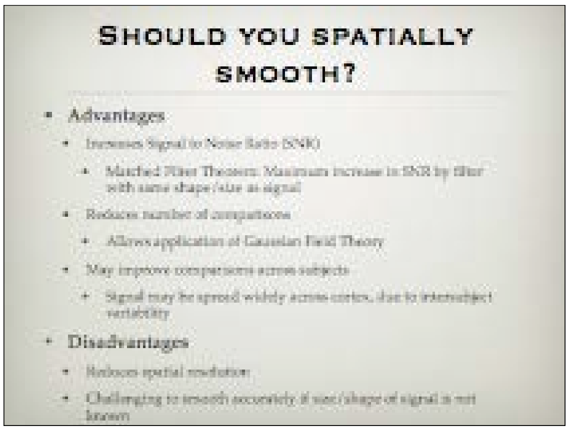
Should you spatially smooth?
Advantages
Increases Signal to Noise Ratio (SNR)
Matched Filter Theorem: Maximum increase in SNR by filter with same shape/size as signal
Reduces number of comparisons
Allows application of Gaussian Field Theory
May improve comparisons across subjects
Signal may be spread widely across cortex, due to intersubject variability
Disadvantages
Reduces spatial resolution
Challenging to smooth accurately if size/shape of signal is not known

50

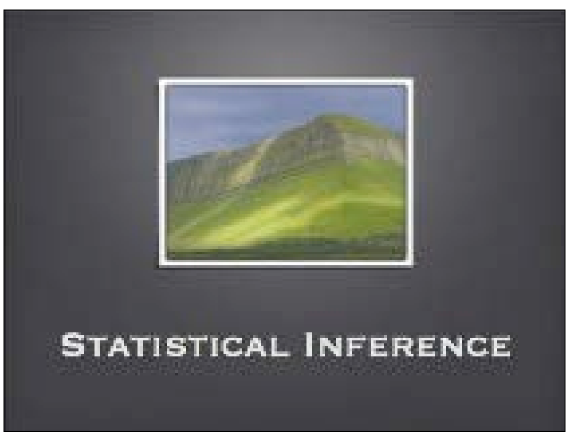
Statistical Inference

51

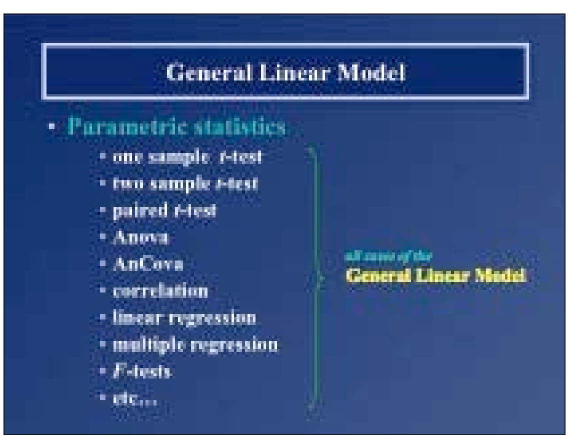
General Linear Model
Parametric statistics
one sample t-test
two sample t-test
paired t-test
Anova
AnCova
correlation
linear regression
multiple regression
F-tests
etc...
all cases of the
General Linear Model

52

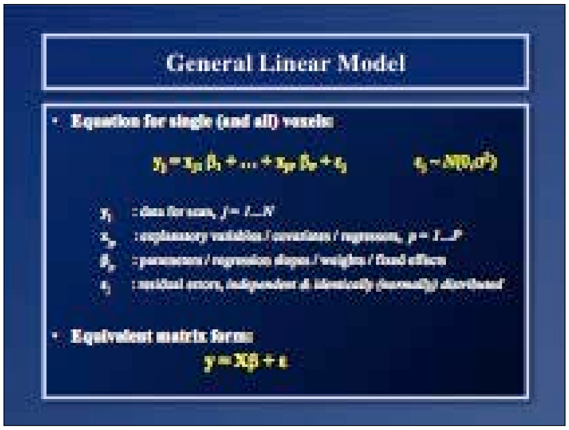
General Linear Model
Equation for single (and all) voxels:
$y_j = x_{j1}\beta_1 + \ldots + x_{jP}\beta_P + \varepsilon_j \qquad \varepsilon_j \sim N(0,\sigma^2)$
y_j : data for scan, $j = 1 \ldots N$
x_{jp} : explanatory variables / covariates / regressors, $p = 1 \ldots P$
β_p : parameters / regression slopes / weights / fixed effects
ε_j : residual errors, independent & identically (normally) distributed
Equivalent matrix form:
$y = X\beta + \varepsilon$

53

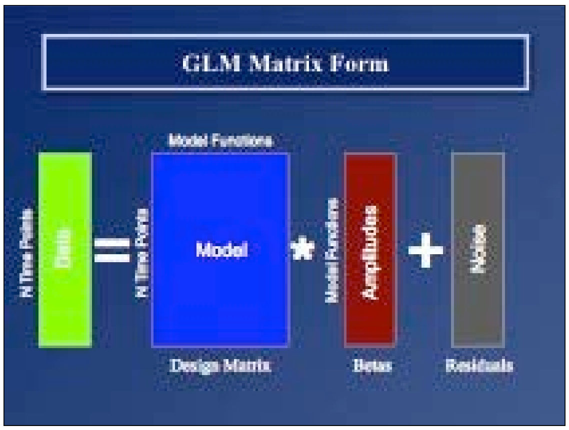
GLM Matrix Form
Model Functions
N Time Points
Data
=
N Time Points
Model
Design Matrix
*
Model Functions
Amplitudes
Betas
+
Noise
Residuals

54

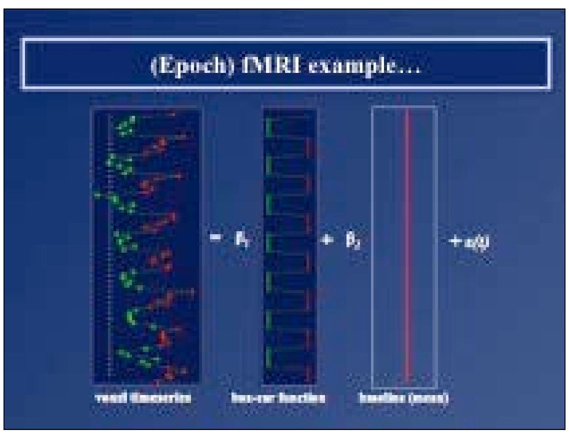
(Epoch) fMRI example…
= β_1
+ β_2
+ $e(t)$
voxel timeseries
box-car function
baseline (mean)

55

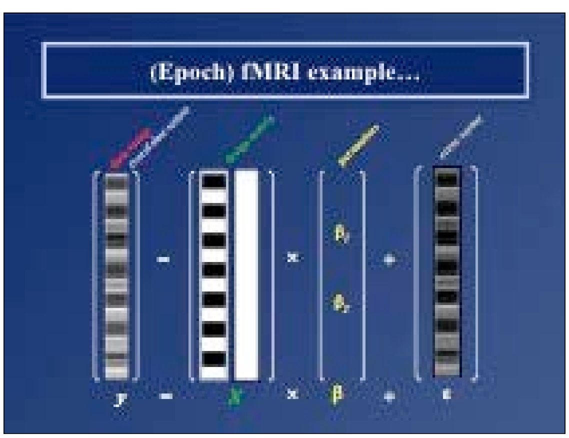
(Epoch) fMRI example…
β_1
β_2
y = X × β + ε

56

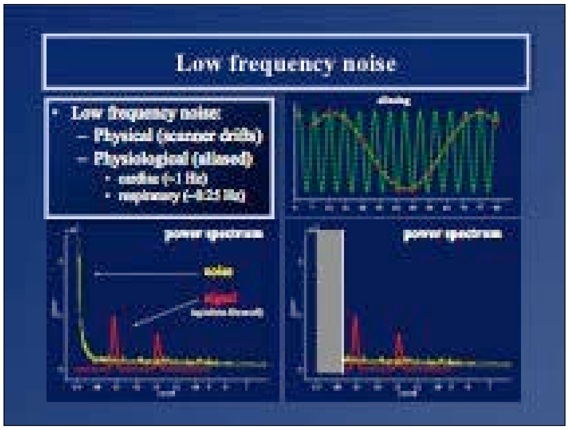
Low frequency noise
Low frequency noise:
– Physical (scanner drifts)
– Physiological (aliased)
• cardiac (~1 Hz)
• respiratory (~0.25 Hz)
power spectrum
noise
signal
power spectrum

57

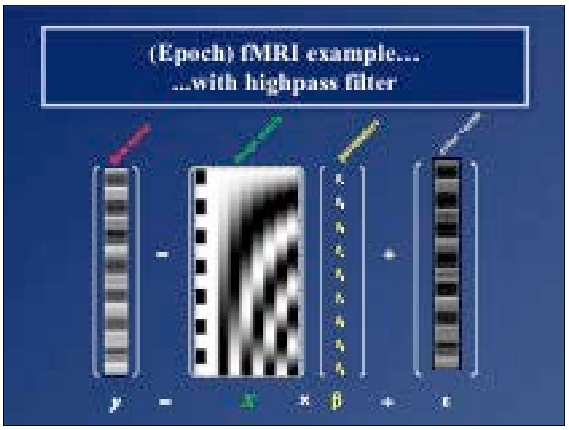
(Epoch) fMRI example…
...with highpass filter
y = X × β + ε

58

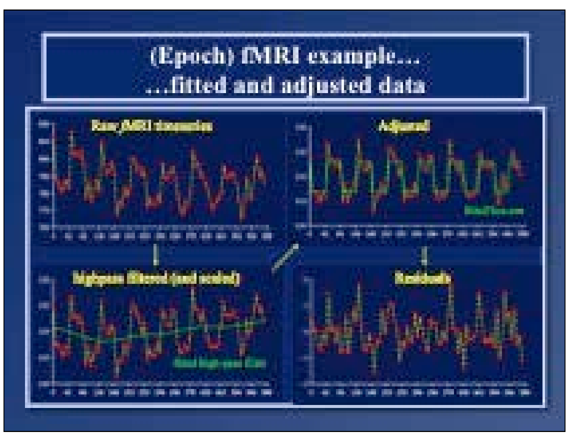
(Epoch) fMRI example…
…fitted and adjusted data
Raw fMRI timeseries
Adjusted
highpass filtered (and scaled)
Residuals

59

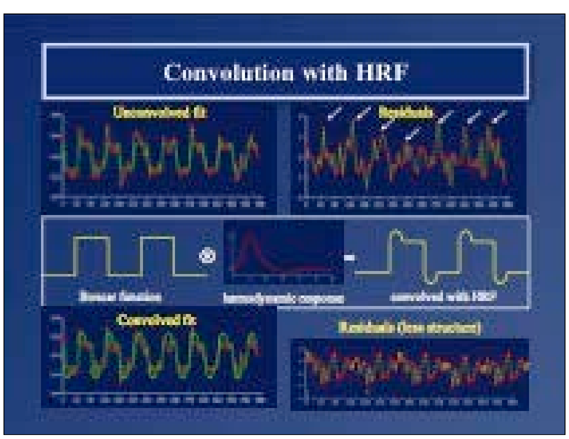
Convolution with HRF
Unconvolved fit
Residuals
Boxcar function
haemodynamic response
convolved with HRF
Convolved fit
Residuals (less structure)

60

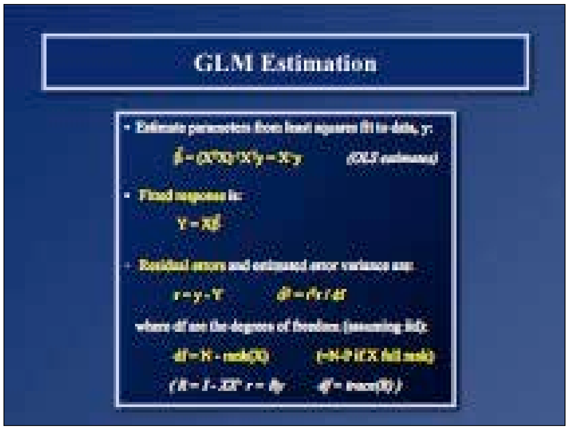
GLM Estimation

61

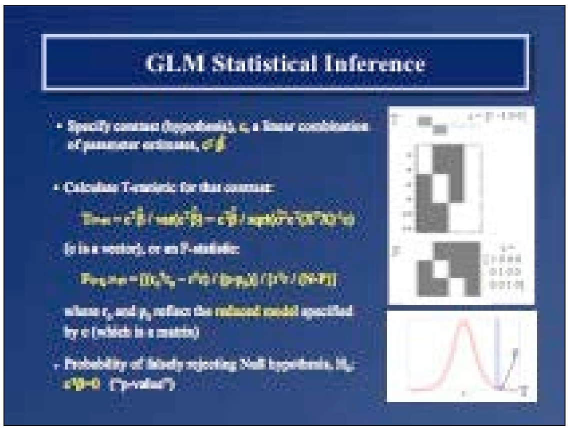
GLM Statistical Inference

62


Multiple Comparison
Correction

63

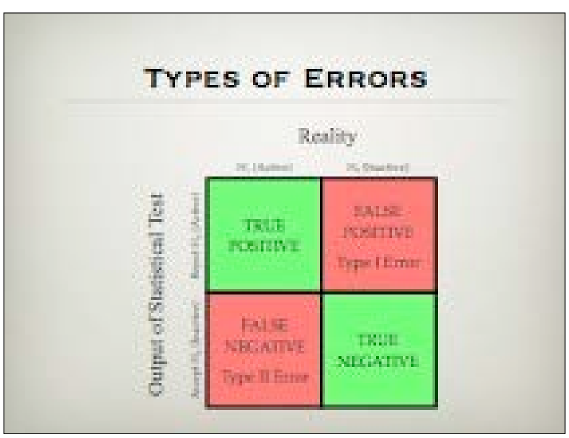
Types of Errors
Reality
Output of Statistical Test
TRUE
POSITIVE
FALSE
POSITIVE
Type I Error
FALSE
NEGATIVE
Type II Error
TRUE
NEGATIVE

64

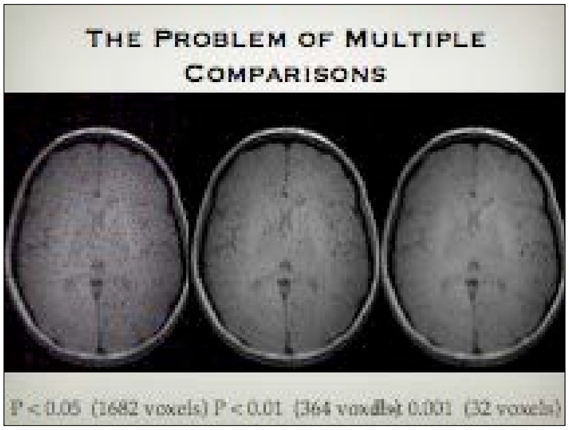
The Problem of Multiple Comparisons
P < 0.05 (1682 voxels) P < 0.01 (364 voxels) P < 0.001 (32 voxels)

65

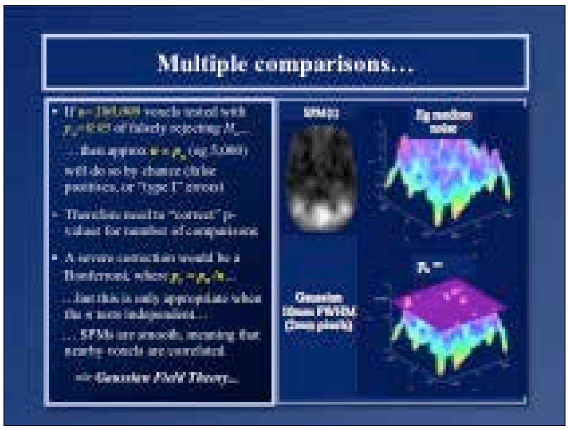
Multiple comparisons…

66

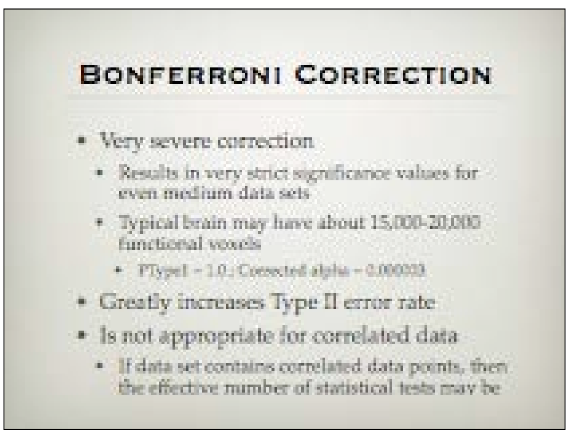
Bonferroni Correction
• Very severe correction
• Results in very strict significance values for even medium data sets
• Typical brain may have about 15,000-20,000 functional voxels
• PType1 ~ 1.0 ; Corrected alpha ~ 0.000003
• Greatly increases Type II error rate
• Is not appropriate for correlated data
• If data set contains correlated data points, then the effective number of statistical tests may be

67

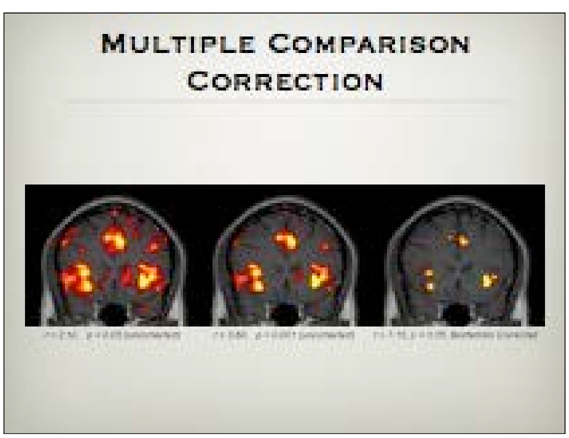
Multiple Comparison Correction

68

Gaussian Field Theory

- Approach developed by Worsley and colleagues to account for multiple comparisons
  - Forms basis for much of SPM
- Provides false positive rate for fMRI data based upon the smoothness of the data
  - If data are very smooth, then the chance of noise points passing threshold is reduced

69

Final Product

Tapping > 0 Both > (Left + Right)

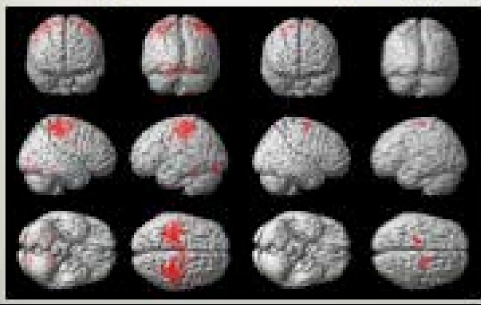

70

Course Paper Assignment

- Journal article review
  - Choose one high impact peer-reviewed journal article from the MRI literature.
  - Write a 3 page critical review of this paper with appropriate comparison to related papers.
  - Due Tuesday December 16th 2008

71